Cloning, expression, purification, structure analysis, biochemical characterization and therapeutic applications of a rhamnogalacturonan acetyl esterase (*Ct*Pae12B) from *Acetivibrio thermocellus* ATCC 27405

PhD Thesis

by

Jebin Ahmed

May 2024

DEPARTMENT OF BIOSCIENCES AND BIOENGINEERING
INDIAN INSTITUTE OF TECHNOLOGY GUWAHATI
GUWAHATI -781039, ASSAM, INDIA

Cloning, expression, purification, structure analysis, biochemical characterization and therapeutic applications of a rhamnogalacturonan acetyl esterase (*Ct*Pae12B) from *Acetivibrio thermocellus* ATCC 27405

A Thesis

Submitted in partial fulfillment
of the requirements for the Degree of

Doctor of Philosophy

by

Jebin Ahmed

Under supervision of
Professor Arun Goyal

May 2024

DEPARTMENT OF BIOSCIENCES AND BIOENGINEERING
INDIAN INSTITUTE OF TECHNOLOGY GUWAHATI
GUWAHATI 781039, ASSAM, INDIA

INDIAN INSTITUTE OF TECHNOLOGY GUWAHATI

DEPARTMENT OF BIOSCIENCES AND BIOENGINEERING

STATEMENT

I do hereby declare that the content embodied in this thesis entitled "**Cloning, expression, purification, structure analysis, biochemical characterization and therapeutic applications of a rhamnogalacturonan acetyl esterase (*Ct*Pae12B) from *Acetivibrio thermocellus* ATCC 27405**" is the result of investigations carried out by me in the Department of Biosciences and Bioengineering, Indian Institute of Technology Guwahati, Guwahati, India under the guidance of Professor Arun Goyal. In keeping with the general practice of reporting scientific observations, due acknowledgements have been made wherever the work described is based on the findings of other investigators.

May, 2024 JEBIN AHMED

(186106119)

INDIAN INSTITUTE OF TECHNOLOGY GUWAHATI

DEPARTMENT OF BIOSCIENCES AND BIOENGINEERING

CERTIFICATE

It is certified that the work described in this thesis entitled "**Cloning, expression, purification, structure analysis, biochemical characterization and therapeutic applications of a rhamnogalacturonan acetyl esterase (*Ct*Pae12B) from *Acetivibrio thermocellus* ATCC 27405**" by Jebin Ahmed (Roll No. 186106119) for the award of degree of Doctor of Philosophy is an authentic record of the results obtained from the research work carried out under my supervision at the Department of Biosciences & Bioengineering, Indian Institute of Technology Guwahati, Guwahati, India and this work has not been submitted elsewhere for a degree.

Prof. Arun Goyal (MTech, PhD)
(FAMI, FBRS, FABAP, FNABS, FNAAS, FIFIB)
(Thesis Supervisor)
Department of Biosciences & Bioengineering
Indian Institute of Technology Guwahati
Guwahati, 781039, India

ACKNOWLEDGEMENTS

It gives me immense pleasure to express my gratitude to all those who have contributed in so many ways in keeping this thesis on track and its completion. I am thankful for all the encouragement, support and motivation to my supervisor, my doctoral committee members, my family, my friends and my colleagues. I would like to thank all those people who made this thesis possible and an unforgettable experience for me. At the end of my thesis, it is a pleasant task to express my thanks to all those who contributed in many ways and had a profound impact on the success of this study deserves special acknowledgement.

First of all, I would like to express my heartfelt gratitude towards the Almighty for blessing me enough in so many ways to go through this incredible journey. I will be forever in debt for bestowing upon me the immense strength, both physically and mentally, to complete this work.

At this moment of accomplishment, I am extremely indebted to my thesis supervisor, Professor Arun Goyal, Department of Biotechnology, IIT Guwahati. This work would not have been possible without his guidance, support and encouragement. Under his guidance I successfully overcame many difficulties and learned a lot. I can't forget how patiently he listened to my problems and provided the necessary instructions. He always used to review my thesis progress, give me valuable suggestions and made corrections numerous times. His unflinching convictions will always inspire me and I hope to continue to work with his noble thoughts. I earnestly thank him for inculcating in me a scientific temperament and appreciable work ethics which helped me to achieve this goal.

I would like to I would also like to express my sincere gratitude to all my doctoral committee members Dr. Shirisha Nagotu, Dr. A. M. Limaye and Dr.

Priyadarshi Satpati for their valuable suggestions and constructive criticism that has led to the successful completion of my thesis.

I am thankful to the Department of Biosciences & Bioengineering and Central Instrumentation Facility (CIF), IITG for providing me with instrumental facilities for my research work.

I sincerely thank Dr. Ravishankar Ramachandran, Principal Scientist and his team member Md Afsar, CSIR-Central Drug Research Institute, Lucknow, India for providing the SAXS facility and data collection.

I would like to specially mention and express my deep gratitude towards Mr. Rushikesh R. Fopase, PhD student, Department of Biosciences and Bioengineering, IITG for his immense support, motivation and power, right from the beginning of this journey. I express my heartfelt appreciation for the courage he has given me at all hard times and kept me going. I am thankful for how he always managed time to support and help me in every difficulty I faced, in spite of his own super busy schedule and made this journey a lot easier than it was. Without his help and continuous moral support, this journey would not have been possible and I will be forever in debt towards his kindness. I wish him a shining and bright future ahead.

I would also like to thank the present and previous heads of the Department of Biosciences & Bioengineering, IIT Guwahati, Prof. K. Pakshirajan, Prof. Latha Rangan and Prof. Rakhi Chaturvedi for providing me with the necessary facilities.

I am also thankful to my seniors Dr. Vikky Rajulapati, Dr. Kedar Sharma, Dr. Krishan Kumar, Dr. Priyanka Nath, Dr. Shweta Singh, Dr. Sumitha Bano, Dr. Abhijeet Thakur and Dr. Kaustubh khaire for their help and suggestions. I am immensely thankful to my research group members Parmeshwar, Maibam, Robin, Madhulika, Ardhendu, Aishwarya, Vishwanath, Shreya, Akshita, Bipasha, Sushrata, Ashwani,

Akshay and Mohana. I am grateful to all the people with whom I have worked in the lab at the Department of Biosciences and Bioengineering for their cooperation and support.

I would like to thank my friends Siddharth, Sahil, Nikhil, Krishnakant, Sonia and my batchmates Meenakshi, Krishna, Nuzelu, Devishmita, Pratyusha, Chitra, Kamal, Simangko and Saswat for their support.

I wish to acknowledge the support received from other teaching and non-teaching staff of the Department of Biosciences and Bioengineering, IITG.

I wish to acknowledge the Ministry of Education, Govt. of India for providing financial assistance and also the Department of Biotechnology, Govt. of India, New Delhi for providing me fellowship through its sponsored project.

My PhD endeavour would not have been successful without the love, trust, support and blessings of my mother. I am filled with profound gratitude towards my mother and wish to make her happy and proud of my achievements. I owe her all the success of my life.

Jebin Ahmed

May, 2024

SYNOPSIS

Introduction

Plants are the primary producers (autotrophs) in the food chain that through the complex process of photosynthesis fulfils the energy requirement of almost all life-forms in different community habitats. Plants store energy in the form of carbohydrates (sugars) in their leaves, seeds, roots etc. Carbohydrates are organic compounds that are polyhydroxy aldehydes or polyhydroxy ketones or change to such substances on simple chemical transformations such as hydrolysis, reduction or oxidation. Carbohydrate components make up to 90% of the primary cell wall which provides protection and structural support to the plant and are also involved in signalling functions. The plant carbohydrates are namely, cellulose, hemicellulose and pectin. Cellulose is a collection of β-1,4-linked glucan chains that interact via hydrogen bonds to form crystalline microfibrils. Hemicelluloses are hetero-polysaccharides that include xyloglucans, arabinoxylans, arabinogalactans, mannans, xylans and mixed-linkage glucans. Among them the most common hemicelluloses are xylan and mannan. Pectin is structurally the most complex polysaccharide constituent of plant cell wall which is found abundantly in primary cell wall and middle lamella. The pectin network also interacts with cellulose and hemicellulose network and other cell wall proteins like extensin and arabinogalactan protein (AGP), covalently and also non-covalently through the ester linkages and hydrogen bonds. Pectin has a prevalent role in plant growth and development, defence mechanism, cell-cell adhesion, providing structural stability to the cell wall, regulation of cell permeability and fruit development. Structural classes of pectic polysaccharides include homogalacturonan (HG), rhamnogalacturonan I (RG I) and rhamnogalacturonan II (RG II) substituted galacturonan like, xylogalacturonan (XGA) and apiogalacturonan (APA). HG, RG II, XGA and APA are characterised by

α-1,4-linked-D- galactopyranosyluronic acid (*GalpA*) backbone. HG is considered as the smooth region of pectin as it is devoid of any side chains, whereas RG I, RG II, XGA and APA are considered as hairy regions of pectin because of the presence of side-chains. RG I is a repeating of monomeric unit [→4)-α-D-*GalpA*-(1→2)-α-L-rhamnopyranosyl (*Rhap*)-(1→]. The *GalpA* residues may be C-6 methylated and acetylated at O-2 or O-3 positions, while 20-80% *Rhap* residues are substituted at C-4 with linear or branched chains of α-L-arabinofuranosyl (*Araf*), β-D-galactopyranosyl (*Galp*) residues and their relative proportion and chain lengths may differ depending on plant source.

Carbohydrate active enzymes are involved that catalyse the breakdown, biosynthesis or modification of carbohydrates or glycoconjugates. Carbohydrate Active Enzyme (CAZy) database provides online and continuously updated access to carbohydrate enzymes based on sequence-based family classification, linking the sequence to its specificity and 3-D structure. As of April 2024, there are 189 families of glycoside hydrolases (GHs), 135 families of glycosyl transferases (GTs), 43 families of polysaccharide lyases (PLs), 20 families of carbohydrate esterases (CEs) and 17 families with auxiliary activities (AAs). CEs are involved in removal of esterified groups present in the polysaccharide side chain. CE12 consists of bacterial and fungal pectin acetyl esterase (PAE), rhamnogalacturonan acetyl esterase (RGAE) and acetyl xylan esterase (AXE). CE12 enzymes usually have a catalytic triad comprising of Ser-His-Asp amino acid residues. In the catalytic triad, the imidazole ring of the histidine acts as a general base and catalyses the nucleophilic attack of the serine oxygen on the acyl carbonyl carbon of the substrate, by abstracting the proton from its hydroxyl group, forming an acyl-enzyme intermediate. The aspartate residue might play a role in correcting the tautomeric orientation of histidine relative to serine and it also might

interact with the imidazole ring to stabilize the ion-pair generated between histidine and the acyl-enzyme intermediate during the transition state. The catalytic triad forms hydrogen bonds among themselves for stabilization. CE12 contains a total of 7378 protein sequences as of April 2024. Of these 7378 protein sequences, 5725 are from bacteria, 1651 are from eukaryota and 2 belong to unclassified sequences. Till date, only 4 bacterial PAEs have been characterized biochemically, *viz*., PaeY from *E. chrysanthemi*, PaeX from *E. chrysanthemi*, YxiM from *B. subtilis* and BliPae from *B. licheniformis*. Out of these four, the crystal structure of only one PAE from *Bacillus subtilis*, 2o14.pdb, has been submitted and is available in the protein data bank. Apart from this, one fungal RGAE from *Aspergillus aculeatus* and 3 bacterial RGAEs from *B. halodurans*, *B. subtilis* and *P. polymyxa* were characterized biochemically. Out of these four RGAEs, only one RGAE from *A. aculeatus*, has been structurally characterized and elucidated. Both RGAE and PAE belong to the Serine-Glycine-Asparagine-Histidine (SGNH) hydrolase family, a new hydrolase family which is different than the glycoside hydrolase family. The SGNH hydrolase family is characterized by the presence of having four conserved blocks of residues, each consisting of completely conserved residues Ser, Gly, Asn and His, respectively. PAEs and RGAEs characterized so far have a typical α/β/α structure containing a central β-sheet.

Acetivibrio thermocellus is a rod-shaped, anaerobic, thermophilic and Gram-positive bacterium and it consists of cellulosome on its cell-surface, an extracellular multi-enzyme complex. The molecular architecture of a putative pectin acetyl esterase (*Ct*Pae12B), a family 12 carbohydrate esterase from *Acetivibrio thermocellus* belonging to gene locus Cthe_3141 under current study is shown below (Fig. 1).

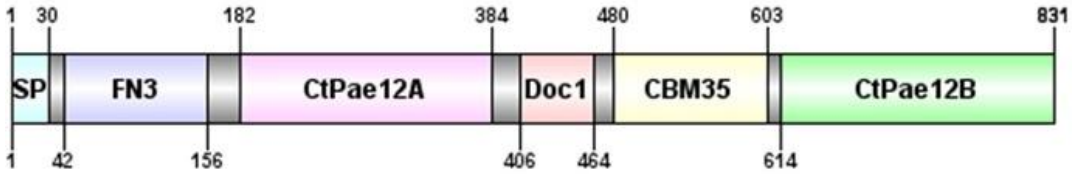

Fig 1. Molecular architecture of the full-length amino acid sequence of locus tag Cthe_3141 (Genbank Accession no. ABN54336.1) showing *Ct*Pae12B catalytic module (green) from *Acetivibrio thermocellus* ATCC 27405.

Current work

The current work entitled "Cloning, expression, purification, structure analysis, biochemical characterization and therapeutic applications of rhamnogalacturonan acetyl esterase (*Ct*Pae12B) from *Acetivibrio thermocellus* ATCC 27405" has been divided into five chapters.

Chapter 1 is the General Introduction, which describes elaborately the major plant cell carbohydrates. An elaborate presentation of pectin and its different structural components are described. A brief explanation of the biosynthesis of pectin wall polymers is mentioned. A detailed introduction to degree of esterification (methylation and acetylation) of pectin is mentioned. The application of pectin in different industrial sectors is mentioned. Different kinds of carbohydrate active enzymes detailed in CAZy database are mentioned. A detailed and elaborated review on the biochemical characters, structure features and different industrial applications of various pectin degrading enzymes are also discussed in this chapter. Detailed features and characteristics of CEs and CE12 family are also mentioned. This chapter also discusses the mechanism of the catalytic action of PAEs and RGAEs and their applications in different sectors. Detailed information on *A. thermocellus* and its cellulosomal structure is also mentioned in this chapter and lastly, the significance of carrying out this current work has been stated along with the specific objectives.

Chapter 2 describes the cloning, expression and purification of the putative pectin acetyl esterase (*Ct*Pae12B) a family 12 carbohydrate esterase (CE12) from *Acetivibrio thermocellus* ATCC 27405 belonging to locus tag Cthe_3141 with Genbank accession no. ABN54336.1. Sequence analysis of locus tag Cthe_3141 from *Acetivibrio thermocellus* ATCC 27405 showed the presence of an N-terminal signal peptide followed by fibronectin type 3 domain, first family 12 carbohydrate esterase catalytic domain *Ct*Pae12A, followed by type 1 dockerin domain, followed by carbohydrate binding module family 35 and second C-terminal family 12 carbohydrate esterase catalytic domain *Ct*Pae12B. The 654 bp of DNA sequence encoding the *Ct*Pae12B was PCR amplified. The restriction enzyme digested fragments of gene encoding *Ct*Pae12B were ligated with linearized pET-28a(+) vector. The ligated mixture was transformed using *E. coli* (DH5α) competent cells and the positive clone of recombinant *Ct*Pae12B was confirmed by using restriction enzymes *NheI* and *XhoI*. The restriction enzyme digested products were electrophoresed and a band of ~5.3 kb was produced for pET-28a(+) vector and a corresponding band of ~0.65 kb was produced from the insert fragment for gene encoding *Ct*Pae12B. *E. coli* BL-21 competent cells were transformed using the recombinant plasmid DNA for protein expression. The hyper-expression of recombinant protein was achieved by using IPTG as an inducer at a final concentration of 0.5 mM. The hyper-expression of the recombinant *Ct*Pae12B was checked and confirmed by SDS-PAGE analysis. The recombinant *Ct*Pae12B was purified from the sonicated cell free extract by immobilized metal ion chromatography (IMAC) using HiTrap chelating sepharose column. The purified *Ct*Pae12B was expressed as a soluble protein and displayed a molecular size of approximately, 25 kDa, as analysed by SDS-PAGE, which was in agreement with the theoretical molecular mass of 26 kDa. The

amount of *Ct*Pae12B protein obtained from 400 mL of culture after IMAC purification was 9 mg with enzyme activity yield 84% and purification fold 18.

Chapter 3 describes the computational and solution structure insights of *Ct*Pae12B. The amino acid sequence of a *Ct*Pae12B was 34.86% identical with 92% query coverage with the amino acid sequence of a pectin acetyl esterase from *Bacillus subtilis* of CE12 family. Multiple sequence alignment with its nearest homologues showed that Ser15, Gly51, His82, Asn83, Asp187, Thr189 and His190 are catalytically important residues of which Ser15, Asp187 and His190 constitute the catalytic triad. The 3-D modeled structure generated by comparative modeling further revealed that it possesses a new α/β hydrolase fold, similar to the fold found in the crystal structure of its nearest homologues (RGAE and YxiM), which is not similar to α/β fold as found in α/β hydrolase family of glycoside hydrolases. CD analysis showed that *Ct*Pae12B is composed of 37.9% α-helices, 16.1% β-sheets and 46.1% random coils which was in agreement with the results predicted by Psipred and 2Struc. *Ct*Pae12B belongs to a new SGNH-hydrolase fold family of which the members of CE12 are a distinct family. The *Ct*Pae12B structure was energy minimized and the refinement was validated. MD simulation of *Ct*Pae12B confirmed that the structure was conformationally stable and compact and the catalytically important residues were also excluded from deformity or any occlusion. The docking studies further revealed the catalytically important residues. The highest binding affinity of *Ct*Pae12B was shown with *p*NPA. Comparative analysis of MD simulated *Ct*Pae12B-*p*NPA structure with only *Ct*Pae12B structure further confirmed the structure stability of the docked complex. The catalytic residues in the docked complex were also stable with minimal fluctuations. The outer loop L4 was found to be comparatively more flexible than the other residues, which might have brought some conformational changes in the structure of *Ct*Pae12B without causing

any distortion in the structure. The best data of *Ct*Pae12B by SAXS analysis was obtained at 3 mg/mL in order to gain an insight into its solution behaviour. The SAXS analysis showed the stable conformational behaviour of *Ct*Pae12B. The Kratky plot further showed the compact nature and lesser flexibility of *Ct*Pae12B. The data from the SAXSMow server showed that the molecular mass of *Ct*Pae12B was thrice of its molecular mass (25 kDa, in monomeric state) at 3 mg/mL. Further, the final dummy atomic model obtained by DAMMIF program fitted manually with three *Ct*Pae12B simulated structures based on existence of hydrophobic interaction between inter protein chains showed an excellent trimeric molecular envelope. The particle size of *Ct*Pae12B at 3 mg/mL determined by dynamic light scattering (DLS) analysis also confirmed that it exists as an elongated homotrimer. However, the DLS analysis at lower concentrations of *Ct*Pae12B than 3 mg/mL showed lower hydrodynamic diameter. Thus, it cannot be concluded that *Ct*Pae12B always exists in a homotrimer structure at all concentrations. The templates used for modeling of *Ct*Pae12B are not yet reported to exist in any higher oligomeric forms. Therefore, the fold analysis, conformations of catalytic residues, ligand binding and conformation analysis by dynamic studies were carried out with template-based homology modeled monomeric form of *Ct*Pae12B. Moreover, the R_g calculated by MD simulation of *Ct*Pae12B trimer modeled structure corroborated with the R_g determined by SAXS analysis of the *Ct*Pae12B trimer formed in solution at 3 mg/mL. The structural insights of pectin acetyl esterase, *Ct*Pae12B illustrated a new hydrolase fold with a compact and stable structure, absence of a nucleophilic elbow and the role of the loops in formation of the catalytic triad in the active-site for covalent catalysis of the substrate. However, more substantial analyses by advanced techniques may lead to its detailed structure elucidation.

Chapter 4 describes the biochemical characterisation of *Ct*Pae12B. *Ct*Pae12B was obtained with maximum yield from commercial medium Luria-Bertani. *Ct*Pae12B displayed thermophilic properties with optimum temperature, 65 ºC and retained 50% of its activity for 5.1 h at 80 ºC. *Ct*Pae12B was stable in both acidic and alkaline environment and displayed maximum activity at pH 8.0. The enzyme, *Ct*Pae12B was drastically inactivated by heavy metal ions, Co^{2+}, Cu^{2+}, Fe^{2+} and Ni^{2+} ions and anionic and non-ionic detergents. However, it was remarkably completely stable at a high concentration, 5 M of urea. Complete inhibition of *Ct*Pae12B activity by 50 mM PMSF showed the importance of the serine residue in catalysis. The enzymatic activity was not affected by any chelating agent showing no involvement of any metal ion for catalysis or structural integrity. The protein melting analysis also confirmed that there is no contribution to thermal stability by any metal ion or chelating agent, corroborating their non-involvement in imparting stability. *Ct*Pae12B showed robustness and superior properties as compared with its homologues as it showed activity against PRG as well as sugar beet pectin, xylan substrates like acetylated birchwood xylan, birchwood xylan, wheat arabinoxylan and also wide range of synthetic substrates. The highest specificity of *Ct*Pae12B against PRG showed its affinity towards the RG region of pectin confirming it to be an RGAE. This result can be explored in managing potato waste generated by many households and food industries like potato chips. *Ct*Pae12B is an efficient enzyme with its alkaline and thermotolerant properties, however, its limitation is that, it is efficient only on acetylated pectic or xylan substrates. It plays no role when the esterified substrate has only methyl groups and does not bear any or have negligible degree of acetylation. However, its broad substrates specificity, high specific activity against PRG (700 U/mg) and thermostable nature makes it a potential candidate

to explore its clinical and pharmaceutical applications like inhibition of cancer cells and drug delivery.

Chapter 5 describes synergistic action, regioselectivity of *Ct*Pae12B and its therapeutic applications in inhibiting colon cancer cells and colon-targeted drug delivery by forming hydrogels. Three pectin degrading enzymes *Ct*Pae12B, pectin methyl esterase (*Ct*PME) and rhamnogalacturonan lyase (*Ct*RGL*f*) were expressed and purified to homogeneity exhibiting single protein bands of ~25 kDa, 35 kDa and 80.2 kDa, respectively. The side chain degrading enzymes *Ct*Pae12B and *Ct*PME showed synergistic action with main chain degrading enzyme *Ct*RGL*f* against PRG, by displaying significant increase in its relative activity by 115%. The regioselectivity of *Ct*Pae12B towards O-2 and O-3 acetylated substrate (PRG) by ^{1}H NMR analysis showed that it had site specificity for acetyl groups at both positions enabling 98% removal of acetyl groups. ^{1}H NMR and HPLC analysis of PRG showed the degree of acetylation (DA) and degree of methylation (DM) to be approx. 21.9% and 7.7%, respectively, indicating higher acetylation and less methylation. The percentage of other mono-saccharides like *GalpA*, *Rhap*, galactose and arabinose calculated from HPLC analysis were 63.5%, 6.5%, 25% and 2.8%, respectively, in PRG. The breakdown products of PRG by only *Ct*RGL*f* and all three *Ct*Pae12B, *Ct*PME and *Ct*RGL*f* showed discrete spots in TLC plate and the smallest molecular mass product displayed was unsaturated RG di-saccharide that had similar mobility as the standard D-*GalpA*. The mass spectrometric analysis of only *Ct*RGL*f* treated and all three *Ct*Pae12B, *Ct*PME, *Ct*RGL*f* treated PRG showed that the smallest degraded product was unsaturated RG di-saccharide with m/z 322. The mass spectrometric analysis also showed that the oligosaccharide products released from PRG upon treatment with all three *Ct*Pae12B, *Ct*PME and *Ct*RGL*f* were de-acetylated and de-methylated as

compared to the products released upon treatment with *Ct*RGL*f* alone. The ATR-FTIR profile also showed de-acetylation and de-methylation of the PRG oligosaccharides upon treatment with all three *Ct*Pae12B, *Ct*PME and *Ct*RGL*f* as compared to acetylated and methylated oligosaccharides produced by only *Ct*RGL*f* treatment of PRG. FESEM analysis showed more porous surface morphology of *Ct*Pae12B-treated PRG as compared to non-enzyme treated PRG. The thermogravimetric (TG) analysis of *Ct*Pae12B-treated PRG showed the degradation temperature to be 254 ± 1.5 ºC. The pore volume (size ≤32 nm) and the total surface area of *Ct*Pae12B-treated PRG was significantly increased as compared with the non-enzyme treated PRG as analysed by Brunauer-Emmett-Teller (BET). The MTT assay showed that PRG polysaccharides (both esterified and de-esterified) were biocompatible with both HEK-293 and HCT-116 cells, while PRG oligosaccharides showed inhibition of HCT-116 cells. As compared to the acetylated and methylated PRG oligosaccharides (cell viability = 65%), the de-acetylated and de-methylated oligosaccharides showed higher inhibition of HCT-116 cells (cell viability = 50%) upon treatment with 1 mg/mL for 48 h. HEK-293 cells showed biocompatibility with all PRG oligosaccharides and no change in cell morphology as compared to the HEK-293 control cells. The cell morphology of the PRG oligosaccharides, *viz*., acetylated and methylated oligosaccharides (AcMeOS), deacetylated and methylated oligosaccharides (dAcMeOS) and deacetylated and demethylated oligosaccharides (dAcdMeOS), treated HCT-116 cells showed fewer number of cells with shrunken and globular shape and loss of cell-cell adhesion as compared to the cell morphology of PRG polysaccharide treated HCT-116 and control HCT-116 cells. The viscosity of doxorubicin hydrochloride (Dox) loaded *Ct*Pae12B-treated PRG hydrogel was higher than *Ct*Pae12B-treated PRG hydrogel without Dox loading. The drug entrapment efficiency of *Ct*Pae12B-treated PRG hydrogel was

remarkably higher than non-enzyme treated PRG hydrogel. The drug release study of *Ct*Pae12B-treated PRG hydrogel at gastric pH 1.2 and intestinal pH 7.4, showed sustainable release as compared with non-enzyme treated hydrogel. The faster rate of drug release by non-enzyme treated PRG hydrogel in gastric pH 1.2 than the *Ct*Pae12B-treated hydrogel showed that the *Ct*Pae12B treatment makes the PRG, a biomaterial more efficient in entrapping the drug and helping in controlled and sustained drug release. *Ct*Pae12B-treated PRG hydrogel showed sustained drug release at intestinal pH 7.4 for 24 h indicating that the *Ct*Pae12B treatment forms a hydrogel for colon targeted drug release. The results showed that *Ct*Pae12B is a highly efficient enzyme for deacetylation and has a potential role in therapeutic applications like inhibiting colon cancer cells and development of biocompatible gel material for controlled drug delivery systems. The role of *Ct*Pae12B can be further explored for developing efficient hydrogel biomaterials for therapeutic applications like entrapment of various anti-cancer drugs and their controlled and sustainable drug release.

CONTENTS

Chapter 1

General Introduction

1 Carbohydrates

Plants are multicellular, eukaryotic organisms that play the most vital role in maintaining life on Earth. Plants are the primary producers (autotrophs) in the food chain that through the complex process of photosynthesis fulfils the energy requirement of almost all life-forms in different community habitats. Plants store energy in the form of carbohydrates (sugars) in their leaves, seeds, roots etc (Forbes *et al*., 1992). Carbohydrates can be metabolized by almost all organisms. Carbohydrates are made up of common basic elements of carbon (C), hydrogen (H) and oxygen (O) and have an empirical formula of $(CH_2O)_n$ where n is $\geq$ 3. Thus, carbohydrates are organic compounds that are polyhydroxy aldehydes or polyhydroxy ketones or change to such substances on simple chemical transformations such as hydrolysis, reduction or oxidation. Classification of carbohydrates is done based on degree of polymerization of the CHO molecule or the number of saccharide units (Wade, 1999). Single polyhydroxy aldehyde or ketone containing carbohydrates are monosaccharides. Four or more carbon atoms together form monosaccharides which exists in cyclic form. Most common monosaccharide is glucose that can be metabolized during cellular respiration to provide energy. 2-10 monosaccharide units unite to form oligosaccharides. Two

monosaccharides unite to form di-saccharides, e.g., sucrose, that consists of a D-Glucose and D-Fructose. Polysaccharides are made by more than 20 monosaccharide units, e.g., cellulose, that is made up of several D-Glucose residues linked by β-(1,4) glycosidic bonds (Nelson, 2008). Cellulose is found abundantly in cell wall of plants. Carbohydrates are stored in the form of starch and glycogen in plants and animals, respectively. Carbohydrates play a great role in structural support and protection of plants and also act as a signalling molecule among several other functions.

1.1 Plant cell carbohydrates

The plant cell wall is a chemically complex structure composed of glycoproteins, aromatic compounds and carbohydrates namely, cellulose, hemicellulose and pectin (Mohnen *et al.*, 2008). Cellulose and hemicellulose are interwoven in a matrix of pectin shown in Fig. 1.1. Carbohydrate components make up to 90% of the primary cell wall which provides protection and structural support to the plant and are also involved in signalling functions. The secondary cell wall contains 10-30% hydrophobic polyphenyl propanoid lignin macromolecules and linear unsubstituted (or lightly substituted) polysaccharides such as cellulose and heteroxylans (Pettolino *et al.*, 2012). Lignin also contains hydroxycinnamyl alcohols (or monolignols), coniferyl alcohol and sinapyl alcohol, with minor amounts of *p*-coumaryl alcohol and it provides strength to cell wall and resistance from pathogenic attack (Boerjan *et al.*, 2003; Ralph *et al.*, 2004). Among all, cellulose is most abundant in plant cell wall. Cellulose is a collection of β-1,4-linked glucan chains that interact via hydrogen bonds to form crystalline microfibrils (Somerville, 2006). Cellulose can also exist in amorphous form (O'Sullivan, 1997). Cellulose aids in maintaining the structure as well as strength of the plant body. Other types of cellulosic polysaccharides like laminarin (β-1,3-linked glucose) and lichenan

(mixed 1,3-1,4-β-D-glucan) are other type of structural glucans (Scheller and Ulvskov, 2010).

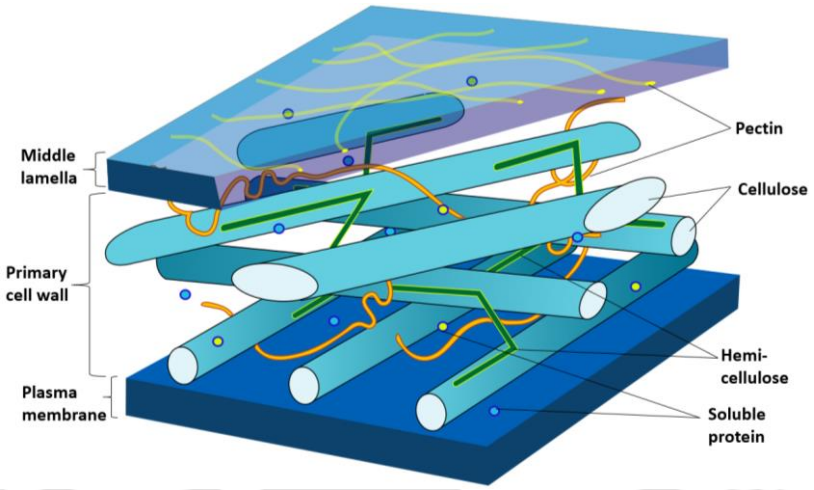

Fig. 1.1 Schematic representation of association between cellulose, hemicellulose and pectin in plant cell wall. (Image source: Wikimedia commons)

In addition to cellulose, plant cell wall contains two categories of heteropolymer matrix polysaccharides *viz.*, hemicellulose and pectin. Hemicelluloses are hetero-polysaccharides that include xyloglucans, arabinoxylans, arabinogalactans, mannans, xylans and mixed-linkage glucans. Among them the most common hemicelluloses are xylan and mannan (Schadel *et al.*, 2009; Keegstra, 2010). Xylan is made of β-1-4 linked xylopyranose residues. Xylan may also contain α-L arabinofuranosyl (arabinoxylan), β-D-glucucopyranosyl uronic acid (β-D-GlcpA) or α-(1→2)-linked 4-O-methyl-D-glucucopyranosyl uronic acid (glucuroxylans) and arabinofuranose and uronic acid (glucuronoarabinoxylan) residues as side chains. Xylan also are decorated by acetyl groups at the O-2 or O-3 position (Scheller and Ulvskov, 2010). Mannans are homo-polymers and contain β-1,4-linked D-mannopyranose and based on the substitutions mannan can be categorised into: **i)** Glucomannan composed of a backbone of β-1,4-linked D-mannopyranosyl residues with randomly distributed β-D-glucose residues in 3:1 ratio (mannose: glucose), **ii)** Galactomannan composed of a backbone of β-1,4-

linked D-mannopyranosyl residues that is substituted with side chains of single α-1,6-linked D-galactopyranosyl residues and **iii)** Galactoglucomannan composed of a backbone of β-1,4-linked D-mannopyranosyl residues and randomly distributed β-D glucose residues linked to mannose residue by β-1,4-linkage and the D-glucose residues are substituted with α-1,6-linked D-galactose residues (Petkowicz *et al.,* 2001, Moreira, 2008). Xyloglucans are composed of β-(1,4) glucose backbone, substituted with α-(1,6)-D-xylose side chains and arabinogalactans consists of β-(1,5) or β-(1,6) linked galactan backbone, substituted with α-(1,3) or α-(1,5) linked L-arabinofuranosyl residues (Bhamidi *et al.,* 2008; Brennan and Harris, 2010). Arabinogalactans are found in plasma membrane and cell wall of plants that play an important role in recognition and signalling events at the cell surface (Ellis *et al*., 2010). Arabinoxylan consists a backbone of β-(1,4) linked D-xylopyranosyl substituted with one or more α-L arabinofuranosyl residues at positions O-2 and O-3 (Cosgrove, 1999).

1.2 Structural components of pectin

Pectin is structurally the most complex polysaccharide constituent of plant cell wall which is found abundantly in primary cell wall and middle lamella (Fig. 1.2) (Caffall and Mohnen, 2009). It plays the most dominant role in holding the cell wall structure together. It is characterized by the presence of monomeric units galactopyranosyluronic acid (*GalpA*) residues (Fig. 1.3A) comprising as much as 30% of dicots, gymnosperms and non-Poales monocot walls (Ridley *et al.,* 2001). Pectin can occur as calcium and magnesium pectate and they can also form salt bridges with Mg^{2+} and Ca^{2+} ions to form insoluble gels (Fig. 1.3B) (Kohn, 1975).

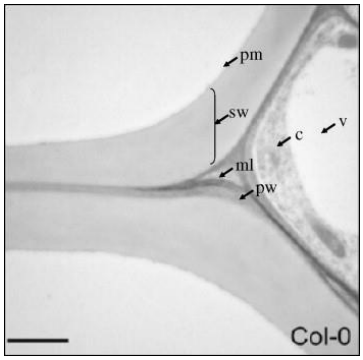

Fig. 1.2 Transmission electron micrograph of WT Arabidopsis thaliana Columbia-O transverse root section showing the clearly delineated middle lamella (ml), primary wall (pw) that is often filled with pectin rich polysaccharide. Additional labeled features of the cell are the secondary wall (sw), plasma membrane (pm), cytosol (c) and vacuole (v). Bar = 2 µM. (Persson *et al*., 2007)

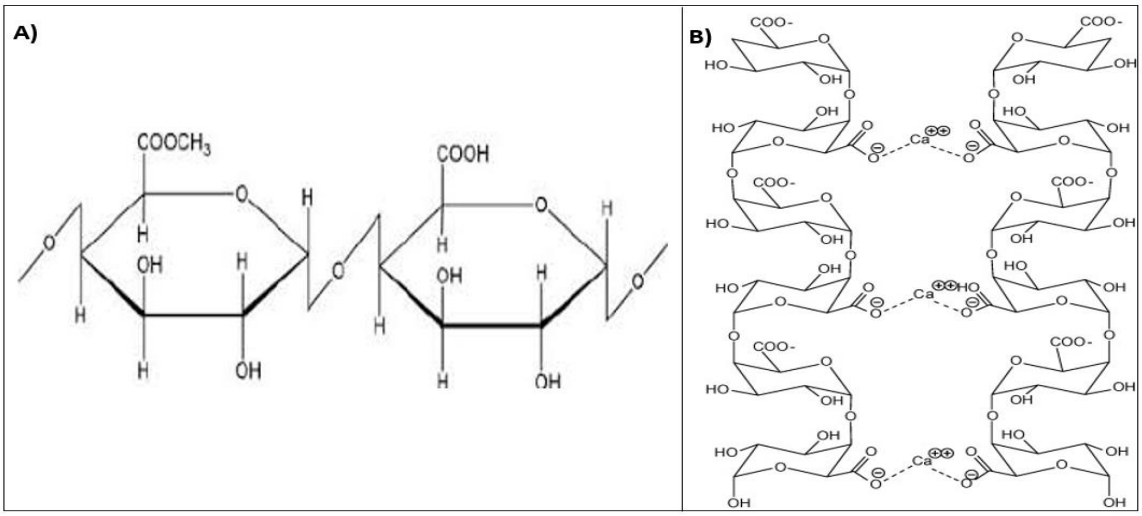

Fig. 1.3 A) Galactopyranosyluronic acid, the monomeric unit of pectin (Akash *et al*., 2015)
B) Salt bridges formed by calcium ions in pectate (Caffall and Mohnen, 2009)

The pectin network also interacts with cellulose and hemicellulose network and other cell wall proteins like extensin and arabinogalactan protein (AGP), covalently and also non-covalently through the ester linkages and hydrogen bonds (Broxterman and Schols, 2018). The complex structure of pectic polysaccharide and their presence is reasonably higher in proportion in dry matter of plant cell wall. The presence of cell wall-based pectin modifying enzymes governs its biological role in morphology, growth, and

development of plants. Pectin has a prevalent role in plant growth and development, defence mechanism, cell-cell adhesion, providing structural stability to the cell wall, regulation of cell permeability and fruit development (Ridley *et al*., 2001). Structural classes of pectic polysaccharides include homogalacturonan (HG), rhamnogalacturonan I (RG I) and rhamnogalacturonan II (RG II) substituted galacturonan like, xylogalacturonan and apiogalacturonan (Caffall and Mohnen, 2009).

1.2.1 Homogalacturonan

Homogalacturonan (HG) comprises of 60% of pectin in plant cell wall and is made up of α-1,4-linked-D- galactopyranosyluronic acid (Fig. 1.4) (Ridley *et al*., 2001). HG is referred as the smooth region of pectin (Schols and Voragen, 1996). The *GalpA* residues in HG may be methyl-esterified at C-6 position and acetyl esterified at the O-2 and O-3 positions (Voragen *et al*., 2009). Highly methyl-esterified pectin molecules are synthesized in the Golgi apparatus and secreted into the plant cell wall where they are subjected to modifications (Ridley *et al*., 2001). The pattern as well as degree of methyl esterification and acetylation depends upon the source as well as the developmental stage and the location of the cell wall. The co-ordination of more than 10 consecutive non-methyl esterified *GalpA* residues of HG that are negatively charged. These negatively charged *GalpA* residues can interact with divalent ions like magnesium and calcium forming salt bridges that can maintain cell wall integrity by providing mechanical strength and cell wall matrix porosity (Caffall and Mohnen, 2009). These interactions affect the cell wall rigidity. The secondary structure of HG chain can exist in four-fold helix (4_1, right-handed), three-fold helix (3_1, right-handed) and (3_2, left-handed) and two-fold helix (2_1) of which the 3_1 helix is most common having three *GalpA* residues per turn (Zdunek *et al*., 2021). HG interaction with divalent ions like magnesium and calcium forms salt bridges that can maintain cell wall

integrity by providing mechanical strength and cell wall matrix porosity (Somerville et al., 2004). HG is abundant in the primary cell wall and particularly dense in the middle lamella of potato (*Solanum tuberosum*) (Bush *et al*., 2001) and sugar-beet pulp (Kobayashi *et al.,* 1993).

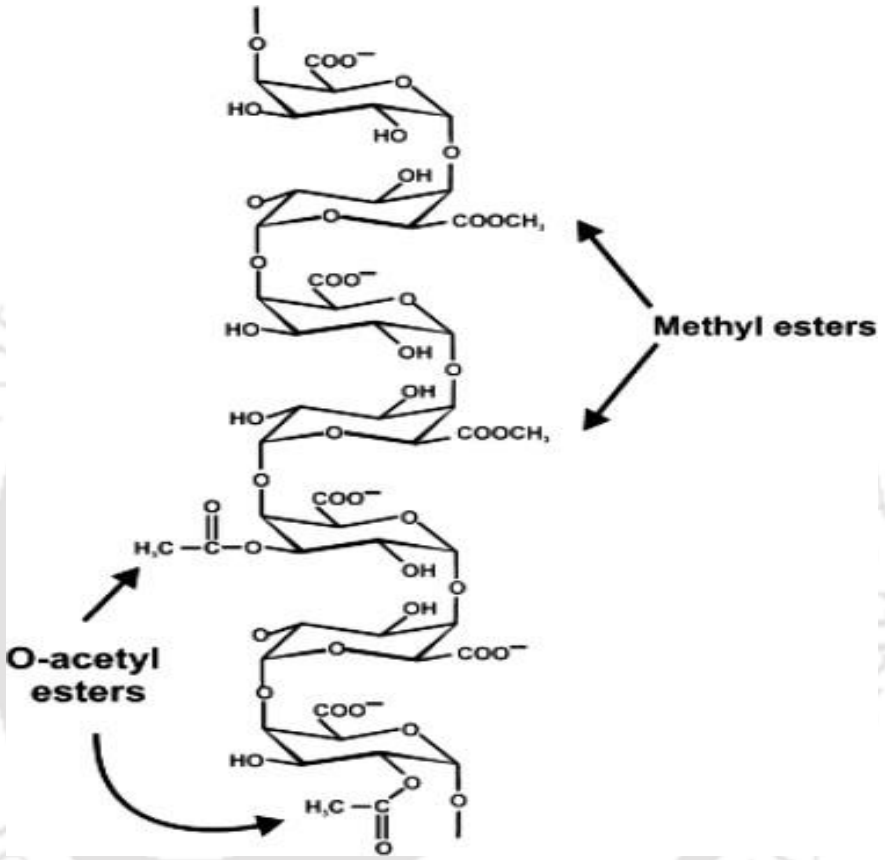

Fig. 1.4 A repeating segment of homogalacturonan and functional groups. Representative sites of methyl esterification at the C-6 and O-acetylation at the O-2 or O-3 of the carbohydrate ring are shown (Ridley *et al.*, 2001).

1.2.2 Rhamnogalacturonan I

Rhamnogalacturonan I (RG I) comprises 20-35% of total pectin and is a highly variable family of polysaccharides (Albersheim *et al*., 1996). RG I is a repeating of monomeric unit [→4)-α-D-*GalpA*-(1→2)-α-L-rhamnopyranosyl (*Rhap*)-(1→] (O'Neill *et al.,* 1996). The *GalpA* residues and *Rhap* residues alternate with each other in the main chain (Mohnen *et al*., 2008). The other major feature of RG-I chains are large substituted side chains. The *GalpA* residues may be C-6 methylated and acetylated

at O-2 or O-3 positions, while 20-80% *Rhap* residues are substituted at C-4 with linear or branched chains of α-L-arabinofuranosyl (*Araf*), β-D-galactopyranosyl (*Galp*) residues and their relative proportion and chain lengths may differ depending on plant source (Fig. 1.5) (O'Neill *et al*., 1996). Other side chains are also present and are generally shorter. It includes α-1, 5-linked L-arabinan that may be substituted with α-1, 2- and α-1, 3-linked arabinose or arabinan branching, β-1, 4-linked D-galactans that may be substituted with O3-linked L-arabinose or arabinan branching and β-1, 3-linked D galactan may be substituted with β-6-linked galactan or arabinogalactan branching. Due to the presence of all these side chains RG I forms a complex structure and is known as the hairy region of pectin (Nakamura *et al*., 2002, O'Neill and York, 2003).

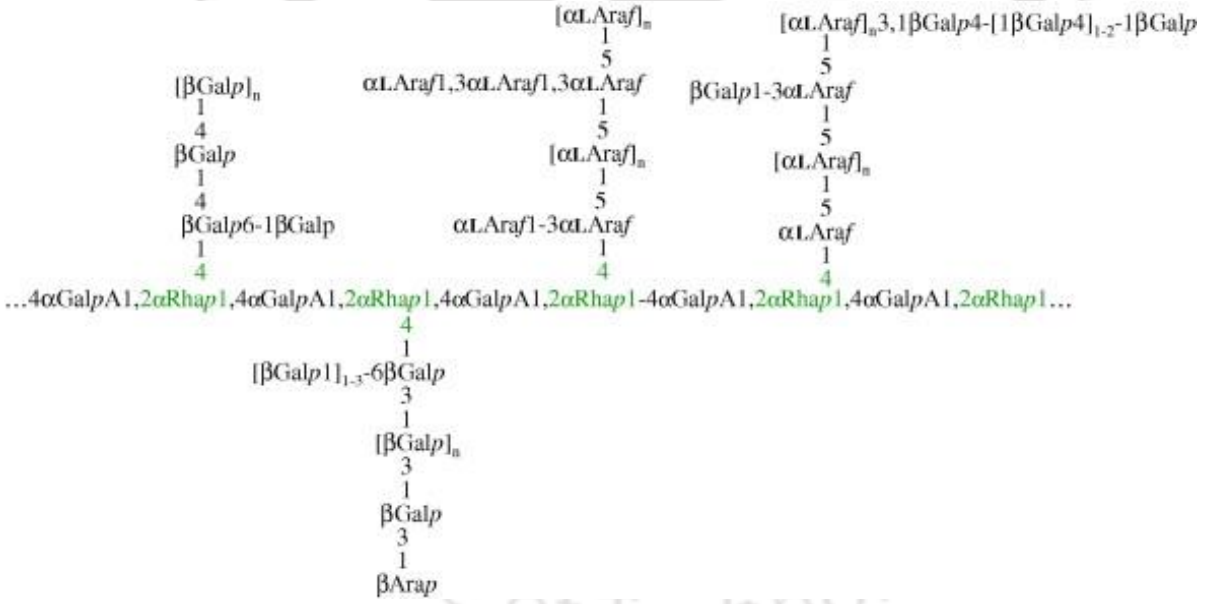

Fig. 1.5 The structure of RG-I backbone and representative side chains (O'Neill and York, 2003).

1.2.3 Rhamnogalacturonan II

Rhamnogalacturonan II are substituted galacturonans that are a diverse group of polysaccharides constituting 2-10% of total pectin. It is composite but structurally most conserved group of pectin found in nature (Mohnen *et al.*, 2008). It is recognized by the presence of a stretch of approximately seven to nine residues long

HG backbone as a repeating unit of 1, 4-linked α-D-*GalpA* residues with four well-defined side chains designated as chain A, B, C and D (Fig. 1.6) (O'Neill *et al*., 1990). Side chain A and B are octasaccharide and nonasaccharide respectively, linked to the HG backbone via β-D apiofuranosyl (*Apif*) at O-2 position and side chain C and D are chemically a disaccharide linked to the O-3 position (Chandrayan *et al*., 2018). RG-II has 12 different types of glycosyl residues in more than 20 linkages. It includes rare sugars species like 2-O-methyl xylose, 2-O-methyl fucose, aceric acid, 2-keto-3-deoxy-d-lyxo heptulosaric acid (Dha) and 2-keto-3-deoxy-d-manno octulosonic acid (Kdo) (Caffall and Mohnen, 2009). Due to the branched structure of RG II, it is also known as the hairy region of pectin. RG-II interacts covalently with HG and RG-I to build a complex macromolecular pectin network (Matsunaga *et al*., 2004). RG II is also associated with borate ion. Borate ion helps in dimerization of two RG II molecules that play a critical role in strength of the plant cell and has a specialized role in meristematic and reproductive system of plants (Caffall and Mohnen, 2009).

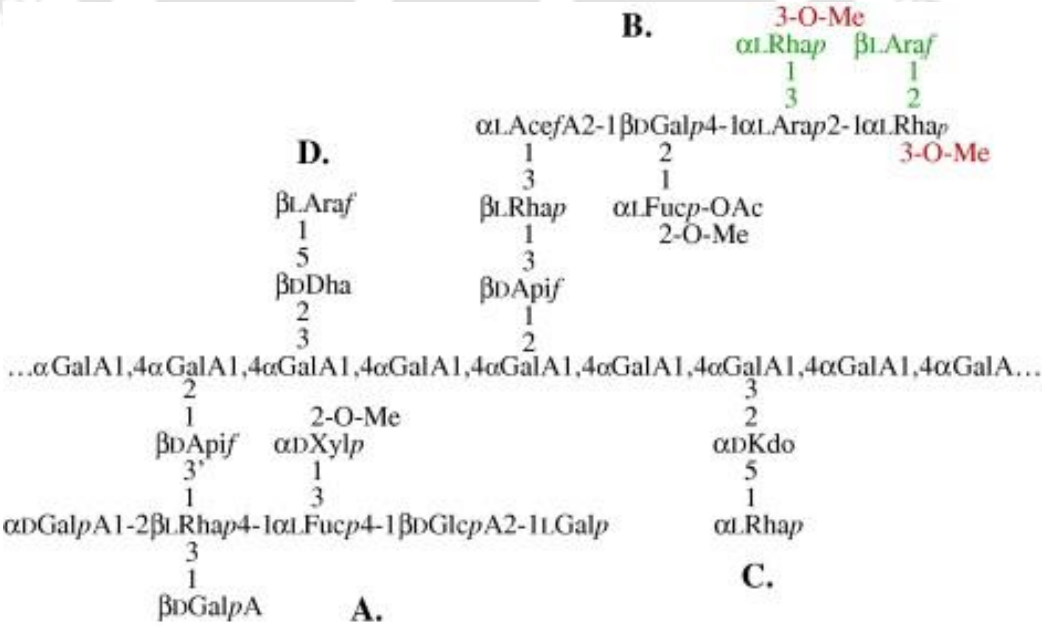

Fig. 1.6 The structure of rhamnogalacturonan II (RG II) or substituted galacturonan (O'Neill *et al*., 2003).

1.2.4 Substituted galacturonans

The other substituted galacturonan is xylogalacturonan (XGA). Based on different sources XGA is characterized by 1,4- or 1,3- or 1,2-linked β-D xylose substitution at O-3 position of the main chain *GalpA* residues (Zandleven *et al*., 2006). XGA may also consist of methyl esterification at O-6 position of *GalpA* backbone together with independent xylose substitutions. AGA characterized by apiose and 3′-linked apibiose at the O-2 position of *GalpA* backbone residues (Caffall and Mohnen, 2009). Due to these substitutions, both XGA and AGA are also considered to be the hairy regions of pectin (Zdunek *et al.*, 2021).

1.3 Biosynthesis of pectin wall polymers

Histochemical analysis of plant cells and various experimental analyses have elucidated that the synthesis of pectic polysaccharides occurs in the cis-Golgi in methylated form and then they move to the cell wall in demethylated form (Wang *et al*., 2020). Epitopes of pectic polysaccharides HG/RG I localized within the cisternae of Golgi suggested that this organelle has the specific location for pectin biosynthetic machinery (Anderson, 2019). Around 65 enzymes activities, including glycosyl transferases, acetyl transferases and methyl transferases are required for the complex structure of pectin (Anderson, 2016). One of the most extensively studied enzymes among these, is galacturonosyltranferase1 (GAUT1) that helps in the formation of the polygalacturonic main chain of pectin by catalysing the transfer of *GalpA* to oligo-*GalpA* acceptor from uridine 5’-diphosphogaluronic acid (UDP-GalA). The macromolecular structural arrangement of pectin constituents into a complex network is still a subject of debate. Available evidences and a few proposed models show that HG, RG I and RG II are linked covalently to one another via their backbone, but the arrangement or position of HG, RG I and RG II chains are yet a matter of research

(Coenen *et al*., 2007). Out of these models, one model suggested that HG chain is associated as a long side chain of RG I next to galactan and arabinan side chains (Vincken *et al*., 2003), while another conventional model suggested that HG, RG I and RG II chains alternate with each other (Willats *et al*., 2006). Yet another model suggested that the structural arrangement of two HG chains alternate with each other with RG I in the core (Yapo, 2011). Earlier studies showed that pectin network integrates with the cellulose or hemicellulose network in a gel-like matrix in PCW, but recent studies carried out using nano image technology showed that pectin exists as filaments known as HG nanofilaments in the PCW (Haas *et al*., 2020). Available evidences also showed that HG, RG I and RG II are linked covalently to each other via their backbone and is also covalently cross linked to xylan and xyloglucan. Xyloglucan on the other hand forms a network with cellulose. Thus, a complex network of pectin, hemicellulose and cellulose provide a complex wall network (Nakamura *et al*., 2002).

1.4 Degree of esterification

Depending on the type of source the structure of pectin varies and; therefore, it is difficult to determine its complexity. Pectin is mainly composed of esterified D-galacturonates linked by α-1,4-glycosidic bond. It also consists of some non-sugar substituents like methanol, acetic acid, phenolic acids and occasionally amide groups. For instance, *GalpA* residues are methyl esterified at C-6 position and acetyl esterified at O-2 and O-3 positions. The degree of methylation (DM) and the degree of acetylation (DAc) are defined as the number of moles of methanol or acetic acid per 100 moles of *GalpA* residues (Morris *et al*., 2010). Degree of esterification (DE) determines the physical properties and industrial quality of pectin and are classified into two broad categories: High methoxy (HM) and Low methoxy (LM) pectin. HM pectin has greater than 50% DE and LM pectin has less than 50% DE (Chandrayan, 2018). HM pectin are

generally hot water soluble and requires minimum amount of soluble solid such as sugar and an acidic pH of 3.0 to form gels. Sugar helps in creating low solubility environment for HM pectin leading to formation of gel by hydrogen bonding between free carboxyl groups on the pectin molecules and between the hydroxyl groups of neighbouring molecules of the solvent at equilibrium condition (May, 1990; Fishman *et al*., 2007). On the other hand, LM pectin need the presence of a controlled amount of calcium or other divalent ions for gelation (May, 1990). Likewise, DAc also effects the gelation of pectin. Acetyl groups are generally found in HG as well as the RG regions of pectin. The HG region of apple and other citrus fruits have very low levels of acetylation but higher level of acetylation is found in HG region of sugar beet and RG region of potato. Presence of acetyl groups negatively effects the gelling property of pectin (Chandrayan, 2018). The degree of methylation in native pectin is generally in the order of DM ≈ 70–80, whereas degree of acetylation is generally much lower e.g., DAc ≈ 35 for sugar beet pectin (Morris *et al.,* 2010). Based on degree of esterification, pectin can be used for various industrial applications like preparing of jam, jellies, fruit preservatives and processing of fruit juices *etc.* (May, 1990).

1.5 Applications of pectin

Pectin is found abundantly in primary cell wall and middle lamella of plants and plays a significant role in cell-cell adhesion, cell signalling, wall porosity, pollen tube growth, fruit development and leaf abscission (Ridley *et al*., 2001). It also promotes upright growth of the plants (Matsunaga *et al*., 2004). Pectin has the gelling property and is used in preparation of jam and jellies. It is also used as a low-calorie food as a fat and/or sugar replacer. Pectin is also used as a frozen barrier and preparation of beverages, confectionery products and barbeque sauces. Pharmaceutical uses of pectin include reduction of blood cholesterol level, prophylactic substance against toxic

cations, removal of heavy metals from gastrointestinal tract and respiratory organs, inhibition of colon cancer cells, as an anti-coagulant and a potential bio-polymer for drug delivery system. Other industrial applications of pectic include use in emulsion stabilizer for water and oil emulsions, production of biodegradable films, sizing agent for paper and textiles and membranes for ultracentrifugation and electrodialysis (Thakur *et al*., 1997).

1.6 Carbohydrate active enzymes

Almost all living organism on earth utilizes carbohydrates as the major source of energy. To metabolize carbohydrate in the living system a variety of carbohydrate active enzymes are involved that catalyse the breakdown, biosynthesis or modification of carbohydrates or glycoconjugates (www.cazy.org). The Carbohydrate Active Enzyme (CAZy) database provides online and continuously updated access to carbohydrate enzymes based on sequence-based family classification, linking the sequence to its specificity and 3- dimensional structure (Lombard *et al.*, 2014). Different classes of carbohydrate active enzymes as mentioned in CAZy database are: i) Glycoside Hydrolases (GHs), ii) Glycosyl Transferases (GTs), iii) Polysaccharide Lyases (PLs) and iv) Carbohydrate Esterases (CEs). The GHs family of enzymes catalyses the hydrolysis and/or rearrangement of glycosidic bonds. GTs are involved in formation or biosynthesis of glycosidic bonds whereas PLs catalyse non-hydrolytic cleavage of glycosidic bonds using a β-elimination mechanism. Apart from these four classes it also consists of a class of enzymes with Auxiliary Activities (AAs). AAs enzymes are grouped in to ligninolytic enzymes, which degrade lignin and the lytic polysaccharide mono-oxygenase that cleaves the mono-oxygen bond from the polysaccharide. As of August 2024, there are 189 families of GHs, 137 families of GTs, 43 families of PLs, 20 families of CEs and 17 families of AAs. CE10 has been removed

from 20 families of CE as most of the members in this family are not active on carbohydrate substrates (Lombard *et al*., 2010). The carbohydrate active enzymes often display a modular form and remains appended as a non- catalytic module known as Carbohydrate Binding Modules (CBMs). CBMs are contiguous amino acid sequence linked to the catalytic module with a linker within a carbohydrate active enzyme with a discreet fold having carbohydrate binding activity (Fig. 1.7) (Taylor *et al*., 2012). There are 97 families of CBMs. For complete utilisation, the complex interaction between the cell wall polysaccharides can be broken down by synergistic action of cellulases, hemicellulases and pectinases. Pectinases and hemicellulases can remove their respective polysaccharide cover, giving an easy access to cellulases for further saccharification and bio-fermentation (Thite and Nerurkar, 2020).

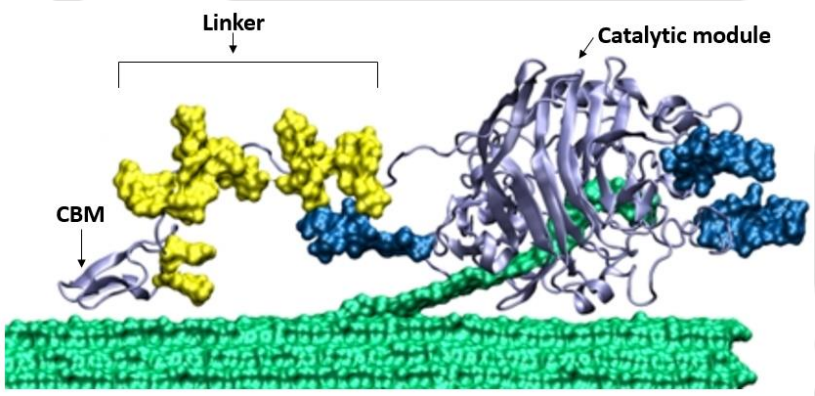

Fig. 1.7 Schematic representation of a modular carbohydrate active enzyme possessing a carbohydrate-binding molecule (CBM) connected to the catalytic domain (CD) via a linker peptide (Adapted from Taylor *et al.*, 2012).

1.7 Pectin degrading enzymes

1.7.1 Different types of pectinolytic enzymes and their applications

Pectinases or pectinolytic enzymes hydrolyses the pectic substances and are most widely distributed in bacteria, fungi and plants. Pectinases break down complex pectin to simple D-galacturonic acids. According to the type of linkages in pectin there

are two categories of pectin degrading enzymes: de-esterifying and de-polymerizing (Hugouvieux-Cotte-Pattat *et al.*, 2014). De-esterifying enzymes belong to the enzyme class carbohydrate esterase. De-polymerizing enzymes like hydrolases and lyases belong to the enzyme classes Glycoside Hydrolase (GH) and Polysaccharide Lyase (PL), respectively (Sathyanarayana and Panda, 2003) (Fig 1.8). GH and PL family enzymes are categorized as endo- (random mode) or exo- (terminal) based on modes of action. The importance of pectinases in the market is growing with its various applications in biotechnological sectors and food processing industries (Fig 1.10). Different types of pectinases have been described in subsequent subsections and key enzymes are listed in Table 1.1.

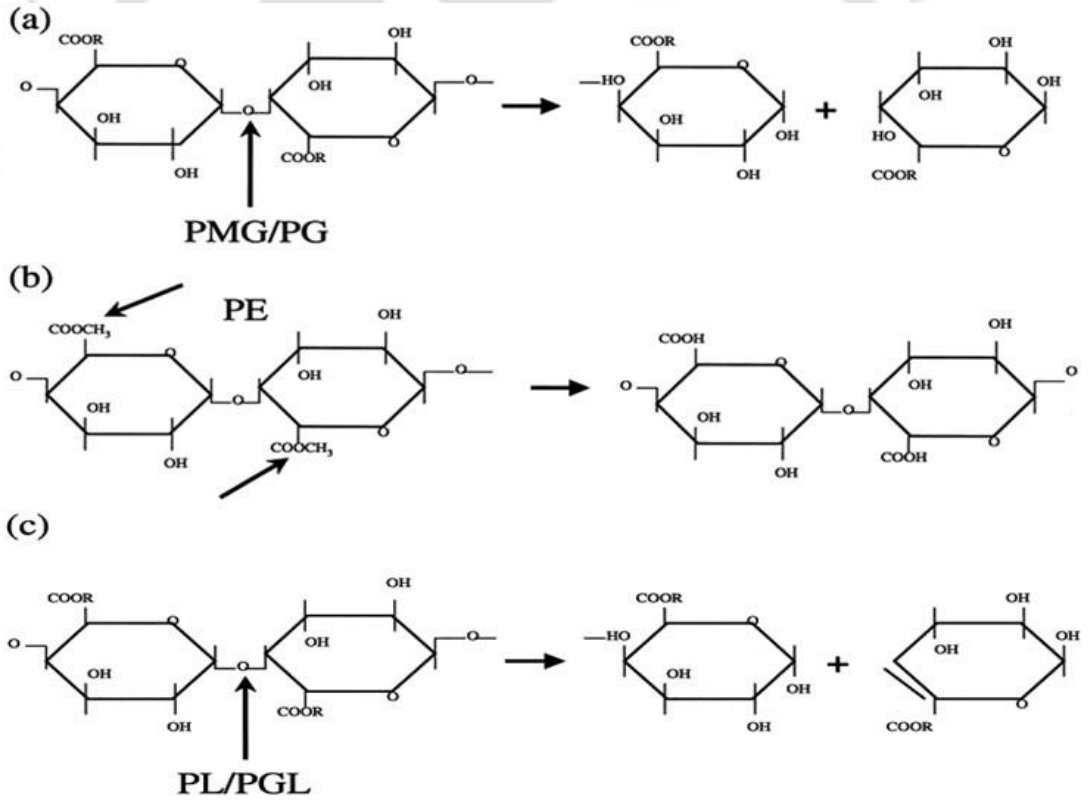

Fig. 1.8 Mode of action of pectinases: (a) R = H for PG and CH_3 for PMG; (b) PE; and (c) R = H for PGL and CH_3 for PL. The arrow indicates the place where the pectinase attacks with the pectic substrates. (PMG: polymethyl galacturonases; PG: polygalacturonases; PE: pectin esterase; PL: pectin lyase; PGL: pectate lyase) (Adapted from Sathyanarayana and Panda, 2003).

1.7.2 Protopectinases

Protopectinase or pectinosinase (EC 3.2.1.99) hydrolyses the protopectin (pectic layer present in PCW close to the cellulose layer that is insoluble in water) and liberates highly polymerized soluble pectin by heterogeneous catalysis (Zapata-Zapata *et al*., 2017). Protopectinases are of two types: i) A type protopectinases belongs to family 28 of GH (http://www.cazy.org) and reacts with the partially methyl-esterified smooth region of protopectin (Zhang *et al*., 2018a) and ii) B type protopectinase belongs to family 43 of GH and reacts with the hairy region of protopectin (Lang *et al*., 2016). Microbial protopectinase is well characterized in different fungi and bacteria with optimal activity within the pH range (3.0–6.1) and temperature 30–40 ºC (Lang *et al*., 2016; Zapata-Zapata *et al*., 2017; Vasco-Correa and Zapata, 2017; Zhang *et al*., 2018a). Use of protopectinases is the most emerged, convenient and eco-friendly strategy to extract pectin from various sources. This green strategy leads to the extraction of pectin without its degradation or producing effluents, which are encountered, while extraction by conventional physical and chemical treatment methods (Patel *et al*., 2022).

1.7.3 Polygalacturonases

Polygalacturonase (PG) catalyses the hydrolytic cleavage of α- (1,4)-glycosidic linkages of polygalacturonic acid chain with the involvement of water across the oxygen bridge, resulting in oligogalacturonides (Karahalil *et al*., 2017). PG belongs to family 28 of GHs. PGs possess a parallel beta-sheet helical structure with aspartic acid present in the catalytic site act as a proton donor (Poondla *et al*., 2017). Depending on the site of cleavage PG are classified into two types. Endo-PG (EC 3.2.1.15) cleaves α-(1,4)-glycosidic linkages of polygalacturonic acid randomly and exo-PG (EC 3.2.1.67) cleaves the glycosidic bond terminally from non-reducing end producing

monogalacturonates (Anand *et al*., 2016). Another class of exo-PG (EC 3.2.1.82) cleaves the penultimate bond from non-reducing end of polygalacturonic acid producing digalacturonates (Anand *et al*., 2017). The optimum activity is in acidic pH range (3.0–6.0) for most of characterized fungal PGs. Acidic PGs are used in clarification of fruit juices like orange, mango, apple and peach where it increases the transmittance of the extracted juice by reducing the colloid formation and viscosity (Anand *et al*., 2017; Amin *et al*., 2020; Ázar *et al*., 2020). PGs with alkaline pH are mostly from bacterial sources and can be used potentially instead of harsh alkali treatments in retting fibres and textile industries by biological depolymerization of the pectic content of gum (Rahman *et al*., 2019). An alkaline PG from a fungal source, *Aspergillus fumigatus* was first reported with application in retting fibres (Anand *et al*., 2016). Most of the PGs from both fungal and bacterial sources show maximum activity in the temperature range, 30–60 ºC. PG activity was found to double by the addition of aluminium oxide (Al_2O_3) microparticles in the medium before inoculation of wild-type *Aspergillus sojae* (Karahalil *et al*., 2017). Similarly, UV light and acridine orange induced mutants of *Bacillus* strain displayed an enhanced exo-PG production and the enzyme activity was increased by 3-fold than wild-type (Muzzamal and Latif, 2016). The optimization of charge-charge interaction of an endo-PG by creating single and double mutants of *Achaetomium* sp. strain Xz8 was reported to have enhanced thermostability of the enzyme, retaining its catalytic activity and structure stability (Tu *et al*., 2015). Thermostable PGs together with cellulases are required for lignocellulosic biomass degradation and have applications in biorefinery for production of biofuel (Ibrahim *et al*., 2021). A purified PG from Mucor circinelloides was also shown to increases the phenolic content in tea leaves during fermentation that increases the quality of tea (Thakur and Gupta, 2012). Furthermore, PGs also find application in

increasing the juice yield when extracted through maceration (Bezus *et al*., 2022), increasing the extraction efficiency of olive oil (Arpana *et al*., 2023), producing pectin oligosaccharides from mango peel with anti-bacterial properties against food pathogens (Long *et al*., 2022) and increasing the bio-accessibility of natural pigment carotenoid from peach and carrot juice promoting many health benefits (Liu *et al*., 2023).

1.7.4 Polymethylgalacturonases

Polymethylgalacturonase (PMG) (EC 3.2.1.41) catalyses the hydrolysis of α-(1,4)-glycosidic bonds of *GalpA* backbone, where at least 75% of the carboxyl groups are esterified with methyl group yielding 6-methyl-D-galacturonate. The optimum pH and temperature for PMG activity is 5.0–6.0 and 30 – 60 ºC, respectively (Karbalaei-Heidari and Rastegari, 2014; Chaurasia *et al*., 2015; Kaur *et al*., 2019). PMG breaks pectin by β-elimination. Like PGs, PMGs are also termed as exo- or endo-enzymes based on the pattern of their action i.e., terminal or random, respectively. PMG belongs to family 28 of Glycoside hydrolases (http://www.cazy.org/GH28.html). PMGs are used in juice and wine clarification, fibre preparation from jute, hemp and linen and also in oil, pigment and flavour extraction from plant materials (Chaurasia *et al*., 2015) and degradation of lignocellulosic wastes for production of biofuels (Gunjal *et al*., 2020).

1.7.5 Pectin methyl esterase

Pectin methyl esterase (PME) belongs to family 8 of carbohydrate esterases (CE) (http://www.cazy.org/CE8.html). PME (EC 3.1.1.11) catalyses the de-esterification of methyl ester linkages in the polygalacturonate chain and releases acidic pectin and methanol (Patidar *et al*., 2016). PME is an accessory enzyme which removes the methoxyl groups from the side chains of pectin backbone making it available for degradation by other de-polymerizing enzymes like hydrolases and lyases (Rajulapati

and Goyal, 2017). PME possesses a right-handed parallel beta-helical structure with Asp-Asp-Arg triad in the catalytic pocket (Rajulapati *et al*., 2018). The optimal temperature for both fungal and bacterial PMEs ranges between 45-50 ºC. The acidic PMEs are mostly found in fungal source with optimal pH ranging between 3.5-5.0 (Patidar *et al*., 2016; Zhang *et al*., 2018b; Zhong *et al*., 2021) and alkaline PMEs (pH 8.0) are generally from bacterial source (Rajulapati and Goyal, 2017). One of the PMEs was reported from the gut microbe *Bacteroides thetaiotaomicron* (BT1017) that displayed no sequence identity with CE8 family and also possessed an α/β fold with Asp-His-Ser as the catalytic triad which was unlike the typical beta-helical structure of PMEs (Duan *et al*., 2020). The methyl esterification activity of this enzyme on RG II domain shows that this is the first PME with no evolutionary link with CE8 family and represents a new family of PME. PMEs are widely used in food processing industries like clarification of juices, increasing the firmness of fruits (Patidar *et al*., 2016; Zhang *et al*., 2018b), formation of jam and jellies in a wide range of pH (Kim *et al*., 2016). PME treatment also increases the aroma release (Kim *et al*., 2016) and in textile industries alkaline PME together with pectate lyase can be used in degumming of fibres and bio scouring of cotton (Rajulapati *et al*., 2020). Pectin with lower degree of methylation help polygalacturonases in delivering higher amount of reduced sugar like galactose and arabinose. MTT assays showed that pectin hydrolysates with low methyl esterification produce more galactose content in pectin hydrolysates that have anti-cancer activity and can inhibit HT-29 colon cancer cells and therefore PMEs can also be potentially used in pharmaceutical industries (Ma *et al*., 2018). However, some other studies reported that highly methylated pectic oligosaccharides like 77% methylation in *Citrus limetta* (Chakraborty et al., 2018) and 68% methylation in *Citrus reticulata* (Rajulapati et al., 2021) caused higher inhibition of HT-29 colon cancer cells as

compared with the non-methylated pectic oligosaccharides. Further, hydrogel beads made from demethylation of methylated pectic oligosaccharides by pectin methyl esterase were demonstrated as sustainable drug delivery material at gastric simulated pH 1.2 and intestinal pH 7.4 for colon-targeted drug delivery (Jung *et al*., 2013). They showed that PME treatment of high methoxy pectin was found to create uniform charge distribution that could form hydrogel beads by ionic interaction with Ca^{2+} ions compared to commercial low methoxy pectin. These PME treated hydrogel beads resulted in better drug entrapment efficiency and drug release. PMEs also find wide applications in removal of methanol from fruit derived alcoholic beverages and biomass exploitation by removing recalcitrance of plant cell wall (Kumar *et al*., 2023).

1.7.6 Pectin/rhamnogalacturonan acetyl esterase

Pectin acetyl esterase (PAE) (EC 3.1.1.6) and rhamnogalacturonan acetyl esterase (RGAE) (3.1.1.86) catalyse the cleaving reaction of acetyl groups in presence of water from O-2 and O-3 positions of galactopyranosyluronic acid of homogalacturonan and rhamnogalacturonan regions of pectin, respectively, producing polygalacturonate and ethanol (Remoroza *et al*., 2014; Ding *et al*., 2019). Bacterial and fungal PAEs belong to CE12 family while plant PAEs belong to CE13 family. CE16 consists of fungal PAEs exclusively (Urbániková, 2021). RGAEs belong to CE12 family. Both PAEs and RGAEs from CE family 12, 13 and 16 possesses an α/β hydrolase fold which was deduced from the crystal structure of an RGAE from *Aspergillus aculeatus* with a different fold from the α/β fold found in GHs (Mølgaard *et al*., 2000). PAEs and RGAEs belong to new SGNH (Serine-Glycine-Asparagine-Histidine) hydrolase superfamily where they lack the nucleophilic elbow as found in the α/β fold of GHs. The catalytic pocket consists of Ser-His-Asp catalytic triad where serine acts a nucleophile. An RGAE (BhRGAE) of CE12 family from *Bacillus*

halodurans was found to have a different fold than the common α/β hydrolase fold possessed by the members of the new SGNH hydrolase superfamily (Navarro-Fernández *et al*., 2008). BLAST analysis of amino acid sequence of BhRGAE revealed that BhRGAE comprised of two domains. The first 135 residues of the protein were similar to the fibronectin type III domain (FnIII) with an immunoglobulin-like β sandwich fold and the rest were similar to RGAE from *Aspergillus aculeatus* representing an α/β/α fold. The later domain contained the catalytic triad (Ser-His-Asp) as present in RGAE. BhRGAE could act in synergy with a xylanase enzyme in deacetylation of acetylated xylan. Acetylation present in the *GalpA* main-chain creates stearic hindrance for hydrolysis action by other pectinases. PAE and RGAE removes this obstacle from acetylated pectin and aids in main chain degradation by PMEs and other de-polymerizing enzymes like lyases and galacturonases (Gama *et al*., 2017). The optimal pH and temperature for both PAEs and RGAEs vary between 7.0-9.0 and 35–50 ºC, respectively. PAEs (PaeY and PaeX) with specific activity towards only the smooth region of pectin i.e., HG, was first isolated and purified from *Erwinia chrysanthemi* 3937 (Shevchik and Hugouvieux-Cotte-Pattat, 1997; Shevchik and Hugouvieux-Cotte-Pattat, 2003). PaeY and PaeX showed increase in specific activity by several folds when acting in synergy with PME and pectate lyase. While another PAE from *Bacillus licheniformis* showed regioselectivity for only O-3 linked acetyl ester groups in HG chain (Remoroza *et al*., 2014). Pectin with higher degree of acetylation is found in sugar beet pulp (about 23–30%) (Shevchik and Hugouvieux-Cotte-Pattat, 1997; Remoroza *et al*., 2014) and okra pod (about 52.2%) (Alba *et al*., 2015). Due to high degree of acetylation present in sugar beet pulp, a polygalacturonase (VdPG2) from *Verticillium dahlia* was found to have low activity against sugar beet pectin as compared with other substrates with lower acetylation like polygalacturonic

acid (Safran *et al*., 2021). PAEs and RGAEs can be exploited to act in synergy with other pectinases and can be used in food industries for gelation (Oosterveld *et al*., 2000), anti-cancer activity (Ma *et al*., 2018) and in the production of biofuel and other value-added products from biomass (Leijdekkers *et al*., 2013; Xiao and Anderson, 2013). Treatment of pectic polysaccharide with high acetyl esterification like sugar beet pulp and okra pod pectin with PAE/RGAE and PME will lead to efficient de-esterification. A brief study on a pectin acetyl esterase on sugar beet pectin reported that enzymatic modification showed porous micro-sponge biomatrix that could be used as a drug delivery material (Savary *et al*., 2003). The enzyme has also been used industrially for the production of β-lactam antibiotics and paper bleaching purposes (Navarro-Fernández *et al*., 2008). Mutation study of the catalytic pocket residues in an RGAE from *Paenibacillus polymyxa* exhibited its cold-adaptation that could be used for the synthesis of cinnamyl acetate by transesterification reaction of cinnamyl alcohol and vinyl acetate (Tang *et al*., 2021).

1.7.7 Pectate lyase

Based on the pattern of action pectate lyase (PGL) are of two types: endo-pectate lyase (EC 4.2.2.2) and exo-pectate lyase (EC 4.2.2.9). PGL belongs to five different families of PLs i.e., PL1, PL2, PL3, PL9 and PL10 (http://www.cazy.org.PL.html). Substrate utilization of PGL is same as endo- and exo-polygalaturonans. PGL cleaves the carbon-oxygen bond of α-(1,4)-glycosidic linkages between low-esterified polygalacturonic acids (Bekli *et al*., 2019) but instead of yielding saturated oligogalacturonates, PGLs yield the same product having an unsaturated C4–C5 bond by β-trans elimination reaction mechanism. Endo-PGL cleaves their substrate randomly producing more than one unsaturated oligogalacturonates (Zhen *et al*., 2020), whereas exo-PGL (EC 4.2.2.9) cleaves their

substrate terminally producing unsaturated di-galacturonates (Wu *et al*., 2020b). Both endo- and exo-PGLs (PL1, PL3 and PL9) possess a right-handed parallel β-helical structure (Chakraborty *et al*., 2015) with a Ca^{2+} ion binding site that acts as a co-factor for its activity (Kudla *et al*., 2007). While a few endo- and exo-PGLs of PL2 family possesses a rare $(\alpha/\alpha)_7$-barrel fold (Abbott and Boraston, 2007) and PL10 family consisting exclusively of endo-PGLs possess an $(\alpha/\alpha)_3$-barrel fold with short β-strands (Novoa de Armas *et al*., 2004). PGL superfamily consists of a characteristic asparagine ladder and catalysis takes part by proton abstraction mechanism by catalytic residues lysine/arginine. PGLs are generally alkaline in nature and their optimum pH ranges between 8.0-10.5 (Zhou *et al*., 2017; Kamijo *et al*., 2019). Optimum temperature ranges from 30 ºC for cold-active PGL (Tang *et al*., 2019) to 70 ºC for thermostable PGL (Zhou *et al*., 2017). Protein engineering of a few pectate lyases by site-saturation mutagenesis was shown to enhance the thermostability of these enzymes (Liang *et al*., 2015; Zhou *et al*., 2015; Wang *et al*., 2018). The evolutionary strategy increased the half-life ($t_{1/2}$) and specific activity of these enzymes, which were later explored for efficient degumming of ramie fibres and bio-scouring of fabrics. The immobilization of PGL (PEL3) with inorganic compound (Cu^{2+} ions) increased its enzyme activity by 2.5-fold forming PEL3/$Cu_3(PO_4)_2 \cdot 5H_2O$ as hybrid nanoflowers (Wu *et al*., 2020a). PGLs have several industrial applications in food and textile industries. PGLs are used in lignocellulosic biomass degradation (Chen *et al*., 2018), textile treatment, bio-scouring of cotton (Chakraborty *et al*., 2017; Zhen *et al*., 2020; Sharma *et al*., 2022), degumming of fibres (Zhou *et al*., 2017; Xu *et al*., 2022) and clarification of juice (Bekli *et al*., 2019; Sheladiya *et al*., 2022). Pectic oligosaccharides (POS) like unsaturated di- and tri-galacturonates obtained by PGL degradation of *Citrus limetta* was shown to

efficiently inhibiting the growth of HT-29 colon-cancer cells by 53–77% (Chakraborty *et al*., 2018).

1.7.8 Pectin lyase

Pectin lyases (PNL) (EC 4.2.2.10) catalyses the breakdown of the α-1,4 glycosidic bond in highly esterified polygalacturonic acid. They have been classified under family 1 polysaccharide lyase (http://www.cazy.org/PL1.html). Unlike PGL, PNL requires highly methyl-esterified pectin and degrades pectic substrates randomly in endo mode, producing unsaturated methyl oligogalacturonates by β-elimination mechanism (Pedrolli and Carmona, 2014). PNLs possess a right-handed β-helical structure and catalysis occurs by proton abstraction by the catalytic arginine residue (Vitali *et al*., 1998). Most of the characterized PNLs are from fungal sources and are acidic in nature with optimum pH ranging between, 5.0–6.0 and are used in fruit-juice clarification (He *et al*., 2018, Liu *et al*., 2022). The optimum temperature of both fungal and bacterial PNLs range between 40 ºC and 50 ºC. Alkaline PNLs are used in retting of fibres (Yadav *et al*., 2017). PNLs are used in extracting cellulose from hemp stalk by enzymatic degumming that can be further used in customized extraction of value-added products like paper pulp, viscose fibres and nano-fibrillated cellulose that can be used in paper, pulp and textile industries (Zhang *et al*., 2023). PNLs are also used in pectic waste-water treatment (Mahesh *et al*., 2016).

1.7.9 Rhamnogalacturonan I rhamnohydrolase

Rhamnogalacturonan I rhamnohydrolase (RGRH) (EC 3.2.1.174) is similar to α-L-rhamnosidase (EC 3.2.1.40) in its activity. Both the enzymes are placed under families, 78 and 106 of GH (http://www.cazy.org/GH.html). RGRH uses an inverting mechanism for hydrolysis of α-1,4 bond between *Rhap* and *GalpA* to cleave the terminal non-reducing end of RG I polymer in an exo-acting mode and liberates

rhamnosyl residues (Mutter *et al*., 1994). While, α-L-rhamnosidase hydrolyses the α-L-rhamnose residues in the terminal non-reducing end of glycosides, flavonoid glycosides, glycolipids, plant pigments and gums (Naumoff and Dedysh, 2012). The optimum pH of RGRH activity ranges between 4.0-5.0 and the optimum temperature between 45-60 ºC (Mutter *et al*., 1994; Matsumoto *et al*., 2017). The optimum pH range of bacterial α-L-rhamnosidases is 5.0-6.0 and that of fungal α-L-rhamnosidases is 5.0-6.5 (Pan *et al*., 2023). The optimum temperature range of α-L-rhamnosidase activity is 40-60 ºC. The α-L-rhamnosidase members of GH78 and GH106 families possess $(\alpha/\alpha)_6$-barrel fold (http://www.cazy.org/ GH78.html) and $(\beta/\alpha)_8$-barrel fold structures (http://www.cazy.org/GH106.html), respectively, but RGRH structure fold is yet to be studied. α-L-Rhamnosidase is used in food industries for increasing the aroma of wine, increasing the quality of juice by removing bitterness caused by flavonoid glycosides narginin, neohespiridin and hesperidin crystals (Matsumoto *et al*., 2017). α-L-Rhamnosidase is effectively used in purification of icariin, a prenylated flavonoid glycoside from a group of epimedium flavonoids (Su *et al*., 2023). Icariin is considered to be the quality marker among all epimedium flavonoids in Chinese medicine for many pharmaceutical advantages like treating cancers. However, RGRH do not act on flavonoid glycosides and hence their industrial applications are yet to be explored (Matsumoto *et al*., 2017).

1.7.10 Rhamnogalacturonan α-1, 2- galacturonohydrolase

Rhamnogalacturonan α-1,2- galacturonohydrolase (RGGH) (EC 3.2.1.173) is classified as a family 28, 138 glycoside hydrolases (http://www. cazy.org/GH28.html). RGGH acts in an exo-acting mode and following retaining mechanism it catalyses the hydrolytic cleavage of α-1,2 glycosidic bond between the L-rhamnopyranosyl and D-galactopyranosyluronic acid of the RG II backbone at the terminal non-reducing end,

liberating monogalacturonate (Coenen *et al*., 2007). The optimum pH and temperature of RGGH purified from *Aspergillus aculeatus* was 4.0 and 50 ºC, respectively (Mutter *et al*., 1998). The 3-dimensional structure of RGGH possesses an $(\alpha/\beta)_8$ TIM barrel fold with two glutamic acid residues acting as catalytic acid/base and nucleophile (Labourel *et al*., 2019). Also, two arginine residues are involved in specifically determining and targeting D-galacturonic acid. The potential applications of this enzyme in industrial sector are also yet to be explored.

1.7.11 Rhamnogalacturonan I hydrolase

Rhamnogalacturonan I hydrolase or Rhamnogalacturonan I endo-hydrolase (RGH) (EC 3.2.1.171) is classified under family 28 of Glycoside Hydrolases (http://www.cazy.org/GH28.html). RGH acts in an endo-mode catalysing the hydrolytic cleavage of α-D-1,4- *GalpA*-α-L-1,2-*Rhap* bond of rhamnogalacturonan chain randomly leaving *Rhap* at the non-reducing end producing oligogalacturonates (Naran *et al*., 2007). The optimum pH and temperature for RGH activity vary between 4.0-5.0 and 30–50 ºC (Fu *et al*., 2001; Normand *et al*., 2010). RGH possesses a right-handed parallel β-helix fold with two aspartic acid residues involved in catalysis (Petersen *et al*., 1997). An acetyl-group tolerant RGH able to degrade acetylated-RG substrates was identified in *Irpex lacteus*, showing the efficiency of the enzyme in acetylated-pectin degradation without synergistic action of any other acetyl esterases (Normand *et al*., 2010).

1.7.12 Rhamnogalacturonan lyases

Rhamnogalacturonan lyases (RGL) are similar to PGLs. Based on the pattern of action RGL are of two types: endo-RGL (EC 4.2.2.23) and exo-RGL (EC 4.2.2.24). RGLs belong to PL4 (bacteria, fungi and plants), PL11 and PL26 (bacteria and fungi) (http://www.cazy. org.PL.html). Endo-RGL (EC 4.2.2.23) acts through random trans-

elimination of the α-1,4 rhamnose-galacturonate glycosidic linkage in the RG I backbone leaving 4-deoxy-β-L-threo-hex-4-enepyranosyluronic acid (unsaturated *GalpA*) at the non-reducing end of one oligomer and rhamnose as a reducing end residue of second oligomer (Iwai *et al*., 2015). Exo-RGL (EC 4.2.2.24) specifically cleaves the terminal *Rhap* residue of RG I releasing unsaturated galacturonosyl rhamnose. Both endo- and exo- RGLs are present in PL4 and PL11 families. PL4 exhibits a β-sandwich structure, while PL11 exhibits an eight-bladed β-propeller structure with a long α-helix in the centre. PL26 consists exclusively of exo-RGL and exhibits 3 domains: i) an anti-parallel $(\alpha/\alpha)_6$-barrel fold, ii) β-sandwich surrounded by five α-helix and iii) antiparallel β-sheets (Kunishige *et al*., 2018). The 3D structure in all the three families exhibits a Ca^{2+} ion binding domain. The optimum pH and temperature for RGL activity ranges between 7.0-8.5 and 30–70 ºC, respectively (Iwai *et al*., 2015; Dhillon *et al*., 2016; Méndez-Yañez *et al*., 2020). Thermo-alkaline RGL has textile industrial application in degumming of jute and bio-scouring of cotton (Dhillon *et al*., 2019). RGL along with polygalacturonase (PG) were found to play a very significant role in efficient herbivorous nutrition of a tortoise leaf beetle (Cassidinae) that live in a symbiotic relationship with its obligate partner *Stammera. Stammera* encodes the genes for RGL and PG that help in depolymerizing pectic substrate in leaf foliage, thereby facilitating access to efficient nutrition of the Cassidinae as compared with other beetles whose symbionts lack these genes (Salem *et al*., 2020).

1.7.13 Unsaturated rhamnogalacturonyl hydrolase

Unsaturated rhamnogalacturonyl hydrolase (*Un*RGH) (EC 3.2.1.172) acts specifically on unsaturated *GalpA* residues at the non-reducing ends of rhamnogalacturonan main chain of RG I (Silva *et al*., 2016). They catalyse the cleavage

of the α-1,2 glycosidic bond between the Δ-4,5 unsaturated-*GalpA* and L-*Rhap* releasing single unsaturated D-*GalpA*. They have been classified into glycoside hydrolase family 105 (GH105) (http://www.cazy.org/GH105.html). UnRGH possesses $(\alpha/\alpha)_6$ hairpin barrel fold overlayed by two β-sheets and a small α-helix, where an aspartic acid residue is involved in catalysis that acts as both acid and base catalysts (Germane *et al*., 2015).

1.7.14 Xylogalacturonan hydrolase

Xylogalacturonase hydrolase (XGH) (EC 3.2.1.-) belongs to family 28 of GH. (http://www.cazy.org/GH28.html). It acts in an endo-manner and catalyses the hydrolytic cleavage of *GalpA* and β-xylose linkage in xylogalacturonan chain producing xylose-galacturonate dimers (Zandleven *et al*., 2006). The crystal structure of an XGH from *Aspergillus tubingensis* showed that it possesses a right-handed parallel β-helix with three short α-helices in four turns (Rozeboom *et al*., 2013). XGH exhibits an inverting mechanism for catalysis like other GH28 members with two catalytic aspartic acid residues acting as acid and base. XGA is specific for xylogalacturonic substrate and has optimum activity between pH 3.0–3.5 and temperature 50 ºC. Xylogalacturonan is abundantly found in the hairy regions of apple pomace and XGH has suitable applications in removal of membrane fouling during apple juice preparation (Herweijer *et al*., 2003). XGH can also act in synergy with PME in methyl esterified xylogalacturonan rich pectin found in pea and soybean (Yamada *et al*., 2021).

1.7.15 Arabinases

Endo-arabinases (EC 3.2.1.99) and α-L-arabinofuranosidases (EC 3.2.1.55) are active on arabinan and on the short side chains of arabinogalactan type I (Beldman *et al*., 1993). Endo-arabinases catalyse the hydrolysis of α-1,5-linked arabinan side chains

of rhamnogalacturonan I and terminal non-reducing arabinose residues are removed by a-L-arabinofuranosidases (Silva *et al*., 2016). They belong to family 43 Glycoside Hydrolases (http://www.cazy.org/GH43.html). Arabinases typically possess a five-blade β-propeller fold where two aspartic acid and one glutamic acid residues help in catalysis by forming a catalytic triad (Farro *et al*., 2018). Bacterial arabinases exhibited an optimum pH of 8.0 (Farro *et al*., 2018), while fungal arabinases showed an optimum pH of 5.5 (Chen *et al*., 2015). Optimum temperature for both bacterial and fungal arabinase ranges from 45-55 ºC (Chen *et al*., 2015, Farro *et al*., 2018). Arabinases along with other cellulases acts synergistically to carry out enzymatic hydrolysis of cellulose (Farro *et al*., 2018). Arabinases are also known to find application in processing and production of fruit and vegetable juices, alcoholic beverages (Chettri and Verma, 2023).

1.8 Other applications of pectinolytic enzymes

Pectin degrading enzymes can act in synergy among themselves and also with other carbohydrate degrading enzymes to find applications in several industrial processes. Mixture of pectinolytic enzymes (endo-PG and PMG) are used in olive oil extraction by reducing the emulsification of pectin (Ortiz *et al*., 2017). Pectinase treatment increases the quality of the extracted oil, retaining its polyphenolic content and malaxation properties. Fermentation of coffee beans by using pectinase (PG, PNL and PME) treatment also increases the quality of coffee by retaining its polyphenol, flavonoid content and antioxidant activity (Haile and Kang, 2019). Pectinase treatment can also be used for removal of the mucilage layer from the coffee beans and speeding up the processing time, flavour and aroma of the coffee (Koshy and De, 2019). PG, PGL, PNL and PME can reduces the viscosity of the animal feed by hydrolysis of non-biodegradable fibres and increasing the absorption of nutrients in the rumen (Murad and Azzaz, 2011). The waste-water released from several citrus processing industries

have higher pectic content. Efficient pectinase treatment can lower this pectic content for water reusability. Pectinases like PG, PNL and PME immobilized in a matrix of functionalized nano-porous activated carbon (FNAC) can effectively degrade pectin and re-cycle waste-water (Mahesh *et al*., 2016). Pectinases also have a great role in paper and pulp industries. Pectin represents "anionic trash" produced from paper pulp during paper-making. Commercial pectinase (Novozymes) treatment from *Bacillus licheniformis* immobilized in chitosan coated microporous resin was found to reduce the cationic demand of white-water by 58% (Liu *et al*., 2012). Xylano-pectinase bio-bleaching is one of the major alternative bleaching techniques emerging in the paper-pulp industries to reduce the environmental pollution load. The pre-treatment of rice-straw paper-pulp by xylano-pectinase reduced the requirement of chemical bleaching by 32% and improved the delignification process, thereby producing the superior quality paper (Nagpal *et al*., 2020). POS produced by the action of different pectinases have anti-microbial activity and can act as potential food prebiotics that can enhance the healthy gut bacteria like *Bifidobacteria*, Bacteroides and can prevent the binding of pathogenic bacteria in the gut ecosystem by competitive anti-adhesive property (Singh and Tingirikari, 2021).

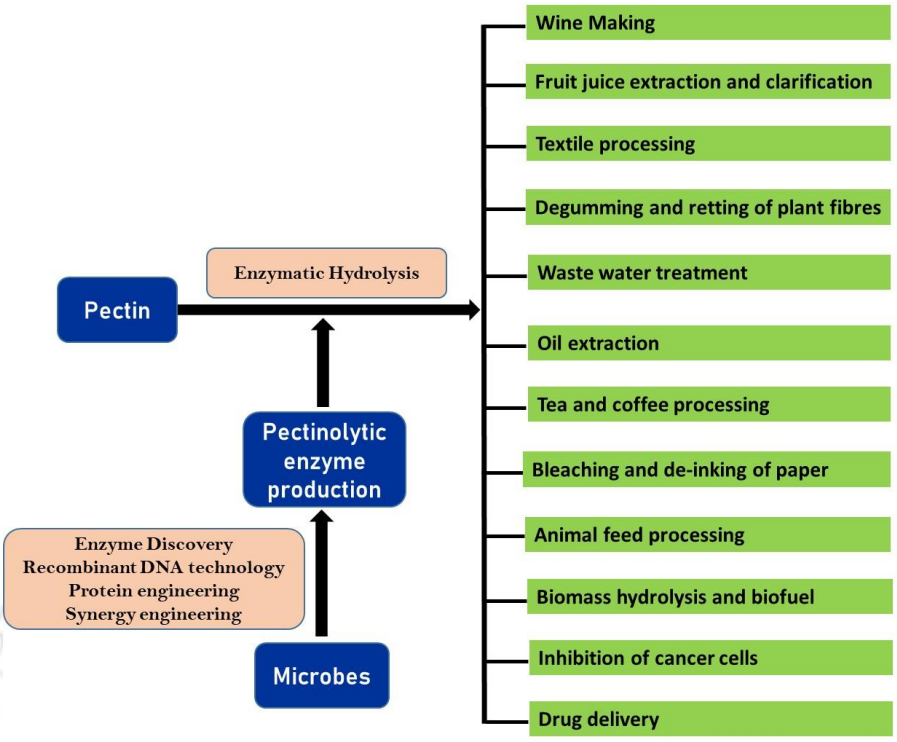

Fig 1.10 Application of different microbial pectinases in different industries.

Table 1.1 Pectinolytic enzymes and their applications.

Enzyme	Enzyme family	EC number	Enzyme activity	Structure fold	Applications	References
Protopectinase	GH28 GH43	3.2.1.-	Endo- & exo-PG	-	Extraction of pectin	Zapata-Zapata *et al*., 2017; Zhang *et al*., 2018
Polygalacturonase	GH28	3.2.1.15 3.2.1.67 3.2.1.82	Endo-PG Exo-PG Exo-PG	Parallel β-helix Parallel β-helix Parallel β-helix	Juice clarification, Retting fibres, Biofuel production, Tea leaf fermentatio	Thakur and Gupta, 2012; Anand *et al*., 2016; Poondla *et al*., 2017 Amin *et al*., 2020; Ibrahim *et al*., 2021
Polymethyl galacturonase	GH28	3.2.1.- 3.2.1.-	Endo-PMG Exo-PMG	-	Juice and wine clarification, fibre processing, oil and flavour	Chaurasia *et al*., 2015
Pectin methyl esterase	CE8	3.1.1.11	PME	Parallel β-helix, α/β/α-fold	Food processing, textile processing, anti-cancer activity	Rajulapati *et al*., 2017; Ma *et al*., 2018; Zhang *et al*., 2018
Pectin/ rhamnogalacturonan acetyl esterase	CE12 CE13 CE16	3.1.1.6 3.1.1.- 3.1.1.86	PAE, RGAE PAE PAE	α/β/α-fold α/β/α-fold α/β/α-fold	Gel formation, biofuel and other value-added products	Mølgaard *et al*., 2000; Xiao and Anderson,2013
Pectate lyase	PL1 PL2 PL3 PL9 PL10	4.2.2.2, 4.2.2.9 4.2.2.2, 4.2.2.9 4.2.2.2 4.2.2.2, 4.2.2.9 4.2.2.2	Endo- & exo-PGL Endo- & exo-PGL Endo-PGL Endo- & exo-PGL Endo-PGL	Parallel β-helix $(\alpha/\alpha)_7$-barrel Parallel β-helix Parallel β-helix $(\alpha/\alpha)_3$-barrel	Textile treatment, degumming of fibres, juice clarification, bio-scouring of cotton, biofuel production	Kudla *et al*., 2007; Zhou *et al*., 2017; Chen *et al*., 2018; Bekli *et al*., 2019; Zhen *et al*., 2020
Pectin lyase	PL1	4.2.2.10	Endo-PNL	β-helix	Textile processing, fibre processing, paper and pulp processing, anti-cancer activity	Chakraborty *et al*., 2015; Yadav *et al*., 2017; He *et al*., 2018; Ckakraborty *et al*., 2018
Rhamnogalacturonan I rhamnohydrolase/α-L-rhamnosidase	GH78 GH106	3.2.1.174 3.2.1.174	Exo-RGRH Exo-RGRH	$(\alpha/\alpha)_6$ $(\beta/\alpha)_8$	Wine aroma, Purification of icariin	Matsumoto *et al*., 2017, Su *et al*., 2023
Rhamnogalacturonan I galacturonohydrolase	GH28	3.2.1.173	Exo-RGGH	$(\beta/\alpha)_8$		Coenen *et al*., 2007, Labourel *et al*., 2019
Rhamnogalacturonan α-1,2- hydrolase	GH28	3.2.1.171	Endo-RGH	-	Degradation of pectin	Naran *et al*., 2007; Normand *et al*., 2010
Rhamnogalacturonan lyase	PL4 PL11 PL26	4.2.2.23 4.2.2.24 4.2.2.24	Endo-RGL Exo-RGL Exo-RGL	β-sandwich+β sheet β-propeller	Degumming of jute and bio-scouring of cotton	Kunishige *et al*., 2018; Dhillon *et al*., 2019
Unsaturated rhamnogalacturonan hydrolase	GH105	3.2.1.172	Exo-RGH	$(\alpha/\alpha)_6$+2 β sheet + α helix	-	Germane *et al*., 2015
Xylogalacturonan hydrolase	GH28	3.2.1.-	Endo-XGH	Parallel β-helix	Juice preparation and processing	Herweijer *et al*., 2003; Rozeboom *et al*., 2013
Arabinases	GH43	3.2.1.99	Endo-arabinase	Five-blade β-propeller	Preparation and processing of juices, alcoholic beverages	Farro *et al*., 2018, Chettri and Verma, 2023

1.9 Carbohydrate esterases

Carbohydrate esterases (CEs) are a class of enzymes that catalyse the de-O or de-N-acylation of substituted saccharides. CEs acts on esterified substrates. CEs hydrolyses esterified substrates releasing an acid and an alcohol; therefore, two classes of substrates are considered for CEs: those in which the sugar plays the role of the acid like pectin methyl esters and pectin acetyl esters, the form of sugar acids involved in such esters is uronic acids and those in which sugar behaves as an alcohol like acetylated xylan (Fazary and JU, 2007). The enzymes under these class shows broad specificity since which is reflected by the fact that they are currently classified into 20 families (www.cazy.org). In terms of substrate specificity, the 20 carbohydrate esterase families represent acetyl xylan esterases (AcXEs), cinnamoyl esterase, carboxyl esterase, S- formylglutathione hydrolase, diacylglycerol O-acyltransferase, trehalose 6-O mycolyltransferase, chitin deacetylases, diacetylchitobiose deacetylase, peptidoglycan deacetylases, cutinase, cephalosporin C- deacetylase, feruloyl esterases, pectin acetyl esterases, pectin methyl esterases, acetylcholine esterase, UDP-3-0-acyl N-acetylglucosamine deacetylase, 4-O-methyl-glucuronoyl methylesterase, glucuronoyl esterases, acetylmannan esterase, N-acetylglucosamine 6-phosphate deacetylase, N-acetylgalactosamine 6-phosphate deacetylase and enzymes catalyzing N-deacetylation of low molecular mass amino sugar derivatives.

1.10 Carbohydrate esterase Family 12

Family 12 carbohydrate esterase (CE12) is represented by pectin acetyl esterase (EC 3.1.1.6), rhamnogalacturonan acetyl esterase (EC 3.1.1.86) and acetyl xylan esterase (EC 3.1.1.72). CE12 contains a total of 7378 protein sequences as of April 2024 (http://www.cazy.org/CE12.html). Of these 7378 protein sequences, 5725 are from bacteria, 1651 are from eukaryota and 2 belongs to unclassified sequences. Pectin

acetyl esterase (PAE) and rhamnogalacturonan acetyl esterase (RGAE) remove the acetyl group from O-2 and O-3 position of *GalpA* of HG and RG I region. Acetylation of *GalpA* residues hinders the hydrolysis action by other main-chain degrading enzymes like polygalacturonases and pectin/pectate or rhamnogalacturonan lyases. PAE/RGAE removes this obstacle from acetylated pectin and aids in main-chain degradation by other de-polymerizing enzymes (Beily, 2012). Till date, only 4 bacterial PAEs have been characterized biochemically, *viz*., PaeY from *E. chrysanthemi* (Shevchik and Hugouvieux-Cotte-Pattat, 1997), PaeX from *E. chrysanthemi* (Shevchik and Hugouvieux-Cotte-Pattat, 2003), YxiM from *B. subtilis* (Bolvig *et al*., 2003) and BliPae from *B. licheniformis* (Remoroza *et al*., 2014) (Table 1.2). Out of these four, the crystal structure of only one PAE from *Bacillus subtilis*, 2o14.pdb, has been submitted and is available in the protein data bank (www.rcsb.org). Apart from this, one fungal RGAE from *Aspergillus aculeatus* (Searle-van Leeuwen *et al*., 1992) and 3 bacterial RGAEs from *B. halodurans* (Navarro-Fernández *et al*., 2008), *B. subtilis* (Martínez-Martínez *et al*., 2008) and *P. polymyxa* (Tang *et al*., 2021) were characterized biochemically (Table 1.2). Out of these four RGAEs, only one RGAE from *A. aculeatus* (1deo.pdb), has been structurally characterized and elucidated (Mølgaard *et al*., 2003). Both RGAE and PAE belong to the Serine-Glycine-Asparagine-Histidine (SGNH) hydrolase family, a new hydrolase family which is different than the glycoside hydrolase family. The SGNH hydrolase family is characterized by the presence of having four conserved blocks of residues, each consisting of completely conserved residues Ser, Gly, Asn and His, respectively (Mølgaard *et al*., 2003, Shevchik and Hugouvieux-Cotte-Pattat, 2003). PAEs and RGAEs characterized so far have a typical α/β/α structure containing a central β- sheet. It deviates from the α/β fold of glycoside hydrolase family in lacking a nucleophilic elbow motif. The active site is an open cleft

with serine-histidine-aspartic acid as the catalytic triad forming an acid-base-nucleophile triad for covalent catalysis (Mølgaard *et al*., 2003).

Table 1.2 Biochemical properties of some CE12 bacterial and fungal pectin/rhamnogalacturonan acetyl esterases.

Protein name	Source	Optimum temperature (°C)	Optimum pH	Substrate specificity	Reference
PAE (PaeY)	*E. chrysanthemi*	50	8	Homo galacturonan	Shevchik and Hugouvieux-Cotte-Pattat, 1997
PAE (PaeX)	*E. chrysanthemi*	50	8.7	Homo galacturonan	Shevchik and Hugouvieux-Cotte-Pattat, 2003
PAE (YxiM)	*B. subtilis*	30	8	Homo galacturonan	Bolvig *et al*., 2003
PAE (BliPAE)	*B. licheniformis*	50	8	O-3-acetylated homo galacturonan	Remoroza *et al*., 2014
RGAE (AaRGAE)	*A. aculeatus*	40	5.5	Rhamno galacturonan	Searle-van Leeuwen *et al*., 1992
RGAE (BhRGAE)	*B. halodurans*	40	8.0	Rhamno galacturonan	Navarro- Fernández *et al*., 2008
RGAE (YesT)	*B. subtilis*	35	8.5	Rhamno galacturonan	Martínez-Martínez *et al*., 2008
RGAE (pp1113)	*P. polymyxa*	30	8.5	Rhamno galacturonan	Tang *et al*., 2021

1.10.1 Mechanism of action of pectin/rhamnogalacturonan acetyl esterase

Pectin/rhamnogalacturonan acetyl esterase, PAE (EC 3.1.1.6 and EC 3.1.1.86) catalyses the removal of the acetyl groups from O-2 and O-3 positions of *GalpA* in homogalacturonan/rhamnogalacturonan region of pectin yielding pectic acid and acetate as shown in Fig. 1.9 (Chandrayan, 2018).

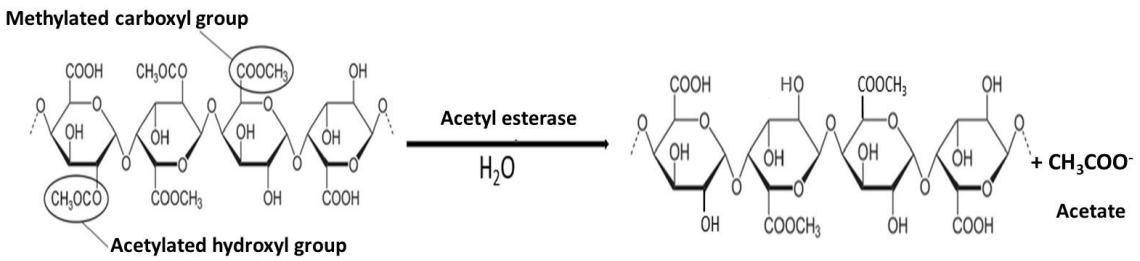

Fig. 1.9 Pectin acetyl esterase action on pectin polysaccharide (Adapted from Schmidt *et al*., 2015).

1.10.2 Applications of pectin/rhamnogalacturonan acetyl esterase

Pectin acetyl esterase (EC 3.1.1.6) and rhamnogalacturonan acetyl esterase (EC 3.1.1.86) are accessory enzymes that targets the acetyl group present in HG, RG I and RG II side chain. As the acetylation of these residues sterically hinders the catalytic function of the corresponding lyases and hydrolases on the main-chain, deacetylation facilitates the action of the lyases and hydrolases (Oosterveld *et al*., 2000; Safran *et al*., 2021). Thus, partial reduction of cell wall acetylation by modulating acetyl transferase and/or acetyl esterase activities might therefore improve microbial viability during fermentation and enhance the conversion efficiency of biomass to biofuel (Leijdekkers *et al.*, 2013). Catalytic efficiency of PME is increased by prior treatment of pectin with PAE, i.e., pre-treatment of pectin with PAE can increase the release of methyl groups by PME (Bolvig *et al*., 2003), thus it can be used in food industry in the production of juices, fruit drinks, wines and can also be used as an exogenous enzyme in fruit and vegetable processing (Chandrayan, 2018). The synergistic effect of PME and PAE also increases the gelation of sugar beet pectin in presence of calcium (Oosterveld *et al*., 2000). PAE is also a potential candidate for modifying pectic polysaccharide as a non-toxic, biodegradable and biocompatible material for colon-targeted drug delivery system (Savary *et al*., 2003). PAEs and RGAEs can be used in food industries for gelation (Oosterveld *et al*., 2000) and in the production of biofuel and other value-added products from biomass (Leijdekkers *et al*., 2013; Xiao and Anderson, 2013). The enzyme has also been used industrially for the production of β-lactam antibiotics and paper bleaching purposes (Navarro-Fernández *et al*., 2008). Cold-adapted PAE/RGAE can be used for the synthesis of cinnamyl acetate by transesterification reaction of cinnamyl alcohol and vinyl acetate (Tang *et al.*, 2021).

1.11 *Acetivibrio thermocellus*

Acetivibrio thermocellus a.k.a *Clostridium thermocellum* and *Hungateiclostridium thermocellum* was first isolated by Viljoen *et al* in 1926 in a study trying to identify the novel organisms with cellulose degrading capability. *A. thermocellus* is a rod-shaped, anaerobic, thermophilic and Gram-positive bacterium (Fig. 1.11) and are capable of directly converting cellulose to ethanol (Bayer *et al*., 2000). Later it was found that apart from cellulose it can also grow on cellobiose, xylose and hemicellulose and produces major fermentation products like carbon-dioxide and hydrogen gas, lactic and formic acid, succinic acid and ethanol depending on the strain. Despite gaining attention for its ethanol producing capacity, it cannot tolerate ethanol after a certain concentration (up to 5 g/L) because of its cell-wall composition.

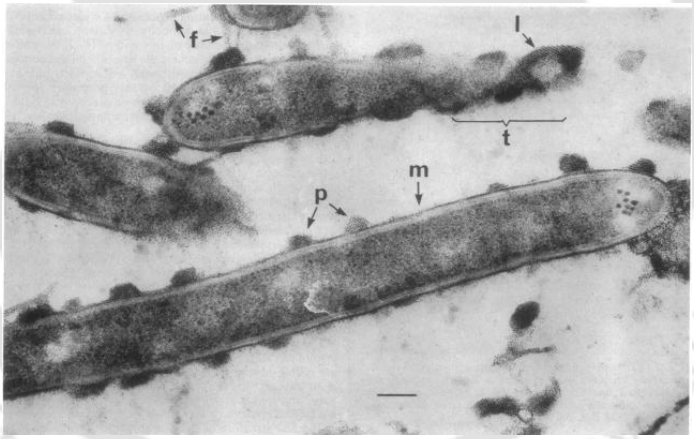

Fig. 1.11 TEM image of cellobiose-grown cells of *C. thermocellum*. Major labels: monolayer (m), the fibrous structures (f) which connect two adjacent cells, (p) the nodulous protuberances (cellulosomes). Bars, 200 nm. (Adopted from Bayer and Lamed, 1986).

An important feature of this organism is the presence of cellulosome (Fig. 1.12) on its cell-surface, an extracellular multi-enzyme complex (Molecular weight, > $2x10^6$ kDa and Diameter 18 nm) that constitutes it as a host organism for many consolidated bioprocessing products (Akinosho *et al*., 2014). Cellulosomes are also reported in *C. cellulovorans*, *A. alkalicellulosi* and *A. clariflavus* (Bayer *et al.*, 1994).

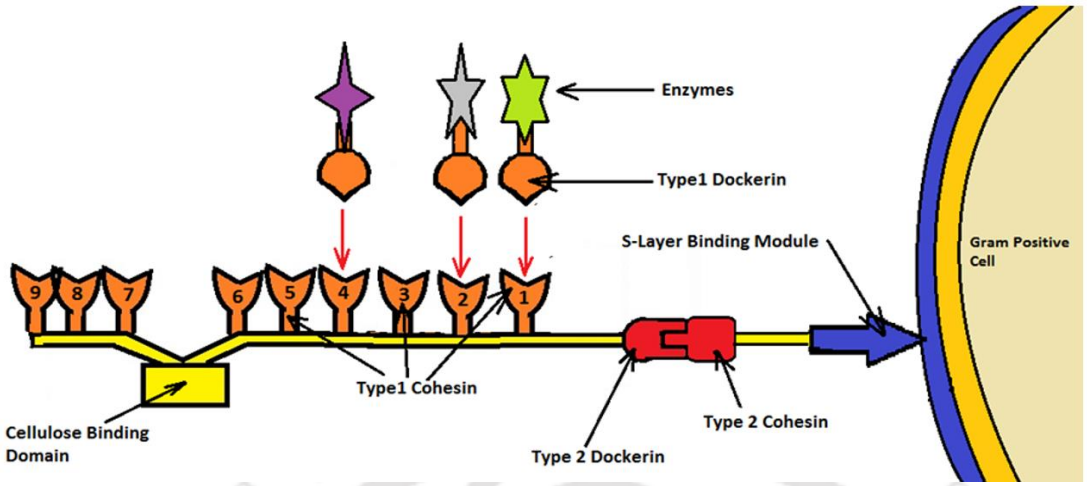

Fig. 1.12 Schematic diagram of cellulosome from *A. thermocellus* (Source 2012.igem.org).

Over 20 distinct enzymes housing pectinases, chitinases, esterases, hemicellulases, cellulases required for the breakdown of lignocellulosic compounds are present in the cellulosomes (Zverlov *et al.,* 2005). Cellulosomes consists of a non-catalytic scaffoldin protein (CipA). This scaffoldin protein consists of nine cohesin type I domain. Cohesin type I binds to dockerin type I domain which connects to the catalytic domains of their respective enzymes through a linker. These specific interactions are very specific for the assembly and function of such big complex. This process takes place in a calcium dependant manner. The cellulosome enzymes are modular in nature. Cellulosome is also assisted with a non-catalytic carbohydrate binding module (CBM) that attaches it to its carbohydrate substrate (Akinosho *et al*., 2014).

1.12 Significance and objectives of the current study

1.12.1 Significance of the study

Pectin degrading enzymes find application in various industrial processes like juice extraction, vegetable puree production, fibre retting, waste water treatment, biomass hydrolysis among other applications. Hence the search for better enzymes that can completely degrade various components of pectin is on. Several enzymes from the cellulosomal complex of *Acetivibrio thermocellus* have been studied but never a pectin/rhamnogalacturonan acetyl esterase belonging to family 12 carbohydrate esterase. *Acetivibrio thermocellus* consists of a gene encoding a putative pectin acetyl esterase belonging to family 12 carbohydrate esterases and this type of enzyme has not been reported from *Acetivibrio thermocellus* till date. Expression and purification of this enzyme will lead to its biochemical and structure characterization. This will give a thermophilic and thermostable pectin degrading enzyme from a thermophilic organism. This enzyme may potentially be applied to modern-day food, beverage, textile, oil and pharmaceutical industries. The proposed study involves the expression and purification of a single domain catalytic module from family 12 carbohydrate esterase, *Ct*Pae12B (GenBank Accession number ABN54336.1) from *Acetivibrio thermocellus* ATCC 27405 genome. BLAST analysis showed that *Ct*Pae12B is a putative pectin acetyl esterase. Biochemical and functional characterization of *Ct*Pae12B will be carried out to determine its activity against different pectin polysaccharides, xylan substrates and synthetic substrates to understand its role in deacetylation of various esterified substrates. Determination of *in-silico* structure activity will help to understand the mode of the enzyme action and the key residues involved in catalysis. Structural study of *Ct*Pae12B, will help to determine the active site of the enzyme and the role of catalytic amino acid residues in binding with the suitable ligands by molecular docking studies. The folding pattern and stability of *Ct*Pae12B will be studied by molecular dynamics simulation. The solution structure elucidation of any bacterial PAE/RGAE of family 12 carbohydrate esterase from *Acetivibrio thermocellus* has not been studied yet. Small angle X-ray scattering (SAXS) and dynamic light scattering (DLS) will help in understanding its behaviour in solution under different protein concentrations. The synergistic action of *Ct*Pae12B with other pectin degrading enzymes like pectin methyl esterase (*Ct*PME) and pectate lyase (*Ct*PL1) or rhamnogalacturonan lyase (*Ct*RGLf) in catalysis of pectic substrate will be analysed. The regioselectivity of *Ct*Pae12B towards

O-2 or O-3 or both O-2 and O-3 acetyl groups will be elucidated. Till date, the effect of deacetylated pectic polysaccharide or pectic oligosaccharides in inhibition of cancer cells has not been reported. Moreover, the use of pectic substrates after surface modification by deacetylation for building the drug delivery material targeting colon has not been studied. Therefore, the study of the effect of deacetylation of pectic substrate on cancer cells and in drug delivery is proposed. The reasons for selecting pectin acetyl esterase (*Ct*Pae12B) of family 12 carbohydrate esterase (CE12) from *Acetivibrio thermocellus* are summarized below:

1. *Ct*Pae12B from *Acetivibrio thermocellus* is a putative pectin acetyl esterase, which shall be thermostable and efficient in hydrolysing the polysaccharides desirable for industries. The de-acetylated pectic polysaccharide can be more efficiently degraded by other pectin degrading enzymes like pectin methyl esterase and pectate or rhamnogalacturonan lyase.
2. Study of biochemical properties of *Ct*Pae12B will elucidate the essential parameters, which would be beneficial for industrial downstream applications.
3. The structural insights and 3-D structure elucidation of *Ct*Pae12B will reveal the molecular determinants of substrate specificity.
4. The synergistic action of *Ct*Pae12B with other pectinases will help in efficient enzymatic hydrolysis of pectic substrates. The regioselectivity analysis of *Ct*Pae12B will help in determination of its site specificity for O-2 or O-3 acetyl groups.
5. The application of *Ct*Pae12B in generating the deacetylated pectic substrates for their significance in inhibition of colon cancer cells (HCT-116) and in building a biomaterial for controlled and sustainable colon-targeted drug delivery.

1.12.2 Specific Objectives

1. Cloning, expression and purification of family 12 carbohydrate esterase (*Ct*Pae12B) from *Acetivibrio thermocellus* ATCC 27405.
2. Structure studies of *Ct*Pae12B by *in-silico* methods like homology modeling, molecular docking, molecular dynamics simulation and their correlation with solution structure determined by SAXS and DLS analysis.
3. Biochemical, functional characterization, optimization of production and substrate specificity of *Ct*Pae12B, a putative pectin acetyl esterase from *Acetivibrio thermocellus* ATCC 27405.
4. Study the role of *Ct*Pae12B in the synergistic action with other pectinases like pectin methyl esterase (*Ct*PME) and main-chain degrading enzyme, pectate lyase (*Ct*PL1) or rhamnogalacturonan lyase (*Ct*RGL*f*) for complete hydrolysis of pectic substrates.
5. Regioselectivity analysis of *Ct*Pae12B.
6. Study the effect of acetylated and methylated pectic polysaccharides and oligosaccharides as well as demethylated and deacetylated oligosaccharides, produced by various combinations of *Ct*Pae12B, *Ct*PME and *Ct*PL1 or *Ct*RGL*f* treatment, on inhibition of colon cancer (HCT-116) cells.
7. Study the effect of deacetylation on surface modification of pectic polysaccharide by *Ct*Pae12B treatment and its use as a biomaterial for drug entrapment and sustainable and controlled colon-targeted drug release.

References

Abbott, D.W., Boraston, A.B. (2007) A family 2 pectate lyase displays a rare fold and transition metal-assisted β-elimination. Journal of Biological Chemistry, 282 (48): 35328–35336.

Akash, Hamid, M.S., Rehman, K., Chen, S. (2015) Natural and synthetic polymers as drug carriers for delivery of therapeutic proteins. Polymer Reviews, 55 (3): 371-406.

Akinosho, H., Kelsey, Y., Dan, C., Arthur, R. (2014) The emergence of *Clostridium thermocellum* as a high utility candidate for consolidated bioprocessing applications. Frontiers in Chemistry, 2: 66.

Alba, K., Laws, A.P., Kontogiorgos, V. (2015) Isolation and characterization of acetylated LM-pectins extracted from okra pods. Food Hydrocolloids, 43: 726–735.

Albersheim, P., Darvill, A.G., O'Neill, M.A., Schols, H.A., Voragen, A.G.J. (1996) A hypothesis: the same six polysaccharides are components of the primary cell walls of all higher plants. Proceedings of International Symposium on Progress in Biotechnology, Pectins and pectinases, Vol. 14 (eds. Visser, J., Voragen, A.G.J.), Elsevier Sciences, Amsterdam, NL, 47–53.

Amin, F., Mohsin, A., Bhatti, H.N., Bilal, M. (2020) Production, thermodynamic characterization, and fruit juice quality improvement characteristics of an exopolygalacturonase from *Penicillium janczewskii*. Biochimica et Biophysica Acta (BBA)- Proteins and Proteomics, 1868 (5): 140379.

Anand, G., Yadav, S., Yadav, D. (2016) Purification and characterization of polygalacturonase from *Aspergillus fumigatus* MTCC 2584 and elucidating its application in retting of *Crotalaria juncea* fiber. 3 Biotech, 6 (2): 1–7.

Anand, G., Yadav, S., Yadav, D. (2017) Production, purification and biochemical characterization of an exo-polygalacturonase from *Aspergillus niger* MTCC 478 suitable for clarification of orange juice. 3 Biotech, 7 (2): 1–8.

Anderson, C.T. (2016) We be jammin': an update on pectin biosynthesis, trafficking and dynamics. Journal of Experimental Botany, 67 (2): 495–502.

Anderson, C.T. (2019) Pectic polysaccharides in plants: structure, biosynthesis, functions, and applications. Extracellular sugar-based biopolymers matrices, biologically-inspired systems, Vol. 12 (eds. Cohen, E., Merzendorfer, H.), Springer, Cham, 487–514.

Arpana, M., Fasim, A., Manjushree, H.K., More, S.S. (2023) An alkalophilic and thermostable polygalacturonase (PGase) from *Pseudomonas* sp. 13159349: purification, biochemical characterization and its efficacy in olive oil extraction. Biologia, 78 (7): 1813-1824.

Ázar, R.I., da Luz Morales, M., Maitan-Alfenas, G.P., Falkoski, D.L., Alfenas, R.F., Guimarães, V.M. (2020) Apple juice clarification by a purified polygalacturonase from *Calonectria pteridis*. Food and Bioproducts Processing, 119: 238–245.

Bayer, E.A., Lamed, R. (1986) Ultrastructure of the cell surface cellulosome of *Clostridium thermocellum* and its interaction with cellulose. Journal of Bacteriology, 167(3): 828-836.

Bayer, E.A., Morag, E., Lamed, R. (1994) The cellulosome-a treasure-trove for biotechnology. Trends in Biotechnology, 12(9): 379-386.

Bayer, E.A., Shoham, Y., Lamed, R. (2000) Cellulose-decomposing prokaryotes and their enzyme systems. The Prokaryotes: An evolving electronic resource for the microbiological community, 3rd ed. (eds. Dworkin, M., Falkow, S., Rosenberg, E., Schleifer, K.H., Stackebrandt, E), Springer, 2, 578–617.

Beily, P. (2012) Microbial carbohydrate esterases deacetylating plant polysaccharides. Biotechnology Advances, 30(6): 1575-1588.

Bekli, S., Aktas, B., Gencer, D., Aslim, B. (2019) Biochemical and molecular characterizations of a novel pH-and temperature-stable pectate lyase from *Bacillus amyloliquefaciens* S6 for industrial application. Molecular Biotechnology, 61 (9): 681–693.

Beldman, G., Searlevanleeuwen, M.J.F., Deruiter, G.A., Siliha, H.A., Voragen, A.G.J. (1993) Degradation of arabinans by arabinanases from *Aspergillus aculeatus* and *Aspergillus niger*. Carbohydrate Polymers, 20: 159-168.

Bezus, B., Esquivel, J.C.C., Cavalitto, S., Cavello, I. (2022) Study of polygalacturonase production by an Antarctic yeast and obtention of dragon fruit juice by maceration at mild temperature. Food Bioscience, 101942.

Bhamidi, S., Scherman, M. S., Rithner, C. D., Prenni, J. E., Chatterjee, D., Khoo, K.H., McNeil, M. R. (2008) The identification and location of succinyl residues and the characterization of the interior arabinan region allow for a model of the complete primary structure of *Mycobacterium tuberculosis* Mycolyl Arabinogalactan. Journal of Biological Chemistry, 283(19): 12992–13000.

Boerjan, W., Ralph, J., Baucher, M. (2003) Lignin biosynthesis. Annual Review of Plant Biology, 54: 519–546.

Bolvig, P.U., Pauly, M., Orfila, C., Scheller, H. V., and Schnorr, K. (2003) Sequence analysis and characterization of a novel pectin acetyl esterase from *Bacillus subtilis*. Advances in Pectin and Pectinase Research, (eds. Voragen, F., Schols, H., Visser, R.), Springer, Dordrecht, 315-330.

Brennan, M., Harris, P.J. (2011) Distribution of fucosylated xyloglucans among the walls of different cell types in monocotyledons determined by immunofluorescence microscopy. Molecular Plant, 4: 144–56.

Broxterman, S. E., Schols, H. A. (2018) Interactions between pectin and cellulose in primary plant cell walls. Carbohydrate Polymers, 192: 263–272.

Bush, M.S., Marry, M., Huxham, I.M., Jarvis, M.C., McCann, M. (2001) Developmental regulation of pectic epitopes during potato tuberization. Planta, 213: 869-880.

Caffall, K.H., Mohnen, D. (2009) The structure, function, and biosynthesis of plant cell wall pectic polysaccharides. Carbohydrate research, 344(14): 1879-1900.

Chakraborty, S., Jagan Mohan Rao, T., Goyal, A. (2017) Immobilization of recombinant pectate lyase from *Clostridium thermocellum* ATCC-27405 on magnetic nanoparticles for bioscouring of cotton fabric. Biotechnology Progress, 33 (1): 236–244.

Chakraborty, S., Rani, A. and Goyal, A. (2018) Pectic oligosaccharides produced from pectin extracted from waste peels of *Citrus limetta* using recombinant endo-pectate lyase (PL1B) inhibit colon cancer cells. Trends in Carbohydrate Research, 10(1).

Chakraborty, S., Sharma, K., Mukherjee, J., N Gupta, M., Goyal, A. (2015) Structural modelling, substrate binding and stability studies of endopectate lyase (PL1B) of family 1 polysaccharide lyase from *Clostridium thermocellum*. Protein and Peptide Letters, 22 (6): 557–568.

Chandrayan, P. (2018) Biological function(s) and application (s) of pectin and pectin degrading enzymes. Biosciences Biotechnology Research Asia, 15(1): 87-100.

Chaurasia, S., Chaurasia, A.K., Chaurasia, S., Chaurasia, S. (2015) Factors affecting the production of poly methyl galacturonase enzyme by *Sclerotium rolfsii Sacc*. International Journal of Applied Sciences and Biotechnology, 3 (1): 89–95.

Chen, L., Gu, W., Xu, H.Y., Yang, G.L., Shan, X.F., Chen, G., Kang, Y.H., Wang, C.F., Qian, A.D. (2018) Comparative genome analysis of *Bacillus velezensis* reveals a potential for degrading lignocellulosic biomass. 3 Biotech, 8 (5): 1–5.

Chen, Z., Liu, Y., Yan, Q., Yang, S. and Jiang, Z. (2015) Biochemical characterization of a novel endo-1, 5-α-l-arabinanase from *Rhizomucor miehei*. Journal of Agricultural and Food Chemistry, 63 (4): 1226-1233.

Chettri, D., Verma, A.K. (2023) Endo-arabinase: Source and application. Glycoside hydrolases: biochemistry, biophysics, and biotechnology foundations and frontiers in enzymology, (eds. Goyal, A., Sharma, S.), Academic Press, 243-254.

Coenen, G.J., Bakx, E.J., Verhoef, R.P., Schols, H.A., Voragen, A.G. (2007) Identification of the connecting linkage between homo-or xylogalacturonan and rhamnogalacturonan type I. Carbohydrate Polymers, 70 (2): 224–235.

Cosgrove, D.J. (1999) Enzymes and other agents that enhance cell wall extensibility. Annual Review of Plant Physiology and Plant Molecular Biology, 50: 391–417.

Dhillon, A., Fernandes, V.O., Dias, F.M., Prates, J.A., Ferreira, L.M., Fontes, C.M., Centeno, M.S., Goyal, A. (2016) A new member of family 11 polysaccharide lyase, rhamnogalacturonan lyase (*Ct*RGLf) from *Clostridium thermocellum*. Molecular Biotechnology, 58 (4): 232–240.

Dhillon, A., Rajulapati, V., Goyal, A. (2019) Bio-scouring of cotton fabric and enzymatic degumming of jute fibres by a thermo-alkaline recombinant rhamnogalacturonan lyase, *Ct*RGLf from *Clostridium thermocellum*. The Canadian Journal of Chemical Engineering, 97(5): 1043-1047.

Ding, J., Zhou, Y., Zhu, H., Deng, M., Long, L., Yang, Y., Wu, Q., Huang, Z. (2019) Identification and characterization of an acetyl esterase from *Paenibacillus* sp. XW-6- 66 and its novel function in 7-aminocephalosporanic acid deacetylation. Biotechnology Letters, 41 (8): 1059–1065.

Duan, C.J., Baslé, A., Liberato, M.V., Gray, J., Nepogodiev, S.A., Field, R.A., Juge, N., Ndeh, D. (2020) Ascertaining the biochemical function of an essential pectin methylesterase in the gut microbe *Bacteroides thetaiotaomicron*. Journal of Biological Chemistry, 295 (52): 18625–18637.

Ellis, M., Egelund, J., Schultz, C., Bacic, A. (2010) Arabinogalactan-proteins: key regulators at the cell surface. Plant Physiology, 153: 403–419.

Farro, E.G.S., Leite, A.E.T., Silva, I.A., Filgueiras, J.G., de Azevedo, E.R., Polikarpov, I. and Nascimento, A.S. (2018) GH43 endo-arabinanase from *Bacillus licheniformis*: Structure, activity and unexpected synergistic effect on cellulose enzymatic hydrolysis. International Journal of Biological Macromolecules, 117: 7-16.

Fazary, A. E., Ju, Y. H. (2007) Feruloyl esterases as biotechnological tools: current and future perspectives. Acta Biochimica et Biophysica Sinica, 39 (11): 811–828.

Fishman, M. L., Cooke, P. H., Chau, H. K., Coffin, D. R., Hotchkiss, A. T. (2007) Global structures of high methoxyl pectin from solution and in gels. Biomacromolecules, 8(2): 573-578.

Forbes, J.C., Forbes, J.C., Watson, D. (1992) Plant growth and development; seed and seedling. Plants in Agriculture. Cambridge University Press, New York, USA, 110-129.

Fu, J., Prade, R., Mort, A. (2001) Expression and action pattern of *Botryotinia fuckeliana* (*Botrytis cinerea*) rhamnogalacturonan hydrolase in *Pichia pastoris*. Carbohydrate Research, 330 (1): 73–81.

Gama, R., Van Dyk, J.S., Burton, M.H., Pletschke, B.I. (2017) Using an artificial neural network to predict the optimal conditions for enzymatic hydrolysis of apple pomace. 3 Biotech, 7 (2): 1–10.

Germane, K.L., Servinsky, M.D., Gerlach, E.S., Sund, C.J. and Hurley, M.M. (2015) Structural analysis of *Clostridium acetobutylicum* ATCC 824 glycoside hydrolase from CAZy family GH105. Acta Crystallographica Section F: Structural Biology Communications, 71(8): 1100-1108.

Gunjal, A.B., Patil, N.N., Shinde, S.S. (2020) Pectinase in degradation of lignocellulosic wastes. Enzymes in Degradation of the Lignocellulosic Wastes. Springer, Cham.

Haas, K.T., Wightman, R., Meyerowitz, E.M., Peaucelle, A. (2020) Pectin homogalacturonan nanofilament expansion drives morphogenesis in plant epidermal cells. Science, 367 (6481): 1003–1007.

Haile, M., Kang, W.H. (2019) Isolation, identification, and characterization of pectinolytic yeasts for starter culture in coffee fermentation. Microorganisms, 7 (10): 401.

He, Y., Pan, L., Wang, B. (2018) Efficient over-expression and application of high-performance pectin lyase by screening *Aspergillus niger* pectin lyase gene family. Biotechnology and Bioproccess Engineering, 23 (6): 662–669.

Herweijer, M.A., Vincken, J.P., Meeuwsen, P.J., van der Vlugt-Bergmans, C.J., Beldman, G., Van Ooyen, A.J., Voragen, A.G. (2003) Endo-xylogalacturonan

hydrolase. Advances in Pectin and Pectinase Research, (eds. Voragen, F., Schols, H., Visser, R.), Springer, Dordrecht, 257–266.

Hugouvieux-Cotte-Pattat, N., Condemine, G., Shevchik, V.E. (2014) Bacterial pectate lyases, structural and functional diversity. Environmental Microbiology Reports, 6: 427–440.

Ibrahim, E., Mahmoud, A., Jones, K.D., Taylor, K.E., Hosseney, E.N., Mills, P.L., Escudero, J.M. (2021) Kinetics and thermodynamics of thermal inactivation for recombinant *Escherichia coli* cellulases, cel12B, cel8C, and polygalacturonase, peh28; biocatalysts for biofuel precursor production. Journal of Biochemistry, 169 (1): 109–117.

Iwai, M., Kawakami, T., Ikemoto, T., Fujiwara, D., Takenaka, S., Nakazawa, M., Ueda, M., Sakamoto, T. (2015) Molecular characterization of a *Penicillium chrysogenum* exo-rhamnogalacturonan lyase that is structurally distinct from other polysaccharide lyase family proteins. Applied Microbiology and Biotechnology, 99 (20): 8515–8525.

Jung, J., Arnold, R.D., Wicker, L. (2013) Pectin and charge modified pectin hydrogel beads as a colon targeted drug delivery carrier. Colloids and Surfaces B: Biointerfaces, 104: 116-121.

Kamijo, J., Sakai, K., Suzuki, H., Suzuki, K., Kunitake, E., Shimizu, M., Kato, M. (2019) Identification and characterization of a thermostable pectate lyase from *Aspergillus luchuensis* var. saitoi. Food Chemistry, 276: 503–510.

Karahalil, E., Demirel, F., Evcan, E., Germeç, M., Tari, C., Turhan, I. (2017) Microparticle-enhanced polygalacturonase production by wild type *Aspergillus sojae*. 3 Biotech, 7 (6): 1–9.

Karbalaei-Heidari, H.R., Rastegari, B. (2014) Isolation and partial characterization of a bacterial thermostable polymethyl galacturonase from a newly isolated *Bacillus* sp. strain BR1390. Iranian Journal of Biotechnology, 12 (4): 41–46.

Kaur, A., Varghese, L.M., Mahajan, R. (2019) Simultaneous production of industrially important alkaline xylanase-pectinase enzymes by a bacterium at low cost under solid-state fermentation conditions. Biotechnology and Applied Biochemistry, 66 (4): 574–585.

Keegstra, K. (2010) Plant Cell Walls. Plant Physiology, 154 (2): 483-486.

Kim, M.J., Ju, H.K., Kim, Y., Yoo, S.H., Kim, Y.S. (2016) Effects of amidation and/or methylesterification of pectin on aroma release at different calcium concentration. Food Hydrocolloids 52: 343–349.

Kobayashi, M., Funane, K., Ueyama, H., Ohya, S., Tanaka, M., Kato, Y. (1993) Sugar composition of beet pulp and their enzymatic hydrolysis. Bioscience Biotechnology and Biochemistry, 57(6): 998-1000.

Kohn, R. (1975) Ion binding on polyuronates alginate and pectin. Pure and Applied Chemistry, 42: 371–397.

Koshy, M., De, S. (2019) Effect of *Bacillus tequilensis* SALBT crude extract with pectinase activity on demucilation of coffee beans and juice clarification. Journal of Basic Microbioly, 59 (12): 1185–1194.

Kudla, U., Milac, A.L., Qin, L., Overmars, H., Roze, E., Holterman, M., Petrescu, A.J., Goverse, A., Bakker, J., Helder, J., Smant, G. (2007) Structural and functional characterization of a novel, host penetration-related pectate lyase from the potato cyst nematode *Globodera rostochiensis*. Molecular Plant Pathology, 8 (3): 293–305.

Kumar, R., Meghwanshi, G.K., Marcianò, D., Ullah, S.F., Bulone, V., Toffolatti, S.L. and Srivastava, V. (2023) Sequence, structure and functionality of pectin methylesterases and their use in sustainable carbohydrate bioproducts: A review. International Journal of Biological Macromolecules, 125385.

Kunishige, Y., Iwai, M., Nakazawa, M., Ueda, M., Tada, T., Nishimura, S., Sakamoto, T. (2018) Crystal structure of exo-rhamnogalacturonan lyase from *Penicillium chrysogenum* as a member of polysaccharide lyase family 26. FEBS letters, 592 (8): 1378–1388.

Labourel, A., Baslé, A., Munoz-Munoz, J., Ndeh, D., Booth, S., Nepogodiev, S.A., Field, R.A. and Cartmell, A. (2019) Structural and functional analyses of glycoside hydrolase 138 enzymes targeting chain A galacturonic acid in the complex pectin rhamnogalacturonan II. Journal of Biological Chemistry, 294(19): 7711-7721.

Lang, C., Yang, R., Yang, Y., Gao, B., Zhao, L., Wei, W., Wang, H., Matsukawa, S., Xie, J., Wei, D. (2016) An acid-adapted endo-α-1, 5-l-arabinanase for pectin releasing. Applied Biochemistry and Biotechnology, 180 (5): 900–916.

Leijdekkers, A. G. M., Bink, J. P. M., Geutjes, S, Schols, H. A., Gruppen, H. (2013) Enzymatic saccharification of sugar beet pulp for the production of galacturonic acid and arabinose; a study on the impact of the formation of recalcitrant oligosaccharides. Bioresource Technology, 128: 518–525.

Liang, C., Gui, X., Zhou, C., Xue, Y., Ma, Y., Tang, S.Y. (2015) Improving the thermoactivity and thermostability of pectate lyase from *Bacillus pumilus* for ramie degumming. Applied Microbiology and Biotechnology, 99 (6): 2673–2682.

Liu, C., Qin, X., Liu, B., Xu, X., Deng, A., Zhang, Y., Zhang, Z. and Zhang, W. (2022) High-yield production of acidic pectin lyase PNLZJ5B for juice processing. Letters in Applied Microbiology, 75(4): 1055-1062.

Liu, J., Bi, J., Liu, X., Liu, D., Lyu, J., Liu, M., Verkerk, R., Dekker, M. and Fogliano, V. (2023) Polygalacturonase treatment affects carotenoid absorption from veggie juice. Food Chemistry, 415: 135748.

Liu, K., Zhao, G., He, B., Chen, L., Huang, L. (2012) Immobilization of pectinase and lipase on macroporous resin coated with chitosan for treatment of whitewater from papermaking. Bioresource Technology, 123: 616–619.

Lombard, V., Bernard, T., Rancurel, C., Brumer, H., Coutinho, P. M., Henrissat, B. (2010) A hierarchical classification of polysaccharide lyases for glycogenomics. Biochemical Journal, 432(3): 437-444.

Lombard, V., Golaconda, R. H., Drula, E., Coutinho, P.M., Henrissat, B. (2014) The carbohydrate-active enzymes database (CAZy) in 2013. Nucleic Acid Research, 42: 490-495.

Long, J., Li, X., Xue, L., Xie, Z., Jiao, A., Bai, Y., Zhou, X., Chen, L., Qiu, C., Xu, X., Jin, Z. (2022) Continuous hydrolysis of mango peel pectin for the production of antibacterial pectic oligosaccharides in packed-bed reactor using immobilized polygalacturonase. Food Bioscience, 50: 102117.

Ma, X., Wang, D., Chen, W., Ismail, B.B., Wang, W., Lv, R., Ding, T., Ye, X., Liu, D. (2018) Effects of ultrasound pre-treatment on the enzymolysis of pectin: kinetic study, structural characteristics and anti-cancer activity of the hydrolysates. Food Hydrocolloids, 79: 90–99.

Mahesh, M., Arivizhivendhan, K.V., Maharaja, P., Boopathy, R., Hamsavathani, V., Sekaran, G. (2016) Production, purification and immobilization of pectinase from *Aspergillus ibericus* onto functionalized nanoporous activated carbon (FNAC) and its application on treatment of pectin containing wastewater. Journal of Molecular Catalysis B: Enzymatic, 133: 43–54.

Martínez-Martínez, I., Navarro-Fernández, J., Daniel Lozada-Ramírez, J., García-Carmona, F. and Sánchez-Ferrer, Á. (2008) YesT: a new rhamnogalacturonan acetyl esterase from *Bacillus subtilis*. Proteins: Structure, Function, and Bioinformatics, 71(1): 379-388.

Matsumoto, S., Yamada, H., Kunishige, Y., Takenaka, S., Nakazawa, M., Ueda, M., Sakamoto, T. (2017) Identification of a novel *Penicillium chrysogenum* rhamnogalacturonan rhamnohydrolase and the first report of a rhamnogalacturonan rhamnohydrolase gene. Enzyme and Microbial Technology, 98: 76–85.

Matsunaga, T., Ishii, T., Matsumoto, S., Higuchi, M., Darvill, A., Albersheim, P., O'Neill, M.A. (2004) Occurrence of the primary cell wall polysaccharide rhamnogalacturonan II in pteridophytes, lycophytes, and bryophytes. Implication for the evolution of vascular plants. Plant Physiology, 134: 339–351.

May, C. D. (1990) Industrial pectins: sources, production and applications. Carbohydrate Polymers, 12(1): 79-99.

Méndez-Yañez, A., González, M., Carrasco-Orellana, C., Herrera, R., Moya-León, M.A. (2020) Isolation of a rhamnogalacturonan lyase expressed during ripening of the Chilean strawberry fruit and its biochemical characterization. Plant Physiology and Biochemistry, 146: 411–419.

Mohnen, D., Bar-Peled, M., Somerville, C. (2008) Biosynthesis of Plant Cell Walls. Chapter 5 Biomass Recalcitrance, (eds. Himmel, M.), Blackwell Publishing, Oxford, 94–187.

Mølgaard, A., Kauppinen, S., Larsen, S. (2000) Rhamnogalacturonan acetyl esterase elucidates the structure and function of a new family of hydrolases. Structure, 8: 373–383.

Moreira, L. R. S. (2008) An overview of mannan structure and mannan-degrading enzyme systems. Applied Microbiology and Biotechnology, 79(2): 165.

Morris, G.A., Kök, M.S., Harding, S.E and Adams, G.A. (2010) Polysaccharide drug delivery system based on pectin and chitosan. Biotechnology and Genetic Engineering Reviews, 27: 257-284.

Murad, H. A., Azzaz, H. H. (2011) Microbial pectinases and ruminant nutrition. Research Journal of Microbiology, 6 (3): 246–269.

Mutter, M., Beldman, G., Schols, H. A., Voragen, A. G. J. (1994) Rhamnogalacturonan α-L-Rhamnopyranohydrolase: a novel enzyme specific for the terminal nonreducing rhamnosyl unit in rhamnogalacturonan regions of pectin. Plant Physiology, 106: 241-250.

Mutter, M., Renard, C. M. G. C., Beldman, G., Schols, H. A., Voragen, A. G. J. (1998) Mode of action of RG-hydrolase and RG-lyase toward rhamnogalacturonan oligomers: characterization of degradation products using RG-rhamnohydrolase and RG-galacturonohydrolase. Carbohydrate Research, 311: 155-164.

Muzzamal, H., Latif, Z. (2016) Improvement of *Bacillus* strains by mutation for overproduction of exopolygalacturonases. Indian Journal of Experimental Biology, 54: 509–517.

Nagpal, R., Bhardwaj, N. K., Mahajan, R. (2020) Synergistic approach using ultrafiltered xylano-pectinolytic enzymes for reducing bleaching chemical dose in manufacturing rice straw paper. Environmental Science and Pollution Research, 27 (35): 44637–44646.

Nakamura, A., Furuta, H., Maeda, H., Takao, T., Nagamatsu, Y. (2002) Analysis of the molecular construction of xylogalacturonan isolated from soluble soybean polysaccharides. Bioscience, Biotechnology and Biochemistry, 66(5): 1155-1158.

Naran, R., Pierce, M.L., Mort, A.J. (2007) Detection and identification of rhamnogalacturonan lyase activity in intercellular spaces of expanding cotton cotyledons. Plant Journal, 50 (1): 95–107.

Naumoff, D.G., Dedysh, S.N. (2012) Lateral gene transfer between the Bacteroidetes and Acidobacteria: the case of α-L-rhamnosidases. FEBS Letters, 586 (21): 3843–3851.

Navarro-Fernández, J., Martínez-Martínez, I., Montoro-García, S., García-Carmona, F., Takami, H. and Sánchez-Ferrer, A. (2008) Characterization of a new rhamnogalacturonan acetyl esterase from *Bacillus halodurans* C-125 with a new putative carbohydrate binding domain. Journal of Bacteriology, 190(4): 1375-1382.

Nelson, D. L., Lehninger, A. L., Cox, M. M. (2008) Lehninger Principles of Biochemistry. Macmillan

Normand, J., Ralet, M.C., Thibault, J.F., Rogniaux, H., Delavault, P., Bonnin, E. (2010) Purification, characterization, and mode of action of a rhamnogalacturonan hydrolase from *Irpex lacteus*, tolerant to an acetylated substrate. Applied Microbiology and Biotechnology, 86 (2): 577–588.

Novoa de Armas, H., Verboven, C., De Ranter, C., Desair, J., Vande Broek, A., Vanderleyden, J., Rabijns, A. (2004) *Azospirillum irakense* pectate lyase displays a toroidal fold. Acta Crystallographica Section D: Biological Crystallography, 60 (6): 999–1007.

O'Neill, M. A., Warrenfeltz, D., Kates, K., Pellerin, P., Doco, T., Darvill, A.G., Albersheim, P. (1996) Rhamnogalacturonan-II, pectic polysaccharide in the walls of growing plant cell, forms a dimer that is covalently cross-linked by a borate ester. Journal of Biological Chemistry, 271: 22923-2290.

O'Neill, M. A., York, W. S. (2003) The composition and structure of plant primary cell walls. The Plant Cell Wall. (Ed. Rose J.K.C.) Ithaca, New York: Blackwell Publishing, CRC Press, 1-54.

O'Neill, M., Albersheim, P., Darvill, A. (1990) The pectic polysaccharides of primary cell walls. Methods in Plant Biochemistry, Vol. 2, (Ed. Dey, P.M.), Academic Press, 415–441.

Oosterveld, A., Beldman, G., Searle-van Leeuwen, M. J. F. and Voragen, A. G. F. (2000) Effect of enzymatic deacetylation on gelation of sugar beet pectin in the presence of calcium. Carbohydrate Polymers, 43: 249-256.

Ortiz, G. E., Ponce-Mora, M. C., Noseda, D. G., Cazabat, G., Saravalli, C., López, M. C., Gil, G. P., Blasco, M., Albertó, E. O. (2017) Pectinase production by *Aspergillus giganteus* in solid-state fermentation: optimization, scale-up, biochemical characterization and its application in olive-oil extraction. Journal of Industrial Microbiology and Biotechnology, 44 (2): 197–211.

O'sullivan, A. C. (1997) Cellulose: the structure slowly unravels. Cellulose, 4 (3): 173-207.

Pan, L., Zhang, Y., Zhang, F., Wang, Z. and Zheng, J. (2023) α-l-rhamnosidase: production, properties, and applications. World Journal of Microbiology and Biotechnology, 39(7): 1-13.

Patel, V.B., Chatterjee, S. and Dhoble, A.S. (2022) A review on pectinase properties, application in juice clarification, and membranes as immobilization support. Journal of Food Science, 87(8): 3338-3354.

Patidar, M.K., Nighojkar, A., Nighojkar, S., Kumar, A. (2016) Purification and characterization of pectin methylesterase produced in solid state fermentation by *Aspergillus tubingensis*. Biotechnology Journal International, 21: 1–10.

Pedrolli, D.B., Carmona, E.C. (2014) Purification and characterization of a unique pectin lyase from *Aspergillus giganteus* able to release unsaturated monogalacturonate during pectin degradation. Enzyme Research, 353915: 1–7.

Persson, S., Caffall, K.H., Freshour, G., Hilley, M.T., Bauer, S., Poindexter, P., Hahn, M., Mohnen, D., Somerville, C. (2007) The Arabidopsis irregular xylem8 mutant is deficient in glucuronoxylan and homogalacturonan, which are essential for secondary cell wall integrity. The plant Cell, 19 (1): 237-255.

Petersen, T.N., Kauppinen, S. and Larsen, S. (1997) The crystal structure of rhamnogalacturonase A from *Aspergillus aculeatus*: a right-handed parallel β helix. Structure, 5(4): 533-544.

Petkowicz, C. D. O., Reicher, F., Chanzy, H., Taravel, F. R., Vuong, R. (2001) Linear mannan in the endosperm of *Schizolobium amazonicum*. Carbohydrate Polymers, 44(2): 107-112.

Pettolino, F., Walsh, C., Fincher, G., Bacic, A. (2012) Determining the polysaccharide composition of plant cell walls. Nature Protocols, 7: 1590–1607.

Poondla, V., Chikati, R., Kallubai, M., Chennupati, V., Subramanyam, R., Obulam, V.S. (2017) Characterization and molecular modeling of polygalacturonase isoforms from *Saccharomyces cerevisiae*. 3 Biotech, 7 (5): 1–3.

Rahman, M., Choi, Y.S., Kim, Y.K., Park, C., Yoo, J.C. (2019) Production of novel polygalacturonase from *Bacillus paralicheniformis* CBS32 and application to depolymerization of ramie fiber. Polymers, 11 (9): 1525.

Rajulapati, V., Dhillon, A., kumar Gali, K., Katiyar, V., Goyal, A. (2020) Green bioprocess of degumming of jute fibers and bioscouring of cotton fabric by recombinant pectin methylesterase and pectate lyases from *Clostridium thermocellum*. Process Biochemistry, 92: 93–104.

Rajulapati, V., Dhillon, A., Goyal, A. (2021) Enzymatically produced pectic-oligosaccharides from fruit waste of *Citrus reticulata* (mandarin) peels display cytotoxicity against colon cancer cells. Bioresource Technology Reports, 15, 100740.

Rajulapati, V., Goyal, A. (2017) Molecular cloning, expression and characterization of pectin methylesterase (*Ct*PME) from *Clostridium thermocellum*. Molecular Biotechnology, 59: 128–140.

Rajulapati, V., Sharma, K., Dhillon, A., Goyal, A. (2018) SAXS and homology modelling based structure characterization of pectin methylesterase a family 8 carbohydrate esterase from *Clostridium thermocellum* ATCC 27405. Archives of Biochemistry and Biophysics, 641: 39–49.

Ralph, J., Lapierre, C., Marita, J.M., Kim, H., Lu, F., Hatfield, R.D., Ralph, S., Chapple, C., Franke, R., Hemm, M.R., Van Doorsselaere, J., Sederoff, R.R., O'Malley, D.M., Scott, J.T., MacKay, J.J., Yahiaoui, N., Boudet, A., Pean, M., Pilate, G., Jouanin, L., Boerjan, W. (2004) Elucidation of new structures in lignins of CAD- and COMT-deficient plants by NMR. Phytochemistry, 57: 993–1003.

Remoroza, C., Wagenknecht, M., Gu, F., Buchholt, H.C., Moerschbacher, B.M., Schols, H.A., Gruppen. H. (2014) A *Bacillus licheniformis* pectin acetylesterase is specific for homogalacturonans acetylated at O-3. Carbohydrate Polymers, (107): 85–93.

Ridley, B.L., O'Neill, M.A., Mohnen, D. (2001) Pectins: structure, biosynthesis, and oligogalacturonide-related signaling. Phytochemistry, 57: 929-967

Rozeboom, H.J., Beldman, G., Schols, H.A., Dijkstra, B.W. (2013) Crystal structure of endo-xylogalacturonan hydrolase from *Aspergillus tubingensis*. The FEBS Journal, 280 (23): 6061–6069.

Safran, J., Habrylo, O., Cherkaoui, M., Lecomte, S., Voxeur, A., Pilard, S., Bassard, S., Pau-Roblot, C., Mercadante, D., Pelloux, J., Sénéchal, F. (2021) New insights into the specificity and processivity of two novel pectinases from *Verticillium dahliae*. International Journal of Biological Macromolecules, 176: 165-176.

Salem, H., Kirsch, R., Pauchet, Y., Berasategui, A., Fukumori, K., Moriyama, M., Cripps, M., Windsor, D., Fukatsu, T., Gerardo, N.M. (2020) Symbiont digestive

range reflects host plant breadth in herbivorous beetles. Current Biology, 30(15): 2875-2886.

Sathyanarayana, N.G., Panda, T. (2003) Purification and biochemical properties of microbial pectinases—a review. Process Biochemistry, 38: 987-996.

Savary, B.J., Nunez, A., Liu, L.S., Yoo, S. (2003) March. Pectin acetylesterase–analysis and application for sugar beet pectin utilization. In Proceedings of the 1st Joint International Beet Research–American Society of Sugar Beet Technologists Congress. Denver, CO: Beet Sugar Development Foundation.

Schadel, C., Blochl, A., Richter, A., Hoch, G. (2009) Short-term dynamics of non-structural carbohydrates and hemicelluloses in young branches of temperate forest trees during bud break. Tree Physiology, 29: 901–911.

Scheller, H.V., Ulvskov, P. (2010) Hemicelluloses. Annual Review of Plant Biology, 61: 263–289.

Schmidt, U., Koch, Lea., Rentschler, Christine., Kurz, T., Endress, Hans-Ulrich., Karbstein, Heike. (2015) Effect of molecular weight Reduction, acetylation and esterification on the emulsification properties of citrus pectin. Food Biophysics, 10: 217-227.

Schols, H.A., Voragen, A.G.J. (1996) Complex pectins: Structure elucidation using enzymes. Pectins and Pectinases. (Eds. Visser J., Voragen A.J.) Elsevier Science, Amsterdam, 3–19.

Searle-van Leeuwen, M.J.F., Van den Broek, L.A.M., Schols, H.A., Beldman, G. and Voragen, A.G.J. (1992) Rhamnogalacturonan acetylesterase: a novel enzyme from *Aspergillus aculeatus*, specific for the deacetylation of hairy (ramified) regions of pectins. Applied Microbiology and Biotechnology, 38: 347-349.

Sharma, N., Sahoo, D., Rai, A.K. and Singh, S.P. (2022) A highly alkaline pectate lyase from the Himalayan hot spring metagenome and its bioscouring applications. Process Biochemistry, 115: 100-109.

Sheladiya, P., Kapadia, C., Prajapati, V., Ali El Enshasy, H., Abd Malek, R., Marraiki, N., Zaghloul, N.S., Sayyed, R.Z. (2022) Production, statistical optimization, and functional characterization of alkali stable pectate lyase of *Paenibacillus lactis* PKC5 for use in juice clarification. Scientific Reports, 12(1): 7564.

Shevchik, V., Hugouvieux-Cotte-Pattat, N. (1997) Identification of a bacterial pectin acetyl esterase in *Erwinia chrysanthemi* 3937. Molecular Microbiology, 24: 1285–1301.

Shevchik, V., Hugouvieux-Cotte-Pattat, N. (2003) PaeX, a Second Pectin Acetylesterase of *Erwinia chrysanthemi* 3937. Journal of Bacteriology, 185 (10): 3091–3100.

Silva, I. R., Jers, C., Meyer, A. S., Mikkelsen, J. D. (2016) Rhamnogalacturonan I modifying enzymes: an update. New Biotechnology, 33(1): 41-54.

Singh, R.P., Tingirikari, J. M. R. (2021) Agro waste derived pectin poly and oligosaccharides: synthesis and functional characterization. Biocatalysis and Agricultural Biotechnology, 101910.

Somerville, C., Bauer, S., Brininstool, G., Facette, M., Hamann, T., Milne, J., Osborne, E., Paredez, A., Persson, S., Raab, T., Vorwerk, S., Youngs, H. (2004) Toward a systems approach to understanding plant-cell walls. Science 306 (5705), 2206–2211.

Somerville C (2006) Cellulose synthesis in higher plants. Annual Review of Cell and Developmental Biology, 22: 53–78.

Su, J., Wu, T., Cao, S., Pei, J. and Zhao, L. (2023) Screening and characterization of a β-xylosidase from *Bifidobacterium* breve K-110 and its application in the biotransformation of the total flavonoids of epimedium to icariin with α-l-rhamnosidase. Bioorganic Chemistry, 132: 106364.

Tang, X.D., Dong, F.Y., Zhang, Q.H., Lin, L., Wang, P., Xu, X.Y., Wei, W. and Wei, D.Z. (2021) Protein engineering of a cold-adapted rhamnogalacturonan acetylesterase: In vivo functional expression and cinnamyl acetate synthesis. Process Biochemistry, 107: 129-137.

Tang, Y., Wu, P., Jiang, S., Selvaraj, J.N., Yang, S., Zhang, G. (2019) A new cold-active and alkaline pectate lyase from Antarctic bacterium with high catalytic efficiency. Applied Microbiology and Biotechnology, 103 (13): 5231–5241.

Taylor, C.B., Talib, M.F., McCabe, C., Bu, L., Adney, W.S., Himmel, M.E., Crowley, M.F., Beckham, G.T. (2012) Computational investigation of glycosylation effects on a family 1 carbohydrate-binding module. Journal of Biological Chemistry, 287(5): 3147 -3155.

Thakur, B.R., Singh, R.K., Handa, A.K., Rao, M.A. (1997) Chemistry and uses of pectin - A review. Critical Reviews in Food Science and Nutrition, 37 (1): 47-73.

Thakur, J., Gupta, R. (2012) Improvement of tea leaves fermentation through pectinases. Acta Microbiologica et Immunologica Hungarica. 59 (3): 321–334.

Thite, V.S., Nerurkar, A.S. (2020) Crude xylanases and pectinases from *Bacillus* spp. along with commercial cellulase formulate an efficient tailor-made cocktail for sugarcane bagasse saccharification. BioEnergy Research, 13 (1): 286–300.

Tu, T., Luo, H., Meng, K., Cheng, Y., Ma, R., Shi, P., Huang, H., Bai, Y., Wang, Y., Zhang, L., Yao, B. (2015) Improvement in thermostability of an *Achaetomium* sp. strain Xz8 endopolygalacturonase *via* the optimization of charge-charge interactions. Applied and Environmental Microbiology, 81 (19): 6938–6944.

Urbániková, L. (2021) CE16 acetylesterases: *in silico* analysis, catalytic machinery prediction and comparison with related SGNH hydrolases. 3 Biotech, 11 (2): 1–21.

Vasco-Correa, J., Zapata, A.D. (2017) Enzymatic extraction of pectin from passion fruit peel (*Passiflora edulis f. flavicarpa*) at laboratory and bench scale. Lebensmittel-Wissenschaft and Technologie, 80: 280–285.

Viljoen, J. A., Fred, E. B., Peterson, W. H. (1926) The fermentation of cellulose by thermophilic bacteria. The Journal of Agricultural Science, 16(1): 1-17.

Vincken, J.P., Schols, H.A., Oomen, R.J.F.J., Mccann, M.C., Ulvskov, P., Voragen, A.G.J., Visser, R.G.F. (2003) If homogalacturonan were a side chain of

rhamnogalacturonan I. Implications for cell wall architecture. Plant Physiology, 132 (4): 1781–1789.

Vitali, J., Schick, B., Kester, H.C., Visser, J., Jurnak, F. (1998) The three-dimensional structure of *Aspergillus niger* pectin lyase B at 1.7-Å resolution. Plant Physiology, 116 (1): 69–80.

Voragen, A, G. J., Coenen Gerd-Jan, Verhoef, R. P., Schols, H. A. (2009). Pectin, a versatile polysaccharide present in plant cell walls. Structural Chemistry, 20(2): 263–275.

Wade Jr, L.G. (1999) Carbohydrates and Nucleic Acids. In Organic Chemistry, (Ed. Jaworski A.) Prentice-Hall Inc, 5, 1101-1154.

Wang, J., Ling, L., Cai, H., Guo, C. (2020) Gene-wide identification and expression analysis of the PMEI family genes in soybean (Glycine max). 3 Biotech, 10 (8): 1–9.

Wang, X., Lu, Z., Xu, T., Selvaraj, J.N., Yi, L., Zhang, G. (2018) Improving the specific activity and thermo-stability of alkaline pectate lyase from *Bacillus subtilis* 168 for bioscouring. Biochemical Engineering Journal, 129: 74–83.

Willats, W.G.T., Knox, P., Mikkelsen, J.D. (2006) Pectin: new insights into an old polymer are starting to gel. Trends in Food Science and Technology, 17 (3): 97–104.

Wu, P., Luo, F., Lu, Z., Zhan, Z., Zhang, G. (2020a) Improving the catalytic performance of pectate lyase through pectate lyase/Cu_3 $(PO_4)_2$ hybrid nanoflowers as an immobilized enzyme. Frontiers of Bioengineering and Biotechnology, 8: 280.

Wu, P., Yang, S., Zhan, Z., Zhang, G. (2020b) Origins and features of pectate lyases and their applications in industry. Applied Microbiology and Biotechnology, 104: 7247–7260.

Xiao, C., Anderson, C.T. (2013) Roles of pectin in biomass yield and processing for biofuels. Frontiers in Plant Science, 4: 67.

Xu, H., Feng, X., Yang, Q., Zheng, K., Yi, L., Duan, S. and Cheng, L. (2022) Improvement on thermostability of pectate lyase and its potential application to ramie degumming. Polymers, 14(14): 2878.

Yadav, S., Maurya, S.K., Anand, G., Dwivedi, R., Yadav, D. (2017) Purification, characterization and retting of *Crotolaria juncea* fibres by an alkaline pectin lyase from *Fusarium oxysporum* MTCC 1755. 3 Biotech, 7 (2): 1–9.

Yamada, H., Kubo, S., Kunishige, Y., Azuma, H., Kotani, Y., Handa, S., Nakazawa, M., Ueda, M., Hasegawa, Y. and Sakamoto, T. (2021) Homogalacturonan and xylogalacturonan region specificity of self-cloning vector-expressed pectin methylesterases (AoPME1–3) in *Aspergillus oryzae*. Enzyme and Microbial Technology, 150: 109894.

Yapo, B.M. (2011) Pectic substances: from simple pectic polysaccharides to complex pectins - a new hypothetical model. Carbohydrate Polymers, 86 (2): 373–385.

Zandleven, J., Beldman, G., Bosveld, M., Schols, H.A., Voragen, A.G. (2006) Enzymatic degradation studies of xylogalacturonans from apple and potato, using xylogalacturonan hydrolase. Carbohydrate Polymers, 65 (4): 495–503.

Zapata-Zapata, A.D., Hours, R.A., Cavalitto, S.F. (2017) Protopectinase-se from *Geotrichum klebahnii*: studies of the adsorption and pectin-solubilization capacity. Dyna, 84 (201): 216–223.

Zdunek, A., Pieczywek, P.M., Cybulska, J. (2021) The primary, secondary, and structures of higher levels of pectin polysaccharides. Comprehensive Reviews in Food Science and Food Safety, 20 (1): 1101–1117.

Zhang, J., Zhao, L., Gao, B., Wei, W., Wang, H., Xie, J. (2018a) Protopectinase production by *Paenibacillus polymyxa* Z6 and its application in pectin extraction from apple pomace. Journal of Food Processing and Preservation, 42 (1): e13367.

Zhang, X., Guo, J., Yu, Y., Hao, X., Xu, Y., Yao, Q., Guo, Y. (2023) Preparation of Pectin Lyase by fermentation for customized extraction of paper pulp, viscose fiber, and nanofibrillated cellulose from hemp stalks. Industrial Crops and Products, 203: 117137.

Zhang, Z., Dong, J., Zhang, D., Wang, J., Qin, X., Liu, B., Xu, X., Zhang, W., Zhang, Y. (2018b) Expression and characterization of a pectin methylesterase from *Aspergillus niger* ZJ5 and its application in fruit processing. Journal of Bioscience and Bioengineering, 126 (6): 690–696.

Zhen, J., Tan, M., Fu, X., Shu, W., Zhao, X., Yang, S., Xu, J., Ma, Y., Zheng, H., Song, H. (2020) High-level extracellular production of an alkaline pectate lyase in *E. coli* BL21 (DE3) and its application in bioscouring of cotton fabric. 3 Biotech, 10 (2): 1-0.

Zhong, L., Wang, X., Fan, L., Ye, X., Li, Z., Cui, Z., Huang, Y. (2021) Characterization of an acidic pectin methylesterase from *Paenibacillus xylanexedens* and its application in fruit processing. Protein Expression and Purification, 179: 105798.

Zhou, C., Xue, Y., Ma, Y. (2017) Cloning, evaluation, and high-level expression of a thermo-alkaline pectate lyase from alkaliphilic *Bacillus clausii* with potential in ramie degumming. Applied Microbiology and Biotechnology, 101 (9): 3663–3676.

Zhou, C., Ye, J., Xue, Y., Ma, Y. (2015) Directed evolution and structural analysis of alkaline pectate lyase from the alkaliphilic bacterium *Bacillus* sp. strain N16-5 to improve its thermostability for efficient ramie degumming. Applied Environmental Microbiology, 81 (17): 5714–5723.

Zverlov, V. V., Schantz, N., Schmitt-Kopplin, P., and Schwarz, W. H. (2005) Two new major subunits in the cellulosome of *Clostridium thermocellum*: xyloglucanase Xgh74A and endoxylanase Xyn10D. Microbiology, 151: 3395–3401.

Chapter 2

Cloning, expression and purification of a putative pectin acetyl esterase (*Ct*Pae12B) a family 12 carbohydrate esterase (CE12) from *Acetivibrio thermocellus* ATCC 27405

2.1 Introduction

Pectin is one of the major polysaccharide constituents of the plant cell wall (PCW) apart from cellulose and hemicellulose. Pectin together with cellulose and hemicellulose assembles to form a complex network in the PCW (Carpita *et al*., 1993). Owing to the presence of this complex polysaccharide network, PCW performs its structural role by providing strength and protection to the plant body (Vincken *et al*., 2003). Cellulose has a homogenous structure whereas hemicellulose and pectin are heterogeneous. Pectin is a highly heterogeneous structure consisting mainly of D-galactopyranosyluronic acid (D-*GalpA*) and the rest is rhamnose (*Rhap*), galactose (*Galp*), xylose (*Xylp*) and arabinose (*Araf*) (Ridley *et al*., 2001). Pectin is present throughout the plant kingdom and is predominantly found in middle lamella and primary cell wall of PCW (O'Neill *et al*., 1996). Pectin contributes towards several functions of PCW like cell signalling, cell-cell adhesion, pollen tube growth, wall porosity, leaf abscission, upright growth of plants (Ridley *et al*., 2001; Matsunaga *et al*., 2004). Pectin encloses cellulose and hemicellulose in a gel like matrix and therefore, primary degradation of pectin is very important for the invading microbes and pathogens for complete disruption of PCW (Lagaert *et al*., 2009). As described

earlier in Chapter 1, the structural components of pectin are mainly homogalacturonan (HG), rhamnogalacturonan I (RG I) and rhamnogalacturonan II (RG II). The primary structural elements of these components are discussed in details in Chapter 1, section 1.2. Other components like xylogalacturonans and apiogalacturonans are also present but are less abundant (Oomen *et al*., 2002). Many industrial applications of commercial pectin obtained mainly from citrus fruits, apple, potato and sugar beet sources has emerged lately. It is being used in the food industry for its gelling properties in the preparation of jam, jellies and marmalades. Pectin is also used in confectionery, acidified milk products and bakery fillings (May, 1990; Rolin, 2002).

The nutrients available in the plants can be used and recycled by degradation of PCW by the varieties of polysaccharide degrading enzymes present in a diverse group of microorganisms (McKie *et al*., 2001; Ochiai *et al*., 2007). Pectin is a recalcitrant carbohydrate and is readily soluble in water than cellulose and hemicelluloses, making the cell prone to microbial degradation (Ochiai *et al*., 2007). Depending on the structural complexity of pectin, its complete degradation needs the recruitment of glycoside hydrolases, polysaccharide lyases as well as carbohydrate esterases (Shevchik and Hugouvieux-Cotte-Pattat, 2003). Carbohydrate esterases removes the methyl esterification present in the side chain (C-6) position of D-*GalpA* (Buccholt *et al*., 2004) and acetyl esterification present in the side chain (O-2 and O-3) positions of D-*GalpA* (Voragen *et al*., 2009). Removal of the methyl and acetyl groups from the side chains of D-*GalpA* gives better access to polysaccharide lyases and glycoside hydrolases. Polysaccharide lyases cleave their substrates *via* a β-elimination mechanism, generating a double bond between C-4 and C-5 in the residue at the non-reducing end (Hugouvieux-Cotte-Pattat *et al.*, 2014). Glycoside hydrolases cleave the glycosidic bonds via an acid-base catalytic mechanism (Koshland *et al*., 1953). Most

of the PCW degrading enzymes possesses a modular nature and often remains appended to a non-catalytic carbohydrate binding module (CBM) (Davis *et al*., 1995).

Pectin acetyl esterase (PAE, EC 3.1.1.6)/rhamnogalacturonan acetyl esterase (RGAE, EC 3.1.1.86) are a group of enzymes belonging to carbohydrate esterases (CE) categorized under sub family 12 (CAZy database, www.cazy.org). PAE/RGAE hydrolyses the acetyl esters present in the O-2 and O-3 positions of D-*GalpA* and releases pectic acid and acetate (Chandrayan, 2018). Pre-treatment of esterified pectin with PAE/RGAE increases the efficiency of pectin methyl esterase in removal of methyl esterification from C-6 position of D-*GalpA* (Bolvig *et al*., 2003). The de-esterified pectate is further degraded by polygalacturonase, pectate lyase and rhamnogalacturonan lyase (Kashyap *et al*., 2001). PAE thus helps in removing the steric hindrance for better penetration of pectin methyl esterase as well as other main-chain degrading enzymes (Shevchik and Hugouvieux-Cotte-Pattat,1997). Pectin acetyl esterase is produced by a wide variety of plants (Christensen *et al*., 1996) fungi (Searle-van Leeuwen, 1996) and bacteria (Shevchik and Hugouvieux-Cotte-Pattat,1997). Till date, only one PAE and one RGAE have been studied in terms of structures and four PAEs and four RGAEs have been functionally characterized from bacterial sources. Among the most studied PAEs from bacterial sources the optimum pH and temperature is in the range of 7.0 -9.0 and 40-50 °C, respectively (Shevchik and Hugouvieux-Cotte-Pattat, 2003; Bolvig *et al*., 2003, Remoroza, 2014). Among the PAE and RGAE whose crystal structures were deduced, only one i.e., a rhamnogalacturonan acetylesterase (Protein name: RGAE, PDB ID: 1DEO) has been structurally characterized. The crystal structure of RGAE showed an α/β fold which is not similar to the fold found in α/β hydrolases with some significant topological differences (Mølgaard *et al*., 2000). Thus, the members of CE12 sub family are distinct members of the new SGNH (Serine-Glycine-Asparagine-Histidine) fold (Mølgaard *et al*., 2000).

In the present study, *Ct*Pae12B is a single catalytic modular protein with locus tag Cthe_3141 and Genbank accession number ABN54336.1 from *Acetivibrio thermocellus* (a.k.a. *Clostridium thermocellum and Hungateiclostridium thermocellum*) ATCC 27405 was cloned and expressed in *Escherichia coli*. The amino acid sequence of *Ct*Pae12B (229 amino acids) was derived from the full-length amino acid sequence of carbohydrate binding family 6 (831 aa) (Uniprot id: A3DK57). The amino acid sequence of carbohydrate binding family 6 was retrieved from NCBI database (https://www.ncbi.nlm.nih.gov/protein/ABN54336.1). The PSI-BLAST analysis of *Ct*Pae12B amino acid sequence revealed its similarity with pectin acetyl esterase (PAE) belonging to carbohydrate esterase family 12 (CE12).

The boundaries for *Ct*Pae12B were identified by submitting the full-length amino acid sequence of carbohydrate binding family 6 in conserved domain database (http://www.ncbi.nlm.nih.gov/cdd/). A molecular architecture of the different domains present in carbohydrate binding family 6 was drawn by using DOG 2.0 (http://dog.biguckoo.org/down.php).

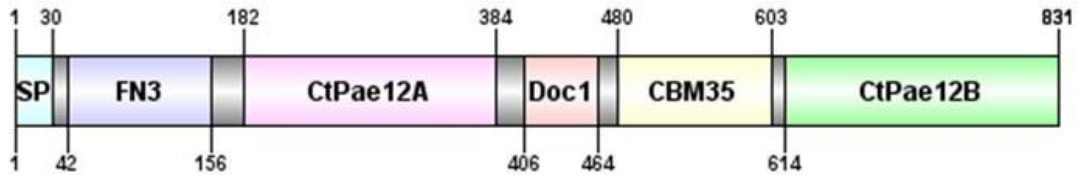

Fig 2.1 Molecular architecture of the full-length amino acid sequence of locus tag Cthe_3141 showing *Ct*Pae12B catalytic module (green) from *Acetivibrio thermocellus* ATCC 27405 developed by using DOG 2.0.

The molecular architecture of modular protein ABN54336.1 from *A. thermocellus* consists of a 30 aa signal peptide, followed by fibronectin type 3 module, (42-156 aa), first catalytic module *Ct*Pae12A (182-384 aa), type 1 dockerin repeat module (406-464 aa), carbohydrate binding module family 35 pectate-lyase like (480-603 aa) and second catalytic module *Ct*Pae12B (614-831 aa) (Fig. 2.1). In the present

study, the gene encoding *Ct*Pae12B was cloned and expressed in *E. coli* and purified by immobilized metal-ion affinity chromatography (IMAC) for further biochemical, functional and structural characterization.

2.2 Materials and Methods

2.2.1 Bacterial strains, plasmid, Chemicals, reagents and kits

The *Escherichia coli* strains DH5α and BL-21 cells used for cloning and expression, respectively, were procured from Novagen, Germany. The expression vector, pET-28a(+), used for both cloning and expression of the gene encoding *Ct*Pae12B was procured from Novagen, Germany. The genomic DNA of *Acetivibrio thermocellus* ATCC 27405 was procured from DSMZ, Germany. Taq DNA polymerase for PCR amplification and the restriction enzymes *NheI* and *XhoI* were acquired from New England Biolabs, UK. The oligonucleotide primers for PCR amplification of genes encoding *Ct*Pae12B were procured from GCC Biotech, India. $MgCl_2$ and dNTPs were procured from GeNei, India. Trizma base (Tris free base). Ethidium bromide, Bradford reagent, DNAse-RNAse free water (pH 8.0), antibiotics kanamycin and components of polyacrylamide gel electrophoresis were obtained from Sigma-Aldrich Co. LLC, USA. Coomassie Brilliant Blue R250 for protein staining, Luria Bertani medium, disodium ethylenediamine tetra acetate salts (EDTA), glucose, sodium hydroxide, pre- stained protein ladder and sodium dodecyl sulphate (SDS) was acquired from Himedia, India whereas, methanol was supplied by Merck, India. The GenElute miniprep, plasmid isolation kit, agarose for preparation of agarose gels for DNA electrophoresis and gel-extraction kit was purchased from was from Sigma-Aldrich, USA. The DNA ladder was purchased from New England Biolabs, USA. T4 DNA ligase and 10x ligase buffers were purchased from Takara Bio Inc., Japan.

2.2.2 PCR amplification of gene encoding *Ct*Pae12B

PCR amplification was performed in a thermal cycler (Applied Biosystems, GeneAmp® PCR System 9700, USA). The gene (654 bp) encoding *Ct*Pae12B, was amplified with the designed oligonucleotide forward and reverse primers using the

Acetivibrio thermocellus ATCC 27405 genomic DNA as template (Table 2.1). The forward primer contains the *NheI* restriction site while reverse primer contains an *XhoI* restriction site. The schematic representation of the amplification of gene encoding *Ct*Pae12B catalytic module is shown in Fig 2.2. The components used for the PCR reaction and the PCR program used for amplification of the gene are tabulated in Table 2.2 and 2.3, respectively.

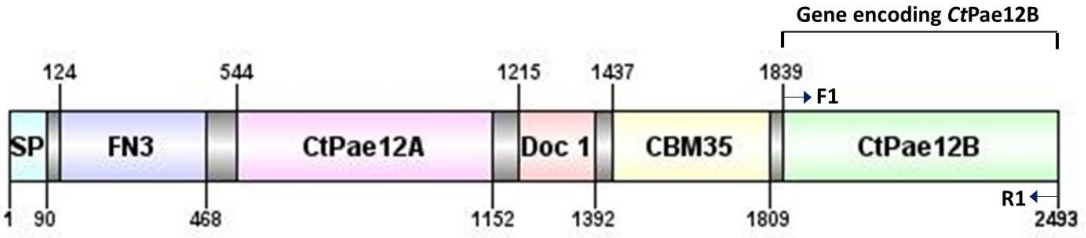

Fig 2.2 Schematic representation showing primers used for PCR amplification of gene encoding *Ct*Pae12B, 654 bp gene sequence (Genbank Accession no. ABN54336.1) from *Acetivibrio thermocellus* ATCC 27504

Table 2.1 Oligonucleotide primer sequences used for cloning of gene encoding *Ct*Pae12B from *Acetivibrio thermocellus*.

Module	Primer name	Primer sequence
*Ct*Pae12B	Forward (F1)	5'-GGTGGTGCTAGCGAAGAAAAAATTACAATTTACATAGCCG-3'
	Reverse (R1)	5'-ACCACCCTCGAGATTGGTTTTCAAATACTTCGCAATATCC-3'

Table 2.2 PCR mixture for amplification of gene encoding *Ct*Pae12B from *Acetivibrio thermocellus.*

PCR components	Volume (µL)	Final concentration
10x reaction buffer	6.0	1x
dNTP mix (2.5 mM)	4.8	0.2 mM
Forward primer (10 µM)	3.6	0.6 µM
Reverse primer (10 µM)	3.6	0.6 µM
Sigma water, pH 8.0	39.6	--
Genomic DNA (86.0 ng/µL)	1.8	2.6 ng
Taq DNA polymerase (5 U/µL)	0.6	0.05 U/µL
Total	60.0	--

Table 2.3 PCR cycles for amplification of gene encoding *Ct*Pae12B from *Acetivibrio thermocellus*.

Steps		Time
I. Denaturation at 95 °C		4 min
II. 35 cycles of	i) Denaturation at 95 °C	20 s
	ii) Annealing at 56 °C	30 s
	iii) Extension at 68 °C	1:00 min
III. Final extension at 68 °C		7:00 min

2.2.3 Agarose gel electrophoresis of PCR amplified products

The PCR amplified gene of interest, encoding *Ct*Pae12B was electrophoresed in 1% (w/v) agarose gel prepared in 1X TAE buffer. 1% (w/v) agarose gel was prepared by dissolving 500 mg of agarose in 50 mL 1X TAE buffer and heated in a microwave oven till the solution turns clear. The solution was allowed to cool to around 50 ºC and 5.0 µL of ethidium bromide (5 mg/mL) was added and mixed well. The solution was then poured on the casting apparatus, comb was placed and the gel was allowed to solidify for about 30 min. A stock solution of TAE buffer was prepared keeping the concentrations of components to 10X (400 mM Tris-acetate, 10 mM EDTA, pH 8.0) (Sambrook and Russell, 2001). The PCR amplified product was mixed with 5X DNA loading dye in a ratio of 4:1 and loaded into the wells of the agarose gel. The gel was run in 1X TAE buffer under constant electric field of 50 volts for about an hour. An ultraviolet illumination system (Biorad XR, USA) was used for visualization of the DNA bands in the agarose gel.

2.2.3.1 Preparation of DNA loading dye

A stock solution of 5X DNA loading dye was prepared by mixing the components mentioned in Table 2.4. The pH of the solution was adjusted to 8.0. While loading into the gel, one part of the 5X loading dye was mixed with 4 parts of the amplified product making the final concentration the loading dye into 1X into the gel.

Table 2.4 Composition of 5X DNA loading dye.

Components	Final concentration (5X)
Tris-HCl	50 mM
Glycerol	25% (w/v)
EDTA	5.0 mM
Bromophenol blue	0.2% (w/v)
Xylene cyanol	0.2% (w/v)

2.2.4 DNA extraction from agarose gel

The PCR amplified DNA was extracted and purified using the gel extraction kit (GenElute™ Gel Extraction Kit, Sigma-Aldrich, USA), according to the protocol provided by the manufacturer as mentioned in section 2.2.4.1. The extracted DNA was eluted in 50 µL elution buffer provided by Gel Extraction Kit.

2.2.4.1 DNA gel extraction protocol

1. The PCR or plasmid DNA band was excised from gel using sharp sterile scalpel and transferred to an empty microcentrifuge tube.
2. Three volume of gel solubilization solution was added to every 1 volume of gel (100 mg ~100 µL) in the microcentrifuge tube and incubated at 50 °C for 10 min (or until the gel slice has completely dissolved).
3. 1 gel volume of 100% isopropanol was added to the microcentrifuge tube and mixed until homogenous.
4. GenElute Binding Column G (DNA binding column) was placed in 2 mL collection tube provided with the kit. 500 µL of the column preparation solution was added to the binding column and centrifuged at 13,000***g*** for 1 min.
5. The above solution containing PCR-amplified or plasmid DNA was added to DNA binding columns and centrifuged at 13,000***g*** for 1 min at room temperature and the flow through was discarded.

6. 700 mL of Wash Solution was added to the binding column and centrifuged at 13,000***g*** for 1 min. Centrifugation was repeated again for 1 min without any additional wash solution to remove excess ethanol.
7. Now the column containing bound DNA was placed in a fresh 1.5 mL sterile microcentrifuge tube. 50 µL of DNAse free water (Sigma-Aldrich Co. LLC, USA) or elution buffer (10 mM Tris-HCl, pH 8.5) was added at the centre of the column. The column was incubated for 2 min at room temperature and centrifuged at 13,000***g*** for 1 min.
9. The PCR amplified or plasmid DNA was eluted from QIAquick spin columns was collected in 1.5 mL sterile microcentrifuge tube. The DNA was stored at -20 ºC for further use.

2.2.5 Preparation of culture medium

For growing the recombinant *E. coli* cells, the most commonly used Luria-Bertani (LB) medium was used by dissolving the ingredients mentioned in Table 2.5, in 800 mL deionized water (Sambrook *et al*., 1989). The final volume was made up to 1 L after adjusting the pH to 7.2. Total medium prepared was divided and transferred in two 1 L conical flasks, 400 mL in each and autoclaved in 121 ºC at 15 psi for 20 min. 200 µL of sterilized and filtered antibiotic, kanamycin (100 mg/mL) was added to each autoclaved and cooled LB medium flask under a sterilized laminar air flow prior to inoculation, making the final concentration of antibiotic 50 µg/mL.

Table 2.5 Composition of Luria-Bertani medium.

Components	Final concentration (%, w/v)
Tryptone	1.0
Yeast extract powder	0.5
Sodium chloride	1.0

2.2.5.1 Preparation of LB-agar medium

Nutrient agar (2%, w/v) was added to LB broth medium and was heated to mix to prepare 100 mL LB-agar medium. The medium was autoclaved as mentioned in section 2.2.5 and 50 µL sterilized and filtered antibiotic, kanamycin (100 mg/mL) was added after cooling of the medium under a laminar air flow. 25 mL of the antibiotic supplemented LB-agar medium were poured into sterilized petri-plates and allowed to solidify for 15-20 min.

2.2.6 Restriction enzyme digestion of the PCR amplified DNA

The purified PCR amplified DNA 80 ng/µL was digested with restriction enzymes (RE) *NheI* and *XhoI* as per the set up described in Table 2.6. The reaction mixtures were incubated in a water bath at 37 ºC for 2 h. The digested PCR fragments were run on 1.0% agarose gel and the desired fragments were extracted using gel extraction kit as mentioned in section 2.2.4.1 and eluted in 50 µL of elution buffer.

Table 2.6 Restriction enzyme digestion set up of PCR amplified DNA.

RE digestion set up	Volume (µL)
10X reaction buffer	2.0
PCR DNAs (80 ng/µL)	12.0
DNAse free water	4.0
*Nhe*I (10 U/µL)	1.0
*Xho*I (10 U/µL)	1.0
Total	20.0

2.2.7 Description of pET-28a(+) vector

The pET vectors were originally constructed by Studier and colleagues (Studier and Moffatt, 1986; Rosenberg, 1987; Studier *et al*., 1990). pET-28a(+) is a translation vector that contain the highly efficient ribosome binding site from the phage T7 major capsid protein. Unique sites sequences of pET-28a(+), numbered by the convention of pBR322 plasmid is shown in the circle map and cloning/expression regions of the coding strand transcribed by T7 RNA polymerase is shown below it in the Fig. 2.3. The

suffix “a” in pET-28 denotes that the reading frame relative to the *BamHI* cloning site recognition sequence, GGATCC, is expressed from the GGA triplet. pET-28a(+) contains a strong bacteriophage T7 lac promoter in N-terminal and Histidine$_6$ tag in both N- and C-terminal, which aids in single step purification using affinity chromatography. The genes cloned in pET vectors remain transcriptionally silent in the uninduced state. Upon induction with IPTG (Isopropyl β-D-1-thiogalactopyranoside), the cloned genes are transcribed by T7 RNA polymerase of the host cell. The positive clones in pET-28a(+) vector are screened on the basis of kanamycin resistance.

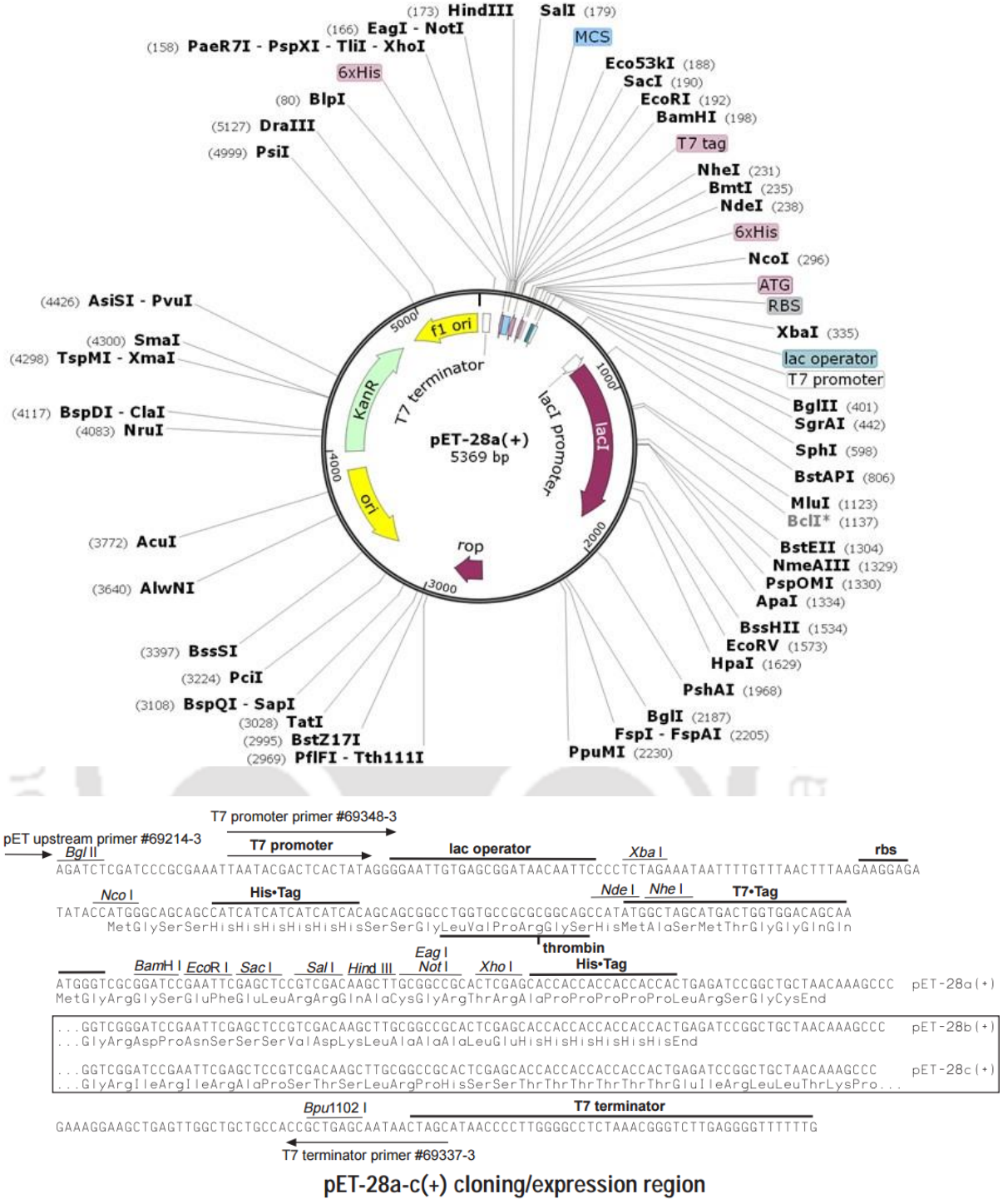

Fig 2.3 Restriction map of the pET-28a(+) expression vector showing multiple cloning site (158-203 bp), restriction enzyme sites, C-terminal His_6-Tag coding sequence (140-157 bp), N-terminal His_6-Tag coding sequence (270-287), T7 promoter (370-386 bp), T7 terminator (26-72 bp), pBR322 origin (3286 bp), kanamycin marker (3995-4807 bp) and a f1 origin (4903-5358). *NheI* cuts at 231 and *XhoI* at 158.

2.2.8 Restriction digestion of pET-28a(+) expression vector for cloning of gene encoding *Ct*Pae12b amplified PCR fragments

For ligation with the PCR amplified gene encoding *Ct*Pae12B, the pET-28a(+) vector (50 ng/µL), 5369 bp was subjected to restriction digestion with *NheI* and *XhoI*. The digestion mixture is mentioned in Table 2.7. The digestion mixture was incubated in a water bath at 37 ºC for 2 h. The *NheI-XhoI* digested pET-28a(+) vector was run on 1% (w/v) agarose gel and purified as described in section 2.2.4.1 and eluted in 50 µL of elution buffer.

Table 2.7 Restriction enzyme digestion set up of pET-28a(+).

RE digestion set up	1X (µL)
10X reaction buffer	2.5
vector pET-28a(+) (50 ng/µL)	20.0
DNAse free water	0.5
*Nhe*I (10 U/µL)	1.0
*Xho*I (10 U/µL)	1.0
Total	25.0

2.2.9 Ligation of *NheI-XhoI* digested PCR fragments into pET-28a(+) vector

The PCR amplified DNA and pET-28a(+) vector digested by restriction enzymes *NheI-XhoI* were ligated using T4 DNA ligase. The molar ratio of insert: vector was kept at 3:1 in the reaction mixture. The amounts of *NheI-XhoI* digested insert DNA of gene encoding *Ct*Pae12B required for cloning was calculated using the following formula (Engler and Richardson, 1982).

$$\frac{\text{ng of vector} \times \text{kb size of insert}}{\text{kb size of vector}} \times \text{insert: vector molar ratio} = \text{ng of insert}$$

$$\frac{55\ \text{ng} \times 0.654\text{kb}}{5.369\text{kb}} \times 3{:}\ 1 = 20.0\ \text{ng of insert (gene encoding } \textit{Ct}\text{Pae12B)}$$

The ligation set up used for digested PCR fragment and pET-28a(+) vector is shown in Table 2.8. The ligation reaction was incubated at 16 ºC for 16 h.

Table 2.8 Ligation set up of PCR inserts and pET-28a(+).

Ligation set up	1X (µL)
2X buffer	5.0
pET-28a(+) vector (22 ng/µL)	2.5
PCR DNA insert (19.0 ng/µL)	1.0
DNAse free water	0.5
T4 DNA ligase (350 U/µL)	1.0
Total	10.0

2.2.10 Preparation of *E. coli* (DH5α) competent cells by calcium chloride method

Day 1

1. 50 µL of culture of *E. coli* DH5α cells from glycerol stock was inoculated into 5.0 mL LB medium (Sambrook *et al*., 1989) contained in a test tube and grown overnight at 37 ºC and 180 rpm.
2. 0.1 M $CaCl_2$, 0.1 M $MgCl_2$ and 0.1 M $CaCl_2$ containing 15% glycerol (v/v) solutions were filter-sterilized by passing through 0.25 µm filter in laminar air flow and kept in refrigerator.

Day 2

3. 1.0 mL culture from day 1 was inoculated into 250 mL LB medium and incubated at 37 ºC with 180 rpm till cell optical density reached 0.4-0.6 at 600 nm.
4. Micro-centrifuge tubes, 50 mL centrifuge tubes (round bottom) and micro tips were autoclaved and kept on ice and placed in a laminar air flow hood.
5. 40 mL culture was transferred aseptically to round bottom centrifuge tubes.
6. The tubes were centrifuged at 4 ºC with 4,000***g*** for 10 min.
7. The step was repeated to centrifuge the entire 250 mL culture.

8. The cell pellet was re-suspended in 3-4 mL sterile, ice-chilled 0.1 M $CaCl_2$ and 0.1 M $MgCl_2$ solution followed by making up the final volume to 20 mL. The cell suspension in centrifuge tubes was kept in ice for 10 min.
9. The tube was centrifuged again at 2,710***g*** at 4 ºC for 10 min.
10. The supernatant was carefully removed and the pellet was re-suspended in 3.0 mL of sterile ice chilled 0.1 M $CaCl_2$ solution.
11. Incubate in ice for 10 min and centrifuge again at 2,710***g*** at 4 ºC for 10 min.
12. The supernatant was carefully removed and the pellet was resuspended in 0.1 M $CaCl_2$ solution containing 15% (v/v) glycerol and 100 µL of competent cells were aliquoted into each 1.5 mL microcentrifuge and kept at -80 ºC for further use.

2.2.11 Transformation of ligated DNA using *E. coli* (DH5α) competent cells

The competent *E. coli* (DH5α) cells were transformed by the heat shock method with the ligated recombinant plasmid containing the gene encoding *Ct*Pae12B. The steps followed in transformation protocol are as follows:

1. The micro-centrifuge tube containing DH5α competent cells (100 µL) was taken out from -80 ºC and kept on ice for 10 min for thawing.
2. 2µL of the recombinant plasmid was added into 100 µL of DH5α competent cells.
3. The tube was gently tapped 4-5 times and incubated on ice for 30 min.
4. The cells were heat shocked at 42 ºC for 42 s.
5. The cells were immediately transferred to ice for 10 min.
6. 1.0 mL of LB medium was added to the transformed cells.
7. The transformed cells were incubated at 37 ºC in a shaking incubator at 180 rpm for 1.5 h.
8. The cells were harvested by centrifugation at 3,000***g*** at 25 ºC for 5 min.

9. 900 µL supernatant was discarded and the cell pellet was then resuspended in remaining 100 µL supernatant.
10. The cells were spread on LB agar plates supplemented with kanamycin at a final concentration 50 µg/mL.
11. The LB agar plates were incubated at 37 ºC for overnight under static condition.
12. The transformation efficiency was calculated using the following equation,

$$\text{Transformation efficiency} = \frac{\text{No. of colonies on LB agar plate} \times \text{Dilution factor}}{\mu\text{g of insert DNA}} = \text{cfu}/\mu\text{g}$$

The colonies with different phenotypes were randomly picked from LB agar plates and inoculated in 10 mL LB medium supplemented with 50 µg/mL kanamycin and incubated at 37 ºC, 180 rpm for 12 h for of plasmid DNA isolation to check for the positive clones.

2.2.12 Isolation of recombinant plasmid DNA

The recombinant plasmid DNA containing the gene encoding *Ct*Pae12B was isolated from *E. coli* (DH5α) cells using plasmid miniprep kit (Sigma-Aldrich Co. LLC, USA) for storage and transformation in expression host. The plasmid DNA isolated using plasmid miniprep kit as described in section 2.2.12.1.

2.2.12.1 Plasmid isolation protocol (Sigma-Aldrich Co. LLC, USA)

1. Total 15 mL of an overnight grown recombinant *E. coli* culture was pelleted by centrifugation at 8,000***g*** for 10 min.
2. Bacterial pellet was resuspended with 200 µL of the Resuspension Solution.
3. Resuspended cells were lysed by adding 200 µL of the lysis solution and by inverting it 6-7 times.

4. The cell debris was precipitated by adding 350 µL of the Neutralization/Binding Solution. The cell debris was precipitated by centrifuging at ≥12,000***g*** or maximum speed for 15 min.
5. The column was prepared by passing 500 µL of the Column Preparation Solution through GenElute Miniprep Binding Column at 12,000***g*** for 1 min.
6. The cleared lysate was transformed from step 3 to the column prepared in step 5 and centrifuged at ≥12,000***g*** for 1 min.
7. 750 µL of the diluted Wash Solution (ethanol added) was added to the column and centrifuge at ≥12,000***g*** for 1 min.
8. Discard flow-through and centrifuge again at ≥12,000***g*** for 10 min, discard flow through.
9. Transfer the Column in a new collection tube and add 40 µL of Elution Solution to the column and centrifuge at ≥12,000***g*** for 1 min. The eluted DNA was stored at -20 ºC for further use.

2.2.13 Screening of recombinant plasmid DNA for identification of positive clones

The purified recombinant plasmid isolated in the last section 2.2.12 was taken in a fresh sterile micro-centrifuge tube for digestion with the restriction enzymes *NheI-XhoI* to check for positive clone. The reaction set up is mentioned in Table 2.9. The reaction mixture was incubated at 37 ºC in a water bath for 1 h. The digested products *viz*. pET-28a(+) vector and the insert DNA of recombinant plasmid were run on 1.0% agarose gel and were visualized under UV transilluminator. The positive clones for the respective recombinant derivatives (insert and vector) were identified based on their respective sizes. Glycerol stocks of *E. coli* (DH5α) cells harbouring the recombinant plasmids was prepared by keeping final concentration of autoclaved glycerol to 20-25%

(v/v). The glycerol stocks in cryo vials of 2 mL were stored at -80 °C and -20 ºC, respectively.

Table 2.9 Restriction enzyme digestion set up of recombinant DNA.

Digestion set up	Volume (µL)
10X buffer	0.5
DNAse free water	1.4
Recombinant plasmid DNA (119 ng/µL)	2.5
*Nhe*I (10 U/µL)	0.3
*Xho*I (10 U/µL)	0.3
Total	5.0

2.2.14 Transformation of recombinant plasmids in *E. coli* BL-21 (DE3) cells for protein expression

50 µL of *E. coli* BL-21 (DE3) competent cells were transformed with 1 µL of the recombinant plasmid DNA isolated by Sigma miniprep method. The protocol for preparation of BL-21 (DE3) competent cells and transformation followed was same as described earlier in section 2.2.10 and 2.2.11, respectively. The BL-21 (DE3) cells containing the recombinant plasmid were spread on LB agar plates with 50 µg/mL kanamycin and grown at 37 ºC for 12 h. The colonies were randomly picked from LB agar plates recombinant cells after 12 h and inoculated into 10.0 mL LB medium supplemented with 50 µg/mL kanamycin and incubated at 37 ºC for 12 h for protein expression.

2.2.15 Expression of recombinant *Ct*Pae12B

Transformed *E. coli* BL-21 (DE3) cells harbouring recombinant plasmids of *Ct*Pae12B was inoculated in 10 mL LB medium containing kanamycin (50 µg/mL) and incubated in a shaking incubator at 37 ºC (180 rpm) till the cell growth reached to mid-exponential phase with absorbance at 600 nm (A_{600}) reached ~0.6. The culture was then induced with IPTG at 1.0 mM final concentration for hyper-expression of recombinant proteins and further incubated at 24 ºC with shaking at 180 rpm for 16 h. The 200 µL

of uninduced and induced cells were centrifuged at 8,000***g*** for 10 min and their supernatant was discarded. The cell pellet was re-suspended in 40 µL distilled water and the protein expression was checked by SDS-PAGE using a 12.5% (w/v) gel.

2.2.16 Sodium dodecyl sulphate-Polyacrylamide gel electrophoresis (SDS-PAGE) analysis of recombinant protein

2.2.16.1 Preparation of SDS-PAGE gel

Based on the respective molecular size, the recombinant proteins are separated on SDS-PAGE gel (Laemmli, 1970; Sambrook *et al*., 1989). The analysis of expression and purification of *Ct*Pae12B was carried out by running SDS-PAGE using a 12.5% (w/v) gel. The resolving gel and stacking gels were prepared by following the protocols from Sambrook *et al*. (1989). The resolving gel was prepared by adding all the components in the order as mentioned in Table 2.10, in a 25 mL beaker, by keeping acrylamide concentration at 12.5% (w/v). Similarly, the stacking gel (4%, w/v) was prepared by dissolving all the components mentioned in Table 2.11. The ingredients used in the preparation of resolving and stacking gels are mentioned in Tables 2.10 and 2.11.

2.2.16.2 Preparation of acrylamide 30% (w/v) solution

The acrylamide solution, 30% (w/v) was prepared by first weighing 0.8 g of bis-acrylamide and transferring it into an amber colour bottle and dissolving in 50 mL of ultra-pure deionized water collected at 18 MΩcm (Millipore, Milli-Q water purification system) using a magnetic stirrer (IKA, C-MAG HS7, Merck, USA). After completely dissolving bis-acrylamide, 29.2 g of acrylamide was added to it and stirred on a magnetic stirrer till the solution became clear. The final volume was adjusted to 100 mL with ultra-pure water by keeping the measuring cylinder (100 mL) wrapped in aluminium foil as acrylamide is light sensitive. The acrylamide solution was then filtered (Whatman No. 1) under dark condition and stored at 4 ºC.

Table 2.10 Composition of SDS-PAGE for preparation of resolving gel.

Components	12.5% (w/v) gel volume (mL)
Acrylamide solution (30%, w/v)	4.2
Deionized water	0.5
SDS (10%, w/v)	1.0
Glycerol (50%, v/v)	1.0
1.5 M Tris-HCl (pH 8.8)	3.3
Ammonium per sulphate (10%, w/v)	0.1
TEMED	0.01

Table 2.11 Composition of SDS-PAGE components for preparation of stacking gel.

Components	4% (w/v) gel volume (mL)
Acrylamide solution (30%, w/v)	0.7
Deionized water	2.8
SDS (10%, w/v)	0.5
0.5 M Tris-HCl (pH 6.8)	1.0
Ammonium per sulphate (10 %, w/v)	0.05
TEMED	0.005

2.2.16.3 Preparation of SDS-PAGE running buffer and sample loading buffer

10X stock solution of running or tank buffer was prepared as described in Table 2.12. The SDS-PAGE gels were run using a 1X running or tank buffer diluted from the 10X stock. The final pH of the buffer was adjusted to 8.3. The 10X buffer was filtered (Whatman, Filter No. 1) and stored at 4 °C. The stock solution of 5X sample loading buffer was prepared by dissolving the components as described in Table 2.13 (Laemmli, 1970). The pH of the buffer was adjusted to 6.8. However, the final concentration while loading to a SDS-PAGE gel was always kept to 1X by mixing 4 volumes of sample (protein) with 1 volume of 5X sample buffer.

Table 2.12 Composition of 10X Tris-Glycine, running or tank buffer.

Components	Final concentration (10X buffer)
Tris-base	0.250 M
Glycine	2.5 M
SDS	1.0% (w/v)

Table 2.13 Composition of 5X sample loading buffer

Components	Final concentration (5X buffer)
Tris-base	62.5 mM
Glycerol	20.0% (v/v)
SDS	2.0% (w/v)
Bromophenol blue	0.025% (w/v)
β-Mercaptoethanol	5.0% (w/v)

2.2.16.4 Preparation of staining and destaining solutions

The staining solution (100 mL) was prepared by dissolving 250 mg or 0.25% (w/v) of Coomassie Brilliant Blue (CBB R-250) dye in 50 mL of deionized water in an amber colour bottle stirring it on a magnetic stirrer for overnight. The solution was filtered (Whatman, Filter No. 1), then 40 mL of methanol and 10 mL of glacial acetic acid were added to finally make the ratio 5:4:1 (deionized water: methanol: glacial acetic acid). The destaining solution was prepared by dissolving deionized water: methanol: glacial acetic in 5:4:1 ratio. The gels were destained by immersing it in destaining solution under gentle shaking condition with change of destaining solution every 30 min, until the protein bands were clearly visible.

2.2.17 Optimization of IPTG concentration for expression of *Ct*Pae12B

The transformed *E. coli* BL-21 (DE3) cells (100 µL) harbouring the recombinant plasmid containing the gene encoding *Ct*Pae12B was inoculated in four different 10 mL LB medium containing kanamycin (50 µg/mL) and incubated in a shaking incubator at 37 ºC and 180 rpm till the cell growth reached to mid-exponential phase with absorbance at 600 nm (A_{600}) reached ~ 0.6. The culture in the four different tubes were then induced with IPTG at 0.25 mM, 0.5 mM, 0.75 mM and 1.0 mM final concentration, for hyper-expression of recombinant proteins and further incubated at 24 ºC with shaking at 180 rpm for 16 h. The 200 µL of uninduced and induced cells were centrifuged at 8,000***g*** for 10 min and their supernatants were discarded. The cell

pellet was resuspended in 40 µL distilled water and the protein expression was checked by SDS-PAGE using 12.5% (w/v) gel.

2.2.18 Purification of recombinant protein, *Ct*Pae12B

The transformed *E. coli* BL-21(DE3) cells containing the recombinant plasmid were grown in 400 mL LB medium (containing 50 µg/mL kanamycin) at 37 ºC to mid-exponential phase (OD = 0.6). To induce recombinant gene expression, IPTG with final concentration 0.5 mM was added to the culture that was further incubated at 24 ºC for 16 h. The cells were pelleted by centrifugation at 8,000***g*** at 4 ºC for 10 min. The cell pellet was resuspended in 50 mM Tris-HCl buffer (pH 7.5) containing 300 mM NaCl. The resuspended cells were subjected to ultra-sonication (Sonics, VCX 750, Vibra cells, USA) for 12 min (10s on and 10s off pulse; 33% amplitude) and the lysed cells were centrifuged at 12,000***g***, 4 ºC for 1 h. The resulting cell supernatant was filtered through 0.45 µm membrane and loaded on to a 5 mL Ni^{2+} ion chelating sepharose column (HiTrap, GE Healthcare, USA). The column bound protein was washed with 30 mL washing buffer (50 mM Tris-HCl buffer, pH 7.5, 300 mM NaCl and 60 mM Imidazole). The bound protein was eluted by using solution containing 50 mM Tris-HCl buffer, pH 7.5, 300 mM NaCl and 300 mM Imidazole. After the use, the column was cleaned using cleaning buffer (50 mM Tris-HCl, pH 8.0, 500 mM NaCl, 50 mM EDTA) and washed with 5 volumes of water and incubated in 1N NaOH at 4 ºC for 2 h. The column was then washed with 50 volumes of water to remove NaOH, and finally stored in 20% (v/v) ethanol at 4 ºC. The eluted enzyme was dialysed (cut off 12-14 kDa) against (50 mM Tris-HCl, pH 7.5, 200 mM NaCl) to remove excess salt and imidazole. The purity and molecular mass of recombinant protein, *Ct*Pae12B was verified by using 12.5% (w/v) SDS-PAGE gel. The gel was stained with Coomassie Brilliant Blue R-250 following conventional procedures and further de-stained for

visualization of the protein bands. The purification fold of *Ct*Pae12B was determined by calculating its enzyme activity against *p*-Nitrophenyl acetate (*p*NPA). The enzymatic activity of *Ct*Pae12B with *p*-nitrophenyl acetate was performed by monitoring the release of *p*-nitrophenol at 410 nm (Wei *et al*., 2014) for 1 min at 65 ºC using a peltier equipped spectrophotometer (Varian, Cary 100-Bio, USA). The standard reaction mixture (1 mL) contained 90 µL of *p*-nitrophenyl acetate (2 mM), 5 µL of *Ct*Pae12B (100 µg/mL) in 905 µL of 50 mM Tris-HCl buffer, pH 8.0. The molar extinction co-efficient (ε), 16,400 M^{-1} cm^{-1} of *p*-nitrophenol was used for calculating the enzymatic activity (Park *et al*., 2021). The amount of enzyme that produced 1 µmol product per min under the reaction conditions was defined as one unit of enzymatic activity. Specific activity was determined by enzymatic activity per mg of the enzyme.

2.2.19 Protein estimation by Bradford and UV method

The concentration of the recombinant protein was determined using the Bradford's method of estimating proteins at a wavelength of 595 nm (Bradford, 1976). Bovine serum albumin (BSA) purchased from Sigma-Aldrich Co. LLC, USA. was used as standard protein. A standard plot of OD at 595 nm versus different concentration of BSA in 10-100 µg/mL was prepared. Commercial Bradford reagent (Sigma-Aldrich Co. LLC, USA) was used for protein content determination. The amount of recombinant protein was estimated using the following equation,

$$[\text{Protein}] = \frac{\Delta A_{595} \times V \times C}{v}$$

Where,

A_{595} = change in absorbance of the sample
V = volume of the protein-buffer mixture (mL)
C = 1 OD equivalent of BSA from standard plot (mg/mL)
v = volume of the enzyme used for assay (mL)

The concentration of the purified protein was also determined from its absorbance at 280 nm using the equation below (Layne, 1957; Stoscheck, 1990). The absorbance was measured after appropriate dilution of the protein using a spectrophotometer (Gene Quant, GE Health care, USA) having a path length of 1 cm. The molar extinction co-efficient for *Ct*Pae12B determined by Expasy protparam was 32320 $M^{-1}cm^{-1}$ (https://web.expasy.org/protparam/).

$$\text{Concentration of protein (mg/mL)} = \frac{\text{Absorbance at 280 nm x Mol. weight (Da)}}{\text{Extinction coefficient } (M^{-1}cm^{-1}) \text{ x Path length (1 cm)}}$$

2.3 Results and Discussion

2.3.1 PCR amplification of *Ct*Pae12B

The PCR amplified gene encoding *Ct*Pae12B, 654 bp, from the genomic DNA of *Acetivibrio thermocellus* ATCC 27405 following the steps mentioned in section 2.2.2 was run on 1.0% (w/v) agarose gel shown in Fig. 2.4. The PCR amplified product displayed a band of size approximately 0.65 kb. The amplified product was further extracted and purified according to the method mentioned in section 2.2.4.1 and stored in -20 ºC for further cloning experiments.

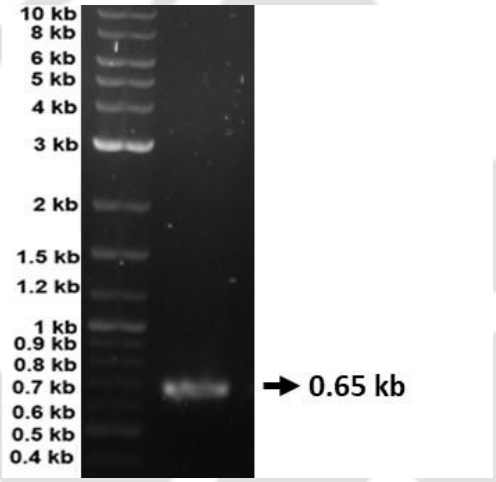

Fig. 2.4 Agarose gel showing PCR amplified fragment of gene encoding *Ct*Pae12B.

2.3.2 Cloning of gene encoding *Ct*Pae12B into pET-28a(+) vector

pET-28a(+) vector and purified PCR amplified gene encoding *Ct*Pae12B were subjected to restriction digestion using *NheI-XhoI* restriction enzymes. The digested insert DNA and vector were purified and were subjected to ligation following the method mentioned in section 2.2.9.

The ligated product was transformed into *E. coli* DH5α competent cells and grown overnight on LB agar plates grown at 37 ºC under stationary condition. The transformation efficiency of *E. coli* DH5α competent cells was 1.2 x10^5 cfu/µg.

2.3.2.1 Isolation of recombinant plasmid DNA and screening of positive clones

Recombinant plasmid DNA from grown colonies after cloning into pET-28a(+) vector grown in LB medium supplemented with 50 µg/mL kanamycin were isolated using Plasmid miniprep kit following the protocol mentioned in section 2.2.12.1. The isolated recombinant plasmid (undigested) as well the digested recombinant plasmid with restriction enzymes *NheI-XhoI* in order to confirm the positive clone were run and visualized after electrophoresis on 1.0% (w/v) agarose gel. The *NheI* and *XhoI* digested plasmid showed the presence of two DNA band equal to the size of pET-28a(+) vector (5.3 kb) and gene encoding *Ct*Pae12B (0.65 kb) confirming the clone of *Ct*Pae12B in to pET-28a(+) vector (Fig. 2.5). Whereas the undigested recombinant plasmid showed a single DNA band of 5.3 kb.

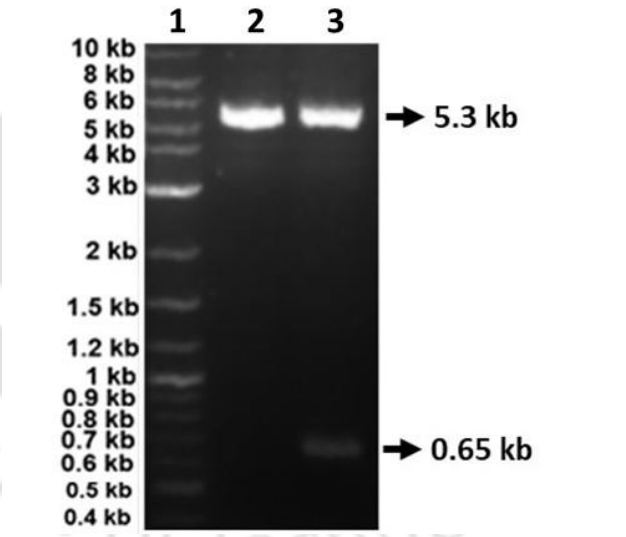

Fig. 2.5 Agarose gel (1.0%, w/v) showing undigested and *NheI-XhoI* digested recombinant plasmid genes, respectively. Lane 1: DNA marker (2-log DNA ladder, NEB, USA), Lane 2: Recombinant plasmid pET-28a(+) (undigested), Lane 3: Digested 0.65 kb fragment of gene encoding *Ct*Pae12B (insert) and vector (5.3 kb, pET-28a(+)).

2.3.3 Expression of recombinant protein *Ct*Pae12B and IPTG concentration optimization for protein expression

Transformed *E. coli* BL-21(DE3) competent cells harbouring the recombinant plasmid was checked for protein expression after induction with 1.0 mM IPTG as mentioned in section 2.2.15. *Ct*Pae12B was seen to be expressed in induced cells (Fig. 2.6A). Expressed *Ct*Pae12B showed the molecular size, approximately, 25 kDa, which was in agreement with the theoretical molecular size, 26 kDa. The minimum final concentration of IPTG required for the expression of *Ct*Pae12B was checked by expressing transformed *E. coli* BL-21(DE3) competent cells with four different concentrations of IPTG. The optimum final concentration of IPTG for *Ct*Pae12B expression was found to be 0.5 mM (Fig 2.6B).

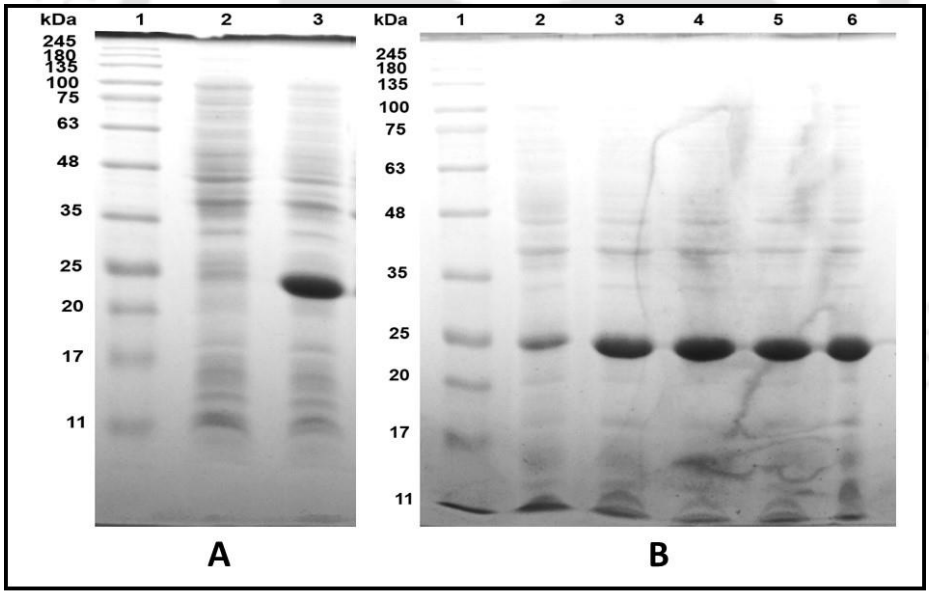

Fig. 2.6 Expression of recombinant *Ct*Pae12B and IPTG concentration optimization for protein expression. A) Expression analysis of *Ct*Pae12B displayed by using 12.5% (w/v) SDS-PAGE gel, 1: Pre-stained protein ladder (Himedia, India); 2: Uninduced cells; 3: Induced cells. B) IPTG concentration optimization, 1: Pre-stained protein ladder (Himedia, India); 2: Uninduced cells; 3: Induced cells (0.25 mM); 4: Induced cells (0.5 mM); 5: Induced cells (0.75 mM) and 6: Induced cells (1.0 mM IPTG).

2.3.4 Purification of recombinant protein *Ct*Pae12B and protein concentration

The recombinant protein *Ct*Pae12B was purified by immobilized metal ion affinity chromatography as described in section 2.2.18 and then dialysed for removal of imidazole and excess salt. The recombinant *Ct*Pae12B expressed as a soluble protein and after purification displayed homogeneous single bands on SDS-PAGE gel, as can be seen in cell free extract (Fig. 2.7). The theoretical molecular mass of the recombinant *Ct*Pae12B including the C-terminal histidine tag was calculated to be 26.0 kDa, which was in close agreement with that observed on SDS-PAGE gel, i.e., 25.0 kDa.

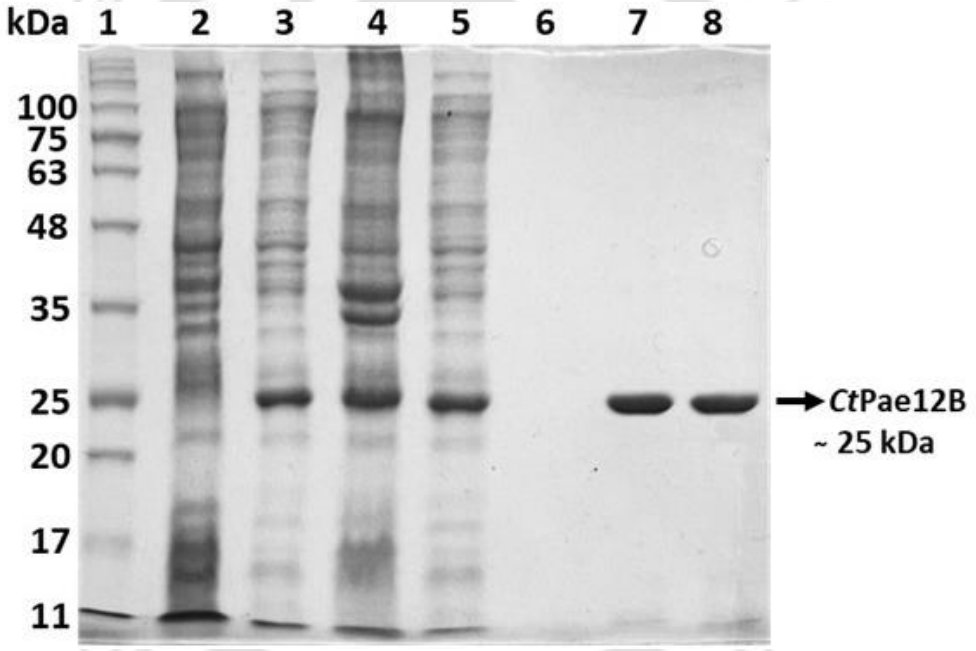

Fig. 2.7 Purification analysis of recombinant *Ct*Pae12B displayed by using 12.5% (w/v) SDS-PAGE gel. 1: Pre-stained protein ladder (Himedia, India); 2: uninduced *E. coli* (DE3) BL-21 cells; 3: induced *E. coli* (DE3) BL-21 cells; 4: cell pellet after sonication; 5: cell free extract after sonication; 6: Last column wash; 7 and 8: purified *Ct*Pae12B protein.

The protein concentration of the purified *Ct*Pae12B obtained from 400 mL culture measured and calculated by both Bradford and UV method as mentioned in section 2.2.19, was 0.9 mg/mL and the total amount of protein obtained was 9 mg. The purification gave the enzymatic activity yield of 84% with a purification fold 18 (Table 2.14).

Table 2.14 Production and purification of *Ct*Pae12B.

Purification step	Volume (mL)	Enzymatic activity (U/mL)	Total activity (U)	Activity yield (%)	Concentration of protein (mg/mL)	Total protein (mg)	Specific activity (U/mg)	Purification fold
Cell free extract	12	34.8 ± 1.7	417	-	16 ± 1	192	2.2	-
IMAC	10	35 ± 1	350	84	0.9 ± 0.2	9	38.9	18

The enzyme activity was calculated by using 2 mM pNPA dissolved in 50 mM Tris-HCl buffer, pH 8.0, at 65 °C for 1 min.

2.4 Conclusion

Sequence analysis of locus tag Cthe_3141 from *Acetivibrio thermocellus* ATCC 27405 showed the presence of an N-terminal signal peptide followed by fibronectin type 3 domain, first family 12 carbohydrate esterase catalytic domain *Ct*Pae12A, followed by type 1 dockerin domain, followed by carbohydrate binding module family 35 and second C-terminal family 12 carbohydrate esterase catalytic domain *Ct*Pae12B. The 654 bp of DNA sequence encoding the *Ct*Pae12B was PCR amplified. The restriction enzyme digested fragments of gene encoding *Ct*Pae12B were ligated with linearized pET-28a(+) vector. The ligated mixture was transformed using *E. coli* (DH5α) competent cells and the positive clone of recombinant *Ct*Pae12B was confirmed by using restriction enzymes *NheI* and *XhoI*. The restriction enzyme digested products were electrophoresed and a band of ~5.3 kb was produced for pET-28a(+) vector and a corresponding band of ~0.65 kb was produced from the insert fragment for gene encoding *Ct*Pae12B. *E. coli* BL-21 competent cells were transformed using the recombinant plasmid DNA for protein expression. The hyper-expression of recombinant protein was achieved by using IPTG as an inducer at a final concentration of 0.5 mM. The hyper-expression of the recombinant *Ct*Pae12B was checked and confirmed by SDS-PAGE analysis. The recombinant *Ct*Pae12B was purified from the sonicated cell free extract by immobilized metal ion chromatography (IMAC) using HiTrap chelating sepharose column. The purified *Ct*Pae12B was expressed as a soluble protein and displayed a molecular size of approximately, 25 kDa, as analysed by SDS-PAGE, which was in agreement with the theoretical molecular mass of 26 kDa. The amount of *Ct*Pae12B protein obtained from 400 mL of culture after IMAC purification was 9 mg with enzyme activity yield 84% and purification fold 18.

References

Bolvig, P.U., Pauly, M., Orfila, C., Scheller, H.V., Schnorr, K. (2003) Sequence analysis and characterization of a novel pectin acetyl esterase from *Bacillus subtilis.* Advances in Pectin and Pectinase Research, (eds. Voragen, F., Schols, H., Visser, R.), Springer, Dordrecht, 315-330.

Bradford, M.M. (1976) A rapid and sensitive method for the quantitation of microgram quantities of protein utilizing the principle of protein-dye binding. Analytical Biochemistry, 72 (1-2): 248-254.

Buchholt, H.C., Christensen, T.M.I.E., Fallesen, B., Ralet, M.C., Thibault, J.F. (2004) Preparation and properties of enzymatically and chemically modified sugar beet pectins. Carbohydrate Polymers, 58: 149–161.

Carpita, N.C., Gibeaut, D.M. (1993) Structural models of primary cell walls in flowering plants: consistency of molecular structure with the physical properties of the walls during growth. Plant Journal, 3: 1–30.

Chandrayan, P. (2018) Biological function(s) and application (s) of pectin and pectin degrading enzymes. Biosciences Biotechnology Research Asia, 15(1): 87-100.

Christensen, T.M.I.E., Nielsen, J.E., Mikkelsen, J.D. (1996) Isolation, characterisation and immunolocalization of orange fruit acetyl esterase. Pectins and pectinases: 723–730.

Davis, G., Henrissat, B. (1995) Structures and mechanisms of glycosyl hydrolases. Structures, 3: 853–859.

Engler, M.J., Richardson, D.C. (1982) DNA ligases. The Enzymes, (ed. Boyer P.D.), Academic Press, San Diego, 15, 3–30.

Hugouvieux-Cotte-Pattat, N., Condemine, G., Shevchik, V.E. (2014) Bacterial pectate lyases, structural and functional diversity. Environmental Microbiology Reports, 6: 427–440.

Kashyap, D.R., Vohra, P.K., Chopra, S., Tewari, R. (2001) Applications of pectinases in the commercial sector: A review. Bioresource Technology, 77: 215–227.

Koshland, D.E. (1953) Stereochemistry and the mechanism of enzymatic reactions. Biological Reviews, 28: 416-436.

Laemmli, U.K. (1970) SDS-page Laemmli method. Nature, 227: 680-685.

Lagaert, S., Beliën, T., Volckaert, G. (2009) Plant cell walls: protecting the barrier from degradation by microbial enzymes. Seminars in Cell and Developmental Biology, 20: 1064–1073.

Layne, E. (1957) Spectrophotometric and turbidimetric methods for measuring proteins. Methods in Enzymology, 3: 447-455.

Matsunaga, T., Ishii, T., Matsumoto, S. (2004) Occurrence of the primary cell wall polysaccharide rhamnogalacturonan II in pteridophytes, lycophytes and

bryophytes: Implications for the evolution of vascular plants. Plant Physiology, 134: 339-351.

May, C.D. (1990) Industrial pectins: Sources, production and applications. Carbohydrate Polymers, 12: 79–99.

McKie, V.A., Vincken, J.P., Voragen, A.G. (2001) A new family of rhamnogalacturonan lyases contains an enzyme that binds to cellulose. Biochemical Journal, 355: 167–177.

Mølgaard, A., Kauppinen, S., Larsen, S. (2000) Rhamnogalacturonan acetylesterase elucidates the structure and function of a new family of hydrolases. Structure, 8: 373–383.

Ochiai, A., Itoh, T., Kawamata, A. (2007) Plant cell wall degradation by saprophytic *Bacillus subtilis* strains: gene clusters responsible for rhamnogalacturonande polymerization. Applied and Environmental Microbiology, 73: 3803-3813.

O'Neill, M.A., Warrenfeltz, D., Kates, K. (1996) Rhamnogalacturonan-II, a pectic polysaccharide in the walls of growing plant cell, forms a dimer that is covalently cross-linked by borate ester in vitro conditions for the formation and hydrolysis of the dimer. Journal of Biological Chemistry, 271: 22923- 22930.

Oomen, R.J., Doeswijk, V.H., Bush, M.S. (2002) In muro fragmentation of the rhamnogalacturonan I backbone in potato (*Solanum tuberosum* L.) results in a reduction and altered location of the galactan and arabinan side-chains and abnormal periderm development. Plant Journal, 30: 403-413.

Park, J.E., Jeong, G.S., Lee, H.W., Kim, H. (2021) Biochemical characterization of a family IV esterase with R-form enantioselectivity from a compost metagenomic library. Applied Biological Chemistry, 64 (1): 1-16.

Remoroza, C., Wagenknecht, M., Gu, F., Buchholt, H.C., Moerschbacher, B.M., Schols, H.A., Gruppen. H. (2014) A *Bacillus licheniformis* pectin acetylesterase is specific for homogalacturonans acetylated at O-3. Carbohydrate Polymers, 107: 85–93.

Ridley, B.L., O'Neill, M.A., Mohnen, D. (2001) Pectins: structure, biosynthesis, and oligogalacturonide-related signalling. Phytochemistry, 57: 929-967.

Rolin, C. (2002) 8 Commercial pectin preparations. Pectins and their Manipulation, (Eds. Seymour G.B., Knox J.P.), CRC Press, Blackwell publishing Ltd., 15, 222-239.

Rosenberg, A.H., Lade, B.N., Chui, D., Lin, S., Dunn, J.J., Studier, F.W. (1987) Vectors for selective expression of cloned DNAs by T7 RNA polymerase. Gene, 56 (1): 125-135.

Sambrook, J., Fritsch, E.F., Maniatis, T. (1989) In (2nd ed.) Molecular Cloning: A Laboratory Manual, Vol. 1. Plainview, Cold Spring Harbor Laboratory Press, Woodbury, New York.

Sambrook, J., Russel, D.W. (2001) In (3rd ed.) Molecular Cloning: A Laboratory Manual, Vol. 1. Cold Spring Harbor Laboratory Press, Woodbury, New York.

Searle-van Leeuwen, M.J.F., Vincken, J-P., Schipper, D., Voragen, A.G.J, Beldman, G. (1996) Acetyl esterases of *Aspergillus niger*: purification and mode of action on pectins. Pectins and Pectinases: 793–798.

Shevchik, V., Hugouvieux-Cotte-Pattat, N. (1997) Identification of a bacterial pectin acetyl esterase in Erwinia chrysanthemi 3937. Molecular Microbiology, 24: 1285–1301.

Shevchik, V., Hugouvieux-Cotte-Pattat, N. (2003) PaeX, a second pectin acetylesterase of *Erwinia chrysanthemi* 3937. Journal of Bacteriology, 185, 10: 3091–3100.

Stoscheck, C.M. (1990) Quantitation of protein. Methods in Enzymology, 182: 50–69.

Studier, F.W., Moffatt, B.A. (1986) Use of bacteriophage T7 RNA polymerase to direct selective high-level expression of cloned genes. Journal of Molecular Biology, 189: 113–130.

Studier, F.W., Rosenberg, A.H., Dunn, J.J., Dubendorff, J.W. (1990) Use of T7 RNA polymerase to direct expression of cloned genes. Methods in Enzymology, 185: 60–89.

Vincken, J.P., Schols, H.A., Oomen, R.J. (2003) If homogalacturonan were a side chain of rhamnogalacturonan I. Implications for cell wall architecture. Plant Physiology, 132: 1781-1789.

Voragen, A.G., Coenen, G.J., Verhoef, R.P., Schols, H.A. (2009) Pectin, a versatile polysaccharide present in plant cell walls. Structural Chemistry, 20: 263–275.

Wei, R., Oeser, T., Zimmermann, W. (2014) Synthetic polyester-hydrolyzing enzymes from thermophilic actinomycetes. Advances in Applied Microbiology, 89: 267-305.

Chapter 3

Computational and solution structure insights of putative pectin acetyl esterase (*Ct*Pae12B)

3.1 Introduction

The polysaccharide network present in the plant cell wall forms the structural unit of the plant body that provides the mechanical strength and support. It also predominantly contributes to the plant defence system that protects them from pathogens. The major components of this polysaccharide network are cellulose, hemicellulose, lignin and pectin (Mohnen *et al*., 2008). Pectin is one of the major components of the plant cell wall that acts as the frontline defence system against pathogenic attacks. Pectin contributes greatly towards the structural complexity of the plant cell wall as it forms a gel-like matrix, interwoven with cellulose and hemicellulose threads (Lagaert *et al*., 2009). Pectin is also known to promote upright growth of the plants (Matsunga *et al*., 2004). Pectin is abundantly found in middle lamella and primary cell wall of plant cells and as described earlier in Chapter 1, pectin is composed of homogalacturonan (HG), rhamnogalacturonan I (RG I) and rhamnogalacturonan II (RG II) (Caffall & Mohnen, 2009). For complete degradation of the plant cell wall, pectic components must be degraded first by pectinases to get access to the cellulose

and hemicellulose networks. Among the three components of pectin, the major industrially and biotechnologically important pectinase is, the HG degrading type (Chandrayan, 2018). HG is a homopolymer of monomeric units, the galactopyranosyluronic acid (*GalpA*) residues linked by α-1,4-linkages and these residues may be methyl-esterified at C-6 position and acetyl esterified at the O-2 and O-3 positions (Voragen *et al*., 2009). As described earlier in Chapter 2, the prior action of the de-esterifying pectinases favours the action of the de-polymerising pectinases for the complete degradation of HG (Shevchik and Hugouvieux-Cotte-Pattat, 2003). Based on the reaction mechanism, the de-polymerising pectinases are of two types: hydrolytic cleavage mechanism followed by polygalacturonases (EC 3.2.1.15) and β-elimination mechanism followed by pectate lyases (EC 4.2.2.9) and pectin lyases (EC 4.2.2.10) (Hugouvieux-Cotte-Pattat *et al.*, 2014). The de-esterifying enzymes are pectin methyl esterase (EC 3.1.1.11) and pectin acetyl esterase (EC 3.1.1.6) (Shevchik and Hugouvieux-Cotte-Pattat, 2003). The degree of methyl and acetyl esterification of HG depends on the type of source. The degree of methylation (DM) and the degree of acetylation (DAc) are defined as the number of moles of methanol or acetic acid per 100 moles of *GalpA* residues (Morris *et al*., 2010). Acetyl groups present in the side chain of HG can create steric hindrance in the action of other pectin degrading enzymes. Pectin acetyl esterase (PAE), an accessory enzyme de-acetylates HG by catalysing the removal of acetyl groups from the side chains of HG producing pectic acid and acetate, making it accessible for degradation by other microbial pectinases for breakdown of other glycosidic bonds (Shevchik and Hugouvieux-Cotte-Pattat, 2003). PAE together with the concerted action of pectin methyl esterase and other pectin depolymerising enzymes can completely degrade the HG containing the acetyl and methyl substitutions in side chain (Shevchik and Hugouvieux-Cotte-Pattat, 2003). PAE belongs to family

12 of carbohydrate esterases (http://www.cazy.org/). Till date, only two 3-Dimensional crystal structures from family 12 carbohydrate esterases have been solved. One is rhamnogalacturonan esterase, RGAE (PDB ID: 1DEO) (Mølgaard *et al*., 2000) from eukaryotic source, *Aspergillus aculeatus* that hydrolyses the cleavage of acetyl group from RG-II (Searle-van Leeuwen, 1992). The second is a pectin acetyl esterase, YxiM (PDB ID: 2O14) (unpublished data) from prokaryotic source, *Bacillus subtilis* 168 that hydrolyses the acetyl group from HG (Bolvig *et al*., 2003). The reported crystal structure of RGAE showed that it possesses a α/β sandwich structure, which is not identical to the fold possessed by the members of α/β hydrolase family of glycoside hydrolases. Ser-His-Asp forms the catalytic triad which is common to these enzymes causing the hydrolytic cleavage of substrates (Lau and Bruice, 1999). Serine acts as a nucleophile and its function is to form an acyl-enzyme intermediate by entering a transacylation reaction with the substrate, which is later hydrolysed to form the product (Lau and Bruice, 1999).

Acetivibrio thermocellus a.k.a *Clostridium thermocellum* and *Hungateiclostridium thermocellum* is a thermostable gram positive, anaerobic, rod-shaped bacterium that contains extracellular multi-enzyme complex (cellulosome) on its cell surface (Akinosho *et al*., 2014). The cellulosome produces over 20 distinct industrially important enzymes required for the decomposition of lignocellulosic compounds (Zverlov *et al.,* 2005). These enzymes are modular in nature, tolerant and efficient for bioconversion which constitutes this host organism for many consolidated bioprocessing products. A gene encoding a putative pectin acetyl esterase (*Ct*Pae12B) of carbohydrate esterase family 12 from *Acetivibrio thermocellus* was earlier cloned, expressed and purified exhibiting a single band soluble protein of molecular mass approximately, 25 kDa (Chapter 2). In the current study, *Ct*Pae12B was structurally

characterised by subjecting its amino acid sequence to 3D homology modeling. The 3D homology structure was refined and validated and subjected to molecular dynamic simulation. The catalytically important amino acid residues of *Ct*Pae12B were analysed by docking studies with various suitable ligands. The aqueous state of the *Ct*Pae12B structure was also studied by small angle x-ray scattering (SAXS) and dynamic light scattering (DLS).

3.2 Materials and methods

3.2.1 Amino acid sequence search and analysis of *Ct*Pae12B

The amino acid sequence of the single catalytic module (here named as *Ct*Pae12B), a family 12 carbohydrate esterase (229 aa) was derived from the full-length amino acid sequence of carbohydrate binding family 6 (831 aa) with locus tag Cthe_3141 and Genbank accession number ABN54336.1 from *Acetivibrio thermocellus* ATCC 27405 (Uniprot id: A3DK57). The amino acid sequence of carbohydrate binding family 6 was retrieved from NCBI database (https://www.ncbi.nlm.nih.gov/protein/ABN54336.1). The boundaries for *Ct*Pae12B were identified by submitting the full-length amino acid sequence of carbohydrate binding family 6 in conserved domain database (http://www.ncbi.nlm.nih.gov/cdd/) and Interproscan (http://www.ebi.ac.uk/interpro/) server analysis. A molecular architecture of the different domains present in carbohydrate binding family 6 was drawn by using DOG 2.0 (http://dog.biguckoo.org/down.php). The PSI-BLAST analysis of *Ct*Pae12B amino acid sequence was also performed against PDB database for analysing the percentage similarity among its homologous proteins (Altschul *et al*., 1997). Multiple sequence alignment (MSA) of *Ct*Pae12B with other similar known sequences was carried out by Clustal Omega tool (http://www.ebi.ac.uk/Tools/msa/clustalo/) (Madeira *et al.*, 2019) available at EMBL-EBI services, for identification of conserved, semi-conserved and active-site residues and were viewed by ESPript 3.0 (http://espript.ibcp.fr/ESPript/ESPript/) (Robert and Gouet, 2014). The amino acid sequences of the homologues obtained after PSI-BLAST, YxiM (Uniprot ID: P42304) (PDB ID: 2O14) from *Bacillus subtilis* strain 168 and RGAE (Uniprot id: Q00017) (PDB ID: 1DEO) from *Aspergillus aculeatus* were obtained from PDB database. The other similar sequences of the carbohydrate esterase

family 12 (CE12) homologues, YesY (Uniprot id: O31528) from *Bacillus subtilis* strain 168, YesT (Uniport id: O31523) from *Bacillus subtilis* strain 168, BliPAE (Uniprot id: Q65DF1) from *Bacillus licheniformis* DSM13, and PaeY (Uniprot id: O32563) from *Dickeya dadantii* 3937, were retrieved from Uniprot database (www.uniprot.org) (Morgat *et al*., 2020). The entire amino acid sequence of each of *Ct*Pae12B, RGAE, yesY, yesT and BliPAE were included for MSA, whereas the sequence of YxiM starts at residue 161 and the sequence of PaeY starts at residue 259.

3.2.2 Homology modeling of *Ct*Pae12B

The 3-dimensional model of single catalytic module, *Ct*Pae12B was generated by submitting the query sequence (with start codon and His-tag at C-terminal) in I-TASSER server (https://zhanglab.ccmb.med.umich.edu/I-TASSER/). I-TASSER predicts the structure by generating a large ensemble of structural conformations (Yang and Zhang, 2015). I-TASSER uses the SPICKER program to cluster all the conformations based on pair-wise structure similarity. The final model of *Ct*Pae12B was obtained as a PDB file that was selected on the basis of highest confidence score (C-score). The C-score is a quantitative measure, typically in the range -5 to 2, which is calculated on the basis of the significance score of threading template alignments and the convergence parameters of the structure assembly simulations used for estimation of the prediction accuracy (Zhang, 2008). Based on Root-Mean Square Deviation (RMSD) values between the residues and the Template modeling (TM) score (structural alignment between the query structure and known structures in the PDB ranging from 0 to 1), the closest homology was reported to be with a rhamnogalacturonan acetyl esterase (PDB ID: 1DEO) from *Aspergillus aculeatus* followed by a pectin acetyl esterase (PDB ID: 2O14) from *Bacillus subtilis*. The topology profile of *Ct*Pae12B was generated through PDBSum server (http://www.ebi.ac.uk/thornton-

srv/databases/pdbsum/Generate.html). Different residues forming the active-site, the active-site volume and the active-site mouth area of the ligand binding pocket of *Ct*Pae12B were calculated by using the computed atlas of surface topography of proteins (CASTp 3.0) server (http://sts.bioe.uic.edu/castp/calculation.html), with a default probe radius of 1.4 Å (Tian *et al*., 2018).

3.2.3 Refinement and validation of modeled structure of *Ct*Pae12B

The 3-D model of *Ct*Pae12B generated by I-TASSER was refined by energy minimization server, YASARA (http://www.yasara.org/minimizationserver.html). This server uses YASARA force field to perform energy minimization. The force field uses an energy function based on knowledge-based potential, where, the protein structure is extensively analysed statistically based on the preferable common structural features and the 3D coordinates extracted from known protein structures from PDB database (Kreiger *et al*., 2009). The energy minimized model was validated by assessing the various structural parameters by using structural analysis and verification server (SAVES v5.0) (http://services.mbi.ucla.edu/SAVES/). The quality assessment of the modeled structure was also carried out by Ramachandran plot using Rampage server. (http://mordred.bioc.cam.ac.uk/~rapper/rampage.php) (Lovell *et al.*, 2003). The statistical Z-score deviation of the modeled structure based on earlier deposited high resolution PDB and NMR structures was calculated using ProSA server (https://prosa.services.came.sbg.ac.at/ prosa.php) (Wiederstein and Sippl, 2007). The thermal stability of the amino acid residues was predicted by I-TASSER server based on normalized B-factor. Template based assignment and profile-based predictions are used to predict the normalized B-factor profile (BFP) of all the residues or atoms present in the protein (Yang *et al*., 2016).

3.2.4 Secondary structure prediction of *Ct*Pae12B

The secondary structural elements (α-helixes, β-sheets and random coils) of *Ct*Pae12B were predicted by web based servers for secondary structure prediction, *viz.* Psipred (http://bioinf.cs.ucl.ac.uk/psipred/) (Jones, 1999) and 2Struc (http://2struc.cryst.bbk.ac.uk/twostruc) (Klose *et al.*, 2010) by Dictionary of Secondary Structures of Proteins (DSSP) method. Further, the secondary structure of *Ct*Pae12B modeled structure was analysed by using I-TASSER server. Moreover, the relative surface accessibility of the amino acid residues was predicted by NetSurfP 2.0 (http://www.cbs.dtu.dk/services/NetSurfP/) (Klausen *et al.*, 2019). The secondary structure of *Ct*Pae12B was also determined by circular dichroism (CD) analysis with purified *Ct*Pae12B at a concentration of 20 µM in 50 mM Tris-HCl buffer of pH 7.5. The CD spectrum at far-UV (190-240 nm) was recorded by a spectro-polarimeter (JASCO J-815, Jasco Corporation) at 25 ºC in a quartz cuvette at a scanning rate of 50 nm/min and 1 nm bandwidth. The molar residual ellipticity (MRE, 10^3.deg.cm^2 dmol^{-1}) was calculated with the help of molar residual weight (g/mol) and millidegrees obtained from the recorded spectrum with path length 0.1 cm and protein concentration (g/L). Molar extinction co-efficient (Δε, decilitre mol^{-1}cm^{-1}) was calculated by dividing the MRE values with factor 3298 (Kelly *et al*., 2005). The difference in Δε values was analysed described as a function of wavelength and the percentage estimate of α-helix and β-sheets present in *Ct*Pae12B was estimated by the K2D3 server (http://cbdm-01.zdv.uni-mainz.de/~andrade/k2d3/). The results obtained from CD were compared with the web-based servers' predicted results.

3.2.5 Molecular dynamic simulation of *Ct*Pae12B

The modeled structure of *Ct*Pae12B was subjected to molecular dynamic (MD) simulation by using GROMACS v5.1.4 software (Berendsen *et al*., 1995) on Param-

Ishan (super computer) facility, Indian Institute of Technology, Guwahati, in order to assess the conformational dynamics and stability of the modeled structure. Gromos 53a6 force field was used to estimate the protein forces. The modeled structure was placed in a single point charge (SPC) cubic box with 12609 solvent (water) molecules. The protein charge of *Ct*Pae12B was neutralized by adding one Cl^- counter ion. Two phase equilibrations were carried out to equilibrate the system. The first phase was carried out under an NVT aggregate in isothermal-isochoric conditions for 500 ps with iteration time 2 fs. The second phase was carried out under an NPT aggregate in isothermal-isobaric conditions for 500 ps with iteration time 2 fs (Hess *et al*., 2008). The equilibrated MD simulation system was used for final MD simulation and was carried out for 100 ns with iteration time 2 fs. The modeled structure was analyzed as a time dependant function throughout the simulation to assess its stability in the solvent system. The variations of the protein backbone of *Ct*Pae12B were evaluated by root mean square deviation (RMSD) and root mean square fluctuation (RMSF) of the amino acids by using the commands gmx_mpi rmsd and gmx_mpi rmsf, respectively. The solvent accessible surface area (SASA) and radius of gyration (R_g) were calculated by using the commands gmx_mpi sasa and gmx_mpi gyrate, respectively.

3.2.6 Molecular docking analysis of *Ct*Pae12B

The molecular docking simulation study was performed to demonstrate the molecular interaction and identification of the active-site catalytically important amino acid residues of *Ct*Pae12B with the suitable ligands by using Autodock 4.2.1 (Morris *et al*., 2009) linked with the viewer MGLTools 1.5.6 (http://mgltools. scripps.edu/). The ligands used for docking simulation with *Ct*Pae12B were *p*-Nitrophenyl acetate (*p*NPA), α-Naphtyl acetate (α-NA), D-galacturonic acid (GalA), 2-O-acetyl-D-galacturonic acid (2aGalA) and 3-O-acetyl-D-galacturonic acid (3aGalA). The ligand

files were derived from PubChem database (http://pubchem.ncbi.nlm.nih.gov). All the ligand files were derived in 3D SDF format and converted to PDB format by using Open Babel 2.3.2a software (Boyle *et al*., 2011). The method of docking followed was as described earlier (Sharma *et al*., 2018). The grid points in the x, y and z dimensions of the active-site grid box were 28, 42 and 26. Spacing around the active-site was 0.375 Å. 50 different conformations were generated by using Lamarckian Genetic Algorithm (LGA) for docking simulation of *Ct*Pae12B with the ligands. Out of these 50 clustered docked conformations ranked on the basis of binding energies, the best matching docked conformations of ligands bound to the active-site of *CtPae12B* with least binding energies were analysed further by using UCSF Chimera software (Pettersen *et al*., 2004). The 2D schematic representation for identification of polar and non-polar interaction between protein-ligand docked complexes was analysed by using Ligplot+ program (Laskowski and Swindells, 2011).

3.2.7 Molecular dynamic simulation of ligand bound *Ct*Pae12B

Molecular dynamic (MD) simulation for determining the interaction of *CtPae12B* with the ligand was performed. Based on the least binding energy between ligand and *Ct*Pae12B, the docked complex of *Ct*Pae12B with *p*-Nitrophenyl acetate (*p*NPA) was selected from section 3.2.6 and was simulated by using GROMACS v5.14. The GROMOS96 43A1 force field was used to calculate the protein forces and PRODRG server was used to generate the ligand topology for *p*NPA. The docked complex was placed in a single point charge (SPC) cubic box with 11,110 solvent (water) molecules. The charge neutralization of *Ct*Pae12B-*p*NPA docked complex was done by adding one Cl^- counter ion. Two phase equilibrations were carried out to equilibrate the system. The first phase was carried out under an NVT aggregate in isothermal-isochoric conditions for 500 ps with iteration time, 2 fs. The second phase

was carried out under an NPT aggregate in isothermal-isobaric conditions for 500 ps with iteration time, 2 fs. The equilibrated MD simulation system was used for final MD simulation and was carried out for 100 ns with iteration time, 2 fs. The interaction of the ligand with the catalytic residues at the active-site in the docked complexes after 100 ns simulation run were visualized by PyMOL V2.3.3 software (Schrödinger, 2017). The complexes were also analysed as a time dependent function throughout the simulation to assess its stability in the solvent system. The RMSD of the ligand bound *Ct*Pae12B after simulation was estimated by gmx_mpi rms command and the fluctuations of the residues in the complex was estimated by gmx_mpi rmsf command. The SASA and radius of gyration (R_g) of the simulated docked complex were also calculated by using the commands gmx_mpi sasa and gmx_mpi gyrate, respectively, and compared with the results obtained after simulation studies of unbound *Ct*Pae12B. The 2-D depiction of the interaction between protein and ligand was prepared with the help of Ligplot+ program.

3.2.8 Small-angle X-ray scattering (SAXS) analysis of *Ct*Pae12B

The small-angle X-ray scattering (SAXS) analysis of *Ct*Pae12B was performed at two different concentrations (3 mg/mL and 5 mg/mL) to analyse its conformational behaviour in solution. SAXS data for *Ct*Pae12B were collected on home source small-angle X-ray scattering system (SAXSpace, Anton Paar). The protein concentrations were measured at A_{280} nm using extinction coefficient 32320 $M^{-1}cm^{-1}$. The scattering pattern was recorded at an incident wavelength of 1.5 Å. A peltier system was used to maintain the temperature to 10 ºC. The scattering pattern of the matched buffer (50 mM Tris-HCl, pH 7.5) was recorded and subtracted from protein samples of each concentration and the absolute scattering pattern of only protein was obtained. The SAXS data analysis program, ATSAS 2.8.4 suite, was used for processing and analysis

of *Ct*Pae12B scattering profiles (Franke *et al*., 2017). The radius of gyration (R_g) of globular and rod shape (R_c) of *Ct*Pae12B for both concentrations were determined by applying the Guinier approximation equation in primusqt (Fournet and Guinier, 1955; Konarev *et al.*, 2003). The persistence length (L) of *Ct*Pae12B was calculated by using the formula [$\sqrt{12}\{(Rg^2) - (Rc^2)\}$] (Goyal *et al*., 2020). The maximum particle dimension (D_{max}) and the distance distribution function plot (P(R)) was evaluated using GNOM software (Svergun, 1992). The molecular mass of *Ct*Pae12B was determined by using the SAXSMoW program (Fischer *et al.*, 2010). DAMMIF program was used to construct 20 *ab initio* models. These 20 independent models were subsequently averaged, clustered and refined by DAMAVER (Volvok and Svergun, 2010) and DAMMIN to create the final *ab initio* shape. The final averaged *ab initio* model was superposed with *Ct*Pae12B modeled structure by using the SUPCOMB program (Kozin and Svergun, 2001). The CRYSOL program was used for fitting of the DAMMIF generated model and homology model of *Ct*Pae12B and were evaluated against experimental SAXS data (Svergun *et al.*, 1995).

3.2.9 Dynamic light scattering (DLS) analysis of *Ct*Pae12B

The apparent hydrodynamic diameter of *Ct*Pae12B at 1mg/mL, 2 mg/mL and 3 mg/mL of *Ct*Pae12B was determined by the Dynamic light scattering (DLS) analysis (Litesizer 500, Particle Analyzer, Anton Paar, Graz, Austria). The protein solutions were centrifuged at 13,000***g*** for 15 min and the supernatant was filtered through a 0.45 µm filter membrane (Fisher Scientific). Measures were taken with 40 mW diode laser of wavelength 658 nm at backscatter angle (175º) at a constant temperature of 25 ºC maintained by a Peltier based temperature controller. The Kalliope software was used for particle size analysis of average of 20 processed runs.

3.2.10 MD simulation of *Ct*Pae12B trimer modeled structure

The modeled structure of *Ct*Pae12B trimer was built by protein-protein docking of the simulated *Ct*Pae12B model by using HDOCK server (http://hdock.phys.hust.edu.cn/). The *Ct*Pae12B-trimer modeled structure was subjected to MD simulation by following the same method as mentioned in section 3.2.5. The modeled trimer structure was placed in a single point charge (SPC) cubic box with 23754 solvent (water) molecules. The protein charge of *Ct*Pae12B trimer model was neutralized by adding three Cl^- counter ions. Two phase equilibrations under NVT aggregate in isothermal-isochoric conditions and NPT aggregate in isothermal-isobaric conditions were carried out sequentially for 500 ps with iteration time 2 fs and then subjected to MD simulation for 100 ns with iteration time 2 fs. The root mean square deviation (RMSD) of *Ct*Pae12B trimer and radius of gyration (R_g) were calculated by gmx_mpi rmsd and gmx_mpi gyrate, respectively.

3.3 Results and Discussion

3.3.1 Sequence analysis of *Ct*Pae12B

The full-length amino acid sequence of carbohydrate binding family 6 (831 aa) was analysed and the domains were drawn using DOG 2.0. The sequence was also analysed by SignalP 3.0 server (http://www.cbs.dtu.dk/services/SignalP-3.0) which showed the presence of N-terminal signal peptide (1-30 aa), followed by fibronectin type 3 module, (42-156 aa), first catalytic module *Ct*Pae12A (182-384 aa), type 1 dockerin repeat module (406-464 aa), carbohydrate binding module family 35 pectate-lyase like (480-603 aa) and second catalytic module *Ct*Pae12B (614-831 aa) (Fig. 3.1). The gene encoding the second catalytic module, *Ct*Pae12B was already cloned earlier, expressed and purified (Chapter 2). *Ct*Pae12B consisting of 229 amino acids (including start codon and His-tag at C-terminal) exhibited a single band of molecular mass, approximately, 25 kDa on SDS-PAGE after purification (Chapter 2). This was in agreement with the molecular mass, 26 kDa, determined by Expasy Protparam server, (https://web.expasy.org/protparam/). The PSI-BLAST analysis of *Ct*Pae12B amino acid sequence against PDB database showed similarity with previously characterized pectin acetyl esterase and rhamnogalacturonan acetyl esterase from CE12 family (Table 3.1). *Ct*Pae12B showed highest percentage identity (34.86%) with pectin acetyl esterase (YxiM) from *Bacillus subtilis* (PDB ID: 2O14) with 92% query cover, followed by rhamnogalacturonan acetyl esterase (RGAE) from *Aspergillus aculeatus* (PDB ID: 1DEO) and mutant RGAE D192N from *Aspergillus aculeatus* (PDB ID: 3C1U). The multiple sequence alignment of *Ct*Pae12B with other homologues of CE12 family was viewed by ESPript 3.0 server (Fig. 3.2). The MSA of *Ct*Pae12B showed 12 α-helices (8α+4η), 7 β-strands and 4 β-turns (TT). As identified and reported in the crystal structure of RGAE (PDB ID: 1DEO) by Mølgaard *et al*., 2000, the residues involved in

catalysis form a catalytic triad comprising Ser9-Asp192-His195 residues, respectively. The results obtained after MSA showed that these three catalytic residues Ser15, Asp187 and His190 corresponding to *Ct*Pae12B amino acid sequence are highly conserved in all the homologues of family 12 carbohydrate esterase depicted by black star (Fig. 3.2). *Ct*Pae12B also displayed the five highly conserved catalytically important residues Ser15, Gly51, Asn83, Asp187 and His190 indicated by black dots (Fig. 3.2). These residues are found in all the members of the serine-glycine-asparagine-histidine (SGNH) hydrolase family of which family 12 carbohydrate esterase is a distinct sub-family (Mølgaard *et al*., 2000; Bolvig *et al.*, 2003).

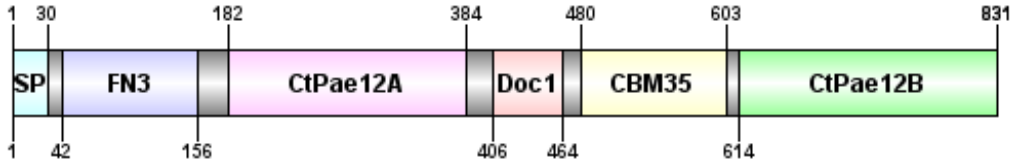

Fig. 3.1 Molecular architecture of the full-length amino acid sequence of locus tag Cthe_3141 showing *Ct*Pae12B catalytic module (Green) from *Acetivibrio thermocellus* ATCC 27405 developed by using DOG 2.0.

Table 3.1 PSI-BLAST analysis of *Ct*Pae12B amino acid sequence against PDB database.

PDB ID	Organism	Enzyme	Enzyme name	Percent identity	Query cover	E-value	Total score
2O14	*Bacillus subtilis*	Pectin acetyl esterase	YxiM	34.86%	92%	7e-79	242
1DEO	*Aspergillus aculeatus*	Rhamnogalacturonan acetyl esterase	RGAE	27.59%	93%	4e-77	233
3C1U	*Aspergillus aculeatus*	Rhamnogalacturonan acetyl esterase	RGAE D192N	27.16%	93%	3e-76	230

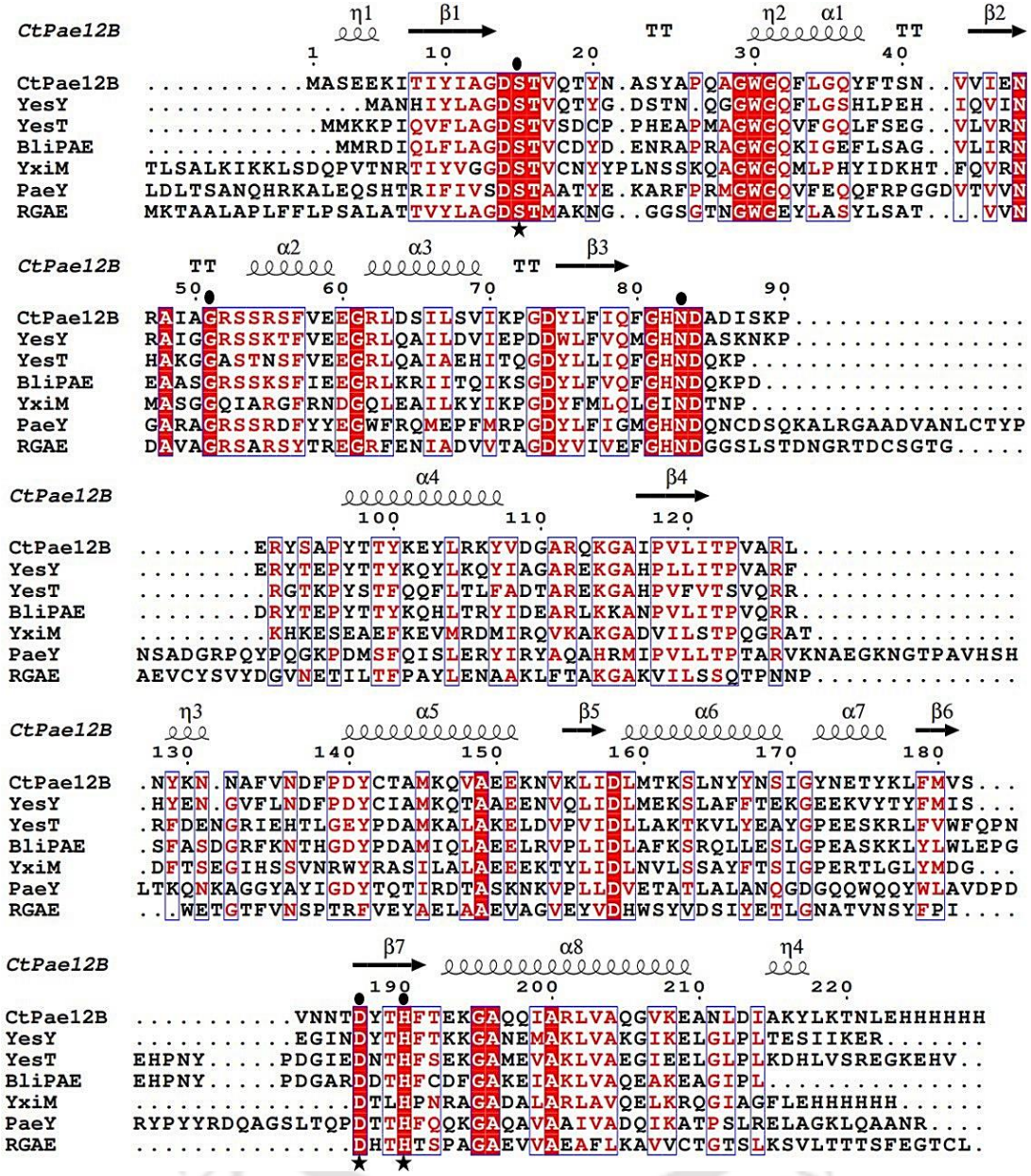

Fig. 3.2 Multiple sequence alignment (MSA) of *Ct*Pae12B with family 12 carbohydrate esterases viz. yesY (Uniprot id: O31528), yesT (Uniprot id: O31523), BliPAE (Uniprot id: Q65DF1), YxiM (Uniprot id: P42304), RGAE (Uniprot id: Q00017), PaeY (Uniprot id: O32563) was performed using ClustalW. The conserved residues are shown in white text with red colour background and semi conserved residues in red colour text shown in blue boxes. The secondary structure elements assignment and the residue numbers correspond to *Ct*Pae12B.

3.3.2 Homology modeling and catalytic mechanism of *Ct*Pae12B

The 3-D modeled structure of *Ct*Pae12B generated by I-TASSER server showed an α/β/α sandwich structure (Fig. 3.3A) which was also found in the reported crystal structure of RGAE (PDB ID: 1DEO) and YxiM (PDB ID: 2O14) of CE12 family. This structure closely resembles the α/β- hydrolase fold, but has a few significant topologically distinguishing features. The residues forming the α3 helix is highly conserved in the α/β hydrolase fold, but not in *Ct*Pae12B and its homologues. Thus, *Ct*Pae12B possesses the SGNH-hydrolase fold, a new hydrolase family of which, CE12 family is a distinct sub family (Mølgaard *et al.,* 2000). The naming and numbering of the residues forming the α-helices, β-strands and loops were identified from the topology profile of *Ct*Pae12B generated by PDBSum server (Fig. 3.3B). The topology plot of *Ct*Pae12B modeled structure showed the presence of 7 β-strands out of which 5 parallel β-strands are involved in the formation of the central β-sheet. This distinguishes the *Ct*Pae12B fold from α/β hydrolase fold that possesses eight central β-sheets (Ollis *et al*., 1992). 12 numbers of α-helices surround the five central β-sheets out of which 4 are η (small length 3_{10}-helix) and 8 medium length α-helices. The catalytic triad of *Ct*Pae12B (identified from MSA with other homologues) is in the order Ser15-His190-Asp187 and lies on the surface (red) of an open catalytic cleft making it accessible to the substrate (Fig. 3.3C). The two loops L1 (green) and L6 (blue) in fig. 3.3C are responsible for the formation of catalytic triad. L1 (14-28 amino acids from N-terminal) lying between β1 and η2, consists of nucleophile Ser15, located on the switch-point of the loop. L6 consists the other two catalytic residues Asp187 and His190. In the *Ct*Pae12B modeled structure, L1 and L6 are observed to bring these three residues closer in the active-site for the formation of catalytic triad. The two catalytic residues (Asp187 and His190) are far away from each other in α/β hydrolase family whereas, they are

only two residues apart in SGNH- hydrolase family (Ollis *et al*., 1992; Mølgaard *et al*., 2000). This signifies that the structure of *Ct*Pae12B is different from the α/β hydrolase fold and belongs to new SGNH- hydrolase family. The superposition of *Ct*Pae12B with the crystal structures of RGAE (PDB ID: 1DEO) and YxiM (PDB ID: 2O14) is shown in Fig. 3.3D. The RMSD value of *Ct*Pae12B superimposed with YxiM was 0.924Å with 163 Cα atoms and with RGAE it was 0.810 Å with 160 Cα atoms, showing an excellent alignment. The superposition also revealed similar orientation of the catalytic residues Ser15-Asp187-His190. The alignment of the catalytic residues (Ser15-Asp187-His190) is almost perpendicular to the central β-sheets in *Ct*Pae12B similar to the other two homologues, YxiM and RGAE of CE12 family as shown in fig. 3.3D, which is a difference with the α/β hydrolase fold, where these three catalytic residues are parallelly aligned (Ollis *et al*., 1992; Mølgaard *et al.,* 2000). The orientation of the catalytic triad of *Ct*Pae12B and the other two homologues YxiM and RGAE, in the active-site is illustrated in fig. 3.3E. In the catalytic triad, (Ser-His-Asp), the imidazole ring of the histidine acts as a general base and catalyses the nucleophilic attack of the serine oxygen on the acyl carbonyl carbon of the substrate, by abstracting the proton from its hydroxyl group, forming an acyl-enzyme intermediate (Lau and Bruice, 1999). The aspartate residue might play a role in correcting the tautomeric orientation of histidine relative to serine and it also might interact with the imidazole ring to stabilize the ion-pair generated between histidine and the acyl-enzyme intermediate during the transition state (Polgar, 2005). The catalytic triad forms hydrogen bonds among themselves for stabilization. The histidine residue (His181) of *Sobemovirus* peptidase forms double and a single hydrogen bond, respectively, with Asp216 and Ser284 in its catalytic triad (Govind *et al*., 2013). In *Ct*Pae12B modeled structure, the bond lengths between the catalytic triad were estimated by using PyMOL v2.3.3. The bond length was found to

be 3.5 Å between Nδ1(His190) and Oδ2(Asp187), 3.1 Å between main chain N (His190) and Oδ1(Asp 187) and 3.5 Å between Nε2(His190) and Oγ(Ser15). The distance range between two nonhydrogen atoms in a hydrogen bond is in the range 2.4-3.5 Å (Berg *et al*., 2002). This showed that the three residues in the catalytic triad of *Ct*Pae12B were within the bond length range for hydrogen bond formation among themselves. The active-site analysis by CASTp server revealed the ligand binding pocket of *Ct*Pae12B (Fig. 3.3F). The computed active-site solvent accessible mouth surface area and volume are 282.75 $Å^2$ and 183.52 $Å^3$, respectively. Amino acid residues forming different subsites in the active-site showed that the catalytically important residues lying in -1 subsite are highly conserved throughout the homologues in CE12 family (Fig. 3.3G). However, the other residues lying in +1 subsite and +2 subsite of the ligand binding pocket, which are catalytically less important are either semi-conserved or less conserved as compared to -1 subsite residues.

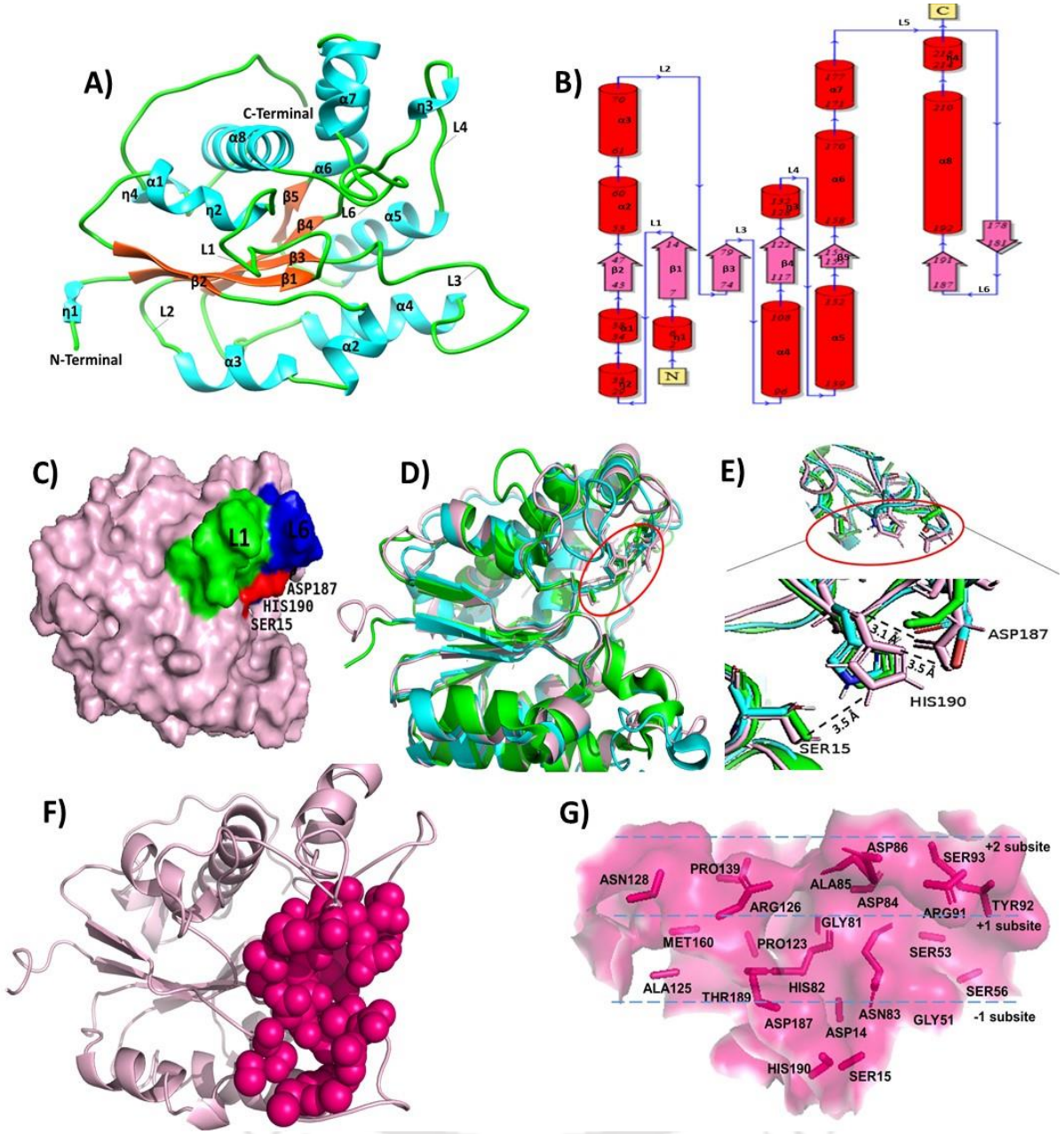

Fig. 3.3 Homology modeling analysis of *Ct*Pae12B. A) 3-D cartoon view of *Ct*Pae12B representing α/β/α structure, B) Topology diagram of *Ct*Pae12B with N- and C-terminal and secondary structure elements (α-helices, β-sheets and turns), C) Surface view of *Ct*Pae12B shows loop1 (L1) in green and loop 6 (L6) in blue forming the catalytic triad (in red), D) Superposition of *Ct*Pae12B modeled structure (pink) with closest homologues YxiM (green) and RGAE (cyan) and catalytic residues in red circle, E) Closer view of the catalytic triad with bond-length profile between the catalytic residues visualized by PyMOL molecular graphics system v2.3.3, F) Active-site volume of *Ct*Pae12B using CASTp server, G) Different residues forming subsites at the active-site.

3.3.3 Refinement and validation of the modeled structure of *Ct*Pae12B

The backbone Ψ and Φ dihedral angles of the amino acid residues of *Ct*Pae12B modeled structure was analysed by Ramachandran plot through RAMPAGE server (Fig. 3.4A). The plot showed 92.5% residues in the favoured region, 6.2% in the allowed region and only 1.3% residues in the disallowed region. The three residues in the disallowed region are Lys89, Ala116 and Thr186. Thr186 lies in L6 that brings the catalytic residues, Asp187 and H190 close to Ser15 in L1, giving this residue (Thr186) a strained conformation. It is also worth mentioning that no residues from L1 was assigned in the disallowed region, which makes it evident that *Ct*Pae12B lacks a nucleophilic elbow motif. Nucleophilic elbow motif is a characteristic motif found in α/β hydrolase family of enzymes, in which the nucleophile is located as a central residue of the motif, bringing it closer to the other two catalytic residues (Asp and His) of the catalytic triad by forming an extremely sharp turn which results in the nucleophile backbone angles (Φ and ψ) in the disallowed region of Ramachandran plot (Ollis *et al*., 1992). ProSA plot for the overall model quality of *Ct*Pae12B showed that the model was error-free and holds position within the X-ray and NMR zones with Z-score of -8.33 (Fig. 3.4B). The local model quality of *Ct*Pae12B assessed by ProSA, the local energy plot as a function of the position of amino acid sequence showed that no part of the modeled structure is erroneous, as no residue has a positive value (Fig. 3.4C). The quality assessment of *Ct*Pae12B was also done by UCLA Saves server, where the structure was mentioned pass by VERIFY 3D as 96.07% residues had average 3D-1D score ≥ 0.2, which indicated the compatibility of amino acids with the modeled structure (Fig. 3.4D). Analysis of the overall quality factor of the *Ct*Pae12B modeled structure by ERRAT server was found to be 84.5%, which further established the excellent quality of *Ct*Pae12B modeled structure (Fig. 3.4E). The normalized B-factor profile (BFP) of

the amino acid residues/atoms of *Ct*Pae12B modeled structure predicted by I-TASSER server (Fig. 3.4F) showed that most of the residues involved in the formation of secondary structural elements, α-helices and β- strands have BFP value lesser than 0, indicating higher stability of the structure. The residues with the predicted BFP values higher than 0, are experimentally less stable structures (Yang *et al*., 2016). The refinement of the model and the results obtained from its quality assessment was justifiable and acceptable for carrying out further studies.

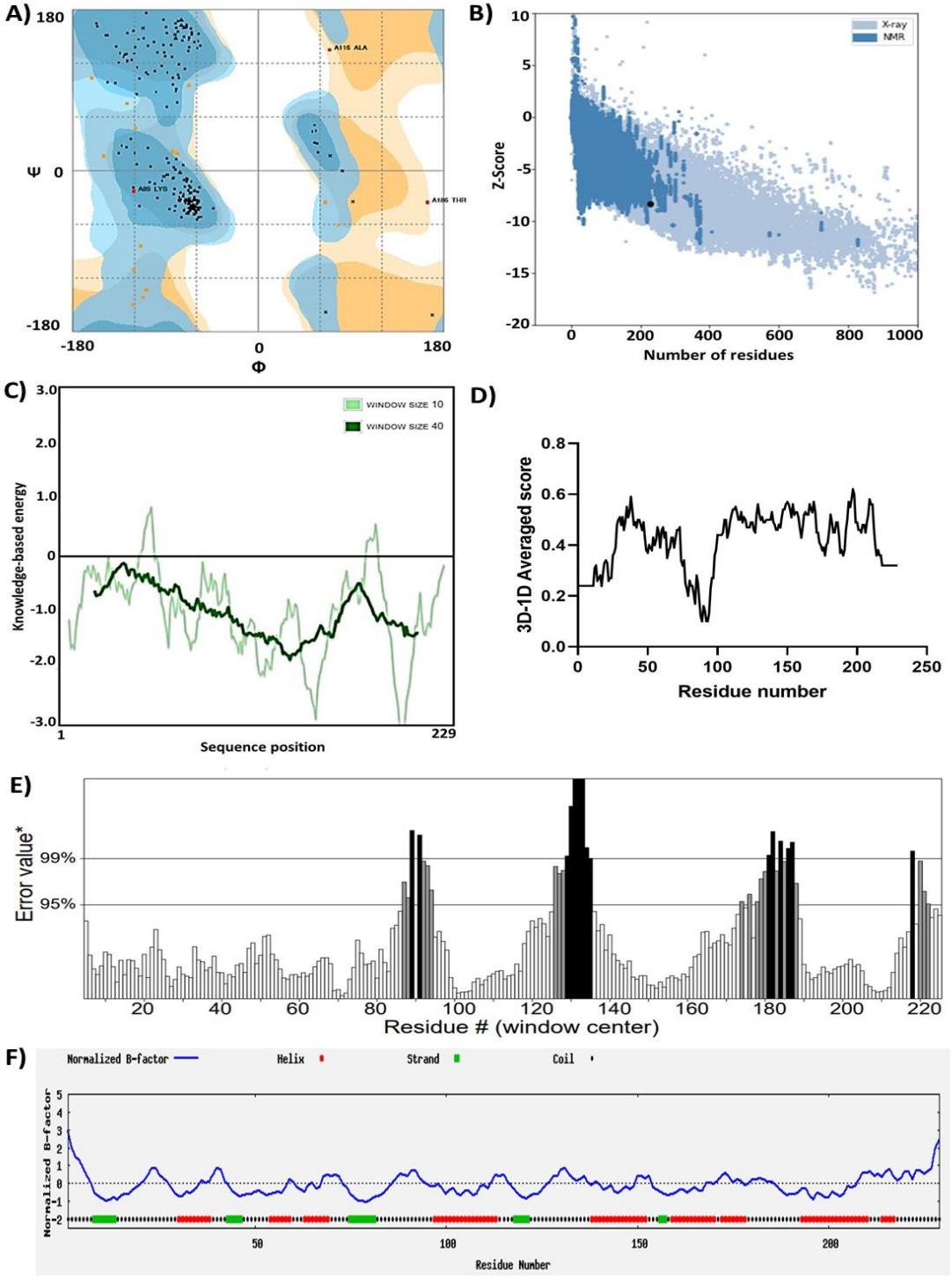

Fig. 3.4 Validation and quality assessment of CtPae12B modeled structure. A) Ramachandran plot generated by RAMPAGE showing favoured, allowed and disallowed regions of the amino acids, B) ProSA plot displays the overall model quality, C) ProSA plot of residue scores, D) VERIFY 3D shows the 3D-1D averaged scores of the amino acid residues, E) ERRAT plot showing the overall quality factor of the modeled structure, F) Normalized B-factor profile indicating thermal stability of the protein residues/atoms predicted by I-TASSER server.

3.3.4 Secondary structure analysis of *Ct*Pae12B

The secondary structure elements of *Ct*Pae12B were predicted from the amino acid sequence by a web-based server PsiPred 4.0. A pictorial representation of the residues involved in formation of helix, strands and coils is shown in fig. 3.5A. It showed that *Ct*Pae12B comprises of 41.4% α-helices, 10.4% β-strands and 48% random coils (Table 3.2). Composition of α-helices, β-sheets and random coils determined by I-TASSER and 2Struc server by DSSP method, from the homology modeled structure are 41.5%, 10%, 48.5% and 38.0%, 13.5%, 48.5%, respectively. The secondary structure results from CD analysis by K2D3 server showed 37.9% α-helices, 16% β-sheets and 46.1% random coils (Fig. 3.5B and Table 3.2). This result corroborated with the secondary structure elements of *Ct*Pae12B predicted by web-based servers. Thus, most of the residues of *Ct*Pae12B folds into α-helices and random coils forming the surface of the protein making it more stable and β-sheets forms the core of the protein. The relative surface accessibility of the residues was also predicted extensively by NetSurfP-2.0 server (Fig. 3.5C). The residues exposed towards the surface of the protein are shown in red and residues buried at 25% threshold, inside the core of the protein are shown in blue (Fig. 3.5C). Solvent accessibility was also determined by I-TASSER on a score from 0 (buried residue at 25% threshold) to 9 (highly exposed residue). 48.5% of residues are buried whereas 51.5% are residues are exposed in the protein surface (Table 3.3). It was observed that around 95% residues forming the β-strands are buried residues forming the protein core and more than 60% residues forming the α-helices and random coils are exposed and lying on the surface of the protein making it highly solvent accessible.

Table 3.2 Secondary structure analysis of *Ct*Pae12B.

Prediction server	α-helices (%)	β-sheets (%)	Random coils (%)
PsiPred	41.4	10.4	48.0
2Struc	38.0	13.5	48.5
I-TASSER	41.5	10.0	48.5
NetSurfP	47.5	12.0	41.2
CD analysis (K2D3)	37.9	16.1	46.1

Table 3.3 Surface accessibility of amino acid residues in *Ct*Pae12B.

Prediction server	Exposed residues (%)	Buried residues (%)
I-TASSER	51.5	48.5
NetSurfP	52.8	47.2

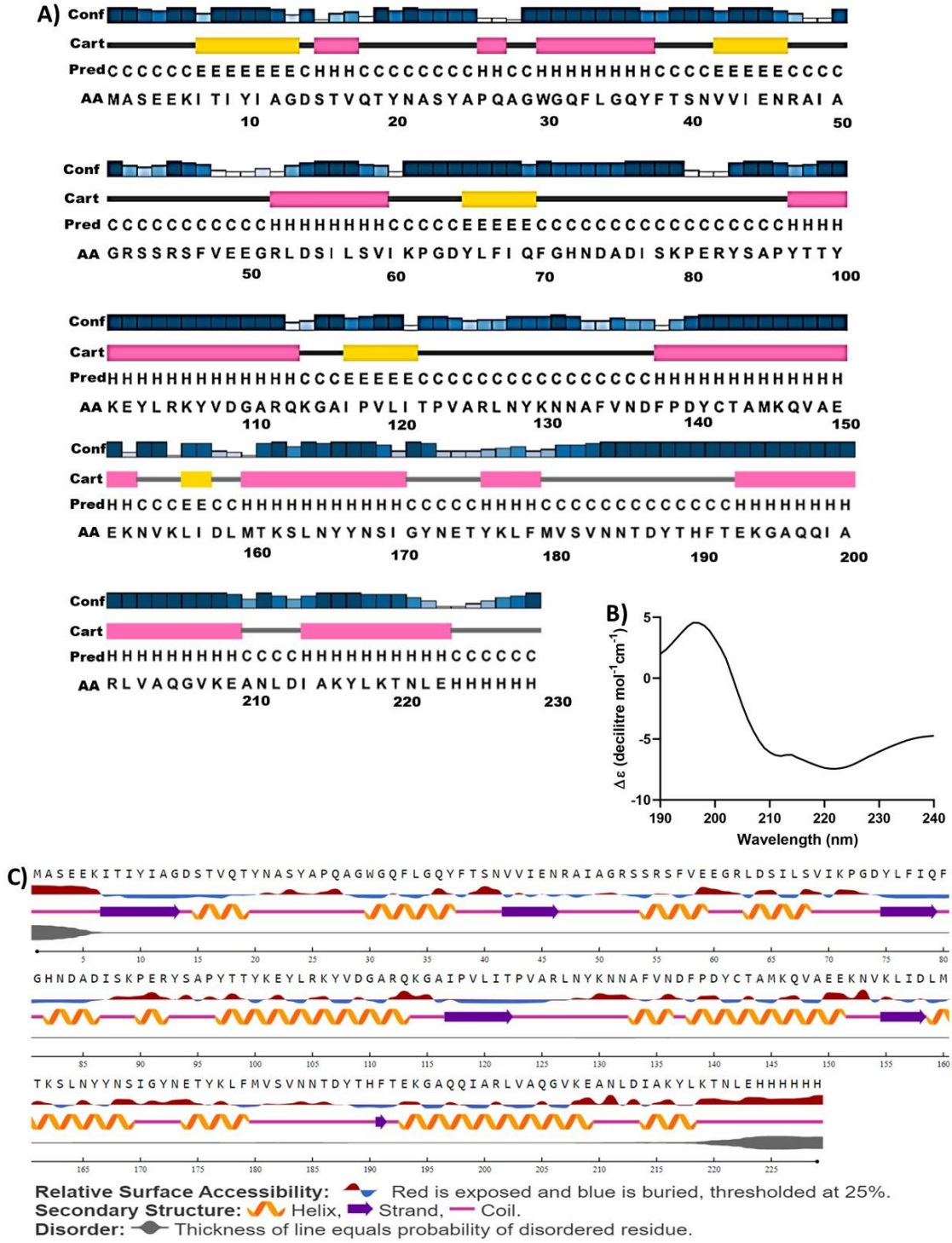

Fig. 3.5 Secondary structure determination of *Ct*Pae12B. A) Secondary structure profile generated by PsiPred, B) Far UV-CD spectrum of *Ct*Pae12B analysed by K2D3 server, C) The secondary structural elements as well as buried and exposed amino acid residues of *Ct*Pae12B predicted by NetSurfP- 2.0.

3.3.5 MD simulation of *Ct*Pae12B modeled structure

The *Ct*Pae12B modeled structure was subjected for molecular dynamics (MD) simulation for 100 ns to analyse the structural dynamics, global compactness and stability of the structure. The root mean square deviation (RMSD) from the original structure was estimated during the entire trajectory from the RMSD values. The resulting RMSD versus time graph showed minimal fluctuation between 0.21 nm to 0.4 nm initially up to 54 ns and then the structure got stabilized after 54 ns up to 100 ns with RMSD between 0.39 nm to 0.33 nm. The average RMSD was found to be 0.36 nm (Fig. 3.6A). The radius of gyration (R_g) remained between 1.78 nm to 1.74 nm throughout the trajectory for up to 100 ns showing excellent global compactness of the structure (Fig. 3.6B). The solvent accessible surface area (SASA) for *Ct*Pae12B reduces from 135 nm^2 to 120 nm^2 up to 40 ns and after that remains relatively unchanged up to 100 ns with average SASA, 118 nm^2 (Fig. 3.6C). The SASA varied only with some minor changes, which suggested that the catalytic residues are not occluded by any deformity and were accessible to the substrate. The root mean square fluctuations (RMSF) of the Cα-atoms of the amino acid residues were calculated after MD simulation to analyse the displacement of atom/atoms from the original structure in various regions of the simulated structure. It was found that the residues present in N- and C- terminal of *Ct*Pae12B are highly flexible. The residues forming secondary structures were found to be less flexible as compared with the ones present in the loop region. The catalytic residues Ser15 lying in L1 and Asp187 and His190 lying in L6 depicted by blue circles, were seen to be comparatively less flexible than the other residues present in L1 and L6 (green circle) (Fig. 3.6D). The results obtained from RMSF values of the amino acid residues after simulation corroborated with the prediction of the inherent fluctuations of atoms/residues by I-TASSER server

mentioned in fig. 3.4F, where the B-factor profile showed lesser mobility of atoms/residues involved in formation of secondary structural elements i.e., α-helices and β-sheets as compared with the other coil/loop regions. The MD simulated structure (yellow) formed after 100 ns was superimposed with *Ct*Pae12B modeled structure (pink) given as input, in Pymol v2.3.3 (Fig. 3.6E). The superposition displayed some variation in the loop regions, but the orientation and region of the catalytic residues were apparently similar (Fig. 3.6E). MD simulation analysis showed that *Ct*Pae12B modeled structure was compact and stable and satisfactory to proceed with further structure analysis.

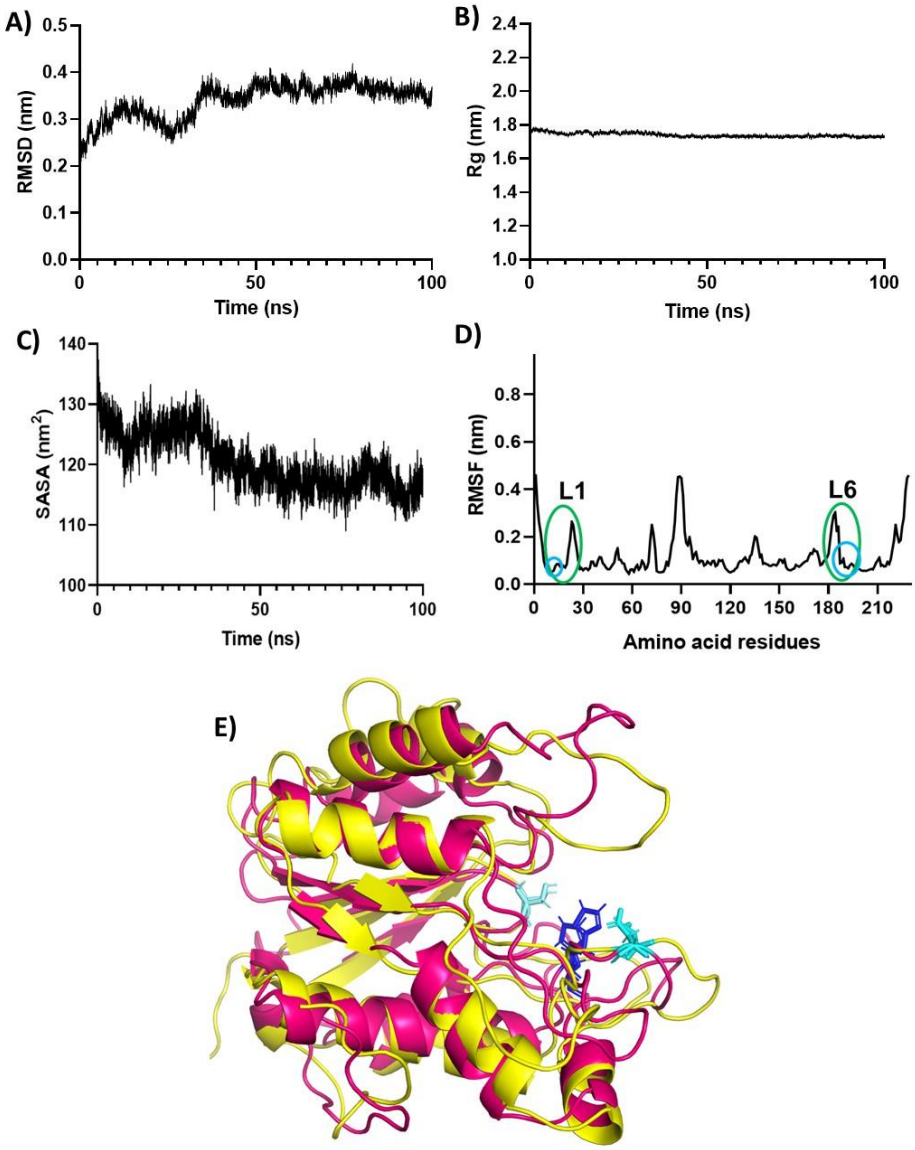

Fig. 3.6 MD simulation analysis of *Ct*Pae12B modeled structure. A) RMSD plot, B) Radius of gyration (Rg) plot, C) SASA plot, D) RMSF plot, E) Superposition of simulated structure (yellow) with homology modeled input structure of *Ct*Pae12B (pink).

3.3.6 Docking analysis of *Ct*Pae12B with ligands

The docking analysis of *Ct*Pae12B carried out by Autodock 4.2.1 tool revealed highest binding affinity with *p*NPA (binding energy, -3.83 kcal/mol) followed by α-NA (-3.69 kcal/mol) as can be seen in Table 3.4. The binding affinity with non-acetylated GalA was the lowest (-1.56 kcal/mol), but with acetylated 3aGalA and 2aGalA it was slightly higher -2.97 kcal/mol and -2.83 kcal/mol, respectively. This showed that

*Ct*Pae12B has higher affinity for acetylated galacturonic acid than non-acetylated galacturonic acid (Table 3.4). The 3D molecular interaction among the active-site residues of the open catalytic cleft of *Ct*Pae12B and the ligands were visualized by UCSF Chimera software (Fig. 3.7). The 2-dimensional interaction of the ligands with the amino acid residues in the catalytic cleft was studied from the depictions obtained from Ligplot software. The *Ct*Pae12B-*p*NPA docked complex is shown in Fig. 3.7A. Two hydrogen bonds were formed between Ser15 and Asn83 of *Ct*Pae12B and *p*NPA. Ser15 formed the hydrogen bond with O1 atom bound to acetyl group of *p*NPA and Asn83 formed hydrogen bond with O4 atom of the acetyl group of *p*NPA. The residues, Ala50, Gly51, His82, Thr189 and His190 of *Ct*Pae12B were involved in forming hydrophobic interactions with *p*NPA (Fig. 3.7B). The docked complex of *Ct*Pae12B with α-NA is shown in Fig. 3.7C. Only one hydrogen bond was formed by Ser15 of *Ct*Pae12B with O-1 atom bound to acetyl group of α-NA. The docking complex was stabilized by other hydrophobic interactions with Ala50, Gly51, His82, Asn83, Thr189 and His190 of *Ct*Pae12B (Fig. 3.7D). The docking conformation of different residues of *Ct*Pae12B with non-acetylated GalA is shown in Fig. 3.7E. 2D analysis of *Ct*Pae12B-GalA complex displayed that GalA forms hydrogen bonds with Ser15, Asn83, His82, Asp187 and Thr189 and hydrophobic interactions with only His190 of *Ct*Pae12B (Fig. 3.7F). The results obtained showed that *Ct*Pae12B has stronger binding affinity for ligands with acetyl groups compared to the ligand with no acetyl group.

Table 3.4 Molecular interactions of the active-site residues of *Ct*Pae12B with ligands.

Ligand	Binding energy (kcal/mol)	Polar interaction	Hydrophobic interaction
p-Nitrophenyl acetate	-3.83	Ser15, Asn83	Ala50, Gly51, His82, Thr189, His190
α-Naphthyl acetate	-3.69	Ser15	Ala50, Gly51, His82, Asn83, Thr189, His190
3-O-acetyl-D-Galacturonic acid	-2.97	Ser15, Thr189, His190	Gly51, His82, Asn83 Asp187
2-O-acetyl-D-Galacturonic acid	-2.83	Ser15, Asn83, His190	Gly51, His82 Thr189
D-Galacturonic acid	-1.56	Ser15, Asn83, His82, Asp187, Thr189	His190

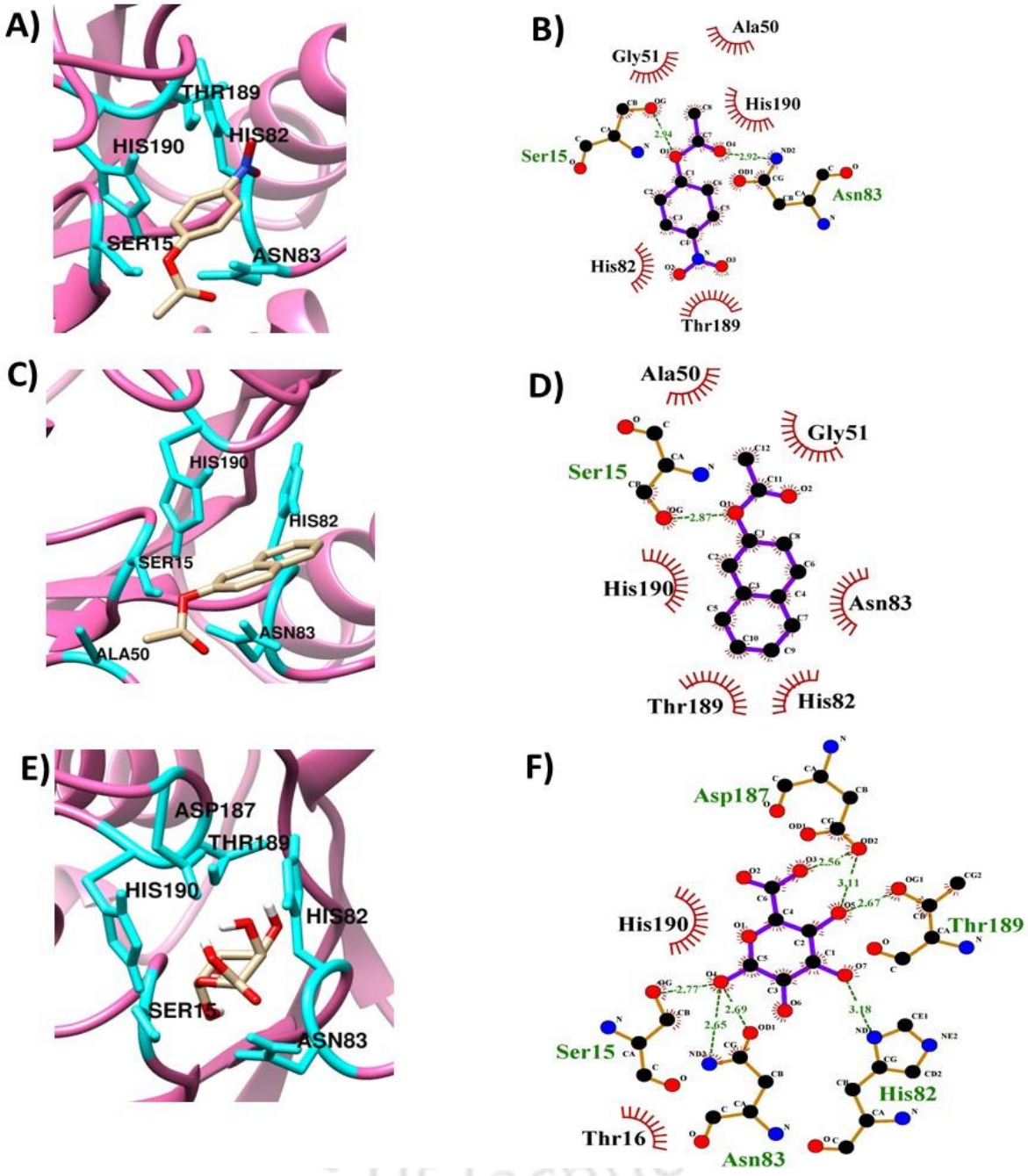

Fig. 3.7 Docking analysis of *Ct*Pae12B with the ligands. A, C, E, showing interaction between active-site residues of *Ct*Pae12B with ligands *p*NPA, α-NA and GalA, respectively (Cyan blue: active-site residues, pink: *Ct*Pae12B protein chain, red and tan: ligand). B, D and F showing 2D schematic representation of orientation of active-site residues of *Ct*Pae12B with ligands *p*NPA, α-NA and GalA, respectively. (dashed green lines: hydrogen bond, combed red arcs: hydrophobic interactions, black balls: carbon atoms, blue balls: nitrogen atoms, red balls: oxygen atoms, purple lines: ligand bonds, light brown lines: amino acid residue bonds).

3.3.7 MD simulation of ligand bound *Ct*Pae12B

The docked complex of *Ct*Pae12B-*p*NPA was subjected to MD simulation for 100 ns and the conformational dynamics of the docked complex was compared with the dynamics of only *Ct*Pae12B catalytic module to analyse various parameters assessing the stability and compactness of the docked complex after simulation. The estimation of root mean square deviation (RMSD) of the docked complex after simulation showed that RMSD value after 50 ns was stabilised on 0.3 nm with ± 0.02 nm oscillation up to 100 ns which is ~0.05 nm less than the RMSD of only *Ct*Pae12B (Fig. 3.8A). This indicated that due to the presence of the ligand (*p*NPA) in the catalytic cleft of *Ct*Pae12B, the RMSD decreased minimally with not much conformational changes in the simulated docked complex compared to only *Ct*Pae12B. The stable RMSD also showed the structure equilibrium and stability of the docked complex. The radius of gyration (R_g) of the docked complex remained between 1.70 nm and 1.67 nm throughout the trajectory up to 100 ns (Fig. 3.8B). R_g of the docked complex is comparatively,~0.06 nm less than the R_g of only *Ct*Pae12B which showed that binding of the ligand increased the global compactness and tightness of the complex. The solvent accessible surface area (SASA) remained approximately 108 nm^2 throughout the trajectory (Fig. 3.8C) up to 100 ns which decreased from SASA of only *Ct*Pae12B by ~18 nm^2 indicating that ligand binding to the catalytic cleft of the *Ct*Pae12B in the docked complex decreased the accessibility of solvent to a small extent. The RMSF plot (Fig. 3.8D) of the MD simulated docked complex showed that like only *Ct*Pae12B the N- and C- terminal residues were highly flexible. The loop region was seen to be more flexible than the residues forming the secondary structural elements. L4 was found to be comparatively more flexible in the docked complex as compared with only *Ct*Pae12B. L4 is an outer loop lying in +2 binding site of *Ct*Pae12B. The flexibility in

L4 might be responsible for some conformational changes in *Ct*Pae12B upon ligand binding. The flexibility in the outer loops upon ligand binding which resulting in conformational changes in the chimeric enzyme has been also previously reported (Nath *et al.,* 2020) The RMSF plot of catalytic residues (Ser15-Asp187-His190) were observed to be stable. No apparent mobility of these residues, signifies that they are geometrically correct and can form productive catalytical conformations. The MD simulation study showing such lower fluctuation and preservation of the catalytic triad (Ser77, His156 and D133) geometry in the active-site of a mutated serine lipase 6B compared to its wild type, helped to deduce that 6B was much closer to a catalytically competent conformation than its wild type (Kamal *et al*., 2012) The interaction of various amino acid residues, Ser15, Ala50, Gly51, His82, Asn83, Thr189 and His190 at the catalytic site of *Ct*Pae12B in the docked complex with *p*NPA (Fig. 4.8E) was developed by Pymol v2.3.3. The RMSF plot reveals that amino acid residues Ser15, Ala50, Gly51, His82, Asn83, Thr189 and His190 interacting with ligand possess lower fluctuation values and less significant changes in both simulated docked complex and only *Ct*Pae12B (Fig. 3.8D). Such lower fluctuation values of these 7 amino acids in the binding site are conducive to the docked *p*NPA immobilization at the catalytic site. Similar significance of ligand and protein residues interaction was reported after 100 ns MD simulated docked complex of Ubiquitin-conjugating Enzyme H5 (UbcH5s) with 1β-hydroxy alantolactone (Xu and Meng, 2020). The 2D schematic representation showed that the amino acid residues His82 and Asn83 formed hydrogen bonds with the ligand whereas Ser15, Ala50, Gly51, His82, Thr189 and His190 showed hydrophobic interactions with 4-NPA in the catalytic cleft after 100 ns (Fig. 3.8F). This differed from the docked complex at 0 ns of *Ct*Pae12B-*p*NPA, where Ser15 of *Ct*Pae12B forms a hydrogen bond with O-atom bound to acetyl group in *p*NPA (Fig. 3.7B). Ser15 acts as

nucleophile in the catalytic triad. Nucleophiles are electron rich species and should theoretically form covalent bond with electron deficient carbon atom of the substrate (Xu and Meng, 2020). The minimal fluctuation in the loop L1, involved in the formation of the catalytic triad, might be responsible for slightly changing the orientation of nucleophile Ser15 making it form non-polar bond with the ligand, thus, fulfilling the hypothesis of covalent bond formation by Ser15 with the substrate for nucleophilic attack. Minimal fluctuations in L1 implies minimal mobilisation signifying stable conformation and no deformity or distortion of the catalytic triad. Comparative analysis of MD simulation of both ligand bound and only *Ct*Pae12B showed the stable and compact structural conformation of the docked complex.

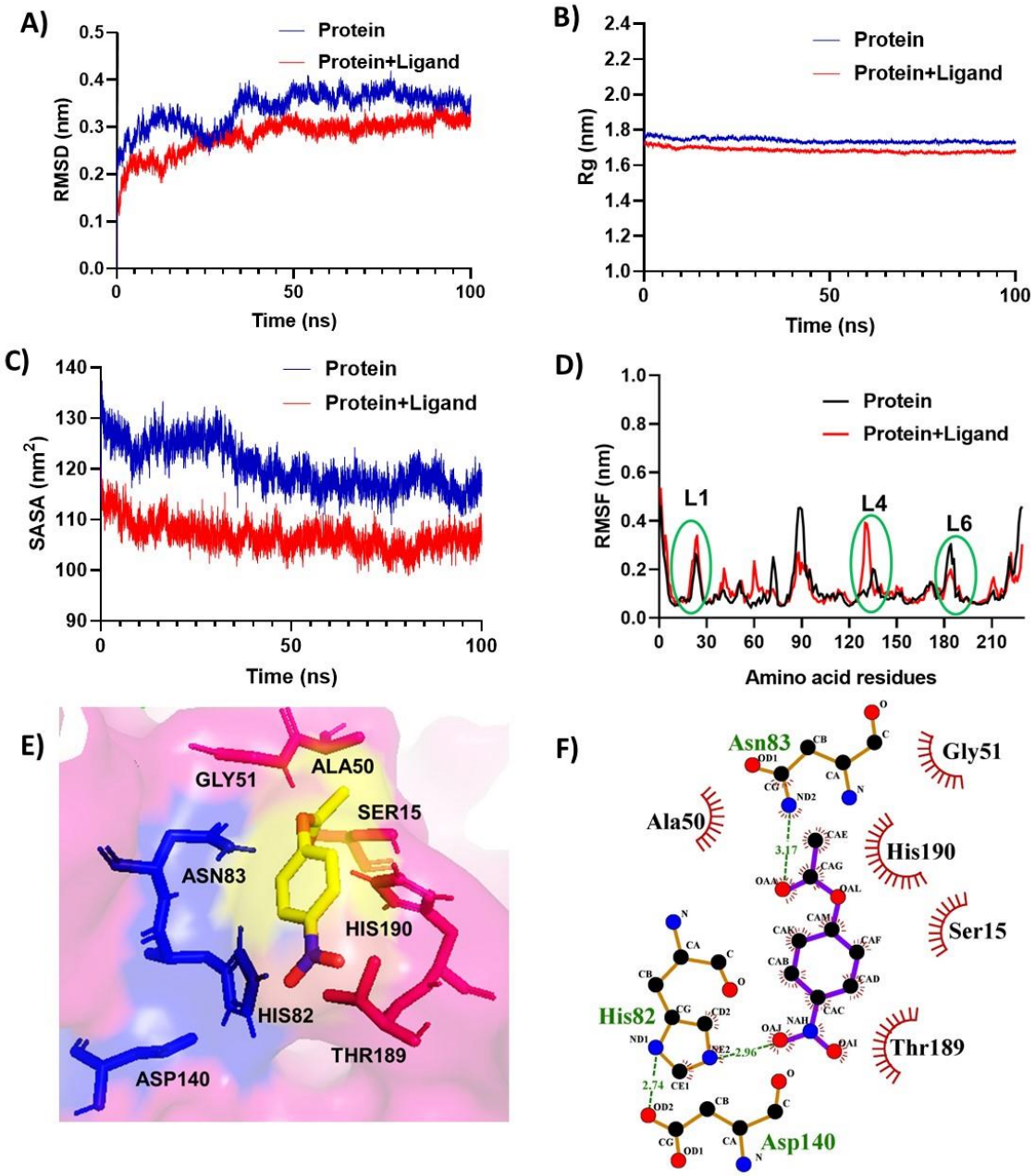

Fig. 3.8 Comparative molecular dynamic simulation analysis of ligand (*p*NPA) bound *Ct*Pae12B and only *Ct*Pae12B. A) RMSD plot, B) Radius of gyration plot, C) SASA plot, D) RMSF plot, E) The interaction of amino acid residues with *p*NPA at the active-site after 100 ns simulation, F) 2D schematic representation of interaction of amino acid residues at the active-site with *p*NPA after 100 ns simulation.

3.3.8 Small angle X-ray and dynamic light scattering analyses of *Ct*Pae12B

The molecular shape and conformation of *Ct*Pae12B in solution was studied by SAXS data analysis. The structural parameters of *Ct*Pae12B obtained by SAXS data processing and analysis are summarized in Table 3.5. The SAXS patterns of *Ct*Pae12B

obtained at 3 and 5 mg/mL are shown in fig. 3.9A. Scattering curves displayed that the conformation of *Ct*Pae12B at 3 mg/mL is intact, monodispersed, free of aggregation of particles and lack of any inter-particle correlation effect. While at a higher concentration, i.e., 5 mg/mL, SAXS pattern showed slight aggregation. Therefore, further SAXS data analysis was carried out for 3 mg/mL protein concentration of *Ct*Pae12B. The fit line to Guinier plot displayed linear behaviour in low q region, which indicated no aggregation effect and excellent monodispersity of *Ct*Pae12B (Fig. 3.9B). Guinier plot gave the radius of gyration for globular shape (R_g), 3.91 (± 0.05) nm and rod shape (R_c), 1.19 (± 0.0) nm. The persistence length of the enzyme molecule was 12.9 nm. The P(R) function analysis acquired by fourier transformation of the *Ct*Pae12B scattering profile displayed the asymmetric profile (Fig. 3.9C) suggesting oligomeric state of *Ct*Pae12B. The maximum dimension (D_{max}) and radius of gyration (R_g) of *Ct*Pae12B estimated from P(R) plot were 13 nm and 3.94 nm. The analysis of Kratky plot displayed bell-shape peak at low Q region confirming the compact, limited flexibility and fully folded structure of *Ct*Pae12B (Fig. 3.9D). The molecular mass of *Ct*Pae12B at 3 mg/mL was determined to be 79.1 kDa from the SAXS scattering profile by SAXSMow server which is triple of molecular mass of *Ct*Pae12B in its monomer state i.e., 25 kDa. This showed that *Ct*Pae12B exists in a homotrimer form at 3 mg/mL protein concentration. 20 independent models averaged and refined by DAMAVER and DAMMIN, respectively, were taken with normalized special discrepancy (NSD) value 0.668 (± 0.059). The *ab initio* dummy model built by DAMMIF was found to be multi-modular and elongated. Superposition of a single *Ct*Pae12B simulated structure with averaged DAM shape covered only one third of the modeled envelope. Since, no web-servers are available for protein-protein docking against SAXS scattering profile for higher oligomeric form of protein other than dimer, three simulated structures of

*Ct*Pae12B were manually fitted in the molecular map (Fig. 3.10A and 3.10B). The alternative view of the molecular envelope is shown in fig. 3.10C and fig 3.10D. The interchain protein-protein interaction predicted by RaptorX-ComplexContact web server (http://raptorx.uchicago.edu/ComplexContact/) showed that *Ct*Pae12B protein chains interact via hydrophobic interaction with highest probability (Jing *et al*., 2020). Thus, using this logic the trimeric molecular envelope was prepared. Furthermore, DLS analysis for particle diameter against the scattering intensity (%) for 1, 2 and 3 mg/mL protein concentrations of *Ct*Pae12B gave single peaks showing excellent monodispersity of the protein (Fig. 3.10E). Apparent hydrodynamic diameter at 3 mg/mL was found to be 5.8 nm (hydrodynamic radius, R_h=2.9 nm) which was in agreement with the theoretical calculated mass of anhydrous sphere of approximately 79 kDa protein (Erickson, 2009). This showed the presence of *Ct*Pae12B as a homotrimer at 3 mg/mL protein concentration. The shape factor ρ (R_g/R_h) at 3 mg/mL *Ct*Pae12B yielded a value greater than 1 (≈ 1.35), which indicated that *Ct*Pae12B is present as an elongated trimer. Similar results were obtained for MurE-MurF fusion protein where the overall ρ factor ≈1 indicated an elongated shape of the molecule (Laddomada *et al*., 2019). The SAXS data of *Ct*Pae12B at lower than 3 mg/mL concentration were collected but not good enough for processing and therefore not included. However, the DLS analysis of *Ct*Pae12B at 1 and 2 mg/mL, revealed the hydrodynamic diameters of 4.1 nm (R_h=2.0 nm) and 4.9 nm (R_h=2.5 nm), respectively (Fig. 3.10E), which suggested that *Ct*Pae12B might be existing as monomer and dimer, respectively, at these concentrations. The hydrodynamic diameter obtained at 1 mg/Ml also corroborates with the R_g (1.8 nm) obtained from MD simulation of the monomeric form of *Ct*Pae12B (Fig. 3.6B). The DLS analysis of *Ct*Pae12B conclusively suggested that with increase in the concentration of protein, the oligomeric form of *Ct*Pae12B also

increases by protein-protein interaction in solution. Therefore, for these reasons, the model was studied and validated by using the template-based monomeric form of *Ct*Pae12B. Similar simulation and structural studies performed with monomeric form of the protein and SAXS analysis showing their higher oligomeric forms, have been earlier reported in human DNAJB6 oligomeric chaperone (Söderberg *et al*., 2018) and an endocellulase of family 9 glycoside hydrolase from *Acetivibrio thermocellus* (Kumar *et al*., 2021).

Table 3.5 SAXS data collection and derived parameters of *Ct*Pae12B.

Data-collection parameter	*Ct*Pae12B
Instrument	SAXSpace Anton-Paar
Wavelength (Å)	1.54
Q range (nm^{-1})	0.135-5.95
Exposure time (min.)	30x2
Temperature (°C)	10
Protein concentration (mg/ml)	3
Structural parameter	
Q range (nm^{-1}) used for R_g analysis	0.15-0.33
I(0) au from Guinier	155980 ± 1317.53
R_g nm from Guinier	3.91 ± 0.05
I(0) from P(R)	154700
R_g nm from P(R)	3.94
D_{max} (nm)	13
Porod volume estimate (nm^3)	96.19
Persistant length (nm)	12.9
Molecular mass determination	
Theoritical molecular mass (kDa)	26.05
Molecular mass from SAXSMoW, (kDa)	79.1
Modeling parameters	
Q range (nm^{-1}) used for structure modeling	0.15-2.04
Resolution (nm)	0.42 ± 0.03
χ^2	0.69
Normalized spatial discrepancy (NSD)	0.668 ± 0.059
Software employed	
Data processing	Primus
P(R) function calculation	GNOM
Ab initio modeling	DAMMIF
Validation and averaging	DAMAVER
Structure superposition	SUPCOMB
3-D graphical representation	Pymol

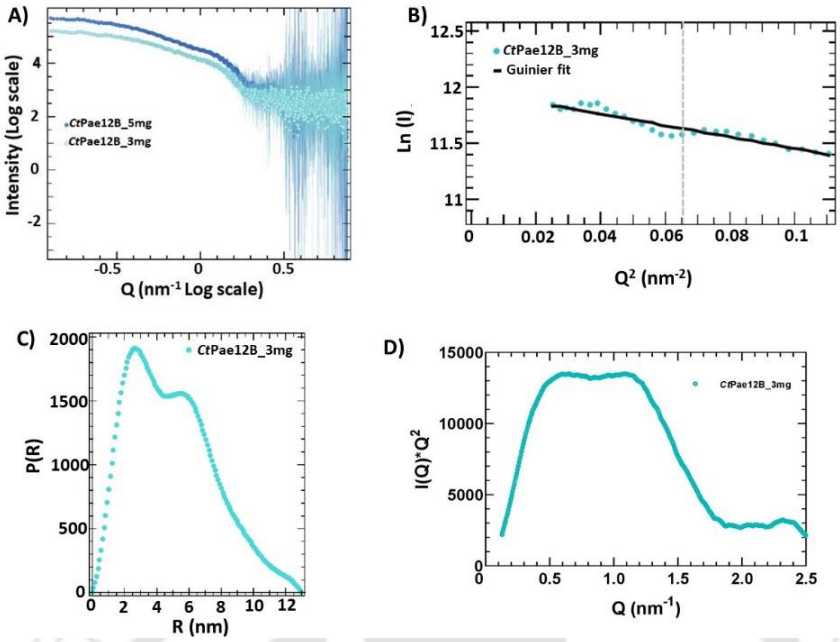

Fig. 3.9 SAXS analysis of *Ct*Pae12B. (A) Intensity profile obtained through SAXS, (B) Guinier plot of the SAXS intensities at 3 mg/mL, (C) P(R) curve of *Ct*Pae12B as a function of R, (D) Kratky plot of SAXS data.

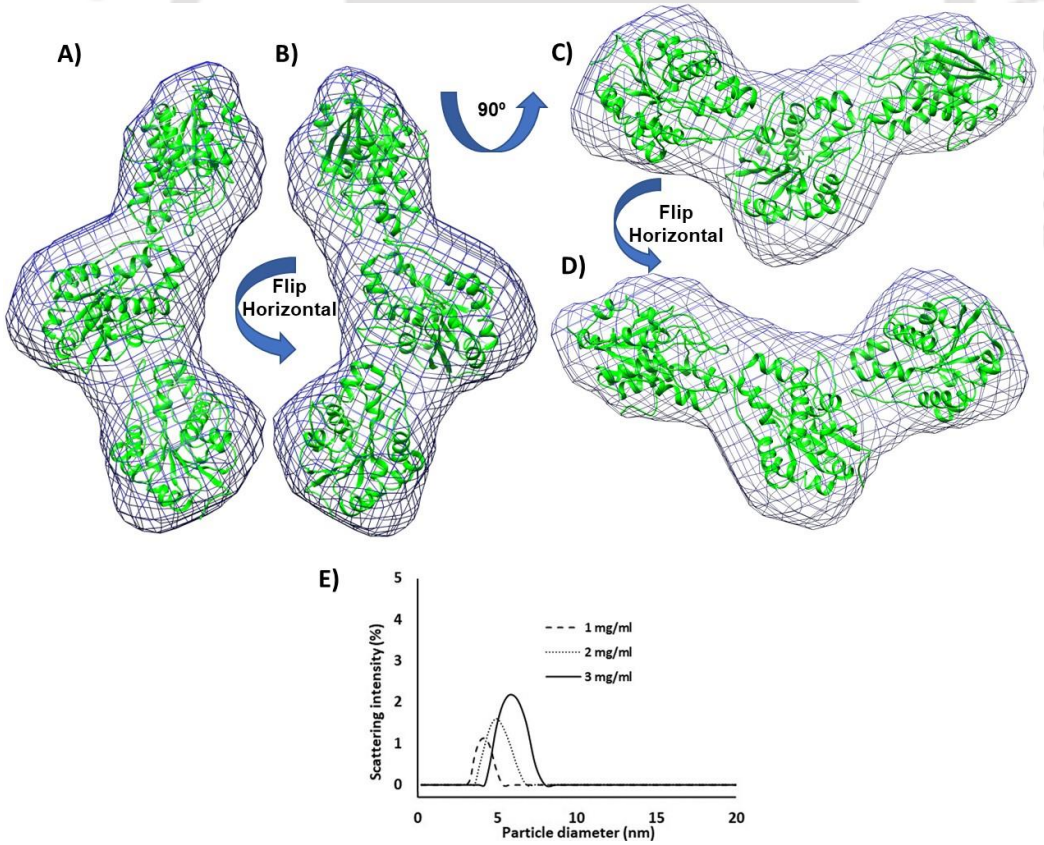

Fig. 3.10 SAXS envelope of *Ct*Pae12B at 3 mg/mL protein concentration. (A) and (B) Molecular map of *ab initio Ct*Pae12B fitted with three simulated structures of *Ct*Pae12B using UCSF Chimera. (C) and (D) Alternative views of the envelope fit of the homotrimer with 90° flip, (E) Particle diameter analysis of *Ct*Pae12B at 1, 2 and 3 mg/mL by DLS.

3.3.9 MD simulation of *Ct*Pae12B trimer modeled structure

The modeled structure of *Ct*Pae12B trimer was subjected to MD simulation for 100 ns to analyse the stability of the structure and global compactness. The variations of the protein backbone of *Ct*Pae12B trimer showed by RMSD versus time graph displayed initially minimal fluctuations between 0.21 nm to 0.27 nm up to 50 ns and there after the structure remained in a stabilized state up to 100 ns with RMSD between 0.27 nm and 0.29 nm. The average RMSD was found to be 0.35 nm (Fig. 3.11A). The radius of gyration (R_g) of the *Ct*Pae12B trimer remained between 3.7 nm to 3.9 nm throughout the trajectory up to 100 ns showing excellent global compactness of the structure (Fig. 3.11B). The R_g of the simulated *Ct*Pae12B trimer corroborated with the R_g of the *Ct*Pae12B (3.94 nm) trimer determined by SAXS analysis (Section 3.3.8). These results showed that *Ct*Pae12B forms a compact trimer oligomer in solution at 3 mg/mL.

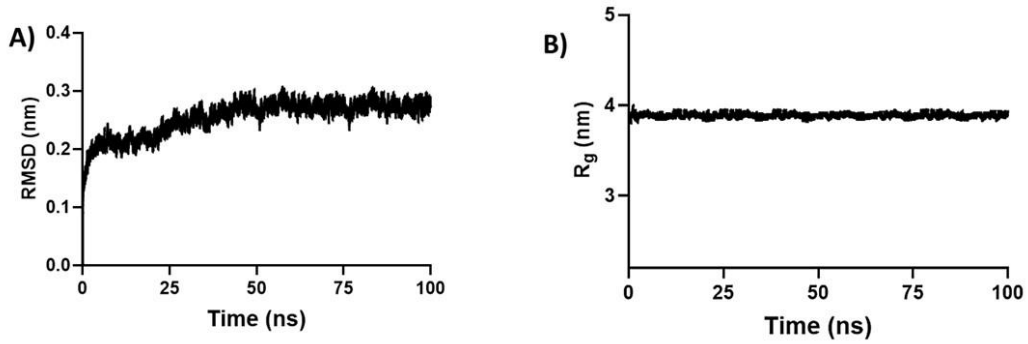

Fig. 3.11 MD simulation of *Ct*Pae12B trimer modeled structure at 100 ns. A) RMSD plot and B) R_g plot.

3.4 Conclusion

The amino acid sequence of a *Ct*Pae12B was 34.86% identical with 92% query coverage with the amino acid sequence of a pectin acetyl esterase from *Bacillus subtilis* of CE12 family. Multiple sequence alignment with its nearest homologues showed that Ser15, Gly51, His82, Asn83, Asp187, Thr189 and His190 are catalytically important residues of which Ser15, Asp187 and His190 constitute the catalytic triad. The 3-D modeled structure generated by comparative modeling further revealed that it possesses a new α/β hydrolase fold, similar to the fold found in the crystal structure of its nearest homologues (RGAE and YxiM), which is not similar to α/β fold as found in α/β hydrolase family of glycoside hydrolases. CD analysis showed that *Ct*Pae12B is composed of 37.9% α-helices, 16.1% β-sheets and 46.1% random coils which was in agreement with the results predicted by Psipred and 2Struc. *Ct*Pae12B belongs to a new SGNH-hydrolase fold family of which the members of CE12 are a distinct family. The *Ct*Pae12B structure was energy minimized and the refinement was validated. MD simulation of *Ct*Pae12B confirmed that the structure was conformationally stable and compact and the catalytically important residues were also excluded from deformity or any occlusion. The docking studies further revealed the catalytically important residues. The highest binding affinity of *Ct*Pae12B was shown with *p*NPA. Comparative analysis of MD simulated *Ct*Pae12B-*p*NPA structure with only *Ct*Pae12B structure further confirmed the structure stability of the docked complex. The catalytic residues in the docked complex were also stable with minimal fluctuations. The outer loop L4 was found to be comparatively more flexible than the other residues, which might have brought some conformational changes in the structure of *Ct*Pae12B without causing any distortion in the structure. The best data of *Ct*Pae12B by SAXS analysis was obtained at 3 mg/mL in order to gain an insight into its solution behaviour. The SAXS

analysis showed the stable conformational behaviour of *Ct*Pae12B. The Kratky plot further showed the compact nature and lesser flexibility of *Ct*Pae12B. The data from the SAXSMow server showed that the molecular mass of *Ct*Pae12B was thrice of its molecular mass (25 kDa, in monomeric state) at 3 mg/mL. Further, the final dummy atomic model obtained by DAMMIF program fitted manually with three *Ct*Pae12B simulated structures based on existence of hydrophobic interaction between inter protein chains showed an excellent trimeric molecular envelope. The particle size of *Ct*Pae12B at 3 mg/mL determined by dynamic light scattering (DLS) analysis also confirmed that it exists as an elongated homotrimer. However, the DLS analysis at lower concentrations of *Ct*Pae12B than 3 mg/mL showed lower hydrodynamic diameter. Thus, it cannot be concluded that *Ct*Pae12B always exists in a homotrimer structure at all concentrations. The templates used for modeling of *Ct*Pae12B are not yet reported to exist in any higher oligomeric forms. Therefore, the fold analysis, conformations of catalytic residues, ligand binding and conformation analysis by dynamic studies were carried out with template-based homology modeled monomeric form of *Ct*Pae12B. Moreover, the R_g calculated by MD simulation of *Ct*Pae12B trimer modeled structure corroborated with the R_g determined by SAXS analysis of the *Ct*Pae12B trimer formed in solution at 3 mg/mL. The structural insights of pectin acetyl esterase, *Ct*Pae12B illustrated a new hydrolase fold with a compact and stable structure, absence of a nucleophilic elbow and the role of the loops in formation of the catalytic triad in the active-site for covalent catalysis of the substrate. However, more substantial analyses by advanced techniques may lead to its detailed structure elucidation.

References

Akinosho, H., Kelsey, Y., Dan, C., Arthur, R. (2014) The emergence of *Clostridium thermocellum* as a high utility candidate for consolidated bioprocessing applications. Frontiers in Chemistry, 2.

Altschul, S.F., Madden, T.L., Schäffer, A.A., Zhang, J., Zhang, Z., Miller, W., Lipman, D. J. (1997) Gapped BLAST and PSI-BLAST: a new generation of protein database search programs, Nucleic Acids Research, 25: 3389–3402.

Berendsen, H.J., Van der Spoel, D., Van Drunen, R. (1995) GROMACS: A message-passing parallel molecular dynamics implementation. Computer Physics Communications, 91(1–3): 43–56.

Berg, J.M., Tymoczko, J.L., Stryer, L. (2002) Biochemistry. 5th edition. New York: W. H. Freeman; Section 1.3, Chemical Bonds in Biochemistry.

Bolvig, P.U., Pauly, M., Orfila, C., Scheller, H.V., Schnorr, K. (2003) Sequence analysis and characterisation of a novel pectin acetyl esterase from *Bacillus subtilis*. Advances in Pectin and Pectinase Research, (Eds. Voragen, A.J.G., Schols, H. and Visser, R.), Springer, Dordrecht, 315-330.

Boyle, N.M.O., Banck, M., James, C.A., Morley, C., Vandermeersch, T., Hutchison, G.R. (2011) Open babel: an open chemical toolbox. Journal of Cheminformatics, 3(1): 1-14.

Caffall, K.H., Mohnen, D. (2009) The structure, function, and biosynthesis of plant cell wall pectic polysaccharides. Carbohydrate Research, 344(14): 1879-1900.

Chandrayan, P. (2018) Biological function(s) and application (s) of pectin and pectin degrading enzymes. Biosciences Biotechnology Research Asia, 15(1): 87-100.

Erickson, H.P. (2009) Size and shape of protein molecules at the nanometer level determined by sedimentation, gel filtration, and electron microscopy. Biological Procedures Online, 11: 32-51.

Fischer, H.D.O.N., Oliveira Neto, M.D., Napolitano, H.B., Polikarpov, I., Craievich, A.F. (2010) Determination of the molecular weight of proteins in solution from a single small-angle X-ray scattering measurement on a relative scale. Journal of Applied Crystallography, 43(1): 101–109.

Fournet, G., Guinier, A. (1955) Small angle scattering of X-rays translated by Walker C.B and Yudowitch, New York, NY: John Wiley and Sons, 7–78.

Franke, D., Petoukhov, M.V., Konarev, P.V., Panjkovich, A., Tuukkanen, A., Mertens, H.D.T., Kikhney, A.G., Hajizadeh, N.R., Franklin, J.M., Jeffries, C.M., Svergun, D. (2017) ATSAS 2.8: a comprehensive data analysis suite for small-angle scattering from macromolecular solutions. Journal of Applied Crystallography, 50(4): 1212-1225.

Govind, K., Murthy, M.R.N., Savithri, H.S. (2013) Chapter 692- Sobemovirus peptidase. Handbooks of Proteolytic Enzymes, 3: 3141-3148.

Goyal, D., Kumar, K., Sharma, K. and Goyal, A. (2019) Small-angle X-ray scattering based structure, modeling and molecular dynamics analyses of a family 5 glycoside hydrolase first endo-mannanase named as *Rf*GH5_7 from

Ruminococcus flavefaciens. Journal of Biomolecular Structure and Dynamics, 38 (15): 4371-4384.

Hess, B., Kutzner, C., Spoel, D.V., Lindahl, E. (2008) GROMACS 4: Algorithms for highly efficient, load-balanced and scalable molecular simulation. Journal of Chemical Theory and Computation, 4(3): 435-447.

Hugouvieux-Cotte-Pattat, N., Condemine, G., Shevchik, V.E. (2014) Bacterial pectate lyases, structural and functional diversity. Environmental Microbiology Reports, 6 (20): 427–440.

Jing, X., Zeng, H., Wang, S. and Xu, J. (2020) A web-based protocol for interprotein contact prediction by deep learning. Protein-protein interaction networks (Eds. Canzar, S., Ringeling, F.R.), Humana, New York, 67-80.

Jones, D.T. (1999) Protein secondary structure prediction based on position-specific scoring matrices. Journal of Molecular Biology, 292: 195-202.

Kamal, M.Z., Mohammad, T.A., Krishnamoorthy, G., Rao, N.M. (2012) Role of active-site rigidity in activity: MD simulation and fluorescence study on a lipase mutant. PloS One, 7(4): e35188.

Kelly, S.M., Jess, T.J., Price, N.C. (2005). How to study proteins by circular dichroism? Biochimica et Biophysica Acta, 1751 (2): 119–139.

Klausen, M.S., Jespersen, M.C., Nielsen, H., Jensen, K.K., Jurtz, V.I., Sønderby, C.K., Sommer, M.O.A., Winther, O., Nielsen, M., Petersen, B., Marcatili. P. (2019) NetSurfP-2.0: Improved prediction of protein structural features by integrated deep learning. Proteins, 87(6): 520-527.

Klose, D.P., Wallace, B.A., Janes, R.W. (2010) 2Struc: The secondary structure server. Bioinformatics, 26(20): 2624–2625.

Konarev, P.V., Volkov, V.V., Sokolova, A.V., Koch, M.H., Svergun, D.I. (2003) PRIMUS: A Windows PC-based system for small-angle scattering data analysis. Journal of Applied Crystallography, 36(5): 1277–1282.

Kozin, M.B., Svergun, D.I. (2001) Automated matching of high-and low-resolution structural models. Journal of Applied Crystallography, 34(1): 33–41.

Krieger, E., Joo, K., Lee, J., Raman, S., Thompson, J., Tyka, M., Baker, D., Karplus, K. (2009) Improving physical realism, stereochemistry, and side-chain accuracy in homology modeling: four approaches that performed well in CASP8, Proteins: Structure, Function and Bioinformatics, 77: 114–122.

Kumar, K., Singh, S., Sharma, K., Goyal, A. (2021) Computational modeling and small-angle X-ray scattering based structure analysis and identifying ligand cleavage mechanism by processive endocellulase of family 9 glycoside hydrolase (*Ht*GH9) from *Hungateiclostridium thermocellum* ATCC 27405. Journal of Molecular Graphics and Modelling, 103: 107808.

Laddomada, F., Miyachiro, M.M., Jessop, M., Patin, D., Job, V., Mengin-Lecreulx, D., Le Roy, A., Ebel, C., Breyton, C., Gutsche, I., Dessen, A. (2019) The MurG glycosyltransferase provides an oligomeric scaffold for the cytoplasmic steps of peptidoglycan biosynthesis in the human pathogen *Bordetella pertussis*. Scientific Reports, 9(1): 1-17.

Lagaert, S., Beliën, T., Volckaert, G. (2009) Plant cell walls: protecting the barrier from degradation by microbial enzymes. Seminars in Cell and Developmental Biology, 20: 1064–1073.

Laskowski, R.A., Swindells, M.B. (2011) LigPlot+: multiple ligand–protein interaction diagrams for drug discovery. Journal of Chemical Information and Modelling, 51: 2778–2786.

Lau, E.Y., Bruice, T.C. (1999) Consequences of breaking the Asp-His hydrogen bond of the catalytic triad: Effects on the structure and dynamics of the serine esterase cutinase. Biophysical Journal, 77(1): 85-98.

Lovell, S.C., Davis, I.W., Arendall III W.B., Bakker, P.I.W., Word, J.M., Prisant, M.G., Richardson, J.S., Richardson, D.C. (2002) Structure validation by Cα geometry: φ/ψ and Cβ deviation. Proteins: Structure, Function & Genetics, 50: 437-450.

Madeira, F., Park, Y.M., Lee, J., Buso, N., Gur, T., Madhusoodanan, N., Basutkar, P., Tivey, A.R.N., Potter, S.C., Finn, R.D., Lopez, R. (2019) The EMBL-EBI search and sequence analysis tools APIs in 2019. Nucleic Acids Research, 47(W1): W636-W641.

Matsunaga, T., Ishii, T., Matsumoto, S. (2004) Occurrence of the primary cell wall polysaccharide rhamnogalacturonan II in pteridophytes, lycophytes and bryophytes. Implications for the evolution of vascular plants. Plant Physiology, 134: 339–351.

Mohnen, D., Bar-Peled, M., Somerville, C. (2008) Biosynthesis of plant cell walls. Biomass Recalcitrance, Chapter 5, (Ed. Himmel, M.), Blackwell Publishing, Oxford, 94–187.

Mølgaard, A., Kauppinen, S., Larsen, S. (2000) Rhamnogalacturonan acetylesterase elucidates the structure and function of a new family of hydrolases. Structure, 8: 373–383.

Morgat, A., Lombardot, T., Coudert, E., Axelsen, K., Neto, T.B., Gehant, S., Bansal, P., Bolleman, J., Gasteiger, E., Castro, E., Baratin, D., Pozzato, M., Xenarios, I., Poux, S., Redaschi, N., Bridge, A. (2020) The UniProt Consortium, Enzyme annotation in UniProtKB using Rhea. Bioinformatics, 36(6): 1896–1901.

Morris G.M., Huey, R., Lindstrom, W., Sanner, M.F., Belew, R.K., Goodsell, D.S., Olson, A.J. (2010) AutoDock4 and AutoDockTools4: automated docking with selective receptor flexibility. Journal of Computational Chemistry, 30: 2785–2791.

Morris, G.A., Kök, M.S., Harding, S.E., Adams, G.A. (2010) Polysaccharide drug delivery system based on pectin and chitosan. Biotechnology and Genetic Engineering Reviews, 27: 257-284.

Nath, P., Sharma, K., Kumar, K., Goyal, A. (2020) Combined SAXS and computational approaches for structure determination and binding characteristics of Chimera (*Ct*GH1-L1-*Ct*GH5-F194A) generated by assembling β-glucosidase (*Ct*GH1) and a mutant endoglucanase (*Ct*GH5-F194A) from *Clostridium thermocellum*. International Journal of Biological Macromolecules, 148: 364-377.

Ollis, D.L., Cheah, E., Cygler, M., Dijkstra, B., Frolow, F., Franken, Sybille M., Harel, M., Remington, S.J., Silman, I., Schrag, J. (1992) The α/β hydrolase fold. Protein Engineering, 5(3): 197-211.

Pettersen, E.F., Goddard, T.D., Huang, C.C., Couch, G.S., Greenblatt, D.M., Meng, E.C., Ferrin, T.E. (2004) UCSF Chimera—a visualization system for exploratory research and analysis, Journal of Computational Chemistry, 2: 1605–1612.

Polgar, L. (2005) The catalytic triad of serine peptidases. Cellular and Molecular Life Sciences, 62: 2161-2172.

Robert, X., Gouet, P. (2014) Deciphering key features in protein structures with the new ENDscript server. Nucleic Acids Research, 42: W320–W324.

Schrödinger, L. (2017) The PyMOL molecular graphics system, Version 2.0. Retrieved from http://www.pymol.org/

Searle-van Leeuwen, M.J.F., van der Broek, L.A.M., Schols, H.A., Beldman, G., Voragen, A.G.J. (1992) Rhamnogalacturonan acetylesterase: A novel enzyme from *Aspergillus aculeatus*, specific for the deacetylation of hairy regions of pectins. Applied Microbiology and Biotechnology, 38: 347–349.

Sharma, K., Antunes, I.L., Ralulapati, V., Goyal, A. (2018) Low resolution SAXS and comparative modelling-based structure analysis of endo-β-1,4-xylanase, a family 10 glycoside hydrolase from *Pseudobacter saltans* comb. nov. International Journal of Biological Macromolecules, 112: 1104-1114.

Shevchik, V., Hugouvieux-Cotte-Pattat, N. (2003) PaeX, a second pectin acetylesterase of *Erwinia chrysanthemi* 3937. Journal of Bacteriology, 185(10): 3091–3100.

Söderberg, C.A., Månsson, C., Bernfur, K., Rutsdottir, G., Härmark, J., Rajan, S., Al-Karadaghi, S., Rasmussen, M., Höjrup, P., Hebert, H., Emanuelsson, C. (2018) Structural modelling of the DNAJB6 oligomeric chaperone shows a peptide-binding cleft lined with conserved S/T-residues at the dimer interface. Scientific Reports, 8(1): 1-15.

Svergun, D.I. (1992) Determination of the regularization parameter in indirect-transform methods using perceptual criteria. Journal of Applied Crystallography, 25(4): 495–503.

Tian, W., Chen, C., Lei, X., Zhao, J., Liang, J. (2018) CASTp 3.0: computed atlas of surface topography of proteins. Nucleic Acids Research, 46: W363–W367.

Volkov, V.V., Svergun, D.I. (2003) Uniqueness of ab initio shape determination in small angle scattering. Journal of Applied Crystallography, 36(3): 860–864.

Voragen, A.G.J., Coenen Gerd-Jan, Verhoef, R.P., Schols, H.A. (2009) Pectin, a versatile polysaccharide present in plant cell walls. Structural Chemistry, 20(2): 263–275.

Wiederstein, M., Sippl, M.J. (2007) ProSA-web: Interactive web service for the recognition of errors in three-dimensional structures of proteins. Nucleic Acids Research, 35(Web Server): W407–W410

Xu, Y., Meng, X. (2020) Molecular simulation elaborating the mechanism of 1β-hydroxy alantolactone inhibiting ubiquitin-conjugating enzyme UbcH5s. Scientific Reports, 10: 141.

Svergun, D.I.B.C.K.M.H.J., Barberato, C., Koch, M.H. (1995) CRYSOL–a program to evaluate X-ray solution scattering of biological macromolecules from atomic coordinates. Journal of Applied Crystallography, 28(6): 768–773.

Yang, J., Zhang, Y. (2015) I-TASSER server: new development for protein structure and function predictions. Nucleic Acids Research, 43: W174-W181.

Yang, J., Wang, Y., Zhang, Y. (2016) ResQ: An approach to unified estimation of B-factor and residue-specific error in protein structure prediction. Journal of Molecular Biology, 428: 693-701.

Zhang, Y. (2008) I-TASSER server for protein 3D structure prediction. BMC Bioinformatics, 9: 40.

Zverlov, V.V., Schantz, N., Schmitt-Kopplin, P., Schwarz, W.H. (2005) Two new major subunits in the cellulosome of *Clostridium thermocellum*: xyloglucanase Xgh74A and endoxylanase Xyn10D. Microbiology, 151: 3395–3401.

Chapter 4

Biochemical characterization of thermotolerant and pH stable rhamnogalacturonan acetyl esterase (*Ct*Pae12B) and its substrate specificity

4.1 Introduction

Pectin backbone is composed mostly of *GalpA* residues linked by α-1,4- bonds (Ridley *et al*., 2001). As described earlier in Chapter 1, the structural components of pectin consist of a smooth region called homogalacturonan (HG) and hairy regions consisting of side chains called rhamnogalacturonan I (RG I) and rhamnogalacturonan II (RG II) (Voragen *et al*., 2009). Some other substituted galacturonans present in pectin are xylogalacturonan (XGA) and apiogalacturonan (AGA) (Fig. 4.1) (Ridley *et al*., 2001). The backbone of HG, RG II, XGA and AGA consists of α-1,4- linked *GalpA* but RG I backbone consists of alternately repeating units of *GalpA* and rhamnopyranosyl (*Rhap*) units (O'Neill *et al*., 1990). HG, RG I, XGA and AGA can have esterification by a methyl group at the C-6 position or acetyl-esterification at the O-2/O-3 position of *GalpA* residue (Fig. 4.1) (Ahmed *et al*., 2021). Owing to its structural complexity, complete hydrolysis of pectin requires a concerted action of many enzymes, commonly called as pectin degrading enzymes (PDEs). PDEs find applications in many industrial sectors like juice processing and clarification, tea and

coffee fermentation, retting fibres, textile processing, paper and pulp processing, degumming of fibres and also in anti-cancer activity (Ahmed *et al*., 2021).

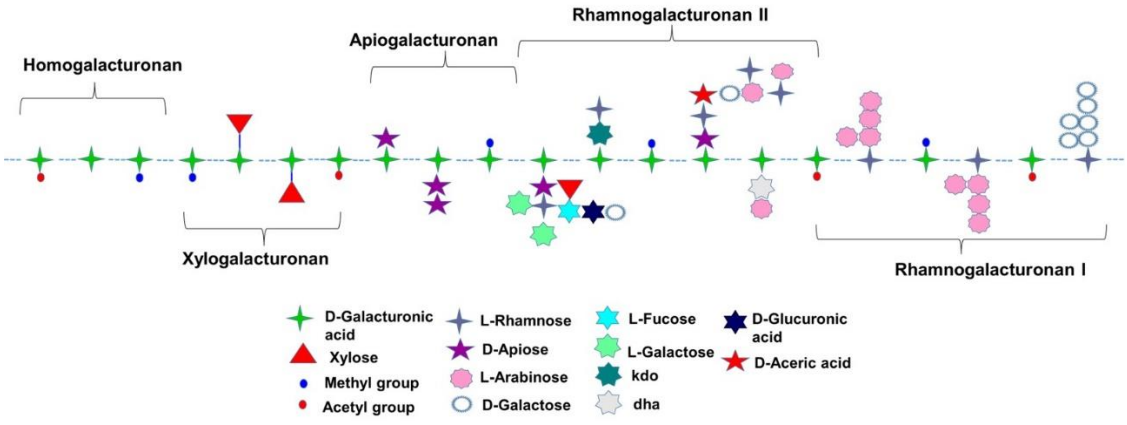

Fig. 4.1 Structure of pectin showing different domains and substitutions present in the side-chains.

Many PDEs are responsible for removing various side-chain substituents (as mentioned in fig. 4.1) from the pectin backbone so that the main-chain can be cleaved for complete hydrolysis. Apart from the long side chains present, methyl and acetyl esterification in the HG and RG regions of pectin causes steric hindrance to other backbone cleaving enzymes, such as pectic lyase and polygalacturonase. Methyl de-esterification is catalysed by pectin methyl esterase (PME) by cleaving the methyl group present at the C-6 position of *GalpA* (Rajulapati and Goyal, 2017), while pectin acetyl esterase (PAE) and rhamnogalacturonan acetyl esterase (RGAE) are involved in de-acetylation, liberating acetyl groups from the O-2/O-3 positions of *GalpA* residues in HG and RG I regions of pectin, respectively. It was reported that due to the presence of acetyl groups in the side chains of HG region of sugar beet pectin, polygalacturonase was unable to cleave the main chain and exhibited lowest activity against sugar beet pectin as compared with other pectic substrates, where no acetyl groups were present (Safran *et al*., 2021). Therefore, the removal of these hindrances in esterified substrates is very important in order to achieve the complete hydrolysis. Many PMEs are studied and reported till date, but not many PAEs and particularly RGAEs. RGAEs are

particularly specific in catalysing the removal of the acetyl ester bonds from the RG I region of pectin compared to the other regions of pectin. PAE (EC 3.1.1.6) and RGAE (EC 3.1.1.6) belong to family 12, carbohydrate esterase (CE) (www.cazy.org). Both PAE and RGAE belong to the SGNH (serine-glycine-asparagine-histidine) family and possess an α/β/α fold structure which is different from the typical α/β hydrolase fold found in glycoside hydrolases (Mølgaard *et al*., 2000). PAE and RGAE are serine esterases where serine plays a very important role in catalysis. Serine belongs to catalytic triad (Ser-His-Asp), where Ser acts as a nucleophile, His as a general base (Lau *et al*., 1999; Mølgaard *et al*., 2000) and Asp plays a role in tautomeric orientation correction and stabilisation during catalysis (Polgár, 2005).

Only a few PAEs and RGAEs have been studied so far in terms of extensive characterization and most importantly the specificity for natural substrates. Bacterial PAEs and RGAEs that have been studied so far showed maximum activity against synthetic substrates and sugar beet pectin. Most of the characterized acetyl esterases of CE12 family did not show any activity against citrus pectin or apple pectin (AP) (Bolvig *et al*., 2003; Remoroza *et al*., 2014). Only a few reports on the specificity of acetyl esterase against both HG and RG region of pectin substrates are available. The regioselectivity of one of the PAEs (BliPAE) from *Bacillus lichenisformis* showed specificity towards deacetylation of only the C-3 position of the HG region of pectin (Remoroza *et al*., 2014). A fungal acetyl esterase from *Aspergillus aculeatus* was also found to be active on both HG and RG regions of pectin (Bonnin *et al*., 2008). Apart from pectic substrates, not much exploration was done against xylan and galactan substrates. The activity of all the characterized PAEs and RGAEs was well studied with sugar beet pectin but not much with the pectin from potato tubers. It has been reported earlier that the RG I region of pectin in potato tubers have a higher degree of acetylation (Schols *et al*., 1996; Oomen *et al*., 2002). No RGAE showing activity against RG region

of potato pectin is reported yet. A few bacterial PAEs found to de-acetylate potato pectin material are BliPAE from *B. licheniformis* (Remoroza *et al*., 2014) and YxiM from *B. subtilis* (Bolvig *et al*., 2003). The acetyl esterase activity can help in degrading potato pectin completely by the concerted action of other PDEs. None of the acetyl esterases reported so far displayed thermostable properties. Henceforth, exploration of a robust enzyme is required that can de-acetylate pectin not only from its smooth region but also its hairy region with high activity having thermostability and pH stability.

In the current study, an RGAE (*Ct*Pae12B) from a thermophile gram-positive bacterium *Acetivibrio thermocellus*, a.k.a. *Clostridium thermocellum* and *Hungateiclostridium thermocellum* was biochemically characterized. This anaerobic bacterium produces thermostable cellulosomal enzymes which can be beneficial for industrial applications. Many enzymes from this organism have been studied but not an RGAE yet. *Ct*Pae12B was cloned, expressed and purified earlier showed a single band protein of molecular mass approx. 25 kDa is described in Chapter 2. *Ct*Pae12B was extensively studied in terms of sequence analysis and structural insights by computational and solution-structure determination methods as described in Chapter 3 (Ahmed *et al*., 2022). It was found to possess an α/β hydrolase fold which was deduced from the crystal structure of an RGAE from *A. aculeatus* (PDB id: 1deo). However, the catalytic action, biochemical properties and substrate specificity of the enzyme still remains to be explored. This study involves phylogenetic analysis of *Ct*Pae12B, screening of different medium for protein production and yield, determination of biochemical properties like optimal pH, optimal temperature, pH and thermostability, effect of different metal ions on its activity and its substrate specificity against various synthetic and natural pectic and xylan substrates.

4.2 Materials and methods

4.2.1 Chemicals, reagents and kits

The synthetic substrate *p*-nitrophenyl acetate was procured from Sigma-Aldrich, USA and β-D-gluco-pentaacetate, triacetin, α-naphthyl acetate and β-naphthyl acetate were procured from Sisco research laboratories (SRL) Pvt. Ltd., India. Natural pectic and xylan substrates potato rhamnogalacturonan, lupin and potato galactan, soybean rhamnogalacturonan, acetylated birchwood xylan, wheat arabinoxylan, rye arabinoxylan and acetic acid analysis kit were procured from Megazyme Ltd., Ireland. Sugar beet pectin was procured from CP Kelco, Germany and citrus pectin with 25%, 55–70% and 80% esterification, apple pectin, birchwood xylan and beechwood xylan were procured from Sigma-Aldrich, USA. The growth media and reagents for the enzyme assays were procured from Sigma-Aldrich, USA and HiMedia Pvt. Ltd., India.

4.2.2 Phylogenetic analysis of *Ct*Pae12B

The catalytic domain, *Ct*Pae12B, located in the locus tag Cthe_3141 has the Genbank accession number ABN54336.1 and Uniprot id: A3DK57. *Ct*Pae12B is present as the second single catalytic domain (614-831 aa) in the molecular architecture of the locus tag, as reported earlier (Ahmed *et al*., 2022). *Ct*Pae12B is a family 12 CE and its phylogenetic relationship with the closest homologues from the same family was studied by using Mega-X software (Kumar *et al*., 2018). The amino acid sequence of *Ct*Pae12B was obtained from NCBI database (https://www.ncbi.nlm.nih.gov/protein/ABN54336.1) and that of its homologues from Uniprot database (http://www.uniprot.org/). The sequence alignment was done by using ClustalW, incorporated within the software, with gap penalty 10. The neighbour-joining phylogenetic tree was constructed using bootstrap method with 1000 replications and Poisson model was used for the correction method.

4.2.3 *Ct*Pae12B production yield under different media

The *E. coli* BL-21 (DE3) cells transformed with the recombinant plasmid containing the gene encoding *Ct*Pae12B were grown in 100 mL of five different autoclaved media, *viz*., Luria-Bertani (LB, pH 7.0), 5× LB (pH 7.0), Terrific Broth (TB, pH 7.2), Tryptone yeast extract (TY, pH 7.0) and Auto induction medium Luria-Bertani (AIM-LB, pH 7.0) medium. The cells were grown and induced with 0.5 mM IPTG as mentioned in the previous Chapter 2, except for the AIM-LB culture. The dry cell weight of the grown cultures from each medium was determined after harvesting the cells as mentioned in Chapter 2. The total amount of purified *Ct*Pae12B obtained from each medium and their individual specific activity with synthetic substrate, *p*-Nitrophenyl acetate was also determined as mentioned in section 2.2.18. The dry cell weight, protein concentration and amount of protein were determined in triplicate and the mean results were presented.

4.2.4 Enzymatic activity assay and substrate specificity of *Ct*Pae12B

The acetyl esterase activity of *Ct*Pae12B was assayed with both synthetic and natural substrates. The synthetic substrates used for the assay were 2 mM *p*-Nitrophenyl acetate, 8.5 mM β-D-glucopentaacetate, 25 mM triacetin, 1 mM of α-naphthyl acetate and 0.95 mM of β-naphthyl acetate. The enzymatic activity of *Ct*Pae12B with *p*-Nitrophenyl acetate was determined as mentioned in section 2.2.18 of Chapter 2. Enzyme assay of *Ct*Pae12B with α- and β-naphthyl acetate was monitored by the release of α- and β- naphthol, respectively, for 1 min at 65 ºC. The standard reaction mixtures contained 95 µL of 1 mM of α-naphthyl acetate or 95 µL of 0.95 mM of β-naphthyl acetate, dissolved in 50 mM Tris-HCl buffer, pH 8.0 and 5 µL of *Ct*Pae12B (100 µg/mL). The naphthol released by acetyl esterase activity of *Ct*Pae12B in both the substrates were detected at 480 nm after adding 50 µL of 5.13 mM Fast red TR salt

hemi (Zinc chloride) (SRL Pvt. Ltd., India) using a spectrophotometer (Multiskan Sky High, Thermo Scientific, USA) following the method reported earlier (Martínez-Martínez *et al*., 2008). The molar extinction co-efficient (ε) used for calculating enzymatic activity was 2708 M^{-1} cm^{-1} and 1871 M^{-1} cm^{-1} for α- and β-naphthol, respectively, determined from the standard curves. The enzyme assay was also performed with pectic polysaccharides, *viz*., 2% (w/v) potato rhamnogalacturonan, 0.5% (w/v) sugar beet pectin, 1% (w/v) citrus pectin, with 25%, 55–70% and 80% esterification, 1% (w/v) apple pectin, 1% (w/v) lupin and potato galactan, 1% (w/v) soybean rhamnogalacturonan and xylan polysaccharides, *viz*., 2% (w/v) acetylated birchwood xylan, 1% (w/v) birchwood xylan, 1% (w/v) beechwood xylan and 1% (w/v) wheat arabinoxylan (low viscosity) and 1% (w/v) rye arabinoxylan. The acetate released by the catalytic action of *Ct*Pae12B (1 min, 65 ºC) on natural pectic, xylan, galactan and synthetic substrates, β-D-glucopentaacetate and triacetin was estimated by using acetic acid kit adapted to a microplate. The standard reaction mixture contained 90 µL of the above-mentioned concentrations of substrates and 10 µL of *Ct*Pae12B (100 µg/mL). The synthetic substrates, triacetin and β-D-glucopentaacetate contained 5 µL of *Ct*Pae12B (100 µg/mL). The substrates were dissolved in 50 mM Tris-HCl buffer, pH 7.2 (due to the intrinsic chemical instability and auto-hydrolysis of the substrates at pH 8.0) (Martínez-Martínez *et al*., 2008; Navarro-Fernández *et al*., 2008). However, enzyme assay for triacetin was performed at pH 8.0 because of its stability. The amount of enzyme that produced 1 µmol product per min under the reaction conditions was defined as one unit of enzymatic activity. Specific activity was determined by enzymatic activity per mg of the enzyme. The background level for the product for each substrate (enzyme blank/control) was subtracted for all data points. All the experiments

involving the specific activity of *Ct*Pae12B were performed in triplicates and the mean results were presented.

4.2.5 Biochemical properties of *Ct*Pae12B

4.2.5.1 Optimum temperature and pH

To determine the optimum temperature of *Ct*Pae12B, the enzyme assays were carried out at different temperatures (30–90 ºC) by using the synthetic substrate, *p*-Nitrophenyl acetate using standard reaction conditions as mentioned in section 2.2.18. The relative activity was calculated in terms of percentage by taking the maximum specific activity (under standard reaction conditions) as 100%. Under the standard reaction conditions, the optimum pH of *Ct*Pae12B was determined by varying the reaction pH. The effect of pH on *Ct*Pae12B activity was investigated by using the buffer systems, *viz*., 50 mM each of citrate phosphate (pH, 2.6–7.0), Tris-HCl (pH, 7.2–9.0), Bicine (pH, 7.6–9.0) and HEPES (pH, 6.8–8.2).

4.2.5.2 Stability analyses of *Ct*Pae12B

The thermostability of *Ct*Pae12B was determined by incubating it at different temperatures (30, 60, 70 and 80 ºC) for 24 h. Aliquots of 5 µL of *Ct*Pae12B (100 µg/mL) incubated at each temperature was taken at various time intervals and the enzymatic activity was assayed under the standard reaction conditions for *p*-Nitrophenyl acetate as mentioned earlier in section 2.2.18. The half-life ($t_{1/2}$) of *Ct*Pae12B at these temperatures was determined by time course of enzyme inactivation acquired for each temperature by plotting relative activity in terms of natural logarithm (ln A/A0) *vs*. time (Nawaz *et al*., 2018). The half-life ($t_{1/2}$) of *Ct*Pae12B was calculated by using the equation, $t_{1/2} = \ln 2/k$, where 'k' is the rate constant that was calculated from the slope of the linear plots (Nawaz *et al*., 2018). The pH stability of *Ct*Pae12B was studied by incubating the enzyme at different pH (2.6–10.6) at 25 ºC for 90 min. The buffer

systems used for pH stability were same as for pH optimization, along with the 50 mM carbonate-bicarbonate (pH, 9.2–10.6). After 90 min incubation, the enzymatic activity was assayed under standard reaction conditions for *p*-Nitrophenyl acetate as mentioned earlier in section 2.2.18.

4.2.6 Kinetic parameters of *Ct*Pae12B

The kinetic parameters study of *Ct*Pae12B were analysed for various natural and synthetic substrates. The synthetic substrates and their concentrations used were β-D-glucopentaacetate (0.01–10 mM), triacetin (0.01–30 mM), α-Naphthyl acetate (0.01–2.0 mM), β-naphthyl acetate (0.01–1.4 mM) and *p*-Nitrophenyl acetate (0.01–3.0 mM). The kinetic parameters were also determined with pectic substrates, potato rhamnogalacturonan (0.01–2.5%, w/v), sugar beet pectin (0.01–1.0%, w/v) and xylan substrates, acetylated birchwood xylan (0.01–2.5%, w/v), birchwood xylan (0.01–1.4%, w/v) and wheat arabinoxylan (0.2–1.4%, w/ v). The reaction was performed according to the method mentioned for each substrate in the section 2.2.18 and 4.2.4. The maximum velocity (V_{max}) and K_m were calculated from Michaelis-Menten curve and Lineweaver Burk plot. The turnover number (k_{cat}) and catalytic efficiency (k_{cat}/K_m) were also determined for each substrate.

4.2.7 Effect of metal ions and chemical agents on *Ct*Pae12B activity

The enzymatic activity of *Ct*Pae12B was determined in the presence of various metal ions and chemical agents. The metal ions used for the investigation were $CaCl_2$, KCl, $MgCl_2$, $MnSO_4$, $CoCl_2$, $NiSO_4$, $CuSO_4$, $FeCl_2$ and LiCl, chelating agents (EGTA and EDTA), detergents (SDS, Triton X100 and Tween 80). *Ct*Pae12B was incubated with different concentrations (1 mM, 2 mM and 5 mM) of the metal ions and chemical agents and the enzymatic activity was determined under the standard reaction conditions for *p*-nitrophenyl acetate as mentioned earlier in section 2.2.18. The effect

of salt (NaCl) at concentration range (20–300 mM), urea (0.1–5 M) and phenylmethylsulfonyl fluoride (PMSF) (1–50 mM), a serine protease/esterase inhibitor (Heymann, 1980) on *Ct*Pae12B activity was also investigated. The treatment of enzyme with PMSF was done to analyse the importance of serine present as a nucleophile in the catalytic triad of family CE12 esterases (Mølgaard, 2003; Ahmed *et al*., 2022). The enzymatic activity was calculated according to the method mentioned in section 2.2.18. The relative activity was calculated in terms of percentage by taking the reaction under standard conditions (devoid of any metal ion or chemical agent) as 100%.

4.2.8 Thermal denaturation study of *Ct*Pae12B

The thermal denaturation of recombinant *Ct*Pae12B was determined by using a UV–visible spectrophotometer (Varian, Cary 100 Bio). One millilitre of 50 µg/mL enzyme in 50 mM Tris-HCl buffer (pH 8.0) was subjected to varying temperatures in the range 25–100 ºC. The absorbance (A_{280}) was measured at an interval of every 2 ºC with a holding time of 2 min. The temperature was controlled by the coupled peltier system. The complete denaturation of the protein was determined by the peak achieved in the melting curve obtained by a plot between absorbance (A_{280}) and the temperature. The melting profile of *Ct*Pae12B was also studied in the presence of 5 mM concentration of each, Ca^{2+} and Mg^{2+} ions and chelating agents, EDTA and EGTA.

4.3 Results and Discussion

4.3.1 Phylogenetic analysis of *Ct*Pae12B

Phylogenetic analysis of *Ct*Pae12B with its closest homologues of family 12 CE, *viz*, PAE (YxiM, Uniprot id: P42304, PDB id: 2O14) from *B. subtilis* strain 168, RGAE (RGAE, Uniprot id: Q00017, PDB id: 1DEO) from *A. aculeatus*, RGAE (YesY, Uniprot id: O31528) from *B. subtilis* strain 168, RGAE (YesT, Uniport id: O31523) from *B. subtilis* strain 168, PAE (BliPAE, Uniprot id: Q65DF1) from *B. licheniformis* DSM13 and PAE (PaeY, Uniprot id: O32563) from *Dickeya dadantii* 3937 (Ahmed *et al*., 2022), was done using Mega-X software. The study showed that *Ct*Pae12B belongs to the same clade with that of YesT, an RGAE from *Bacillus subtilis* (Fig. 4.2). The branch length between them was less showing minimal sequence divergence. The bootstrap value, 95% showed strong support for the phylogenetic analysis.

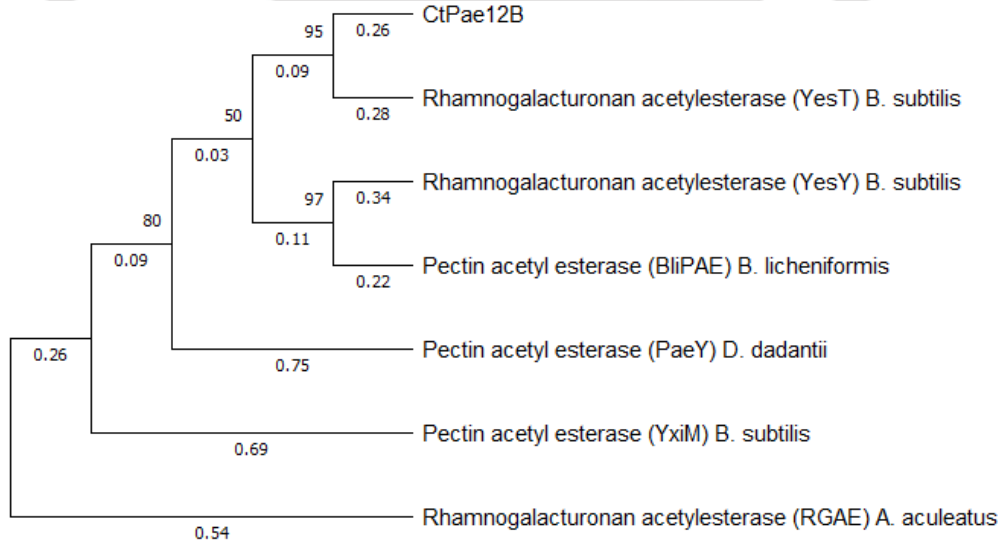

Fig. 4.2 Phylogenetic analysis of *Ct*Pae12B with its closest homologues from CE12 family, RGAE (YesY, Uniprot id: O31528) from *B. subtilis* strain 168, RGAE (YesT, Uniport id: O31523) from *B. subtilis* strain 168, PAE (BliPAE, Uniprot id: Q65DF1) from *B. licheniformis* DSM13, PAE (PaeY, Uniprot id: O32563) from *Dickeya dadantii* 3937, PAE (YxiM, Uniprot id: P42304, PDB id: 2O14) from *B. subtilis* strain 168 and RGAE (RGAE, Uniprot id: Q00017, PDB id: 1DEO) from *A. aculeatus.*

4.3.2 *Ct*Pae12B production yield under different media

The production of *Ct*Pae12B in 100 mL of five different compositions of media was studied. The *E. coli* BL-21 (DE3) cells were grown in respective medium at 24 ºC, 180 rpm for 16 h. The dry cell weight of the grown culture after 16 h of incubation in each medium was determined. The maximum dry cell weight 3.14 ± 0.3 g, was found in AIM-LB medium, followed by LB, TY, TB and 5X-LB medium (Table 4.1). However, the total amount of protein produced by growing the cells in LB medium was highest, i.e., 1.5 mg with protein concentration 0.6 mg/mL followed by AIM-LB, TB, TY and 5X -LB (Table 4.1). The protein yield obtained based on the cell dry weight was 0.71 mg/g for LB medium and 0.84 mg/g for TB medium (Table 4.1). However, the cost of LB medium is half the cost of the TB medium. Therefore, based on the total amount of protein (1.5 mg) produced by 100 mL of LB medium and its cost-effectiveness, LB (1X) medium was chosen as the best medium for *Ct*Pae12B production. The dry cell weight as well as the total amount of protein was least for 5X-LB medium. This could be probably because of the composition of LB medium, where the catabolizable amino acids are the main carbon source for *E. coli* instead of sugars (Sezonov *et al*., 2007). LB consists of tryptone (10 g/L) which is a casein (cow-milk protein) obtained from pancreatic digest and yeast extract (5 g/L) from *S. cerevisiae*. Upon inoculation with *E. coli* culture, highly concentrated LB medium produces metabolites by catabolizing the amino acids increasing the alkalinity and thus, increasing the pH of the medium under aerobic conditions (Kram *et al*., 2015). Highly alkaline medium can cause cell death and faster attaining of stationary phase in *E. coli* growth curve. This study showed that the concentration of the media components can be further optimized for enhancing the cell mass and the expressed protein content.

Table 4.1 Purified *Ct*Pae12B protein yield after production in different media.

Medium	Dry cell wt. (g)	Protein concentration (mg/mL)	Total volume of protein (mL)	Total protein (mg)	Protein yield (mg/g of cell dry wt.)
LB	2.1 ± 0.1	0.6 ± 0.2	2.5	1.5	0.71
AIM-LB	3.14 ± 0.31	0.55 ± 0.11	2.5	1.38	0.44
TB	1.6 ± 0.2	0.6 ± 0.3	2.25	1.35	0.84
TY	2.0 ± 0.2	0.3 ± 0.2	2.5	0.75	0.38
5X-LB	0.9 ± 0.2	0.3 ± 0.3	1.5	0.45	0.05

4.3.3 Biochemical properties of *Ct*Pae12B

4.3.3.1 Optimum temperature and pH

*Ct*Pae12B showed maximum activity at temperature, 65 ºC. It retained ~80% of its relative activity at 90 ºC (Fig. 4.3A). Overall, *Ct*Pae12B retained more than 50% of its activity across the temperature range, 30 ºC to 90 ºC. The optimum pH for maximum *Ct*Pae12B activity was found to be 8.0. The maximum activity at pH 8.0 was found in two buffer systems, i.e., Tris-HCl and HEPES buffer (Fig. 4.3B). The optimum pH 8.0 for PAE (BliPAE) from *B. lichenisformis* (Remoroza *et al*., 2014), RGAE (BhRGAE) from *B. halodurans* (Navarro-Fernández *et al*., 2008), PAE (YxiM) from *B. subtilis* (Bolvig *et al*., 2003) and PAE (PaeY) from *E. chrysanthemi* (Shevchik and Hugouvieux-Cotte-Pattat, 1997) was reported earlier. Other PAEs and RGAEs which have maximum activity at alkaline pH (8.5) are, RGAE (pp1113) from *Paenibacillus polymyxa* (Tang *et al*., 2021), RGAE (YesT) from *B. subtilis* (Martínez-Martínez *et al*., 2008) and PAE (PaeX) from *E. chrysanthemi* (Table 4.3) (Hugouvieux-Cotte-Pattat, 2003). While, fungal RGAE from *A. aculeatus* was reported to have maximal activity at acidic pH 5.5 (Searle-van Leeuwen *et al*., 1992).

4.3.3.2 Stability analysis of *Ct*Pae12B

*Ct*Pae12B showed temperature stability up to 60 ºC for 24 h. The half-life ($t_{1/2}$) of *Ct*Pae12B calculated at different temperatures showed 18.9 days (~ 453 h) at 30 ºC, 10.4 days (~ 250.5 h) at 60 ºC, 2.3 days (~ 56 h) at 70 ºC and 5.1 h at 80 ºC (Fig. 4.3C).

The enzyme remained stable for 6.5 months at 4 ºC (data not shown). The high optimum temperature and high temperature stability of the enzyme *Ct*Pae12B exhibited its typical nature of being thermophilic as it belongs to a thermophile *A. thermocellus*. The pH stability of *Ct*Pae12B showed retaining of its maximum activity in a wide range of pH. The enzyme retained approximately 98% activity from acidic pH 4.0 to alkaline pH 10.5 (Fig. 4.3D). The PAEs that showed enzyme stability at both acidic and alkaline pH were BliPAE from *B. licheniformis*, pH range, 5.0-8.0 (Remoroza *et al*., 2014) and YxiM from *B. subtilis*, pH range, 4.0-9.0 (Bolvig *et al*., 2003) as also mentioned in Table 4.3.

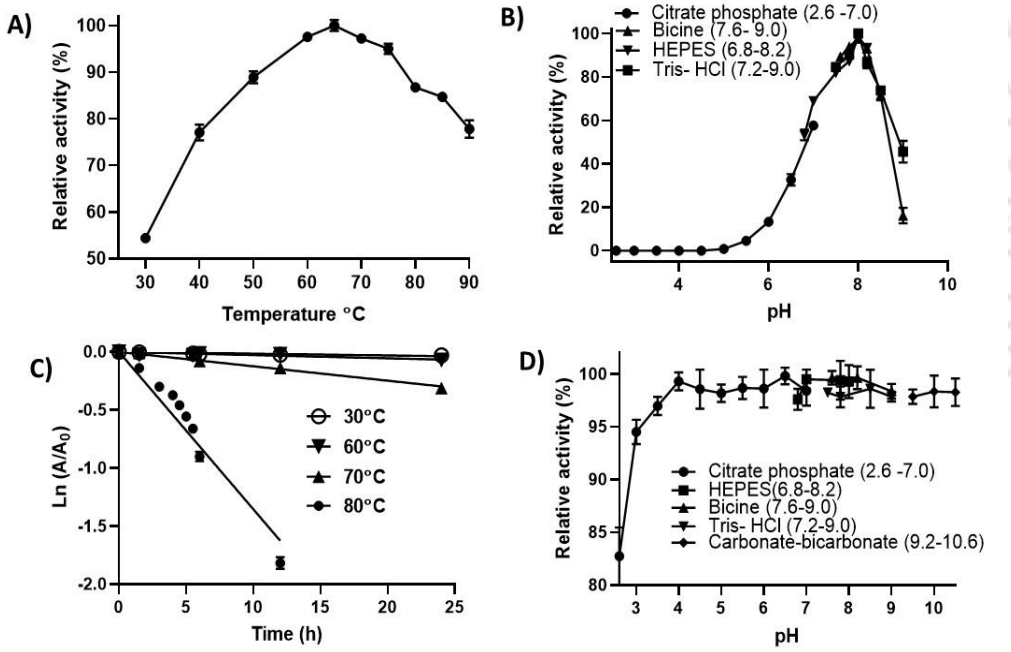

Fig. 4.3 Biochemical properties of *Ct*Pae12B. A) Optimum temperature for *Ct*Pae12B activity, B) Optimum pH for *Ct*Pae12B activity, C) Thermal inactivation curve of *Ct*Pae12B plotted in terms of natural logarithm of relative activity vs time, D) pH stability of *Ct*Pae12B. The plots were generated using graphpad prism 8.0.1 software.

4.3.4 Substrate specificity of *Ct*Pae12B

The substrate specificity of *Ct*Pae12B towards various natural and synthetic substrates was determined. Among the natural pectic substrates, *Ct*Pae12B showed highest specific activity, 700 ± 10 U/mg with potato rhamnogalacturonan (Table 4.2). It was also found to be active in releasing acetate from sugar beet pectin (42 ± 1.4 U/mg). Sugar beet pectin has mostly acetylated HG as compared with acetylated RG as reported in an earlier study (Remoroza *et al*., 2014). The lower specific activity of *Ct*Pae12B against sugar beet pectin might be due to the presence of lower degree of acetylation (16.5% acetylation) mainly located in the HG region. As *Ct*Pae12B showed highest specific activity against the RG I region of pectin in de-acetylation as compared with HG region, therefore it was named as an RGAE. The presence of methyl esterification in the side chains of sugar beet pectin causes steric hindrance to the catalytic action of acetyl esterase while removing the acetyl groups and therefore pre-treatment by PME is required to enhance the activity of acetyl esterase (Remoroza *et al*., 2014). *Ct*Pae12B did not show any activity against citrus pectin, apple pectin and also galactan substrates. This could be because of negligible degree of acetylation as compared with the higher degree of methylation in citrus pectin and apple pectin (Bolvig *et al*., 2003; Thibault *et al*., 2003). No acetate release was detected with soybean rhamnogalacturonan either, due to the lack of acetylation in the RG region of soybean (Nakamura *et al*., 2002). Whereas, *Ct*Pae12B was found to deacetylate acetylated birchwood xylan, birchwood xylan and wheat arabinoxylan but no activity was found with rye arabinoxylan and beechwood xylan. On contrary to these findings, a PAE (YxiM) from *B. subtilis* was reported to deacetylate rye arabinoxylan but not wheat arabinoxylan (Bolvig *et al*., 2003). Earlier reports showed that a few RGAEs, BhRGAE from *B. halodurans* (Navarro-Fernández *et al*., 2008) and YesT from *B. subtilis* were able to deacetylate

acetylated birchwood xylan (Table 4.3). A study on a PAE (BliPAE) from *B. licheniformis* showed its inability to deacetylate acetylated xylan substrates (Remoroza *et al*., 2014). *Ct*Pae12B is the first RGAE to show such high activity against a potato RG polymer. It is noteworthy that most of the other homologues of *Ct*Pae12B were studied using mainly sugar beet pectin as a substrate and other natural substrates were not explored for deacetylation. Other than natural substrates, *Ct*Pae12B was also able to liberate the products from the synthetic substrates, *viz*. *p*-Nitrophenyl acetate, α- and β-Naphthyl acetate, β-D-glucopentaacetate and triacetin (Table 4.2). The substrate specificity of *Ct*Pae12B resembles more with the properties of RGAEs than PAEs as it efficiently deacetylates potato rhamnogalacturonan and follows the catalytic trend of other characterized RGAEs in de-acetylating the xylan substrates as well. *Ct*Pae12B was also found to be active against sugar beet pectin as observed earlier with a fungal RGAE from *Aspergillus aculeatus* (Bonnin *et al*., 2008). They reported that the fungal RGAE was able to liberate acetate from the HG region of sugar beet pectin. Moreover, *Ct*Pae12B displayed significant activity against the synthetic substrate, triacetin which is contrary to RGAE from *A. aculeatus* (Shevchik and Hugouvieux-Cotte-Pattat, 1997). They reported that the fungal enzyme was not able to deacetylate triacetin, as it specifically deacetylated only the ramified regions of pectin (Shevchik and Hugouvieux-Cotte-Pattat, 1997). This showed that *Ct*Pae12B possess broad substrate specificity as it displayed activity against all the synthetic substrates taken in this study. Moreover, *Ct*Pae12B could also deacetylate xylan along with the pectic substrates.

Table 4.2 Specificity and specific activity of *Ct*Pae12B against various natural and synthetic substrates.

Natural substrate	Specific activity (U/mg)
Potato rhamnogalacturonan (2%, w/v)	700 ± 10
Acetylated birchwood xylan (2%, w/v)	90 ± 5
Birchwood xylan (1%, w/v)	43 ± 2
Sugar beet pectin (0.5%, w/v)	42 ± 1
Wheat arabinoxylan (1%, w/v)	26 ± 2
Citrus pectin (1%, w/v)	0
Apple pectin (1%, w/v)	0
Soybean rhamnogalacturonan (1%, w/v)	0
Lupin galactan (1%, w/v)	0
Potato galactan (1%, w/v)	0
Synthetic substrate	**Specific activity (U/mg)**
β-D-glucopentaacetate (8.5 mM)	750 ± 3
*Triacetin (25 mM)	540 ± 9
*β-Naphthyl acetate (0.95 mM)	130 ± 5
**p*-Nitrophenyl acetate (2 mM)	102 ± 2
*α-Naphthyl acetate (1 mM)	85 ± 3

* The enzymatic activity was performed at pH 8.0 (50 mM Tris-HCl buffer)

Table 4.3 Biochemical parameters of *Ct*Pae12B and its homologous enzymes.

Organism/Name of enzyme	Optimum temperature (° C)	Optimum pH	Thermo Stability	pH stability	Subs-trate	K_m, mg/mL for natural and mM for synthetic substrates, resp.	References
A. thermocellus/ RGAE	65	8.0	60 ºC, 24 h	4.0-10.5	PRG SBP ABX *p*NPA bGP	13.4 ± 1.1 1.4 ± 0.1 7.1 ± 0.6 0.62 ± 0.09 1.2 ± 0.3	This study
A. aculeatus/ RGAE	40	5.5	50 ºC, 20 h	5.0	PRG SBP BX *p*NPA bGP	- 0 0 - -	Searle-van Leeuwen *et al*., 1992
E. chrysanthemi/ PAE (PaeY)	50	8.0	50 ºC, 2 h	-	PRG SBP Xylan *p*NPA bGP	- 25 ± 13 - 6 ± 1.2 -	Shevchik and Hugouvieux-Cotte-Pattat, 1997
E. chrysanthemi/ PAE (PaeX)	-	8.7	-	-	PRG SBP Xylan *p*NPA bGP	- ND, 2 ± 1% acetate release - ND -	Shevchik and Hugouvieux-Cotte-Pattat, 2003
B. subtilis/ PAE (YxiM)	-	8.0	-	4.0-9.0	PRG Potato pectin SBP RAX *p*NPA bGP	- ND, 24% acetate release 12 ND, 11% acetate release 1.6 -	Bolvig *et al*., 2003
B. licheniformis/ PAE (BliPAE)	50	8.0	50 ºC, 1 h	5.0-8.0	PRG SBP Xylan *p*NPA bGP	- ND, 37% acetate release - ND -	Remoroza *et al*., 2014
B. halodurans/ RGAE (BhRGAE)	40	8.0	Up to 50 ºC	Above 8.0	PRG SBP ABX *p*NPA bGP	- - ND 14.1 9.1	Navarro-Fernández *et al*., 2008
B. subtilis/ RGAE (YesT)	35	8.5	35-40 ºC	7.0-9.0	PRG SBP ABX bGP *p*NPA	- - ND, 0.02 µmoles acetate release 9.1 2.8	Martínez-Martínez *et al*., 2008
P. polymyxa/ RGAE (pp1113)	30	8.5	Up to 40 ºC	-	PRG SBP Xylan bGP *p*NPA	- - - - 2.22 ± 0.49	Tang *et al*., 2021

ND: Not determined

(PRG- Potato rhamnogalacturonan, SBP- Sugar beet pectin, bGP- β-D-glucopentaacetate, *p*NPA- para-Nitrophenyl acetate, ABX- acetylated birchwood xylan, RAX- rye arabinoxylan, BX- birchwood xylan)

4.3.5 Kinetic parameters of *Ct*Pae12B

Among synthetic substrates, the kinetic parameters determined for *Ct*Pae12B showed maximum velocity (V_{max}), 770 ± 10 U/mg (Fig. 4.4), for β-D-glucopentaacetate (Table 4.4). The Michaelis-Menten constant (K_m) determined from the Michaelis-Menten equation and Lineweaver Burk plot was 1.2 ± 0.3 mM, for β-D-glucopentaacetate. The K_m value determined earlier for both RGAEs, BhRGAE and YesT was 9.1 mM, using substrate, β-D-glucopentaacetate (Table 4.3) (Martínez-Martínez *et al*., 2008; Navarro-Fernández *et al*., 2008). The lower K_m value of *Ct*Pae12B towards β-D-glucopentaacetate showed its high substrate affinity. The catalytic efficiency (k_{cat}/K_m) 267 $s^{-1}mg^{-1}mL$ of *Ct*Pae12B was also maximum with β-D-glucopentaacetate among all the synthetic substrates used. Most of the previously reported enzymes showed affinity for *p*-Nitrophenyl acetate and a comparative analysis showed that *Ct*Pae12B has significantly higher affinity for *p*-nitrophenyl acetate (K_m, 0.62 ± 0.09 mM) as compared with the K_m value of RGAEs, BhRGAE from *B. halodurans*, K_m, 14.1 mM (Navarro-Fernández *et al*., 2008), YesT from *B. subtilis*, K_m, 2.8 mM (Martínez-Martínez *et al*., 2008) and PAEs, PaeY from *E. chrysanthemi*, K_m, 6 ± 1.2 mM (Shevchik and Hugouvieux-Cotte-Pattat, 1997) and YxiM from *B. subtilis*, K_m, 1.6 (Bolvig *et al*., 2003) as listed in Table 4.3. The value of V_{max}, 770 ± 10 U/mg was maximum against potato rhamnogalacturonan among all the natural substrates tested (Fig. 4.5) and the K_m value was 13.4 ± 1.1 mg/mL (Table 4.4). Moreover, *Ct*Pae12B showed maximum catalytic efficiency i.e., 24 $s^{-1}mg^{-1}mL$ with potato rhamnogalacturonan among all the natural substrates. There is no report available on the activity of RGAEs with RG region of potato pectin. However, a PAE, YxiM from *B. subtilis* released 24% of the total acetate groups from potato pectin (Bolvig *et al*., 2003) (Table 4.3). The V_{max}, 50 ± 3 U/mg, of *Ct*Pae12B with sugar beet pectin was

much lower than potato rhamnogalacturonan. Among xylan substrates, *Ct*Pae12B gave maximal velocity (V_{max}) with acetylated birchwood xylan followed by birchwood xylan and wheat arabinoxylan (Table 4.4).

Table 4.4 Kinetic parameters of *Ct*Pae12B with natural and synthetic substrates.

Synthetic substrate	V_{max} (U/mg)	K_m (mM)	k_{cat} (s^{-1})	k_{cat}/K_m ($s^{-1}mM^{-1}$)
β-D-glucopentaacetate	770 ± 10	1.2 ± 0.3	321	267
Triacetin	570 ± 10	4.5 ± 0.5	238	53
β-Naphthyl acetate	143 ± 7	0.36 ± 0.04	60	165
p-Nitrophenyl acetate	118 ± 9	0.62 ± 0.09	49	79
α-Naphthyl acetate	100 ± 10	0.45 ± 0.03	41.6	92.6
Natural substrate	V_{max} (U/mg)	K_m (mg/mL)	k_{cat} (s^{-1})	k_{cat}/K_m ($s^{-1}mg^{-1}mL$)
Potato rhamnogalacturonan	770 ± 10	13.4 ± 1.1	321	24
Sugar beet pectin	50 ± 3	1.4 ± 0.1	20.8	15
Acetylated birchwood xylan	105 ± 9	7.1 ± 0.6	43.8	6
Birchwood xylan	50 ± 5	4.5 ± 0.5	20.8	4.6
Wheat arabinoxylan	33 ± 4	4.5 ± 0.5	13.8	3

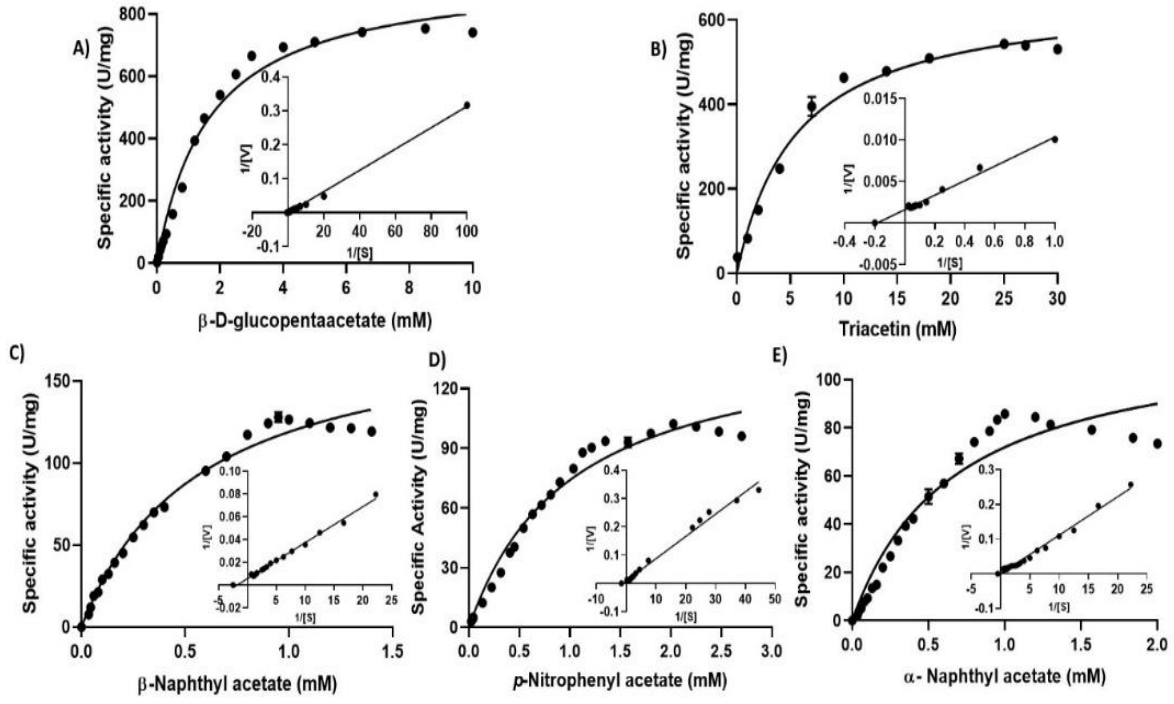

Fig. 4.4 Kinetics of *Ct*Pae12B with various synthetic substrates. A) β-D-glucopentaacetate, B) Triacetin, C) β-naphthyl acetate, D) *p*-nitrophenyl acetate, E) α-naphthyl acetate.

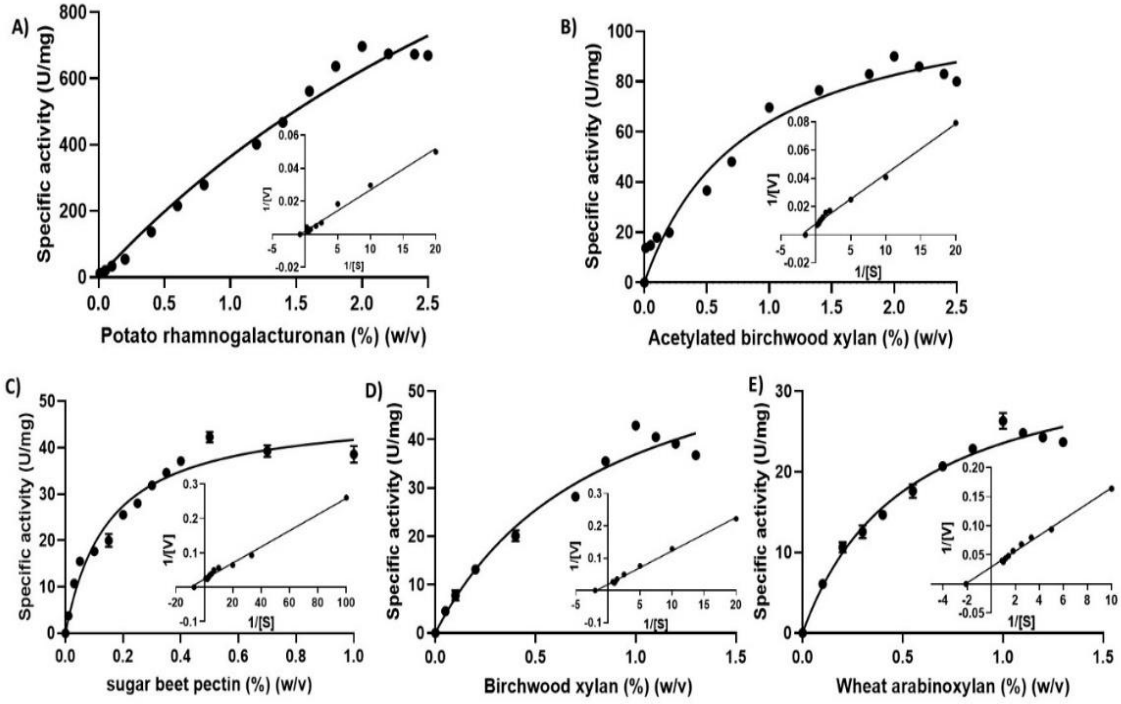

Fig. 4.5 Kinetics of *Ct*Pae12B with natural pectic and xylan substrates. A) Potato rhamnogalacturonan, B) Acetylated birchwood xylan, C) Sugar beet pectin, D) Birchwood xylan, E) Wheat arabinoxylan.

4.3.6 Effect of metal ions and chemical agents on *Ct*Pae12B activity

The results of the effect of metal ions and other chemical agents on the enzyme activity of *Ct*Pae12B are reported in Table 4.5. None of the metal ion used enhanced the enzymatic activity of *Ct*Pae12B. BhRGAE, an RGAE from *B. halodurans* was also reported to have no enhancement in the enzymatic activity by any metal ion (Navarro-Fernández *et al*., 2008). A low inactivation (10%) of enzyme was observed in the presence of 5 mM Mn^{2+} ions, whereas, a number of other metal ions like Ni^{2+}, Cu^{2+}, Co^{2+} or Fe^{2+}, at 5 mM concentration, significantly inhibited the activity of *Ct*Pae12B (Table 4.5). The presence of heavy metal ions may have inhibited the activity by occupying and blocking the catalytic cleft preventing catalysis of the substrate as also reported earlier (Karaca *et al*., 2010). Ca^{2+} and Mg^{2+} ions did not show any change in the enzymatic activity. The enzymatic activity was inhibited in the presence of all the

detergents SDS, Triton X100 and Tween 80. It is noteworthy that *Ct*Pae12B retained 100% of its residual activity in the presence of high concentration, 5 M urea. Similar results for an endoglucanase D (EGD) from *A. thermocellus* showed that 5 M urea concentration does not affect the enzymatic activity (Tokatlidis *et al*., 1991). The secondary structure of the enzyme, EGD was found intact in the presence of urea up to 8 M concentration. However, a pectin methyl esterase, *Ct*PME, from *A. thermocellus* was earlier reported to show 75% inhibition at 5 M concentration of urea (Rajulapati and Goyal, 2017). *Ct*Pae12B is the first RGAE to exhibit stable activity at such high molar concentration of urea. *Ct*Pae12B lost 30% activity in the presence of 0.3 M NaCl concentration (Table 4.5). The chelating agents, EDTA and EGTA, did not show any effect on the activity of *Ct*Pae12B. The enzymatic activity of *Ct*Pae12B was completely inhibited in the presence of 50 mM of a serine protease/esterase inhibitor, PMSF. This showed the importance of serine residue present in the catalytic triad of the enzyme (Ahmed *et al*., 2022). This result was consistent with the findings which are reported earlier, where two RGAEs, BhRGAE from *B. halodurans* and YesT from *B. subtilis* were completely inhibited by 30 mM and (Navarro-Fernández *et al*., 2008) and 50 mM PMSF (Martínez-Martínez *et al*., 2008), respectively.

Table 4.5 Effect of metal ions and chemical agents on *Ct*Pae12B activity.

Metal ions	Relative activity (%)	
	1 mM	5 mM
K^+	99 ± 1	99 ± 1
Li^+	99.3 ± 1.3	99 ± 1
Mg^{2+}	99 ± 1	100 ± 1
Ca^{2+}	99.5 ± 0.5	100 ± 1
Mn^{2+}	95 ± 2	90 ± 1
Ni^{2+}	83.7 ± 2.1	38.4 ± 2.5
Co^{2+}	79.4 ± 1.8	18 ± 2
Cu^{2+}	63 ± 2	23.3 ± 2.5
Fe^{2+}	56 ± 2	0
Detergents	1 mM	5 mM
SDS	32 ± 3	0
Triton X100	90 ± 1 (0.1% v/v)	66.4 ± 1.1 (0.5% v/v)
Tween 80	92 ± 1 (0.1 % v/v)	68.6 ± 0.5 (0.5% v/v)
Chelating agents	1 mM	5 mM
EGTA	98.2 ± 0.6	98 ± 1
EDTA	100 ± 1	99 ± 1
Inhibitors and chaotropic agents		
NaCl	84.3 ± 0.7 (0.1 M)	69.2 ± 1.6 (0.3 M)
Urea	99.5 ± 0.5 (1 M)	100 ± 1 (5 M)
PMSF	52.7 ± 1.6 (0.01 M)	0 (0.05 M)

4.3.7 Thermal denaturation study of *Ct*Pae12B

The thermal denaturation analysis of *Ct*Pae12B determined by the single melting peak showed that it completely unfolded at 94 ºC, when no metal ions or chelating agents were present (Fig. 4.6A). The melting peak did not shift in the presence of 5 mM of Ca^{2+} or Mg^{2+} ions (Fig. 4.6B). This showed that both these metal ions do not contribute to the thermal stability of the enzyme. The melting peak also remained unchanged when analysed in the presence of 5 mM of the chelating agents EDTA (Fig. 4.6C) and EGTA (Fig. 4.6D). It was further concluded that *Ct*Pae12B does not have any bound divalent ion required for its stability, activity or structural integrity. These results corroborated with the results of *Ct*Pae12B activity where it is reported that there is no change in the enzyme activity in the presence of Ca^{2+} or Mg^{2+} metal ions and the chelating agents as described in Section 4.3.6.

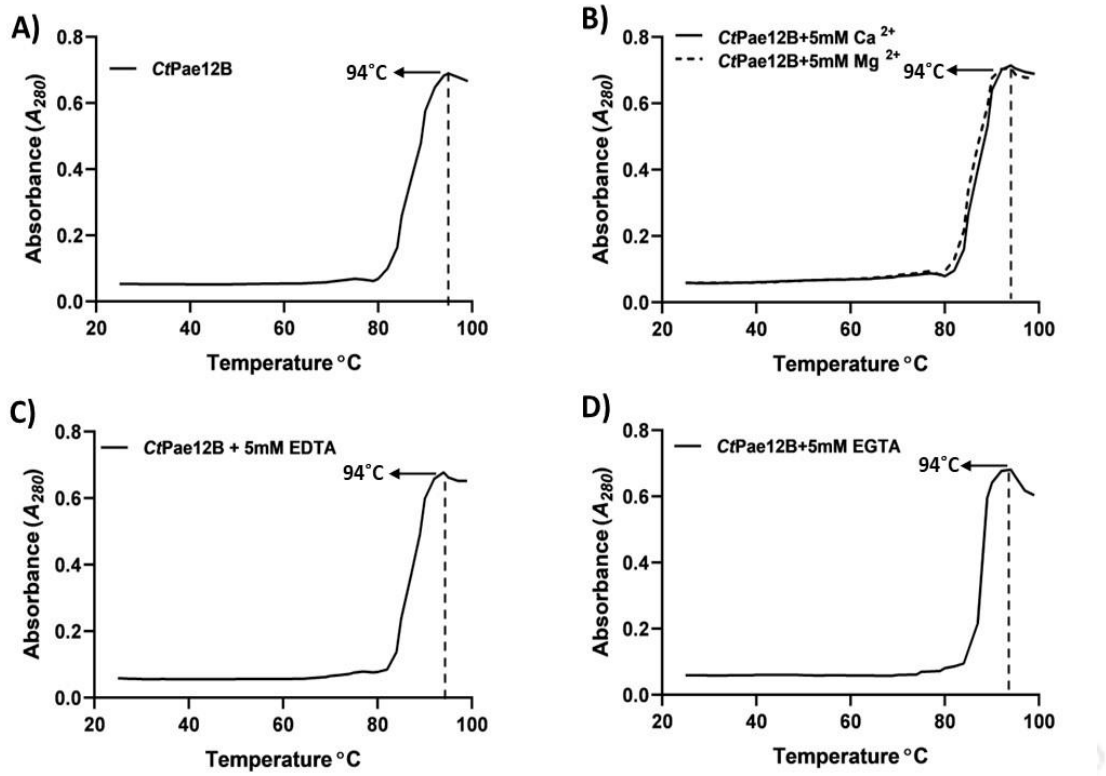

Fig. 4.6 Protein melting analysis of *Ct*Pae12B. A) *Ct*Pae12B without any metal ion or chelating agent, B) *Ct*Pae12B in the presence of 5 mM Ca^{2+} or Mg^{2+} ions, C) *Ct*Pae12B in presence of 5 mM EDTA and D) *Ct*Pae12B in presence of 5 mM EGTA.

4.4 Conclusion

Rhamnogalacturonan acetyl esterase, *Ct*Pae12B was obtained with maximum yield from commercial medium LB. *Ct*Pae12B displayed thermophilic properties with optimum temperature, 65 ºC and retained 50% of its activity for 5.1 h at 80 ºC. *Ct*Pae12B was stable in both acidic and alkaline environment and displayed maximum activity at pH 8.0. The enzyme, *Ct*Pae12B was drastically inactivated by heavy metal ions, Co^{2+}, Cu^{2+}, Fe^{2+} and Ni^{2+} ions and anionic and non-ionic detergents. However, it was remarkably completely stable at a high concentration, 5 M of urea. Complete inhibition of *Ct*Pae12B activity by 50 mM PMSF showed the importance of the serine residue in catalysis. The enzymatic activity was not affected by any chelating agent showing no involvement of any metal ion for catalysis or structural integrity. The protein melting analysis also confirmed that there is no contribution to thermal stability by any metal ion or chelating agent, corroborating their non-involvement in imparting stability. *Ct*Pae12B showed robustness and superior properties as compared with its homologues as it showed activity against PRG as well as sugar beet pectin, xylan substrates like acetylated birchwood xylan, birchwood xylan, wheat arabinoxylan and also wide range of synthetic substrates. The highest specificity of *Ct*Pae12B against PRG showed its affinity towards the RG region of pectin confirming it to be an RGAE. This result can be explored in managing potato waste generated by many households and food industries like potato chips. *Ct*Pae12B is an efficient enzyme with its alkaline and thermotolerant properties, however, its limitation is that, it is efficient only on acetylated pectic or xylan substrates. It plays no role when the esterified substrate has only methyl groups and does not bear any or have negligible degree of acetylation. However, its broad substrates specificity, high specific activity against PRG (700 U/mg) and thermostable nature makes it a potential candidate to explore its clinical and pharmaceutical applications like inhibition of cancer cells and drug delivery.

References

Ahmed, J., Kumar, K., Sharma, K., Fontes, C.M., Goyal, A. (2022) Computational and SAXS-based structure insights of pectin acetyl esterase (CtPae12B) of family 12 carbohydrate esterase from *Clostridium thermocellum* ATCC 27405. Journal of Biomolecular Structure and Dynamics, 40(18): 8437-8454.

Ahmed, J., Thakur, A., Goyal, A. (2021) Emerging trends on the role of recombinant pectinolytic enzymes in industries-an overview. Biocatalysis and Agricultural Biotechnology, 38: 102200.

Bolvig, P.U., Pauly, M., Orfila, C., Scheller, H.V., Schnorr, K. (2003) Sequence analysis and characterization of a novel pectin acetyl esterase from *Bacillus subtilis*. Advances in Pectin and Pectinase Research, (eds. Voragen, F., Schols, H., Visser, R.), Springer, Dordrecht, 315-330.

Bonnin, E., Clavurier, K., Daniel, S., Kauppinen, S., Mikkelsen, J.D.M., Thibault, J.F. (2008) Pectin acetylesterases from *Aspergillus* are able to deacetylate homogalacturonan as well as rhamnogalacturonan. Carbohydrate Polymers, 74(3): 411-418.

Heymann E. (1980). Carboxylesterases and amidases. Enzymatic Basis of Detoxification, (Ed. Jakoby W.B.), Academic Press, New York, 2, 291–323.

Karaca, A., Cetin, S.C., Turgay, O.C., Kizilkaya, R. (2010) Effects of heavy metals on soil enzyme activities. Soil Heavy Metals, Springer, Berlin, Heidelberg, 237-262.

Kram, K.E., Finkel, S.E. (2015) Rich medium composition affects Escherichia coli survival, glycation, and mutation frequency during long-term batch culture. Applied and Environmental Microbiology, 81(13): 4442-4450.

Kumar, S., Stecher, G., Li, M., Knyaz, C., Tamura, K. (2018) MEGA X: molecular evolutionary genetics analysis across computing platforms. Molecular Biology and Evolution, 35(6): 1547.

Lau, E.Y., Bruice, T.C. (1999) Consequences of breaking the Asp-His hydrogen bond of the catalytic triad: Effects on the structure and dynamics of the serine esterase cutinase. Biophysical Journal, 77(1): 85–98.

Martínez-Martínez, I., Navarro-Fernández, J., Daniel Lozada-Ramírez, J., García-Carmona, F., Sánchez-Ferrer, Á. (2008) YesT: a new rhamnogalacturonan acetyl esterase from *Bacillus subtilis*. Proteins: Structure, Function, and Bioinformatics, 71(1): 379-388.

Mølgaard, A. (2003) Rhamnogalacturonan Acetylesterase, a Member of the SGNH-Hydrolase Family. Advances in Pectin and Pectinase Research, (Eds. Voragen, F., Schols, H., Visser, R.), Springer, Dordrecht, 299-313.

Mølgaard, A., Kauppinen, S., Larsen, S. (2000) Rhamnogalacturonan acetylesterase elucidates the structure and function of a new family of hydrolases. Structure, 8 (4): 373–383.

Nakamura, A., Furuta, H., Maeda, H., Takao, T., Nagamatsu, Y. (2002) Structural studies by stepwise enzymatic degradation of the main backbone of soybean soluble polysaccharides consisting of galacturonan and rhamnogalacturonan. Bioscience, Biotechnology and Biochemistry, 66(6): 1301-1313.

Navarro-Fernández, J., Martínez-Martínez, I., Montoro-García, S., García-Carmona, F., Takami, H., Sánchez-Ferrer, A. (2008) Characterization of a new rhamnogalacturonan acetyl esterase from *Bacillus halodurans* C-125 with a new putative carbohydrate binding domain. Journal of Bacteriology, 190 (4): 1375-1382.

Nawaz, M.H., Ferreira, J.C., Nedyalkova, L., Zhu, H., Carrasco-López, C., Kirmizialtin, S., Rabeh, W.M. (2018) The catalytic inactivation of the N-half of human hexokinase 2 and structural and biochemical characterization of its mitochondrial conformation. Bioscience Reports, 38 (1).

O'Neill, M., Albersheim, P., Darvill, A. (1990) The pectic polysaccharides of primary cell walls. Methods in Plant Biochemistry, (Ed. Dey D.M.), Academic Press, London, 1990, 415-441.

Oomen, R.J.F.J., Doeswijk-Voragen, C.H., Bush, M.S., Vincken, J.P., Borkhardt, B., Van den Broek, L.A., Corsar, J., Ulvskov, P., Voragen, A.G., McCann, M.C., Visser, R.G. (2002) In muro fragmentation of the rhamnogalacturonan I backbone in potato (*Solanum tuberosum* L.) results in a reduction and altered location of the galactan and arabinan side-chains and abnormal periderm development. The Plant Journal, 30 (4): 403-413.

Polgár, L. (2005) The catalytic triad of serine peptidases. Cellular and Molecular Life Sciences, 62: 2161–2172.

Rajulapati, V., Goyal, A. (2017) Molecular cloning, expression and characterization of pectin methylesterase (*Ct*PME) from *Clostridium thermocellum*. Molecular Biotechnology, 59 (4): 128-140.

Remoroza, C., Wagenknecht, M., Gu, F., Buchholt, H.C., Moerschbacher, B.M., Schols, H.A., Gruppen, H. (2014) A *Bacillus licheniformis* pectin acetylesterase is specific for homogalacturonans acetylated at O-3. Carbohydrate Polymers, 107: 85-93.

Ridley, B.L., O'Neill, M.A., Mohnen, D. (2001) Pectins: structure, biosynthesis, and oligogalacturonide-related signaling. Phytochemistry, 57: 929–967.

Safran, J., Habrylo, O., Cherkaoui, M., Lecomte, S., Voxeur, A., Pilard, S., Bassard, S., Pau-Roblot, C., Mercadante, D., Pelloux, J., Sénéchal, F. (2021) New insights into the specificity and processivity of two novel pectinases from *Verticillium dahliae*. International Journal of Biological Macromolecules, 176: 165-176.

Schols, H.A., Voragen, A.G.J. (1996) Complex pectins: Structure elucidation using enzymes. Pectins and Pectinases, (Eds. Visser J., Voragen A.G.J.), Elsevier Science B.V., Amsterdam, Netherlands, 3-19.

Searle-van Leeuwen, M.J.F., Van den Broek, L.A.M., Schols, H.A., Beldman, G., Voragen, A.G.J. (1992) Rhamnogalacturonan acetylesterase: a novel enzyme from *Aspergillus aculeatus*, specific for the deacetylation of hairy (ramified) regions of pectins. Applied Microbiology and Biotechnology, 38 (3): 347-349.

Sezonov, G., Joseleau-Petit, D., d'Ari, R. (2007) *Escherichia coli* physiology in Luria-Bertani broth. Journal of Bacteriology, 189 (23): 8746-8749.

Shevchik, V.E., Hugouvieux-Cotte-Pattat, N. (2003) PaeX, a second pectin acetyl esterase of *Erwinia chrysanthemi* 3937. Journal of Bacteriology, 185 (10): 3091–3100.

Shevchik, V.E., Hugouvieux-Cotte-Pattat, N. (1997) Identification of a bacterial pectin acetyl esterase in *Erwinia chrysanthemi* 3937. Molecular Microbiology, 24 (6): 1285-1301.

Tang, X.D., Dong, F.Y., Zhang, Q.H., Lin, L., Wang, P., Xu, X.Y., Wei, W., Wei, D.Z. (2021) Protein engineering of a cold-adapted rhamnogalacturonan acetylesterase: In vivo functional expression and cinnamyl acetate synthesis. Process Biochemistry, 107: 129-137.

Thibault, J.F., Ralet, M.C. (2003) Physico-chemical properties of pectins in the cell walls and after extraction. Advances in Pectin and Pectinase Research, (Eds. Voragen, F., Schols, H., Visser, R.), Springer, Dordrecht, 91-105.

Tokatlidis, K., Dhurjati, P., Millet, J., Béguin, P., Aubert, J.P. (1991) High activity of inclusion bodies formed in *Escherichia coli* overproducing *Clostridium thermocellum* endoglucanase D. FEBS Letters, 282 (1): 205-208.

Voragen, A.G., Coenen, G.J., Verhoef, R.P., Schols, H.A. (2009) Pectin, a versatile polysaccharide present in plant cell walls. Structural Chemistry, 20: 263–275.

Chapter 5

Synergistic action, regioselectivity of rhamnogalacturonan acetyl esterase (*Ct*Pae12B) on potato rhamnogalacturonan I and its therapeutic applications in inhibiting colon cancer cells and colon-targeted drug delivery by forming hydrogels

5.1 Introduction

Plant cell wall has a complex structure that is mainly composed of three carbohydrate polysaccharides, namely, cellulose, hemicellulose and pectin (Ahmed *et al.*, 2021). Of these polysaccharides, pectin has the most complex structure consisting of mainly three components as described earlier in Chapter 1, *viz*. homogalacturonan (HG), rhamnogalacturonan I (RG I) and rhamnogalacturonan II (RG II). Two other types of pectin constituents are substituted galacturonan, *viz.* xylogalacturonan (XGA) and apiogalacturonan (AGA) (Zdunek *et al.*, 2021). Both HG and RG II have a *GalpA* backbone, whereas RG I consists of a backbone with alternating *GalpA* and rhamnopyranosyl (*Rhap*), {(→4)-α-D-*GalpA*-(1→2)-α-L-*Rhap*-(1→)} residues (Mohnen *et al.*, 2008). Both HG and RG I can have methyl esterification at the C-6 position and acetyl esterification at O-2 and O-3 positions of *GalpA* residue (Ahmed et al., 2021). Removal of esterification can modify the substrate surface by removing steric hindrance or surface charge that in-turn help the main chain degrading enzymes

like pectate lyase and rhamnogalacturonan lyase by providing them better accessibility (Shevchik and Hugouvieux-Cotte-Pattat, 1997; Oosterveld *et al.*, 2000). Due to high acetyl esterification in sugar beet pectin (degree of acetylation, 31%), the enzyme activity of polygalacturonase isolated from *Verticillium dahlia* was lower than that against polygalacturonic acid (Safran *et al.*, 2021). The synergistic action of accessory enzymes like methyl esterase and acetyl esterase with main chain degrading enzyme can thereby increase the degradation of substrate. The site specificity of an acetyl esterase for acetyl groups present at both O-2 and O-3 positions can result in to efficient deacetylation. If an acetyl esterase is specific in removing acetyl group from either O-2 or O-3 acetylated positions in a substrate where both O-2 and O-3 are acetylated, efficient deacetylation will not be achieved. A pectin acetyl esterase from *Bacillus licheniformis* was shown to remove only 30% of the total acetyl groups present in the substrate that had acetyl groups present at both O-2 and O-3 positions, due to its site specificity for acetyl groups present at only O-3 position (Remoroza *et al.*, 2014). Pectin acetyl esterase is also found in fruits, like apple and play a very important role in fruit ripening by deacetylation leading to pectin degradation and loosening of the cell-wall (Wu *et al.*, 2021). Wu *et al.* (2021) reported that down-regulation of the pectin acetyl esterase in apple increased its flesh crispness and firmness, thus, increasing its shelf-life.

Till date, a few pectin acetyl esterase (PAE) and rhamnogalacturonan acetyl esterase (RGAE) have been studied mostly based on their biochemical characterization and characteristics of the degraded products. Only few reports have focused on the application that can be performed by deacetylating pectin. For instance, a mutated RGAE (pp1113) from *Paenibacillus polymyxa* was analysed for its adaption to exhibit high activity at 0 ºC (Tang *et al.*, 2021). Tang *et al.* (2021) showed that the cold adapted

RGAE was used for the synthesis of cinnamyl acetate by transesterification reaction of cinnamyl alcohol and vinyl acetate. Pectin polysaccharide, pectin oligosaccharides as well as highly methylated pectin oligosaccharides (68%) were explored for their anti-cancer activity on HT-29 colon cancer cells (Rajulapati *et al.*, 2021). It was reported earlier that pectic oligosaccharides as well as RG oligosaccharides show anti-cancer activity by arresting the malignant factor galectin-3 and anti-apoptotic protein survivin (Mallikarjuna and Dharmesh, 2018) and G2/M cell cycle arrest (Cheng *et al.*, 2013). The *GalpA* moiety in pectin are reported to deactivate Galectin-3, a protein responsible for metastasis of cancer cells, by binding to its carbohydrate recognition domain (Inohara and Raz, 1994). Till date, the effect of deacetylated polysaccharide and oligosaccharide from pectin or any of its moieties on any cancer cell line has not been reported. However, the deacetylated chitosan oligosaccharides produced from chitin were reported to inhibit A549 lung cancer cells (Huang *et al.*, 2004) and PC3 prostate cancer cells, A549 lung cancer cells and HepG2 hepatoma cells (Park *et al.*, 2011). De-acetylation of highly acetylated substrate like sugar beet pectin can modify the surface of the substrate improving its gelation capacity (Oosterveld *et al.*, 2000). A study performed earlier showed that deacetylation of highly acetylated sugar beet pectin with pectin acetyl esterase can make the surface more porous that can be further used as a biomaterial (Savary *et al.*, 2003). Methylated pectic oligosaccharides modified with pectin methyl esterase by demethylation were demonstrated as sustainable drug delivery materials at gastric simulated pH 1.2 and intestinal pH 7.4 (Jung *et al.*, 2013).

The earlier reported results on effect of pectic polysaccharides, pectin oligosaccharides, methylated pectic oligosaccharides as well as demethylated pectic oligosaccharides and deacetylated chitosan oligosaccharides on cancer cell inhibition inspired to study the effect of PRG polysaccharides, PRG oligosaccharides and de-

esterified PRG oligosaccharides on cell viability of colon cancer cells. Also, the earlier reported results on methyl esterase modified pectin hydrogels in drug delivery studies inspired to study the effect of deacetylation of PRG on forming hydrogel and study its drug release kinetics in different simulated bowel conditions with an aim to build a material for colon-targeted drug delivery.

In the present study, three enzymes, namely rhamnogalacturonan acetyl esterase (*Ct*Pae12B), pectin methyl esterase (*Ct*PME) and rhamnogalacturonan lyase (*Ct*RGL*f*) from *Acetivibrio thermocellus, a.k.a Clostridium thermocellum* were purified and the synergistic action of *Ct*Pae12B and *Ct*PME with *Ct*RGL*f* was explored by determining the relative activity of *Ct*RGL*f* after *Ct*Pae12B and *Ct*PME enzymatic treatment. Regioselectivity of the enzyme, *Ct*Pae12B was analysed by ^{1}H NMR (Nuclear Magnetic Resonance) studies towards O-2 and O-3 acetylated *GalpA* residues in PRG and percentage of deacetylation was determined. The degree of acetylation and methylation in PRG were determined by ^{1}H NMR and high-performance liquid chromatography (HPLC) studies. De-esterified oligosaccharides were produced by enzymatic action of *Ct*Pae12B, *Ct*PME and *Ct*RGL*f* and were characterized by thin layer chromatography (TLC), electrospray ionisation mass spectrometry (ESI-MS) and attenuated total reflectance Fourier transformation infrared spectroscopy (ATR-FTIR) studies. The surface morphology and characters of *Ct*Pae12B-treated PRG were analysed by field emission scanning electron microscopy (FESEM), thermogravimetric analysis (TGA) and Brunauer-Emmett-Teller (BET) studies. Further, the role of PRG polysaccharides and oligosaccharides produced by only *Ct*RGL*f* treatment and all three *Ct*Pae12B, *Ct*PME and *Ct*RGL*f* treatment were explored for inhibition of colon cancer cells HCT-116. The use of *Ct*Pae12B deacetylated PRG polysaccharide as a biomaterial drug delivery carrier for sustainable colon targeted drug release was explored. This is

the first report on the effect of de-acetylated rhamno-galacturonates on inhibition of HCT-116 colon cancer cells and the effect of deacetylation by a rhamnogalacturonan acetyl esterase on formation of efficient hydrogel that can be used for controlled and sustainable colon-targeted drug release.

5.2 Materials and methods

5.2.1 Chemicals, substrate and cell lines

The chemicals and reagents like IPTG (isopropyl-β-D-thiogalactopyranoside), Trizma base, hydrochloric acid, sulphuric acid, anti-cancer drug doxorubicin hydrochloride (Dox), Bradford reagent, isopropanol, sodium hydroxide pellets, phosphate buffer saline (PBS) and rhamnose (*Rhap*) were purchased from Himedia Pvt. Ltd., India. Deuterium oxide (D_2O), dimethyl sulfoxide (DMSO) and TLC plates were purchased from Merck Chemical Co. (Darmstadt, Germany). D-Galactopyranosyluronic acid (*GalpA*), imidazole, paraformaldehyde and 3-(4,5-dimethylthiazol-2-yl)-2,5-diphenyl tetrazolium bromide (MTT), 4′,6-diamidino-2-phenylindole (DAPI) and phalloidin-fluorescein isothiocyanate (FITC) were purchased from Sigma Aldrich Co. LLC, USA. Low-glucose Dulbecco′s Modified Eagle′s medium (DMEM), foetal bovine serum (FBS) and penicillin-streptomycin were purchased from Gibco, Thermo Fischer Scientific, USA. The substrate, potato rhamnogalacturonan I (PRG) was purchased from Megazyme Ltd., Ireland. The mammalian cell lines HEK-293 and HCT-116 were procured from National Centre for Cell Science (NCCS), Pune, India.

5.2.2 Purification of *Ct*Pae12B, *Ct*PME and *Ct*RGL*f*

*Ct*Pae12B, *Ct*PME and *Ct*RGL*f* were purified by following the methods reported earlier by (Dhillon *et al.*, 2016; Rajulapati and Goyal, 2017; Ahmed *et al.*, 2023). All three enzymes, *Ct*Pae12B, *Ct*PME and *Ct*RGL*f* were expressed by *E. coli* BL-21 (DE3) cells, harbouring the respective recombinant plasmids by growing in 400 mL, 200 mL and 600 mL Luria-Bertani (LB) medium, respectively, supplemented with 50 µg/mL kanamycin at 37 ºC, 180 rpm. 0.5 mM IPTG for *Ct*Pae12B and 1 mM IPTG for *Ct*PME and *Ct*RGL*f*, were used to induce the cells after the cell-growth reached the mid-

exponential phase (A_{600} = 0.6). After induction, the cells harbouring the recombinant plasmids of *Ct*Pae12B and *Ct*PME were grown at 24 ºC for 16 h, 180 rpm (Rajulapati and Goyal, 2017; Ahmed *et al.*, 2023) and that of *Ct*RGL*f* was grown at 16 ºC for 20 h, 180 rpm (Dhillon *et al.*, 2016). The induced cells were pelleted down (8,000***g***, 4 ºC) for 10 min and sonicated (Sonics, vibra cells) at 33 % amplitude with pulse gap of 10 s on and 10 s off for 15 min. The sonicated cells were pelleted down at 12,000***g***, 4 ºC for 1 h and the filtered (0.45 µm membrane) supernatant was subjected for purification by using Ni^{2+} ion chelating column (HiTrap, GE Healthcare, USA). The resuspension buffer, equilibration buffer and wash buffer used for the purification of *Ct*Pae12B, *Ct*PME and *Ct*RGL*f* was 50 mM Tris-HCl buffer, pH 8.5, 300 mM NaCl, 60 mM imidazole and the elution buffer was 50 mM Tris-HCl buffer, pH 8.5, 300 mM NaCl, 350 mM imidazole. The eluted proteins were further dialysed several times against 50 mM Tris-HCl buffer, pH 8.5 dialysis buffer using dialysis tube of cut-off size 12-14 kDa. The homogeneity of the eluted proteins was analysed by SDS-PAGE by using 12% (w/v) gel. The proteins concentration were determined by using Bradford reagent (Bradford, 1976) and by UV method by using molar extinction co-efficient of the proteins *viz.* 32,320 $M^{-1}cm^{-1}$ for *Ct*Pae12B (Ahmed *et al.*, 2023), 43,570 $M^{-1}cm^{-1}$ for *Ct*PME (Rajulapati and Goyal, 2017) and 1,53,725 $M^{-1}cm^{-1}$ for *Ct*RGL*f* determined by Expasy Protparam (https://web.expasy.org/protparam/).

5.2.3 Synergistic action of *Ct*Pae12B and *Ct*PME with *Ct*RGL*f* against PRG

It was mentioned earlier that the removal of acetyl and methyl esterification from side chains of pectin can enhance the activity of the main-chain degrading enzymes like pectate lyases (Shevchik and Hugouvieux-Cotte-Pattat, 1997). It was reported that *Ct*Pae12B has a specific activity of 700 ± 10 U/mg against PRG in Chapter 4 (Ahmed *et al.*, 2023), *Ct*PME has a specific activity of 0.9 ± 0.13 U/mg against PRG (Rajulapati

and Goyal, 2017) and *Ct*RGL*f* has a specific activity of 9.1 U/mg against PRG (Dhillon *et al.,* 2016). Therefore, the synergistic action of the enzymes *Ct*Pae12B and *Ct*PME were analysed to determine, whether the deacetylation by *Ct*Pae12B and/or demethylation by *Ct*PME enhance the relative activity of *Ct*RGL*f* against PRG. The effect of the catalytic action of *Ct*Pae12B and *Ct*PME against PRG was analysed individually as well as in different sequential combination to check the relative activity of *Ct*RGL*f* against PRG. For maximum deacetylation and demethylation of PRG, the concentration of the enzymes, *Ct*Pae12B and *Ct*PME were individually optimized followed by the optimization of their reaction time, in order to get the maximum relative activity of *Ct*RGL*f* against PRG. The enzymes treatment on PRG were given in a sequential manner. The specific activity of only *Ct*RGL*f* against PRG was taken as 100% and all other activities of *Ct*RGL*f* against *Ct*Pae12B or *Ct*PME or both treated PRG were calculated relative to it.

5.2.3.1 Optimization of concentration and reaction time of *Ct*Pae12B for maximum *Ct*RGL*f* activity

For *Ct*Pae12B concentration optimization, 1 mL reaction mixture was set up by taking 0.5% (w/v) PRG dissolved in 50 mM Tris-HCl buffer, pH 7.2 and 10 µL of different concentrations (0.1, 0.15, 0.2, 0.25 and 0.3 mg/mL) of *Ct*Pae12B and incubated at 65 ºC for 1 min as reported earlier (Ahmed *et al.*, 2023). The de-acetylated PRG was precipitated with ice-cold absolute ethanol (95%) followed by centrifugation at 13,000***g*** for 5 min. The precipitated de-acetylated PRG was washed with sterile MilliQ water thrice to remove any ethanol or acetic acid released during the reaction. The de-acetylated PRG sample obtained by each *Ct*Pae12B concentration was further treated by *Ct*RGL*f* to determine its activity. For *Ct*RGL*f* treatment, the deacetylated PRG was dissolved in 1 mL of 50 mM Tris-HCl buffer, pH 8.5, 3 mM $CaCl_2$, 10 µL of

0.22 mg/mL *Ct*RGL*f* for 5 min at 70 ºC. The reaction was stopped by incubating on ice for 5 min and then centrifuged at 13,000***g*** for 5 min as reported earlier (Dhillon *et al.*, 2016). The supernatant was analysed for the presence of unsaturated galacturonates by taking absorbance at 235 nm against an enzyme-blank. The enzyme activity was calculated by using the molar extinction coefficient, 4600 $M^{-1}cm^{-1}$, of unsaturated *GalpA*, as per the method reported earlier (Dhillon *et al.*, 2016).

After optimizing the concentration of *Ct*Pae12B required for maximum *Ct*RGL*f* relative activity against deacetylated PRG, the reaction time (1-7 min) of *Ct*Pae12B required for maximum deacetylation of PRG was also optimized in order to get the maximum *Ct*RGL*f* activity following the same reaction conditions as mentioned above. Upon optimizing the *Ct*Pae12B concentration and reaction time required for maximum deacetylation in PRG, the concentration and reaction time of *Ct*PME was also optimized in a similar manner.

5.2.3.2 Optimization of enzyme concentration and reaction time of *Ct*PME for maximum *Ct*RGL*f* activity

For *Ct*PME concentration optimization, 1 mL reaction mixture was set up by dissolving 0.5% (w/v) PRG in 50 mM Tris-HCl buffer, pH 8.5 and incubated with 10 µL of different *Ct*PME concentrations (0.05, 0.1, 0.2, 0.3 and 0.4 mg/mL) at 50 ºC for 15 min followed by incubation on ice to stop the reaction as reported earlier (Rajulapati and Goyal, 2017). The de-methylated PRG was precipitated with 95% ice-cold ethanol followed by centrifugation at 13,000***g*** for 5 min. The precipitated de-methylated PRG was washed with sterile MilliQ water thrice to remove any ethanol or methanol released during the reaction. The demethylated PRG obtained by each concentration of *Ct*PME was further subjected to *Ct*RGL*f* treatment by following the reaction conditions as mentioned above. After optimizing the concentration of *Ct*PME required for maximum

*Ct*RGL*f* relative activity against PRG, the reaction time (15-20 min) of *Ct*PME for maximum demethylation of PRG was optimized in order to obtain maximum *Ct*RGL*f* activity.

The optimized enzyme concentration and reaction time of *Ct*Pae12B and *Ct*PME were further used to determine the relative activity of *Ct*RGL*f* against PRG after sequential treatment with only *Ct*Pae12B, only *Ct*PME, both *Ct*Pae12B and *Ct*PME with first *Ct*Pae12B treatment followed by *Ct*PME and also both *Ct*Pae12B and *Ct*PME in the reverse order. After each treatment, the deacetylated or demethylated or both deacetylated and demethylated PRG was precipitated by ethanol (95%) and washed thrice with Milliq and finally the relative activity of *Ct*RGL*f* was determined as mentioned above.

5.2.4 Regioselectivity of *Ct*Pae12B in de-acetylation of PRG

The acetyl esterification is present in O-2 and O-3 positions of *GalpA* residues in HG and RG I constituents of pectin (Ahmed *et al.*, 2021). The regioselectivity of *Ct*Pae12B towards O-2 and O-3 positions of *GalpA* in PRG was analysed by ^{1}H NMR. A reaction mixture of 1 mL was set up by dissolving 1% (w/v) PRG in 50 mM Tris-HCl buffer, pH 7.2 and incubated with 10 µL of 0.1 mg/mL *Ct*Pae12B at 65 ºC for 12 h. An equal amount of PRG without enzyme was also incubated under similar reaction conditions. The non-enzyme treated and *Ct*Pae12B-treated polysaccharides were precipitated with 3 volumes of absolute ethanol (95%, ice-cold) and centrifuged at 13,000***g*** for 15 min. The supernatant was discarded and an additional wash was given to the precipitated polysaccharides with 500 µL ice-cold 95% ethanol and was subjected to lyophilization (ScanVac, Labogene, Denmark) for 16 h. The lyophilized polysaccharides were then dissolved in 600 µL D_2O. A 600 MHz NMR (Bruker, ASCEND 600, Karlsruhe, Germany) spectrometer fitted with 5 mm probe was used to

record the ^{1}H NMR spectra at 25 ºC. The ^{1}H NMR was later analysed by using TopSpin 4.3 software (Bruker, Karlsruhe, Germany).

5.2.5 Quantitative analysis of degree of esterification in PRG by ^{1}H NMR and HPLC

5.2.5.1 Determination of degree of acetylation and methylation by ^{1}H NMR

The percent degree of acetylation and methylation in non-enzyme treated PRG was determined by ^{1}H NMR spectroscopy (Bruker, ASCEND 600, Karlsruhe, Germany). 1% (w/v) PRG was dissolved in 600 µL D_2O and subjected for ^{1}H NMR. The NMR instrument parameters were also kept same as mentioned in section 5.2.4. The different peaks in the NMR spectra were assigned to respective H-atoms present in different positions of *GalpA* residues of PRG. The percent degree of methylation (DM) was calculated by using the integral values of the proton signals as shown in the formula (Rosenbhom *et al.*, 2003).

$$DM\ (\%) = \frac{(I_{COOCH3} + I_{H1}) - I_{COOH}}{(I_{COOCH3} + I_{H1}) + I_{COOH}} \times 100 \qquad \text{Eqn. (1)}$$

Where, $COOCH_3$ and COOH represent the methyl-esterified carboxylate and carboxylate groups, respectively, adjacent to H-5 proton. The percent degree of acetylation (DA) was calculated from the integral values of the proton signals as shown in the formulae (Kasaai, 2010).

$$DA\ (\%) = \{[1/3 \times (I_{CH3\ (O\text{-}2)} + I_{CH3\ (O\text{-}3)})] / [1/2 \times (I_{H\text{-}2} + I_{H\text{-}3})]\} \times 100 \qquad \text{Eqn. (2)}$$

$$DA\ (\%) = [1/3 \times (I_{CH3\ (O\text{-}2)} + I_{CH3\ (O\text{-}3)}) / I_{H\text{-}1}] \times 100 \qquad \text{Eqn. (3)}$$

Where, CH_3 represent the acetyl groups present in O-2 and O-3 positions. H-2 and H-3 are the protons present in the O-2 and O-3 positions, respectively. The acetyl signals were also compared with H-1 proton signal as it is considered as the internal standard (Heux *et al.*, 2000; Kasaai, 2010).

5.2.5.2 Determination of degree of acetylation and methylation by HPLC

HPLC (Shimadzu Corporation, Japan) technique was also used for the determination of percent degree of methylation and acetylation as well as percentage of *GalpA*, *Rhap* and other mono-saccharides present in PRG. The percent degree of methylation and acetylation was determined by using the protocol as mentioned by Melton and Smith. (2001a). 1% (w/v) PRG was dissolved in 1 mL ice-cold isopropanol/NaOH solution (50% v/v Isopropanol solution/0.4 M NaOH). The mixture was allowed to stand for 2 h and then centrifuged at 2,000***g*** for 10 min at 25 ºC. The supernatant was carefully removed and transferred into septum vials for analysis by HPLC connected to an Ion exclusion column (Phenomenex Rezex ROA (H^+) (300 × 7.8 mm) attached to a guard column Phenomenex Rezex ROA (H^+) (50 × 7.8 mm). Isocratic mode was used to run the system by using the mobile phase, 5 mM H_2SO_4 at a flow rate of 0.6 mL/min, 25 ºC and acquisition time 27 min. 15 µL injection volume was kept constant for different concentrations of standards and the sample and the detection was done by both ultra-violet (UV) and refractive index (RI) detectors. The percent of components in the unknown sample was calculated from the respective retention time peak area. The formula used for the calculation of percent DM and DA was as below,

DA or DM (%) = (millimoles of methanol or acetic acid/millimoles of *GalpA*) x 100 Eqn. (4)

Millimoles of *GalpA* was calculated from the total percentage of *GalpA* residues present in PRG following the method reported earlier (Melton and Smith., 2001a). To calculate the total *GalpA* present, 1% (w/v) PRG was dissolved in 1 mL sterile Milliq water and treated with 2 M trifluoracetic acid (TFA) for 5 h at 80 ºC as reported earlier (Rajulapati *et al.,* 2021). 1 mL TFA treated solution was filtered through 0.45 µm filter membrane and subjected to HPLC analysis for mono-saccharides quantification using the same

instrument methods and parameters as used for determination of DM and DA. Total percentage of *GalpA* in PRG was calculated from the standard curve of different *GalpA* concentrations, determined from the peak area in the chromatogram following the method reported earlier (Melton and Smith, 2001b). Similarly, the amount of other mono-saccharides like *Rhap*, xylose, galactose and arabinose were calculated from their respective standard curves. All the resulting chromatogram were analysed by Lab Solutions Software integrated with the HPLC system.

5.2.6 TLC and ESI-MS analysis of the breakdown products of PRG

5.2.6.1 TLC analysis of only *Ct*RGL*f* treated and all three *Ct*Pae12B, *Ct*PME and *Ct*RGL*f* sequentially treated products of PRG

The breakdown products of the PRG treated only with *Ct*RGL*f* and with all three *Ct*Pae12B, *Ct*PME, *Ct*RGL*f* were qualitatively analysed by using TLC technique. For PRG treated only with *Ct*RGL*f*, 1 mL of the reaction mixture was set up by dissolving 1% (w/v) PRG in 50 mM Tris-HCl, pH 8.5 and incubated with 10 µL of 0.22 mg/mL *Ct*RGL*f* and 3 mM $CaCl_2$ at 70 ºC for 2 h. For PRG treated with *Ct*Pae12B, *Ct*PME and *Ct*RGL*f*, 1 mL reaction mixture consisting 1% (w/v) PRG was subjected to sequential enzymatic treatment with 10 µL of 0.2 mg/mL *Ct*Pae12B for 1 h, followed by 10 µL of 0.3 mg/mL *Ct*PME for 1 h and 0.22 mg/mL *Ct*RGL*f* in presence of 3 mM $CaCl_2$ for 2 h following the same reaction conditions (pH and temperature) and method for each enzyme as described in synergistic action of enzymes in section 5.2.3. The high molecular weight undigested polysaccharides from both the only *Ct*RGL*f* treated PRG and PRG treated with *Ct*Pae12B, *Ct*PME, *Ct*RGL*f* were precipitated by adding 3 volumes of absolute ethanol (95%) and the supernatant containing enzyme degraded low molecular weight products was obtained by centrifuging at 13,000***g*** for 10 min. The supernatant was concentrated by drying in oven at 60 ºC for 16 h to 20 µL

(approx.). 0.8 µL of the above concentrated supernatant was loaded as spots on the TLC plate along with standards D-galacturonic acid and rhamnose. A mixture of 1-butanol, acetic acid and water in the ratio, 5.5:2.5:2 was used as the mobile phase. A solution containing 1 mL of 37.5% HCl, 2 mL aniline, 10 mL 85% H_3PO4, 100 mL ethyl acetate, 2 g diphenylamine (diphenylamine-aniline-phosphoric acid reagent) was used for staining the TLC plate. The spots on the TLC plate were developed after drying it for 1 h at 70 ºC.

5.2.6.2 ESI-MS analysis of only *Ct*RGL*f* treated and all three *Ct*Pae12B, *Ct*PME and *Ct*RGL*f* sequentially treated products of PRG

The same concentrated supernatant obtained from TLC analysis (acetylated oligosaccharides and de-acetylated, de-methylated oligosaccharides) were diluted by Milli-Q water (Millipore, USA) to 1 mL, filtered through 0.2 µm filter membrane using a syringe filter and analysed by ESI-MS (Agilent Technologies, USA). The samples were analysed by negative ion mode in the scanning range, 50-3200 m/z. The system was run in dual Agilent Jet Stream-Electron Spray Ionization (AJS-ESI) mode. The nozzle voltage was set to 1000 V and capillary voltage was set to 3500 V. The nebulizer was set at 20 psig. The drying gas temperature was kept at 300 ºC at a flow rate of 10 L/min. Sample volume of 5 µL was injected with an ejection speed of 400 µL/min for 1 min. The mobile phase composed of 50% acetonitrile and 50% water containing 0.1% ammonia was run at a flow rate of 0.3 mL/min. The mass spectra for both acetylated and de-acetylated products were analysed by Mnova software (Mestrelab Research, Spain) (https://mestrelab.com/download/mnova/).

5.2.7 ATR-FTIR of *Ct*RGL*f* treated and all three *Ct*Pae12B, *Ct*PME and *Ct*RGL*f* treated products of PRG

The removal of acetyl and methyl groups from *Ct*RGL*f*, *Ct*Pae12B and *Ct*PME treated PRG oligosaccharides was analysed by comparing their spectra with that of

*Ct*RGL*f* treated PRG oligosaccharides using FT-IR (Shimadzu Corporation, Japan) in ATR mode. Both, only *Ct*RGL*f* treated and *Ct*RGL*f*, *Ct*Pae12B and *Ct*PME treated PRG oligosaccharides, were prepared and concentrated to 20 µL, following the same method as mentioned for TLC analysis (section 5.2.6.1), out of which 10 µL was taken for ATR-FTIR. The spectra were recorded in wavenumber range, 4000-400 cm^{-1} with 64 scans per sample. The peaks were analysed after baseline correction.

5.2.8 FESEM, TGA and BET analyses of *Ct*Pae12B-treated PRG

FESEM for the surface morphology of non-enzyme treated and *Ct*Pae12B-treated PRG, TGA for degradation temperature and phase shift of *Ct*Pae12B-treated PRG and BET for surface area and pore volume analysis of non-enzyme treated and *Ct*Pae12B-treated PRG, were used.

5.2.8.1 FESEM analysis of non-enzyme treated and *Ct*Pae12B-treated PRG

Non-enzyme treated PRG and *Ct*Pae12B-treated PRG were prepared and dried using the same method as described for regioselectivity analysis in section 5.2.4. The dried PRG polysaccharides were mounted on the carbon-tape attached FESEM stub and were gold-coated by sputter (Hitachi E-1010 ion sputter). The surface morphology was analysed by FESEM (Zeiss, Sigma, Germany) at accelerating voltage of 5.0 kV and magnification range from 15-50 KX magnification.

5.2.8.2 TGA analysis of *Ct*Pae12B-treated PRG

A reaction mixture of 1 mL was set up by dissolving 2% (w/v) PRG dissolved in 50 mM Tris-HCl buffer, pH 7.2 and was incubated with 20 µL of 0.1 mg/mL *Ct*Pae12B at 65 ºC for 1 h. The treated polysaccharide was ethanol precipitated (3 volumes, 95%) and the dried in hot air oven at 50 ºC for overnight. The dried polysaccharide was subjected to TGA (Netzsch STA 449F3A-0232-M, USA) in order to determine its degradation temperature and phase shift. Argon gas was used to remove oxygen from

the chambers and also to purge the *Ct*Pae12B-treated PRG placed in Al_2O_3 crucible placed in the jacket chamber. An empty Al_2O_3 crucible was used to subtract the weight of the crucible. The temperature range, 25-1000 ºC was set and the gas was heated at a linear rate of 10 ºC/min. Derivative of weight loss (%/min) was determined from derivative of the thermogravimetric (DTG) curve.

5.2.8.3 BET analysis of non-enzyme treated and *Ct*Pae12B-treated PRG

The total surface area and pore volume of the treated and non-treated PRG samples were determined by BET analysis. 2% (w/v) dried *Ct*Pae12B-treated PRG was prepared by using the same method as for TG analysis. An equal amount of PRG under same reaction conditions without any enzyme treatment was also prepared. Both treated and non-treated polysaccharides were degassed at 150 ºC for 3 h and were subjected to N_2 adsorption/desorption measurements by using Quantachrome (Autosorb-IQ MP, USA) at -196 ºC.

5.2.9 Effect of *Ct*Pae12B, *Ct*PME and *Ct*RGL*f* treated PRG on colon cancer HCT-116 cells

The biocompatibility and cytotoxicity studies of the *Ct*Pae12B, *Ct*PME and *Ct*RGL*f* treated PRG products were studied by using both normal human embryonic kidney (HEK-293) cells and adult human colorectal carcinoma (HCT-116) cells. The effect of five PRG products, untreated PRG polysaccharide with both acetylation and methylation (AcMePS), *Ct*Pae12B and *Ct*PME treated deacetylated and demethylated PRG polysaccharide (dAcdMePS), *Ct*RGL*f* treated PRG giving acetylated and methylated oligosaccharides (AcMeOS), *Ct*Pae12B and *Ct*RGL*f* treated PRG giving deacetylated and methylated oligosaccharides (dAcMeOS) and *Ct*Pae12B, *Ct*PME, *Ct*RGL*f* treated PRG giving deacetylated and demethylated oligosaccharides (dAcdMeOS), on the cell lines were studied. The oligosaccharides were prepared after

sequential enzymatic reactions with the respective enzymes as mentioned in section 5.2.3. While dAcdMePS was prepared by following the same methods as used for the preparation of de-acetylated PRG mentioned in section 5.2.4. Mammalian cells, HEK-293 and HCT-116 were grown in low glucose DMEM supplemented with 10% (v/v) FBS and 1% (v/v) antibiotic solution containing 50 µg/ml streptomycin and 50 IU/ml penicillin. The incubator used for the cell growth and adherence was set at 37 ºC, 5% CO_2 and 95% RH (relative humidity). 1.5 x 10^4 cells (both HEK-293 and HCT-116) were seeded in 96-well tissue-culture plates and allowed to adhere by incubating for 12 h. After adherence, the media was removed and washed with 1X PBS buffer, pH 7.4. Both HEK-293 and HCT-116 cells were treated with 0.2, 0.4, 0.6, 0.8 and 1 mg/mL of each of AcMePS, dAcdMePS, AcMeOS, dAcMeOS or dAcdMeOS in serum-free DMEM and incubated for 24 h and 48 h. HEK-293 and HCT-116 cells in serum-free DMEM without any PRG product were kept as controls. After incubation, the medium was removed from the wells and the cell viability was analysed by MTT reduction assay method (Mosmann, 1983). 100 µl of 0.5 mg/mL MTT reagent was added in each well and incubated for 4 h. After incubation, the MTT reagent was removed carefully without removing the formazan crystals which were later dissolved in 100 µl DMSO. The absorbance of the plate was taken at 570 nm by a microplate reader (Multiskan Sky High, Thermo Scientific, USA). The cell viability was calculated as per the method mentioned earlier (Fopase *et al.*, 2020b).

$$\text{Cell viability (\%)} = \frac{(A_{570}\text{Treated cells})}{(A_{570}\text{Control cells})} \text{ x } 100 \qquad \text{Eqn. (5)}$$

The morphology of HEK-293 and HCT-119 cells after treatment with PRG product was analysed by inverted fluorescence microscopy imaging (Olympus, Japan). For this, 5 x 10^4 cells of both the cell lines were added on 24-well cell plate loaded with poly-L-

Lysine coated cover slips. The cells were allowed to adhere by incubating for 12 h. After incubation, the media was removed and cells were washed with 1X PBS buffer, pH 7.4 and thereafter, 1 mg/mL of each of dAcdMePS, AcMeOS, dAcMeOS and dAcdMeOS were added in serum-free DMEM and incubated for 48 h. The control wells were without any PRG products in serum-free DMEM. After incubation, the serum-free media was removed and the cover slips were washed with 1X PBS buffer, pH 7.4. The cells were fixed in the lysine coated cover slips with 4% paraformaldehyde solution for 15 min. After fixing, the cell walls were permeabilized by treating with Triton X-100 solution. Finally, the cells were stained with DAPI for nucleus staining and phalloidin-FITC for visualization of cytoskeletal F-actin filaments.

5.2.10 Drug entrapment, viscosity and drug release analysis of *Ct*Pae12B-treated PRG hydrogel

5.2.10.1 Drug entrapment by *Ct*Pae12B-treated and non-enzyme treated PRG hydrogels

For hydrogel formation, 1 mL of reaction mixture was set up by dissolving 2% (w/v) PRG in 50 mM Tris-HCl buffer, pH 7.2 and incubated with 20 µL of 0.1 mg/mL *Ct*Pae12B at 65 °C for 1 h. The de-acetylated PRG was precipitated with absolute ethanol (95%) followed by centrifugation at 13,000***g*** for 10 min. The precipitated polysaccharide was washed thrice with sterile MilliQ water. As reported earlier, the presence of acetyl groups hinders the gelation property of pectin (Said *et al.*, 2023). Another study also stated that de-acetylated chitosan polymers could form thermo-reversible gel (Chenite *et al.*, 2001). Therefore, the removal of acetyl groups from PRG helped in hydrogel formation with water. An equal amount of non-enzyme treated PRG was also subjected to form hydrogel with water in the similar manner. Both *Ct*Pae12B-treated and non-enzyme PRG were loaded with 1 mL of 0.5 mg/mL of an anti-cancer drug, doxorubicin (Dox) and kept at a slow-stirring condition at 4 ºC for 16 h. The free

Dox that was not trapped in the hydrogel and was present in the solution was measured by taking absorbance at 480 nm (A_{480}) and drug entrapment efficiency of the hydrogels was calculated by using the formula (Panwar *et al.*, 2010).

$$\text{Drug entrapment efficiency (\%)} = \frac{\text{Concentration of drug loaded} - \text{Concentration of free drug}}{\text{Concentration of drug loaded}} \text{x100} \quad \text{Eqn. (6)}$$

5.2.10.2 Viscosity analysis of Dox loaded and without Dox loaded *Ct*Pae12B-treated PRG hydrogel

The viscosity (η) of *Ct*Pae12B-treated PRG hydrogel and its viscosity after drug loading was analysed in terms of centi-poise (cP) by using a rheometer (Anton Paar MCR72, Austria) applying varying shear rate (γ, *a.k.a* flow behaviour) in the range 0-100 1/s. The temperature at 25 °C was set with the help of a peltier system connected to the instrument. For viscosity analysis, hydrogel was prepared from total 40 mg PRG treated with *Ct*Pae12B. For this, two separate 1 mL reactions were set, each containing 2% (w/v) PRG dissolved in 50 mM Tris-HCl buffer, pH 7.2 and incubated with 20 µL of 0.1 mg/mL *Ct*Pae12B at 65 ºC for 1 h. The de-acetylated PRG was precipitated with 3 volumes of absolute ethanol (95%) followed by centrifugation at 13,000***g*** for 10 min. The precipitated polysaccharide was washed thrice with sterile MilliQ water. The ~40 mg *Ct*Pae12B-treated PRG hydrogel was loaded with 1 mL of 0.5 mg/mL of Dox and kept at a slow-stirring condition at 4 ºC for 16 h. Both Dox loaded *Ct*Pae12B-treated PRG hydrogel as well as without Dox loaded *Ct*Pae12B-treated PRG hydrogel were analysed for their viscosity with increasing shear rate by loading them separately between removable circular parallel metal plates (20 mm diameter) with a gap of 1 mm diameter between the plates attached to a rheometer.

5.2.10.3 Drug release analysis by *Ct*Pae12B-treated and non-enzyme treated PRG hydrogels

The drug loaded hydrogel preparations were analysed for *in-vitro* drug release using the simulated gastro-intestinal tract pH and time required for gastric emptying and small intestinal transit as described by Jung *et al.* (2013). The drug release was analysed by placing the drug-loaded hydrogels in dialysis membrane (12-14 kDa) and dialysed against 50 mL 0.1 M HCl solution, pH 1.2, for 2 h at 37 ºC and 120 rpm, mimicking the pH in gastric condition and bowel movement time. After 2 h, the hydrogels were sequentially immersed for 3 h in 50 mL 1X PBS solution, pH 7.4 at 37 ºC and 120 rpm, mimicking the pH in small-intestine condition and transient time. The hydrogels were kept for an additional 21 h (total 24 h) in 1X PBS, pH 7.4 and absorbance of the total drug released was taken at different time intervals to study the rate of complete drug release under the intestinal pH condition. The amount of Dox released was calculated from the standard curve and the rate of drug release was calculated. Volume of the dissolution bath medium was made up after every measurement.

5.2.11 Statistical analysis

Three individual experiment set ups were carried out for all the experiments in enzyme activity, cell viability assay and amount of drug entrapment and release assays. All the experiments in each set up were done in triplicates and the results were presented as the mean ± standard deviation. Each independent group was examined by one-way ANOVA followed by significant difference t-test and statistically significant results were presented with probability value less than 0.05 ($p<0.05$). All the experiments to visualize the cell morphology were done in duplicate.

5.3 Results and Discussion

5.3.1 Purification of *Ct*Pae12B, *Ct*PME and *Ct*RGL*f*

The enzymes namely, rhamnogalacturonan acetyl esterase (*Ct*Pae12B), pectin methyl esterase (*Ct*PME) and rhamnogalacturonan lyase (*Ct*RGL*f*) purified by immobilized metal affinity chromatography (IMAC) displayed single band on SDS-PAGE analysis using 12% (w/v) gel with the expected molecular size as reported earlier (Dhillon *et al.*, 2016; Rajulapati and Goyal, 2017; Ahmed *et al.*, 2023). *Ct*Pae12B, *Ct*PME and *Ct*RGL*f* showed single protein band of molecular size, approximately, 25 kDa, 35 kDa and 80.2 kDa, respectively (Fig. 5.1), which were in agreement with their theoretical molecular weights as reported earlier (Dhillon *et al.*, 2016; Rajulapati and Goyal, 2017; Ahmed *et al.*, 2023). The amount of purified *Ct*Pae12B, *Ct*PME and *Ct*RGL*f* was 8.8 ± 0.2 mg, 10.5 ± 0.5 mg and 0.31 ± 0.04 mg, respectively.

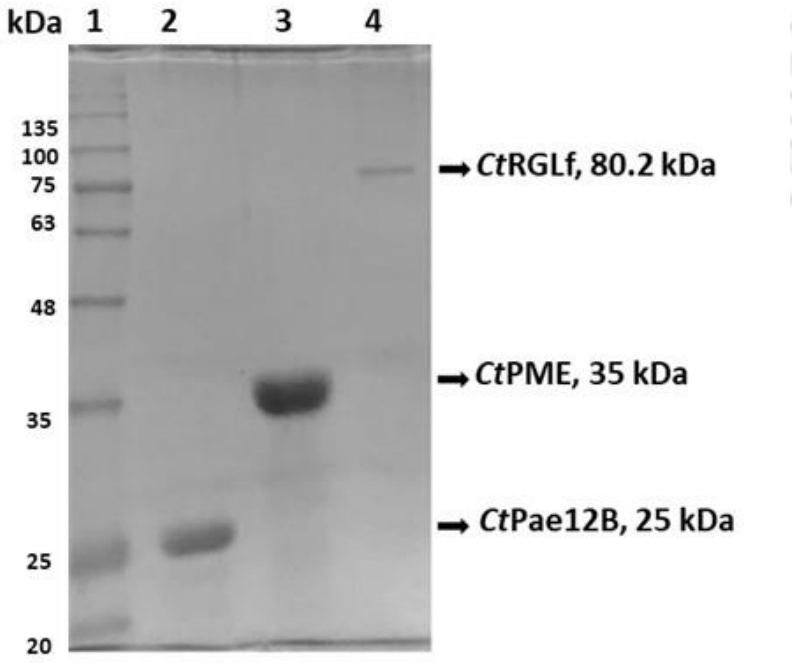

Fig. 5.1 SDS-PAGE analysis of purified proteins *Ct*Pae12B, *Ct*PME and *Ct*RGL*f* using 12% (w/v) gel. Lane 1- Protein marker (Himedia, India), Lane 2- Purified *Ct*Pae12B, Lane 3- Purified *Ct*PME, Lane 4- Purified *Ct*RGL*f*.

5.3.2 Synergistic action of *Ct*Pae12B and *Ct*PME with *Ct*RGLf against PRG

The optimized *Ct*Pae12B concentration, 0.2 mg/mL and optimized reaction time of 5 min, gave maximum relative activity of *Ct*RGL*f* against PRG as compared with the activity of only *Ct*RGL*f* against PRG. While, the optimized enzyme concentration and reaction time for *Ct*PME was 0.3 mg/mL and 15 min, respectively. The relative activity of *Ct*RGL*f* against PRG after treatment of *Ct*Pae12B and *Ct*PME under various combinations is shown in Table 5.1. The prior treatment of PRG with *Ct*PME enhanced only 11% of the total relative activity of *Ct*RGL*f* against PRG (Table 5.1). While, the prior treatment of PRG with *Ct*Pae12B significantly enhanced by 90% of the total relative activity of *Ct*RGL*f* against PRG. This could be probably due to low content of methylation in PRG, as the specific activity of *Ct*PME was only 0.9 U/mg against PRG as compared with 18.1 U/mg against 85% methylated citrus pectin as reported earlier (Rajulapati and Goyal, 2017). However, a high specific activity i.e. 700 U/mg of *Ct*Pae12B against PRG was reported earlier in Chapter 4, suggesting a higher content of acetyl groups present in PRG (Ahmed *et al.*, 2023). As a result, relative activity of *Ct*RGL*f* after the removal of acetyl group from PRG increased, showing that the catalytic action of RG lyase increased after the removal of the steric hindrance posed by the acetyl groups present in higher percentage as compared with methyl groups in the side chains. A 10% increase in the relative activity (total 200%) of *Ct*RGL*f* was observed after treating PRG first with *Ct*PME followed by *Ct*Pae12B as compared with (total 190%), obtained after the treatment of PRG with *Ct*Pae12B alone indicating that the removal of both methyl and acetyl group enhanced the activity of *Ct*RGL*f*. Interestingly, it was observed that the relative activity of *Ct*RGL*f* against PRG increased by 15% when first treated with *Ct*Pae12B followed by *Ct*PME (total 215%) rather than reverse order as above (total 200%). This indicated that the removal of acetyl groups

gives a better penetration ability to *Ct*PME for efficient demethylation. A study reported earlier on the catalytic action of pectin methyl esterase (PemA) and pectin acetyl esterase (PaeY) from *Dickeya dadantii* on sugar beet pectin showed that prior removal of methyl group by PemA enhanced the deacetylation activity of PaeY and hence increased the pectate lyases activity (Shevchik and Hugouvieux-Cotte-Pattat, 1997). Another study performed on sugar beet pectin by using a pectin acetyl esterase (YxiM) from *Bacillus subtilis* and pectin methyl esterase (PME) from *Aspergillus aculeatus* showed that YxiM treatment followed by PME could reduce the percent degree of methylation (DM) from 66.1% to 1.2% and percent degree of acetylation (DA) from 24% to 19.2% as compared to DM 11.1% and DA 18.2% obtained when treated first with PME followed by YxiM showing that the prior treatment with YxiM resulted in higher overall de-esterification than with the prior treatment with PME (Bolvig *et al.*, 2003).

Table 5.1 Synergistic action of *Ct*Pae12B and *Ct*PME with *Ct*RGLf against PRG.

Sequence of enzyme treatment	Relative activity of *Ct*RGL*f* (%)
*Ct*RGL*f*	100 ± 2
*Ct*PME + *Ct*RGL*f*	111 ± 3
*Ct*Pae12B + *Ct*RGL*f*	190 ± 2
*Ct*PME + *Ct*Pae12B + *Ct*RGL*f*	200 ± 3
*Ct*Pae12B + *Ct*PME + *Ct*RGL*f*	215 ± 4

All experiments were performed with 0.5% (w/v) PRG. The relative activity is presented as the mean of the triplicates ± standard deviation.

5.3.3 Regioselectivity of *Ct*Pae12B in de-acetylation of PRG

The localization of the acetyl groups present in *GalpA* residues can be confirmed by ^{1}H NMR (Ishii, 1997). As reported earlier, a single acetyl group present at O-2 position of non-methyl esterified *GalpA* residue shows a chemical shift at 2.00-2.04 ppm and that present in O-3 positions shows a chemical shift at 2.09-2.11 ppm,

respectively (Remoroza *et al.,* 2014). They also mentioned that various chemical signals can be observed at 2.18-2.21 ppm for methyl-esterified *GalpA* residues with O-2 or O-3 acetylation or double acetylation. ^{1}H NMR spectrum of non-enzyme treated PRG polysaccharide showed signals at 2.01 ppm and 2.10 ppm corresponding to non-methyl esterified *GalpA* with acetyl groups present at both O-2 and O-3 positions, respectively (Fig. 5.2). Whereas, the ^{1}H NMR spectrum of *Ct*Pae12B-treated PRG polysaccharide displayed significantly reduced chemical signals at both 2.015 ppm and 2.095 ppm (Fig. 5.2). This indicated that *Ct*Pae12B could significantly de-acetylate acetyl groups (approx. 98%) from both specific sites O-2 and O-3 positions of non-methyl esterified acetyl esterified *GalpA* residues of PRG, showing regio-selectivity for both the positions. A pectin acetyl esterase from *Bacillus licheniformis* removed only 30% of total acetyl groups in sugar beet pectin that contained acetyl groups at both O-2 and O-3 positions, because the enzyme had site specificity for only the acetyl groups present at O-3 position (Remoroza *et al.,* 2014).

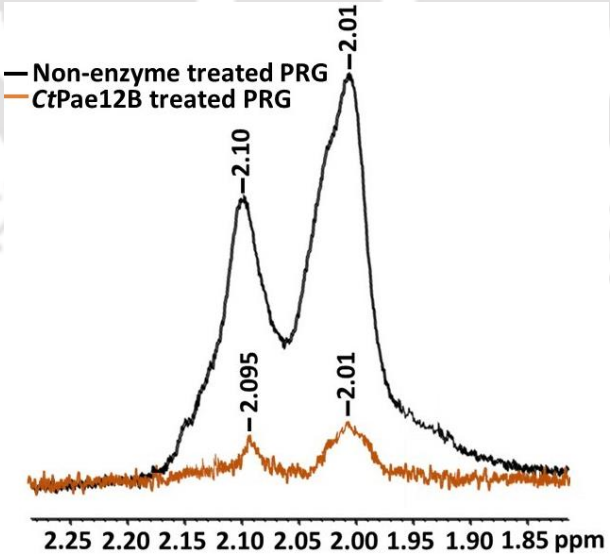

Fig. 5.2 ^{1}H NMR spectra of non-enzyme treated PRG polysaccharide and *Ct*Pae12B-treated PRG polysaccharide.

5.3.4 Quantitative analysis of degree of esterification in PRG by ^{1}H NMR and HPLC

5.3.4.1 Determination of degree of acetylation and methylation by ^{1}H NMR

The ^{1}H NMR spectra of the non-enzyme treated PRG polysaccharide is shown in fig. 5.3A. The integral values of the H-5 proton adjacent to methyl esterified carboxylate at 5.04 ppm and carboxylate at 4.51 ppm were 2.40 and 6.28, respectively. The integral value of H-1 proton (internal standard) at 5.01 ppm was found to be 4.85. Using equation 1, the percent DM was calculated to be 7.17%. This very less percent DM indicated that the *GalpA* residues of PRG are very scantly methylated corroborating the low 0.9 U/mg specific activity of *Ct*PME against PRG (Rajulapati and Goyal, 2017). A study earlier reported 13% methylation in the RG I region of potato which accounted for very less methylation (Schols and Voragen, 1994). The integral values of acetyl groups at O-2 position (2.01 ppm) was 1.99 and that at O-3 position (2.10 ppm) was 1.10. The percent degree of acetylation was calculated by comparing the integral values of acetyl groups at O-2 and O-3 positions with integral value of H-2 proton at 3.75 ppm, i.e., 6.60 and H-3 proton at 3.91 ppm, i.e., 3.59 using equation 2 and that with internal standard H-1 using equation 3. The DA was calculated to be approximately, 20.2% and 21.2% by using equation 2 and 3, respectively. The percent DA showed that PRG is highly acetyl-esterified as compared with methyl esterification corroborating the high specific activity of *Ct*Pae12B (700 U/mg) against PRG as described in Chapter 4 (Ahmed *et al.*, 2023). Another study performed on potato pectin using ^{1}H NMR reported DM and DA in the range of 21.5-37.4% and 9.2-15.4%, respectively (Yang *et al.*, 2018). Most of the methyl esterification in potato may be confined to the HG region instead of RG I region, as RG I region is known to contain

acetyl groups at O-2 and O-3 positions, with no or very less methyl groups (Komalavilas and Mort, 1989; O'Neill and York, 2003).

5.3.4.2 Determination of degree of acetylation and methylation by HPLC

The HPLC analysis of different standards *GalpA*, galactose, xylose, rhamnose, arabinose, acetic acid and methanol showed the retention time, 11.20 min, 12.53 min, 12.55 min, 13.23 min, 13.70 min, 18.73 min and 22.60 min, respectively (Fig. 5.3B). The amount of acetic acid and methanol released from PRG upon isopropanol/NaOH treatment was calculated from the peak area at retention time, 18.72 min and 22.60 min, respectively (Fig. 5.3C). The percentage of total acetyl and methyl groups present in PRG polysaccharide calculated by equation 4, were 21.94% and 7.78%, respectively, with respect to total *GalpA* percentage (63.3%) in PRG, that was obtained after TFA treatment. The total percentage of *GalpA* after TFA treatment was calculated from the peak area at retention time 11.20 min with respect to its standard curve (Fig. 5.3D). The other mono-saccharides detected in the TFA treated PRG sample were *Rhap,* galactose and arabinose with retention time at 13.25 min, 12.52 min and 13.72, respectively (Fig. 5.3D). The percentage of *Rhap,* galactose and arabinose in PRG calculated from their respective standard curves were 6.5%, 25% and 2.8%, respectively. DA and DM in PRG measured by HPLC method corroborated with that of ^{1}H NMR.

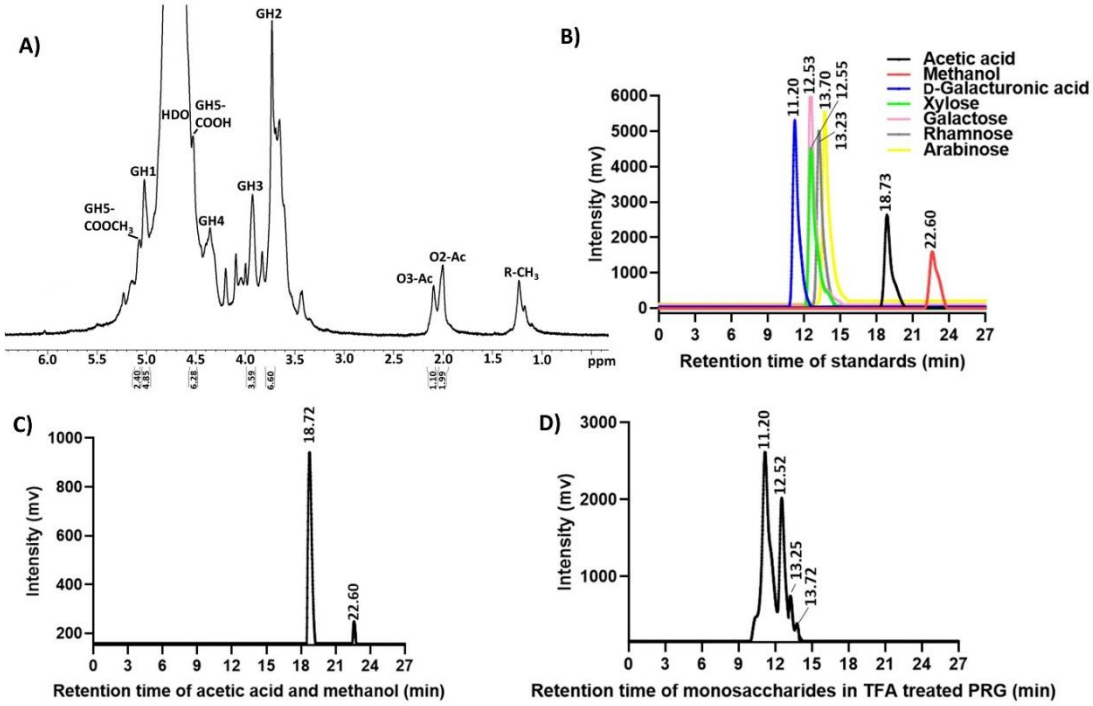

Fig. 5.3 A) ^{1}H NMR spectrum of non-enzyme treated PRG. "G" stands for *GalpA*, "Ac" for acetyl and R-CH$_3$ for methyl group present in *Rhap* residues. HPLC chromatogram showing the B) retention time of all the standards used, C) retention time and peak area of acetic acid and methanol released from PRG upon isopropanol/NaOH treatment, D) retention time and peak area of the released mono-saccharides, *GalpA*, galactose, rhamnose and arabinose, upon TFA treatment.

5.3.5 Thin layer chromatography (TLC) and ESI-MS analysis of breakdown products of PRG

5.3.5.1 TLC analysis of breakdown products of PRG

The degraded products of PRG by the treatment with only *Ct*RGL*f* and *Ct*Pae12B, *Ct*PME, *Ct*RGL*f* were analysed by TLC technique. D-*GalpA* (lane 1) and rhamnose (lane 2) were used as standards (Fig. 5.4A). The *Ct*RGL*f* degraded products (lane 4) and *Ct*Pae12B, *Ct*PME, *Ct*RGL*f* degraded products (lane 5) showed almost same pattern of mobility in the TLC plate as not much difference could be made by removal of acetyl groups from oligosaccharides. The mobility of the products showed almost 6 discrete spots on the TLC plate (Fig. 5.4A). Of all the spots, the farthest spot was observed to have travelled a distance almost equal to the standard, D-*GalpA* (lanes 4 and 5). It was reported earlier that the unsaturated disaccharide unit of RG I showed

mobility similar to D-*GalpA* (Ochiai *et al.*, 2007; Dhillon *et al.*, 2016). This was further confirmed by ESI-MS.

5.3.5.2 ESI-MS analysis of breakdown products of PRG

The mass spectrometry profile generated for *Ct*RGL*f* lysed PRG is shown in Fig. 5.4B. The smallest molecular mass product was unsaturated (un) RG disaccharide (*UnGalpA*+*Rhap*) showing a peak at m/z 322.53 (Fig. 5.4B and Table 5.2). The molecular mass of unsaturated RG disaccharide was earlier shown to be 322 (Ochiai *et al.*, 2007). The corresponding peaks at different m/z values in Fig. 5.4B are as follows. The second peak at m/z 351.05 corresponded to deprotonated unsaturated di-galacturonate (*UnGalpA*+*GalpA*-H^+). The third peak at m/z 364.06 corresponded to acetylated unsaturated RG disaccharide (*UnGalpA*+*Rhap*+Ac). The fourth peak at m/z 393.04 corresponded to deprotonated acetylated unsaturated di-galacturonate (*UnGalpA*+*GalpA*+Ac-H^+). The fifth peak at m/z 527.08 corresponded to deprotonated unsaturated tri-galacturonate (*UnGalpA*+*GalpA*+*GalpA*-H^+). The sixth peak at m/z 660.05 corresponded to deprotonated unsaturated RG tetra-saccharide (*UnGalpA*+*Rhap*+ *UnGalpA*+*Rhap*-H^+). The seventh peak at m/z 703.12 corresponded to acetylated unsaturated RG tetra-saccharide (*UnGalpA*+*Rhap*+*UnGalpA*+*Rhap*+Ac). The eighth peak at m/z 746.084 corresponded to acetylated unsaturated tetra-galacturonate (*UnGalpA*+*GalpA*+*GalpA*+*GalpA*+Ac). The ninth peak at m/z 921.16 corresponded to deprotonated acetylated unsaturated penta-galacturonate (*UnGalpA*+*GalpA*+*GalpA*+*GalpA*+*GalpA*+Ac-H^+) and the tenth peak at m/z 1098.17 corresponded to double acetylated and single methylated unsaturated RG hexa-saccharide (*UnGalpA*+*Rhap*+*UnGalpA*+*Rhap*+*UnGalpA*+*Rhap*+2Ac+Me) (Table 5. 2).

The mass spectrometry profile of the lysed products of the combined catalytic action of *Ct*Pae12B, *Ct*PME, *Ct*RGL*f* are shown in Fig. 5.4C. The various peaks corresponding to different m/z values in Fig. 5.4C are tabulated in Table 5.3. The smallest molecular mass peak at m/z 322.53 corresponded to unsaturated RG di-saccharide (*UnGalpA+Rhap).* The second peak at m/z 351.06 corresponded to deprotonated unsaturated di-galacturonate (*UnGalpA+GalpA*-H^+). The third peak at m/z 527.08 corresponded to deprotonated unsaturated tri-galacturonate (*UnGalpA+GalpA+GalpA*-H^+). The fourth peak at m/z 661.0 corresponded to unsaturated RG tetra-saccharide (*UnGalpA+Rhap+UnGalpA+Rhap*). The fifth peak at m/z 704.12 corresponded to unsaturated tetra-galacturonate (*UnGalpA+GalpA+GalpA+GalpA*). The sixth peak at m/z 879.04 corresponded to deprotonated unsaturated penta-galacturonate (*UnGalpA+GalpA+GalpA+GalpA+GalpA*-H^+) and the seventh peak at m/z 1000.07 corresponded to unsaturated RG hexa-saccharide (*UnGalpA+Rhap+UnGalpA+Rhap+UnGalpA+Rhap*). The m/z values of all the peaks in fig. 5.4C corresponded to the oligosaccharides with no acetyl or methyl groups present. Moreover, the intensities of the de-acetylated oligo-saccharides increased in fig. 5.4C as compared with the intensities of the de-acetylated oligosaccharides in fig. 5.4B. This showed that the oligosaccharides were efficiently de-acetylated as well as de-methylated. Fig. 5.4B showed that the oligosaccharides with methylation were significantly less as compared with the acetylated oligosaccharides.

The ESI-MS analyses showed that the catalytic action of *Ct*RGL*f* released both unsaturated galacturonates and unsaturated rhamno-galacturonates of different degree of polymerisation. This could be because of the dispersed distribution of *GalpA* and *Rhap* backbone in the commercial PRG polysaccharide chain. The composition of

constituents in PRG polysaccharide chain was determined to be approx. 63.3% *GalpA* and 6.5% *Rhap* by HPLC (section 5.3.4) which also corroborated with the composition of PRG constituents mentioned at Megazyme web-page (https://www.megazyme.com/rhamnogalacturonan-i-potato). Due to the dispersed distribution of *Rhap* residues in the polysaccharide chain, the cleavage sites of *Ct*RGL*f* between *Rhap* and *GalpA* residues could be in such a way that, both galacturonates and rhamno-galacturonates were released. However, the major products with higher intensity were observed to be rhamno-galacturonates as compared to galacturonates by MS.

It is worth mentioning here that the smallest molecular mass unit of *Ct*RGL*f* degraded PRG product was unsaturated RG disaccharide, which, however, was not the case with the smallest molecular mass product released from *Ct*RGL*f* degraded soybean rhamnogalacturonan I (Dhillon *et al.*, 2016). They reported that the smallest released product unit was larger than unsaturated disaccharide unit of RG I (Dhillon *et al.*, 2016). However, further confirmation about the degree of polymerisation of the smallest released product unit was not done by mass spectrometry or any other technique in their study. The RG I lyase releasing unsaturated RG disaccharide as the smallest molecular mass product was earlier reported by Ochiai *et al.*, (2007). Wang *et al.*, (2022) also reported the release of unsaturated RG up to octa-saccharides, with unsaturated RG di-saccharide being the smallest unit released by RG lyase from *Bacteroides ovatus*.

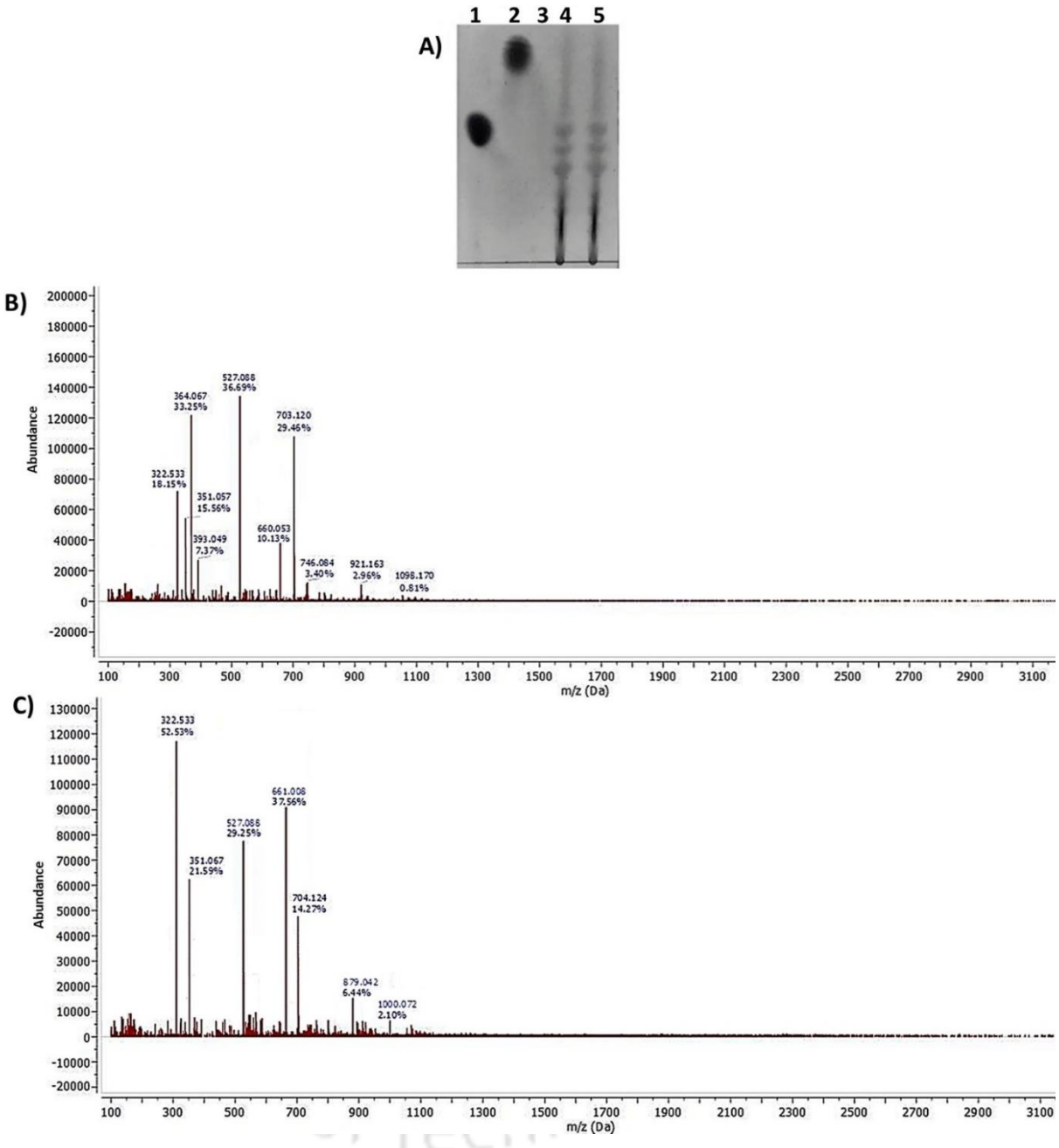

Fig. 5.4 A) TLC analysis of enzyme-degraded products of PRG. Lane 1- Standard *D-GalpA*, lane 2- standard *Rhap*, lane 3- 0 min, lane 4- *Ct*RGL*f* degraded products and lane 5- *Ct*Pae12B, *Ct*PME, *Ct*RGL*f* degraded products. B) ESI-MS analysis of *Ct*RGL*f* degraded products and C) ESI-MS analysis of *Ct*Pae12B, *Ct*PME, *Ct*RGL*f* degraded products.

Table 5.2. Oligosaccharide species released from *Ct*RGL*f* treated PRG and their respective m/z and relative abundance.

Oligosaccharide species released from *Ct*RGL*f* treated PRG	m/z	Relative abundance
UnGalpA+Rhap	322.53	18.15
UnGalpA+GalpA-H^+	351.05	15.56
UnGalpA+Rhap+Ac	364.06	33.25
UnGalpA+GalpA+Ac-H^+	393.04	7.37
UnGalpA+GalpA+GalpA-H^+	527.08	36.69
UnGalpA+Rhap+UnGalpA+Rhap-H^+	660.05	10.13
UnGalpA+Rhap+UnGalpA+Rhap+Ac	703.12	29.46
UnGalpA+GalpA+GalpA+GalpA+Ac	746.08	3.40
UnGalpA+GalpA+GalpA+GalpA+GalpA+Ac-H^+	921.16	2.96
UnGalpA+Rhap+UnGalpA+Rhap+UnGalpA+Rhap+2Ac+Me	1098.17	0.81

Table 5.3. Oligosaccharide species released from *Ct*Pae12B, *Ct*PME and *Ct*RGL*f* treated PRG and their respective m/z and relative abundance.

Oligosaccharide species released from *Ct*Pae12B, *Ct*PME *Ct*RGL*f* treated PRG	m/z	Relative abundance (%)
UnGalpA+Rhap	322.53	52.53
UnGalpA+GalpA-H^+	351.06	21.59
UnGalpA+GalpA+GalpA-H^+	527.08	29.25
UnGalpA+Rhap+UnGalpA+Rhap	661.08	37.56
UnGalpA+GalpA+GalpA+GalpA	704.12	14.27
UnGalpA+GalpA+GalpA+GalpA+GalpA-H^+	879.04	6.44
UnGalpA+Rhap+UnGalpA+Rhap+UnGalpA+Rhap	1000.07	2.10

5.3.6 ATR-FTIR analysis of acetylated and de-acetylated PRG oligosaccharides

The FT-IR spectra of *Ct*RGL*f* treated PRG producing oligosaccharides with both acetylation and methylation (Ac and Me) and *Ct*Pae12B, *Ct*PME, *Ct*RGL*f* treated PRG producing oligosaccharides with deacetylation (dAc) and demethylation (dMe) are shown in fig. 5.5. The most intense band at 3435 cm^{-1} corresponded to the O-H stretching bond and the peak at 2938 cm^{-1} was assigned to C-H stretching bond. With acetyl and methyl esterification, the peak height of the O-H stretching bond decreases, while the peak height of the C-H stretching bond increases (Synytsya *et al.*, 2003). Therefore, an increase in peak height of the O-H stretching bond and decrease in peak height of the C-H stretching bond observed in the red curve showed that *Ct*Pae12B, *Ct*PME, *Ct*RGL*f* treated PRG oligosaccharides were de-esterified as compared with the

black curve that shows only *Ct*RGL*f* treated PRG oligosaccharides, with intact esterification (Fig. 5.5). The methyl esterified carboxyl group as well as carbonyl vibration band of acetyl groups were assigned to the peaks at 1748 cm^{-1} as reported earlier (Synytsya *et al.*, 2003; Peng *et al.*, 2016). The dAc and dMe of PRG led to the reduction in the intensity of the peak at 1748 cm^{-1}. The carbonyl group of the non-methylated carboxylic group is represented by the peak at 1626 cm^{-1} (Peng *et al.*, 2016). The intensity of peak at 1626 cm^{-1} did not increase significantly upon dAc and dMe of PRG showing that the free carbonyl groups of non-methylated carboxylates remained almost constant upon dMe, indicating low amount of methyl group present in PRG oligosaccharides. A small peak at 1253 cm^{-1} was assigned to acetyl group (Synytsya *et al.*, 2003) and another peak at 1068 cm^{-1} also attributed to the acetyl group as reported earlier (Synytsya *et al.*, 2003; Yang *et al.*, 2018). Both the peaks decreased or rather vanished in the de-esterified oligosaccharides. FT-IR analysis showed that prior treatment of PRG with *Ct*Pae12B and *Ct*PME resulted in both efficient dAc and dMe of the *Ct*RGL*f* hydrolysed PRG oligosaccharides.

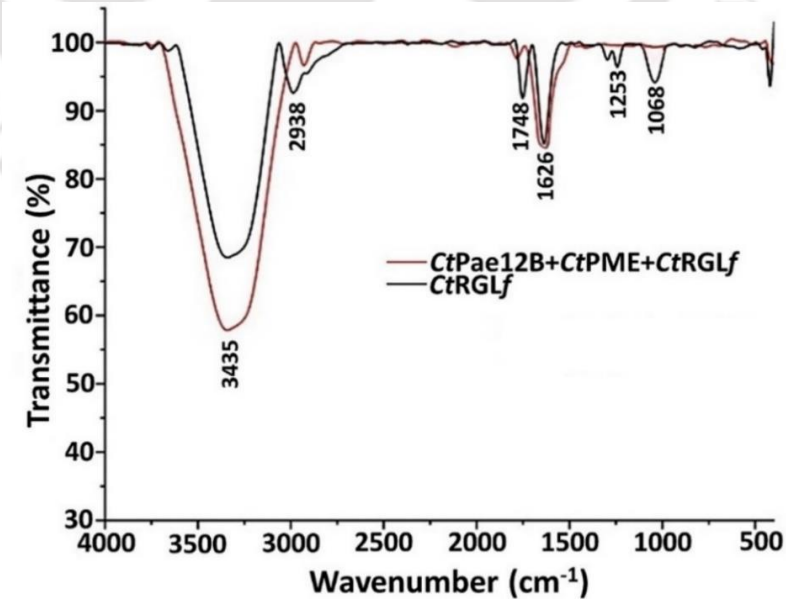

Fig. 5.5 ATR FT-IR spectra of only *Ct*RGL*f* treated PRG and *Ct*Pae12B, *Ct*PME and *Ct*RGL*f* treated PRG.

5.3.7 FESEM, TGA and BET analysis

5.3.7.1 FESEM analysis of non-enzyme treated and *Ct*Pae12B-treated PRG

Enzymatic modification of the pectin surface has been widely studied earlier in terms of solubility, viscosity, cross-linking and gelation (Cao *et al.*, 2020) but not much focus has been given yet on studying its surface morphology. The surface morphology of the PRG polysaccharide without any enzyme treatment by FESEM analysis at 15.00 KX magnification displayed rough and only slightly porous surface (Fig. 5.6A). While, the *Ct*Pae12B-treated PRG showed a more porous surface at 15.00 KX magnification (Fig. 5.6B). A more distinct view of the pores on the surface displayed in Fig. 5.6B is shown under 50.00 KX magnification (Fig. 5.6C). A brief study on a pectin acetyl esterase on sugar beet pectin reported that enzymatic modification showed porous micro-sponge biomatrix that could be used as a drug delivery material (Savary *et al.*, 2003).

5.3.7.2 TGA analysis of *Ct*Pae12B-treated PRG

The TG analysis of the *Ct*Pae12B-treated PRG showed decrease in weight with the increasing temperature in the range 25-1000 ºC (Fig. 5.6D). The DTG and TG curves showed that the initial 7% weight loss occurred at 154-211 ºC. This small amount of weight loss was due to evaporation of moisture from the *Ct*Pae12B-treated dry PRG. In the next stage, in the temperature range 211-334 ºC, the percent weight was reduced to 41% from 7% due to pyrolytic de-polymerization of the *Ct*Pae12B-treated PRG. The third stage was marked by reduction in percent weight to 66% from 41% that occurred in the temperature range, 334-803 ºC. The percent weight further reduced by 10% (i.e. total 76%) in the temperature range 803-1000 ºC. 24% of the total weight of the enzyme treated PRG remained after heating up to 1000 ºC which accounted to a total mass of 1.24 mg from initial mass, 5.17 mg. The DTG curve showed the degradation

temperature, 254 ± 1.5 ºC. The DTG derived degradation peak was observed at 220 ºC for potato pectin in a study reported earlier (Hu *et al.*, 2022), while that of citrus pectin was 250 ºC (Einhorn-Stoll and Kunzek, 2009).

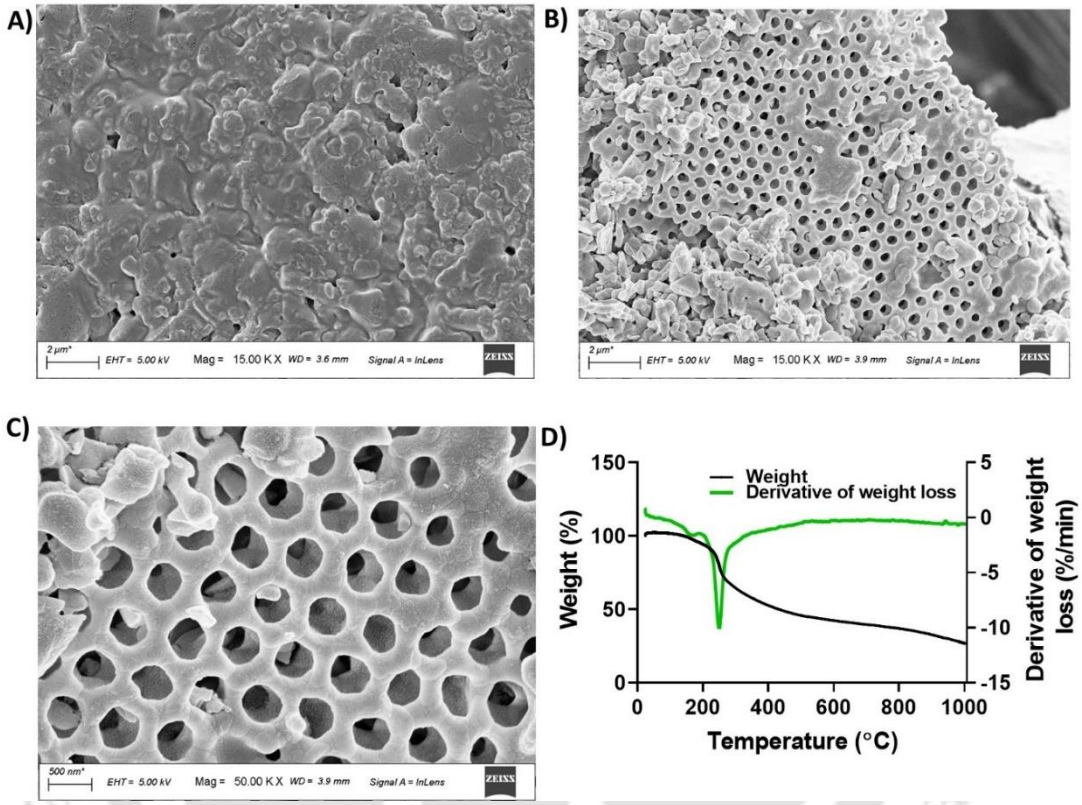

Fig. 5.6 Surface morphology analysis by FESEM of A) non-enzyme treated PRG at 15.00 KX magnification, *Ct*Pae12B-treated PRG at B) 15.00 KX magnification and C) 50.00 KX magnification. D) Thermal degradation by TG and DTG analysis of *Ct*Pae12B-treated PRG.

5.3.7.3 BET analysis of non-enzyme treated and *Ct*Pae12B-treated PRG

Further, the total surface area and pore volume of pores ≤32 nm of both non-enzyme-treated and *Ct*Pae12B-treated PRG polysaccharides were analysed by BET. The non-enzyme-treated PRG showed a total surface area of 69.85 m^2/g, while the *Ct*Pae12B-treated PRG showed a total surface area more than double, 146.05 m^2/g, of the non-enzyme treated PRG. The total pore volume of pores (≤32 nm) was measured to be 0.29 cc/g for the non-enzyme treated PRG, whereas for *Ct*Pae12B-treated PRG, the pore volume was calculated to be almost 4 times more, 1.16 cc/g, than the non-

enzyme treated PRG. Both the surface area and pore volume were larger in the *Ct*Pae12B-treated PRG as compared with the non-enzyme treated PRG. The porous structure, larger surface area and higher pore volume of the *Ct*Pae12B-treated PRG, makes it a potential polysaccharide material for drug delivery purposes.

5.3.8 Effect of *Ct*Pae12B, *Ct*PME and *Ct*RGL*f* treated PRG on colon cancer HCT-116 cells

The biocompatibility and toxicity of PRG products AcMePS, dAcdMePS, AcMeOS, dAcMeOS and dAcdMeOS were analysed by MTT assay. Cell viability was calculated upon treatment with the PRG products by using equation 5. The HEK-293 cells showed biocompatibility with 1 mg/mL PRG polysaccharides AcMePS and dAcdMePS with about 99% cell viability upon incubation for 24 h and 48 h, respectively (Fig. 5.7A and 5.7B). The PRG oligosaccharides AcMeOS, dAcMeOS and dAcdMeOS at 1 mg/mL were also seen to have no toxic effect on HEK-293. Each of PRG oligosaccharides AcMeOS, dAcMeOS and dAcdMeOS at 1 mg/mL was biocompatible with HEK-293 cells with cell viability 97.5%, 95.3% and 95.4%, respectively, upon incubation for 48 h (Fig. 5.7B). In case of HCT-116 cell line, PRG polysaccharides, AcMePS and dAcdMePS at 1 mg/mL were biocompatible with HCT-116 cells showing cell viability 91.6% and 90.9%, respectively, upon incubation for 48 h (Fig. 5.7C and 5.7D). However, cell viability of HCT-116 cells decreased upon treatment PRG oligosaccharides. AcMeOS at 1 mg/mL decreased the cell viability of HCT-116 to 78% upon incubation for 24 h and 65% upon incubation for 48 h. dAcMeOS and dAcdMeOS showed quite similar patterns of cell viability upon incubation with HCT-116. dAcMeOS at 1 mg/mL showed cell viability of 71% upon incubation for 24 h and 50.5% upon incubation for 48 h. Similarly, dAcdMeOS at 1 mg/mL showed cell viability of 69.5% upon incubation for 24 h and 49.8% upon

incubation for 48 h (Fig. 5.7C and 5.7D). The results showed that the acetylated and methylated oligosaccharides showed only 35% inhibition of the HCT-116 cells, while, interestingly, both de-acetylated and de-methylated oligosaccharides as well as deacetylated and methylated oligosaccharides could cause inhibition of HCT-116 cells up to 50% (Fig. 5.7D). Earlier reports showed that highly methylated pectic oligosaccharides like 77% methylation in *Citrus limetta* (Chakraborty *et al.,* 2018) and 68% methylation in *Citrus reticulata* (Rajulapati *et al.,* 2021) caused higher inhibition of HT-29 colon cancer cells as compared with the non-methylated pectic oligosaccharides. The similar inhibition pattern obtained by both dAcMeOS and dAcdMeOS, can be explained by the reason that the amount of methyl groups present in PRG (approx. 7%) was quite low to show any significant effect on cell inhibition. However, PRG was seen to be highly acetylated (approx. 21%) and from MTT assays it became clear that the removal of acetyl groups from PRG oligosaccharides increases the inhibition of HCT-116 cells. This could be explained by the fact that deacetylation helps in better cellular uptake of the oligosaccharides and therefore, cytotoxicity, as also mentioned earlier (Huang *et al.,* 2004; Park *et al.*, 2011).

The cell morphology of HEK-293 cells did not change upon treatment with any of the PRG products dAcdMePS, AcMeOS, dAcMeOS and dAcdMeOS (Fig. 5.7E). The morphology of HEK-293 cells upon treatment with AcMePS is not shown as it showed similar cell viability and cell morphology as dAcdMePS. While, the morphology of dAcdMePS treated HCT-116 did not change with respect to the control (Fig. 5.7F). However, the morphology of AcMeOS, dAcMeOS and dAcdMeOS treated HCT-116 showed more shrunken and globular structure as shown by the phalloidin-FITC staining (Fig. 5.7F) than the control (untreated). The cell-cell attachments were also lost and fewer number of cells were only present that could be visualized as compared to the

control and dAcdMePS treated HCT-116 cells. Considering the number of cells in HCT-116 control to be 100%, the number of cells in AcMeOS treated cells were approx. 65% and 50% for dAcMeOS and dAcdMeOS treated cells (Fig. 5.7F).

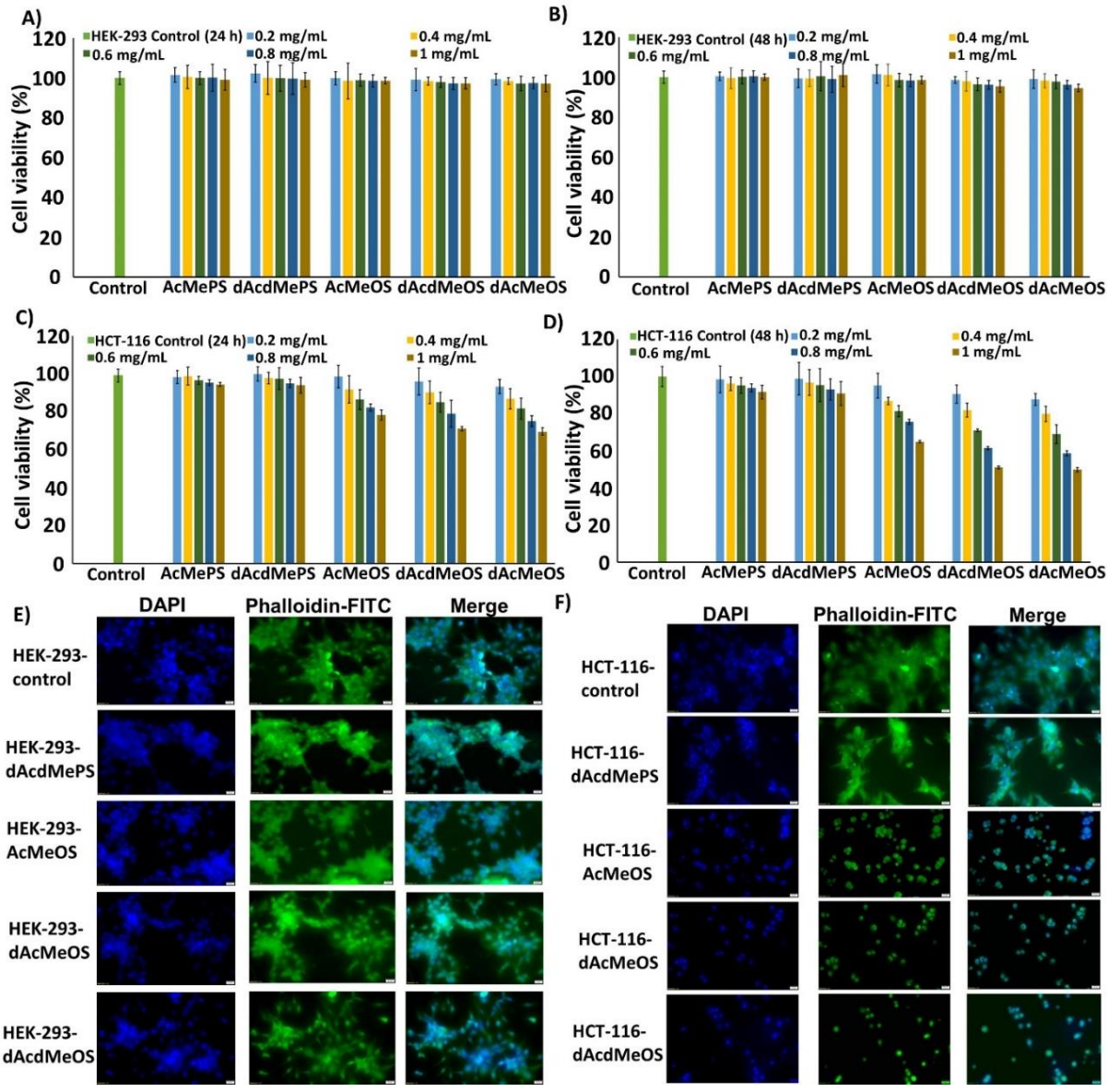

Fig. 5.7 MTT assay after treatment with different concentrations of PRG products of A) HEK-293 cells upon 24 h incubation, B) HEK-293 cells upon 48 h incubation, C) HCT-116 cells upon 24 h incubation, D) HCT-116 cells upon 48 h incubation. Cellular morphology after 48 h incubation with 1 mg/mL of different PRG products of E) HEK-293 cells and F) HCT-116 cells.

5.3.9 Drug entrapment, viscosity and drug release analysis of *Ct*Pae12B-treated PRG hydrogel

5.3.9.1 Drug entrapment by *Ct*Pae12B-treated and non-enzyme treated PRG hydrogels

After loading the drug, Dox, to the two hydrogels prepared by *Ct*Pae12B-treated PRG and non-enzyme treated PRG, the drug entrapment efficiency was analysed by equation 6. The drug entrapment efficiency of *Ct*Pae12B-treated PRG hydrogel was calculated to be 93.4 ± 2% and that of non-enzyme treated PRG hydrogel was 63.4 ± 3%. Thus, *Ct*Pae12B-treated hydrogel showed better drug entrapment efficiency than non-enzyme treated PRG hydrogel. The non-enzyme treated hydrogel loaded with Dox exhibited a light red colour (Left panel, Fig. 5.8A) as compared with the *Ct*Pae12B-treated hydrogel loaded with Dox that exhibited a blood red colour of Dox because of higher entrapment efficiency (Right panel, Fig. 5.8A).

5.3.9.2 Viscosity analysis of Dox loaded *Ct*Pae12B-treated PRG hydrogel and *Ct*Pae12B-treated PRG hydrogel without Dox

The viscosity variation of the drug (Dox) loaded *Ct*Pae12B-treated PRG hydrogel and only *Ct*Pae12B-treated PRG hydrogel (without Dox) against the increasing shear rate is shown in fig. 5.8B. The log-log plot of viscosity and shear rate showed linear behaviour indicating pseudo-plastic or shear thinning characteristics as the viscosity in both the hydrogels decreased with increase in shear rate as also reported earlier (El-Naggar *et al.*, 2020). From the curve of viscosity *vs.* shear rate (Fig. 5.8B), it was clear that the hydrogel loaded with Dox showed higher viscosity, i.e. 98050 cP at lowest shear rate 1.75 s^{-1} as compared with *Ct*Pae12B-treated hydrogel without Dox, i.e. 93180 cP. At higher shear rate 100 s^{-1}, the viscosity of Dox loaded PRG hydrogel decreased to 323 cP and that of *Ct*Pae12B-treated hydrogel without Dox to 148 cP. These results indicated that the hydrogel prepared by *Ct*Pae12B-treated PRG was viscous enough for

drug loading studies and that its viscosity increased significantly on addition of Dox. One of the studies reported earlier showed that when viscosity was studied as a function of shear rate, an increase in viscosity of pectin hydrogels loaded with Dox was observed as compared to the viscosity of pectin alone (Bosio *et al.*, 2012).

5.3.9.3 Drug release analysis by *Ct*Pae12B-treated and non-enzyme treated PRG hydrogels

Both the hydrogel preparations, *Ct*Pae12B-treated and non-enzyme treated PRG hydrogels were analysed for drug release at gastric simulated pH 1.2 for 2 h and subsequently at intestinal fluid simulated pH 7.4 for 3 h to 24 h. At the end of 2 h, at pH 1.2, the cumulative percent drug release was higher (almost double) i.e. 67.5 ± 2.3% from non-enzyme treated hydrogel as compared with the cumulative percent drug release from *Ct*Pae12B-treated hydrogel, i.e. 38.8 ± 2.5% (Fig. 5.8C). Therefore, higher drug loss was observed in the gastric pH by non-enzyme treated PRG hydrogel as compared with *Ct*Pae12B-treated PRG hydrogel. This showed that *Ct*Pae12B-treated PRG hydrogel helps in sustainable drug release at gastric conditions. The drug release rate at pH 1.2 from both the hydrogels was calculated after fitting to the zero-order kinetic model using equation 7 (Gami *et al.*, 2020; Sontakke *et al.*, 2022).

$$Q_t/Q_e = K_o t \qquad \text{Eqn. (7)}$$

Where Q_t is the amount of drug released in time t, Q_e is the amount of drug released at equilibrium, K_o is the zero-order rate constant and t is time. The K_o for non-enzyme treated hydrogel calculated from equation 7 was 0.0057 min^{-1} with R^2=0.99, while for *Ct*Pae12B-treated hydrogel, the K_o was calculated to 0.0033 min^{-1} with R^2=0.99 (Fig. 5.8D and Table 5.4). Therefore, a lower drug release rate was achieved at pH 1.2 by *Ct*Pae12B-treated PRG hydrogel as compared with non-enzyme treated PRG hydrogel,

showing that *Ct*Pae12B-treated PRG hydrogel was better for sustainable colon-targeted drug release.

Both the hydrogels were placed subsequently at pH 7.4 with remaining amount of Dox entrapped in them and the amount of drug release was monitored at various time intervals. At 132 min, complete drug release (100 ± 3.6%) was observed for non-enzyme treated hydrogel at pH 7.4, while for the *Ct*Pae12B-treated hydrogel the cumulative accumulated drug release at 180 min was 78.6 ± 3% (Fig. 5.8E). At the end of 26 h (2 h at pH 1.2 and 24 h at pH 7.4), the total drug released from *Ct*Pae12B-treated hydrogel was 87.5 ± 3.2% showing a very sustainable release (Fig. 5.8D). About 50% of total drug was released from *Ct*Pae12B-treated hydrogel when placed for 24 h at pH 7.4. Due to less drug entrapment and higher amount of drug already released at pH 1.2, the non-enzyme treated hydrogel formulation reached its equilibrium in a very less time (132 min) at pH 7.4. In contrast, *Ct*Pae12B-treated hydrogel showed much better drug entrapment efficiency and sustainable release at both pHs 1.2 and 7.4. The rate of drug release was calculated by fitting the amount of drug release in first order kinetic model for both the hydrogels. The equation used for data fitting was as mentioned earlier (Fopase *et al.*, 2020a).

$$Q_t = A \{1- \exp (-k \times t)\} \qquad \text{Eqn. (8)}$$

Where, A is constant and k is the rate constant. The drug release rate calculated for non-enzyme treated PRG hydrogel from equation 8 at pH 7.4 was 0.02 min^{-1} with R^2=0.99 and that for *Ct*Pae12B-treated PRG hydrogel was 0.009 min^{-1} with R^2=0.99 (Fig. 5.8F and Table 5.4). The drug release rate of non-enzyme treated PRG hydrogel was very high as compared with *Ct*Pae12B-treated PRG hydrogel, indicating that *Ct*Pae12B treatment is better for slower and sustainable drug release at intestinal pH conditions.

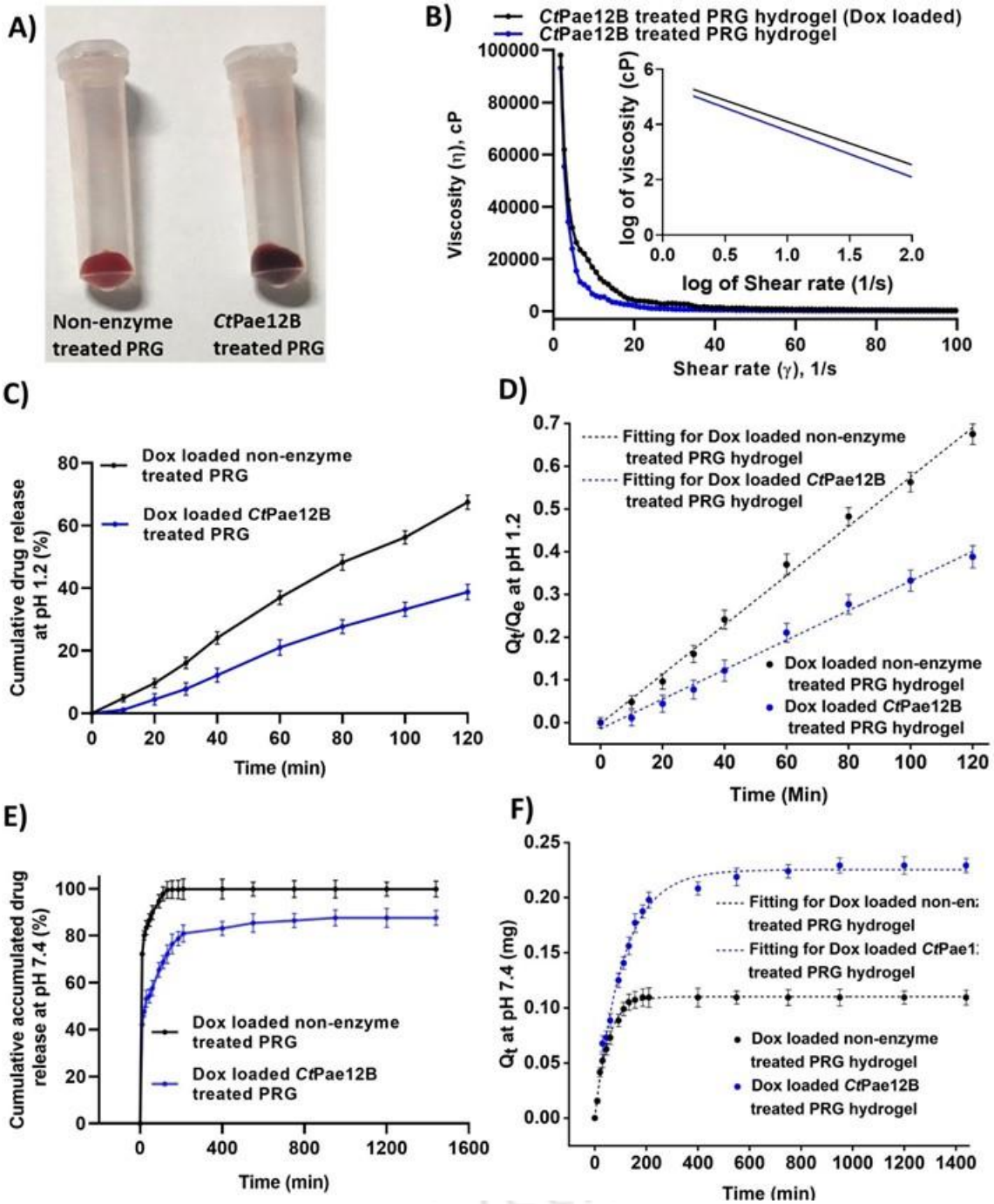

Fig. 5.8 A) Dox loaded non-enzyme treated hydrogel (left panel) and Dox loaded *Ct*Pae12B-treated PRG hydrogel (right panel), B) Viscosity as a function of shear rate of *Ct*Pae12B-treated PRG hydrogel loaded with Dox and *Ct*Pae12B-treated PRG hydrogel without Dox C) Cumulative percent drug release profile of non-enzyme treated and *Ct*Pae12B-treated PRG hydrogels at pH 1.2, D) Fitting of drug release (Q_t/Q_e) by both non-enzyme treated and *Ct*Pae12B-treated PRG hydrogels at pH 1.2 in zero-order kinetic model, E) Cumulative percent drug release profile of non-enzyme treated and *Ct*Pae12B-treated PRG hydrogels at pH 7.4, F) Fitting of drug release (Q_t) by both non-enzyme treated and *Ct*Pae12B-treated PRG hydrogels at pH 7.4 in first order kinetic model.

The drug release rate of *Ct*Pae12B-treated PRG hydrogel was 3 times more at pH 7.4 (0.009 min^{-1}) as compared with pH 1.2 (0.0033 min^{-1}), showing its efficiency as a colon-targeted drug carrier. An earlier study reported that hydrogels prepared from citrus pectin showed less than 1% release rate of indomethacin at pH 1.2 as compared with 5-20% when immersed at pH 7.4 (Jung *et al.*, 2013). Another study also reported that biodegradable hydrogels released less Dox at pH 1.2 (20-23%) for 10 h as compared to an increase to 52% at pH 7.4 for 10 h (Xu *et al.*, 2018).

Table 5.4. Drug release parameters of PRG hydrogels.

Hydrogel	pH	Dox release (%)	Kinetic model	Rate constant (min^{-1})	R^2 of curve fitting
Non-enzyme treated PRG hydrogel	1.2	67.5 ± 2.3	Zero-order (Eqn. 6)	0.0057	0.99
	7.4	100 ± 3.6	First order (Eqn. 7)	0.02	0.99
*Ct*Pae12B-treated PRG hydrogel	1.2	38.8 ± 2.5	Zero-order (Eqn. 6)	0.0033	0.99
	7.4	80 ± 3.4	First order (Eqn. 7)	0.009	0.99

5.4 Conclusion

Three pectin degrading enzymes *Ct*Pae12B, *Ct*PME and *Ct*RGL*f* were expressed and purified to homogeneity exhibiting single protein bands of ~25 kDa, 35 kDa and 80.2 kDa, respectively. The side chain degrading enzymes *Ct*Pae12B and *Ct*PME showed synergistic action with main chain degrading enzyme *Ct*RGL*f* against PRG, by displaying significant increase in its relative activity by 115%. The regioselectivity of *Ct*Pae12B towards O-2 and O-3 acetylated substrate (PRG) by ^{1}H NMR analysis showed that it had site specificity for acetyl groups at both positions enabling 98% removal of acetyl groups. ^{1}H NMR and HPLC analysis of PRG showed the DA and DM to be approx. 21.9% and 7.7%, respectively, indicating higher acetylation and less methylation. The percentage of other mono-saccharides like *GalpA*, *Rhap*, galactose and arabinose calculated from HPLC analysis were 63.5%, 6.5%, 25% and 2.8%, respectively, in PRG. The breakdown products of PRG by only *Ct*RGL*f* and all three *Ct*Pae12B, *Ct*PME and *Ct*RGL*f* showed discrete spots in TLC plate and the smallest molecular mass product displayed was unsaturated RG di-saccharide that had similar mobility as the standard D-*GalpA*. The mass spectrometric analysis of only *Ct*RGL*f* treated and all three *Ct*Pae12B, *Ct*PME, *Ct*RGL*f* treated PRG showed that the smallest degraded product was unsaturated RG di-saccharide with m/z 322. The mass spectrometric analysis also showed that the oligosaccharide products released from PRG upon treatment with all three *Ct*Pae12B, *Ct*PME and *Ct*RGL*f* were de-acetylated and de-methylated as compared to the products released upon treatment with *Ct*RGL*f* alone. The ATR-FTIR profile also showed de-acetylation and de-methylation of the PRG oligosaccharides upon treatment with all three *Ct*Pae12B, *Ct*PME and *Ct*RGL*f* as compared to acetylated and methylated oligosaccharides produced by only *Ct*RGL*f* treatment of PRG. FESEM analysis showed more porous surface morphology of *Ct*Pae12B-treated PRG as compared to non-enzyme treated PRG. The TGA of

*Ct*Pae12B-treated PRG showed the degradation temperature to be 254 ± 1.5 ºC. The pore volume (size ≤32 nm) and the total surface area of *Ct*Pae12B-treated PRG was significantly increased as compared with the non-enzyme treated PRG as analysed by BET. The MTT assay showed that PRG polysaccharides (both esterified and de-esterified) were biocompatible with both HEK-293 and HCT-116 cells, while PRG oligosaccharides showed inhibition of HCT-116 cells. As compared to the acetylated and methylated PRG oligosaccharides (cell viability = 65%), the de-acetylated and de-methylated oligosaccharides showed higher inhibition of HCT-116 cells (cell viability = 50%) upon treatment with 1 mg/mL for 48 h. HEK-293 cells showed biocompatibility with all PRG oligosaccharides and no change in cell morphology as compared to the HEK-293 control cells. The cell morphology of the PRG oligosaccharides, AcMeOS, dAcMeOS and dAcdMeOS, treated HCT-116 cells showed fewer number of cells with shrunken and globular shape and loss of cell-cell adhesion as compared to the cell morphology of PRG polysaccharide treated HCT-116 and control HCT-116 cells. The viscosity of Dox loaded *Ct*Pae12B-treated PRG hydrogel was higher than *Ct*Pae12B-treated PRG hydrogel without Dox loading. The drug entrapment efficiency of *Ct*Pae12B-treated PRG hydrogel was remarkably higher than non-enzyme treated PRG hydrogel. The drug release study of *Ct*Pae12B-treated PRG hydrogel at gastric pH 1.2 and intestinal pH 7.4, showed sustainable release as compared with non-enzyme treated hydrogel. The faster rate of drug release by non-enzyme treated PRG hydrogel in gastric pH 1.2 than the *Ct*Pae12B-treated hydrogel showed that the *Ct*Pae12B treatment makes the PRG, a biomaterial more efficient in entrapping the drug and helping in controlled and sustained drug release. *Ct*Pae12B-treated PRG hydrogel showed sustained drug release at intestinal pH 7.4 for 24 h indicating that the *Ct*Pae12B treatment forms a hydrogel for colon targeted drug release. The results showed that *Ct*Pae12B is a highly efficient enzyme for deacetylation and has a potential role in therapeutic applications

like inhibiting colon cancer cells and development of biocompatible gel material for controlled drug delivery systems. The role of *Ct*Pae12B can be further explored for developing efficient hydrogel biomaterials for therapeutic applications like entrapment of various anti-cancer drugs and their controlled and sustainable drug release.

References

Ahmed, J., Kumar, K., Goyal, A. (2023) A thermotolerant and pH stable rhamnogalacturonan acetylesterase (*Ct*Pae12B), a family 12 carbohydrate esterase from *Clostridium thermocellum* with broad substrate specificity. International Journal of Biological Macromolecules, 226: 1560-1569.

Ahmed, J., Thakur, A., Goyal, A. (2021) Emerging trends on the role of recombinant pectinolytic enzymes in industries-an overview. Biocatalysis and Agricultural Biotechnology, 38: 102200.

Bolvig, P.U., Pauly, M., Orfila, C., Scheller, H.V., Schnorr, K. (2003) Sequence analysis and characterization of a novel pectin acetyl esterase from *Bacillus subtilis*. Advances in Pectin and Pectinase Research, (eds. Voragen, F., Schols, H., Visser, R.), Springer, Dordrecht, 315-330.

Bosio, V.E., Machain, V., López, A.G., De Berti, I.O.P., Marchetti, S.G., Mechetti, M., Castro, G.R. (2012) Binding and encapsulation of doxorubicin on smart pectin hydrogels for oral delivery. Applied Biochemistry and Biotechnology, 167: 1365-1376.

Bradford, M.M. (1976) A rapid and sensitive method for the quantitation of microgram quantities of protein utilizing the principle of protein-dye binding. Analytical Biochemistry, 72: 248–254.

Cao, L., Lu, W., Mata, A., Nishinari, K., Fang, Y. (2020) Egg-box model-based gelation of alginate and pectin: A review. Carbohydrate Polymers, 242: 116389.

Chakraborty, S., Rani, A., Goyal, A. (2018) Pectic oligosaccharides produced from pectin extracted from waste peels of *Citrus limetta* using recombinant endo-pectate lyase (PL1B) inhibit colon cancer cells. Trends in Carbohydrate Research, 10(1).

Cheng, H., Zhang, Z., Leng, J., Liu, D., Hao, M., Gao, X., Tai, G., Zhou, Y. (2013) The inhibitory effects and mechanisms of rhamnogalacturonan I pectin from potato on HT-29 colon cancer cell proliferation and cell cycle progression. International Journal of Food Sciences and Nutrition, 64(1): 36-43.

Chenite, A., Buschmann, M., Wang, D., Chaput, C., Kandani, N.J.C.P. (2001) Rheological characterisation of thermosgelling chitosan/glycerol-phosphate solutions. Carbohydrate Polymers, 46(1): 39-47.

Dhillon, A., Fernandes, V.O., Dias, F.M., Prates, J.A., Ferreira, L.M., Fontes, C.M., Centeno, M.S.J., Goyal, A. (2016) A New Member of Family 11 Polysaccharide Lyase, Rhamnogalacturonan Lyase (*Ct*RGLf) from *Clostridium thermocellum*. Molecular Biotechnology, 58: 232-240.

Einhorn-Stoll, U., Kunzek, H. (2009) Thermoanalytical characterisation of processing dependent structural changes and state transitions of citrus pectin. Food Hydrocolloids, 23 (1): 40–52.

El-Naggar, N.E.A., Hussein, M.H., Shaaban-Dessuuki, S.A., Dalal, S.R. (2020) Production, extraction and characterization of *Chlorella vulgaris* soluble

polysaccharides and their applications in AgNPs biosynthesis and biostimulation of plant growth. Scientific Reports, 10(1): 3011.

Fopase, R., Pathode, S.R., Sharma, S., Datta, P., Pandey, L.M. (2020a) Lipopeptide and essential oil based nanoemulsion for controlled drug delivery. Polymer-Plastics Technology and Materials, 59 (18): 2076-2086.

Fopase, R., Saxena, V., Seal, P., Borah, J.P., Pandey, L.M. (2020b) Yttrium iron garnet for hyperthermia applications: synthesis, characterization and *in-vitro* analysis. Materials Science and Engineering: C, 116: 111163.

Gami, P., Kundu, D., Seera, S.D.K., Banerjee, T. (2020) Chemically crosslinked xylan–β-Cyclodextrin hydrogel for the in vitro delivery of curcumin and 5-Fluorouracil. International Journal of Biological Macromolecules, 158: 18-31.

Heux, L., Brugnerotto, J., Desbrieres, J., Versali, M.F., Rinaudo, M. (2000) Solid state NMR for determination of degree of acetylation of chitin and chitosan. Biomacromolecules, 1(4): 746-751.

Hu, Q., Shi, B., Dong, N., Yu, X., Xiao, C., Lei, Z., Li, F., Ren, T., Liu, J. (2022) Physicochemical and morphological characteristics of potato pectin with *in-situ* acid-induced gelation. Journal of Food Science, 87(9): 3965-3977.

Huang, M., Khor, E., Lim, L.Y. (2004) Uptake and cytotoxicity of chitosan molecules and nanoparticles: effects of molecular weight and degree of deacetylation. Pharmaceutical Research, 21: 344-353.

Inohara, H., Raz, A. (1994) Effects of natural complex carbohydrate (citrus pectin) on murine melanoma cell properties related to galectin-3 functions. Glycoconjugate Journal, 11: 527-532.

Ishii, T. (1997) O-Acetylated oligosaccharides from pectins of potato tuber cell walls. Plant Physiology, 113(4): 1265–1272

Jung, J., Arnold, R.D., Wicker, L. (2013) Pectin and charge modified pectin hydrogel beads as a colon-targeted drug delivery carrier. Colloids and Surfaces B: Biointerfaces, 104: 116-121.

Kasaai, M.R. (2010) Determination of the degree of N-acetylation for chitin and chitosan by various NMR spectroscopy techniques: A review. Carbohydrate Polymers, 79(4): 801-810.

Komalavilas, P., Mort, A.J. (1989) The acetylation of O-3 of galacturonic acid in the rhamnose-rich portion of pectins. Carbohydrate Research, 189: 261-272.

Mallikarjuna, S.E., Dharmesh, S.M. (2018) Swallow root (*Decalepis hamiltonii*) pectic oligosaccharide (SRO1) induces cancer cell death via modulation of galectin-3 and survivin. Carbohydrate Polymers, 186: 402-410.

Melton, L.D., Smith, B.G. (2001a) Determining the degree of methylation and acetylation of pectin. Current Protocols in Food Analytical Chemistry, (1): E3-4.

Melton, L.D., Smith, B.G. (2001b) Determination of the uronic acid content of plant cell walls using a colorimetric assay. Current Protocols in Food Analytical Chemistry, (1): E3-3.

Mohnen, D., Bar-Peled, M., & Somerville, C. (2008). Chapter 5. Biosynthesis of Plant Cell Walls. Biomass Recalcitrance, (ed. Himmel, M.), Blackwell Publishing, Oxford, 94–187.

Mosmann, T., (1983) Rapid colorimetric assay for cellular growth and survival: application to proliferation and cytotoxicity assays. Journal of Immunological Methods, 65(1-2): 55-63.

O'Neill, M. A., York, W. S. (2003) The composition and structure of plant primary cell walls. *The plant cell wall (annual plant reviews*), (ed. Rose, J. K. C), Oxford: Blackwell Publishing, 1–54.

Ochiai, A., Itoh, T., Kawamata, A., Hashimoto, W., Murata, K. (2007) Plant cell wall degradation by saprophytic *Bacillus subtilis* strains: gene clusters responsible for rhamnogalacturonan depolymerization. Applied and Environmental Microbiology, 73(12): 3803-3813.

Oosterveld, A., Beldman, G., Searle-van Leeuwen, M.J.F., Voragen, A.G.J. (2000) Effect of enzymatic deacetylation on gelation of sugar beet pectin in the presence of calcium. Carbohydrate Polymers, 43(3): 249-256.

Panwar, P., Pandey, B., Lakhera, P.C., Singh, K.P. (2010) Preparation, characterization, and in vitro release study of albendazole-encapsulated nanosize liposomes. International Journal of Nanomedicine, 101-108.

Park, J.K., Chung, M.J., Choi, H.N., Park, Y.I. (2011) Effects of the molecular weight and the degree of deacetylation of chitosan oligosaccharides on antitumor activity. International Journal of Molecular Sciences, 12(1): 266-277.

Peng, X.Y., Mu, T.H., Zhang, M., Sun, H.N., Chen, J.W., Yu, M. (2016) Effects of pH and high hydrostatic pressure on the structural and rheological properties of sugar beet pectin. Food Hydrocolloids, 60: 161-169.

Rajulapati, V., Goyal, A. (2017) Molecular cloning, expression and characterization of pectin methylesterase (*Ct*PME) from *Clostridium thermocellum*. Molecular Biotechnology, 59: 128-140.

Rajulapati, V., Dhillon, A., Goyal, A. (2021) Enzymatically produced pectic-oligosaccharides from fruit waste of *Citrus reticulata* (mandarin) peels display cytotoxicity against colon cancer cells. Bioresource Technology Reports, 15: 100740.

Remoroza, C., Wagenknecht, M., Gu, F., Buchholt, H.C., Moerschbacher, B.M., Schols, H.A., Gruppen, H. (2014) A *Bacillus licheniformis* pectin acetylesterase is specific for homogalacturonans acetylated at O-3. Carbohydrate Polymers, 107: 85-93.

Rosenbohm, C., Lundt, I., Christensen, T.I., Young, N.G. (2003) Chemically methylated and reduced pectins: preparation, characterisation by ^{1}H NMR spectroscopy, enzymatic degradation, and gelling properties. Carbohydrate Research, 338(7): 637-649.

Safran, J., Habrylo, O., Cherkaoui, M., Lecomte, S., Voxeur, A., Pilard, S., Bassard, S., Pau-Roblot, C., Mercadante, D., Pelloux, J., Sénéchal, F. (2021) New insights into the specificity and processivity of two novel pectinases from *Verticillium dahliae*. International Journal of Biological Macromolecules, 176: 165-176.

Said, N.S., Olawuyi, I.F. & Lee, W.Y. (2023). Pectin hydrogels: Gel-forming behaviours, mechanisms, and food applications. Gels, 9(9), 732.

Savary, B.J., Nunez, A., Liu, L.S., Yoo, S. (2003) March. Pectin acetylesterase–analysis and application for sugar beet pectin utilization. In *Proceedings of the 1st Joint International Beet Research–American Society of Sugar Beet Technologists Congress. Denver, CO: Beet Sugar Development Foundation*.

Schols, H.A., Voragen, A.G. (1994) Occurrence of pectic hairy regions in various plant cell wall materials and their degradability by rhamnogalacturonase. Carbohydrate Research, 256(1): 83-95.

Shevchik, V.E., Hugouvieux-Cotte-Pattat, N. (1997) Identification of a bacterial pectin acetyl esterase in *Erwinia chrysanthemi* 3937. Molecular Microbiology, 24(6): 1285-1301.

Sontakke, A.D., Fopase, R., Pandey, L.M., Purkait, M.K. (2022) Development of graphene oxide nanoscrolls imparted nano-delivery system for the sustained release of gallic acid. Applied Nanoscience, 12(9): 2733-2751.

Synytsya, A., Čopíková, J., Matějka, P., Machovič, V.J.C.P. (2003) Fourier transform Raman and infrared spectroscopy of pectins. Carbohydrate Polymers, 54(1): 97-106.

Tang, X.D., Dong, F.Y., Zhang, Q.H., Lin, L., Wang, P., Xu, X.Y., Wei, W., Wei, D.Z. (2021) Protein engineering of a cold-adapted rhamnogalacturonan acetylesterase: *In vivo* functional expression and cinnamyl acetate synthesis. Process Biochemistry, 107: 129-137.

Wang, W., Mayo, K.H., Yuan, Y., Zhou, Y. (2022) Biochemical characterization of two rhamnogalacturonan lyases from *Bacteroides ovatus* ATCC 8483 with preference for RG-I substrates. Frontiers in Microbiology, 12: 799875.

Wu, B., Shen, F., Chen, C.J., Liu, L., Wang, X., Zheng, W.Y., Deng, Y., Wang, T., Huang, Z.Y., Xiao, C., Zhou, Q. (2021) Natural variations in a pectin acetylesterase gene, MdPAE10, contribute to prolonged apple fruit shelf life. The Plant Genome, 14(1): e20084.

Xu, L., Qiu, L., Sheng, Y., Sun, Y., Deng, L., Li, X., Bradley, M., Zhang, R. (2018) Biodegradable pH-responsive hydrogels for controlled dual-drug release. Journal of Materials Chemistry B, 6(3): 510-517.

Yang, J.S., Mu, T.H., Ma, M.M. (2018) Extraction, structure, and emulsifying properties of pectin from potato pulp. Food Chemistry, 244: 197-205.

Zdunek, A., Pieczywek, P.M., Cybulska, J. (2021) The primary, secondary, and structures of higher levels of pectin polysaccharides. Comprehensive Reviews in Food Science and Food Safety, 20(1): 1101-1117.

List of publications

List of articles published/submitted from Ph.D. Thesis Work

Research articles

1. **Jebin Ahmed,** Krishan Kumar, Kedar Sharma, Carlos MGA Fontes and Arun Goyal, 2022. Computational and SAXS-based structure insights of pectin acetyl esterase (*Ct*Pae12B) of family 12 carbohydrate esterase from *Clostridium thermocellum* ATCC 27405. ***Journal of Biomolecular Structure and Dynamics,*** 40(18): 8437-8454. (JIF 2.7).

2. **Jebin Ahmed**, Krishan Kumar and Arun Goyal, 2023. A thermotolerant and pH stable rhamnogalacturonan acetylesterase (*Ct*Pae12B), a family 12 carbohydrate esterase from *Clostridium thermocellum* with broad substrate specificity. ***International Journal of Biological Macromolecules***, 226: 1560-1569. (JIF 7.7).

Submitted

1. **Jebin Ahmed** and Arun Goyal, 2024. One-pot biocatalysis of potato rhamnogalacturonan and the role of its deacetylation in efficient inhibition of colon cancer cells and hydrogel mediated colon-targeted drug delivery. ***International Journal of Biological Macromolecules.*** **(Submitted).**

Review article

1. **Jebin Ahmed,** Abhijeet Thakur and Arun Goyal, 2021. Emerging trends on the role of recombinant pectinolytic enzymes in industries-an overview. ***Biocatalysis and Agricultural Biotechnology,*** 38: 102200. (JIF 3.4).

List of research articles in collaboration with others

1. Vishwanath Yadav, **Jebin Ahmed**, Abhijeet Thakur, Poorvi Vishwakarma, Shubha Singh, Punit Kaur and Arun Goyal, 2022. Structural insights of a putative β-1, 4-xylosidase (*Ps*GH43F) of glycoside hydrolase family 43 from *Pseudopedobacter saltans*. ***International Journal of Biological Macromolecules***, 221: 751-762. (JIF 7.7).

2. Shubha Singh, **Jebin Ahmed**, Parmeshwar Vitthal Gavande, Carlos MGA Fontes and Arun Goyal, 2023. Structural and functional insights into the glycoside hydrolase family 30 xylanase of the rumen bacterium *Ruminococcus flavefaciens*. ***Journal of Molecular Structure***, 1272: 134155. (JIF 4.0).

3. Parmeshwar Vitthal Gavande, Krishan Kumar, **Jebin Ahmed** and Arun Goyal, 2023. Multifunctionality and mechanism of processivity of family GH5 endoglucanase, *Rf*GH5_4 from *Ruminococcus flavefaciens* on lignocellulosic polymers. ***International Journal of Biological Macromolecules***, 224: 1395-1411. (JIF 7.7).

4. **Jebin Ahmed**, Ashish Poonia and Arun Goyal, 2024. Deciphering the structure of a distinctive trimodular cellulosomal licheninase (*Rf*GH16_21), a family 16 glycoside hydrolase from *Ruminococcus flavefaciens* by computational and experimental methods. ***Journal of Biomolecular Structure and Dynamics***, 42(6): 3094-3107. (JIF 2.7).

5. Ardhendu Mandal, **Jebin Ahmed**, Shweta Singh and Arun Goyal, 2024. Structure elucidation of a multi-modular recombinant endoglucanase, *At*GH9C-CBM3A-CBM3B from *Acetivibrio thermocellus* ATCC 27405 and its substrate binding analysis. ***International Journal of Biological Macromolecules***, p. 133212 (JIF=7.7).
6. Yumnam Robinson Singh, **Jebin Ahmed** and Arun Goyal, 2024. Small angle X-ray scattering and *in-silico* based structure and function analysis of a novel xylobiohydrolase (AcGH30A) from *Acetivibrio clariflavus*. ***Journal of Biomolecular Structure and Dynamics***. (**Accepted**). (JIF 2.7).

Book chapters

1. **Jebin Ahmed,** Abhijeet Thakur and Arun Goyal, 2021. CHAPTER 1: Industrial Wastewater and Its Toxic Effects. In (Ed. Maulin P. Shah) Biological Treatment of Industrial Wastewater, 1–14, **The Royal Society of Chemistry**.
2. **Jebin Ahmed** and Arun Goyal, 2024. Emerging Trends in Novel Technological Advancements in Oligosaccharide Production and Their Potential Applications as Prebiotics with Beneficial Effects. In (Ed. P. Verma) Industrial Microbiology and Biotechnology: An Insight into Current Trends, pp.153-174, **Springer**, Singapore.

List of conferences

1. **Jebin Ahmed**, Krishan Kumar and Arun Goyal, 2021. Cloning, expression, purification and biochemical characterization of pectin acetyl esterase (*Ct*Pae12B) a family 12 carbohydrate esterase from *Clostridium thermocellum*. **International Conference on Biotechnology for Sustainable Agriculture, Environment and Health (BSAEH – 2021)**. 04-08th April, Jaipur, India. (Flash talk and poster presentation).

2. **Jebin Ahmed**, Krishan Kumar, Kedar Sharma, Carlos M. G. A. Fontes and Arun Goyal, 2021. Computational and SAXS-based structure insights of pectin acetyl esterase (*Ct*Pae12B) of family 12 carbohydrate esterase from *Clostridium thermocellum* ATCC 27405. **International conference on Biotechnology for Resource Efficiency, Energy, Environment, Chemicals and Health.** 01-04th December, Dehradun, Uttarakhand, India. (Flash talk and poster presentation).

3. **Jebin Ahmed**, Krishan Kumar, Kedar Sharma, Carlos M. G. A. Fontes and Arun Goyal, 2022. Biochemical characterization and in silico analysis of pectin acetyl esterase (*Ct*Pae12B) a family 12 carbohydrate esterase from *Clostridium thermocellum*. **Research Conclave**, January 20-23rd, IIT Guwahati, Assam. (Poster presentation and 3-min thesis presentation).

4. **Jebin Ahmed**, Ashish Poonia and Arun Goyal, 2022. Structure illustration of a distinctive trimodular cellulosomal licheninase (*Rf*GH16_21), a family 16 glycoside hydrolase from *Ruminococcus flavefaciens* by *in-silico* and experimental methods. **International Carbohydrate Conference on "Emerging Trends in Glycochemistry, Glycobiology and Technology**" (CARBO-XXXVI). 5th – 7th December, 2022, Indian Institute of Technology Bombay, Powai, Mumbai, India. (Poster presentation).

5. **Jebin Ahmed** and Arun Goyal, 2023. Highly efficient de-acetylation by a rhamnogalacturonan acetyl esterase (*Ct*Pae12B), a family 12 carbohydrate esterase from *Clostridium thermocellum*. **Research and Industrial Conclave**, 14-16th May, IIT Guwahati, Assam (Poster presentation).

VITAE

The author was born on November 15, 1922 in the city of Guwahati, (Assam). She passed the Secondary Examination (10th Class) conducted by Secondary Education Board of Assam, Assam in 2009 and Higher Secondary Examination (12 th Class) conducted by Assam Higher Secondary Education Council, Assam in 2011. She completed Integrated Master in Science (Bioscience and Bioinformatics) from Tezpur Central University, Tezpur, Assam in July, 2018.

Ms. Jebin Ahmed joined the Ph.D. program in December, 2018 at Department of Biosciences and Bioengineering, Indian Institute of Technology Guwahati, Guwahati 781039, Assam, India. She successfully completed the course work with 9.00/10 CPI. She received Institute Fellowship (IIT Guwahati) from January 2019 to December 2023, under the scheme run by the Ministry of Education, New Delhi. From January 2024 to March,2024 she received fellowship from a DBT sponsored project in School of Energy Science and Engineering under Prof. Arun Goyal. She delivered the open (PhD Synopsis) Seminar on April 30, 2024 and presented her thesis work before the Doctoral Committee and her performance was satisfactory. She submitted the PhD thesis in May 2024.